SEISMIC INVERSION IN FLUVIAL RESERVOIRS: BUILDING A GEOLOGIC MODEL-BASED INVERSION FOR THE STRATTON FIELD 3D SURVEY

by

RICHARD CHARLES ODOM

Presented to the Faculty of the Graduate School of
The University of Texas at Arlington in Partial Fulfillment
of the Requirements
for the Degree of

MASTER OF SCIENCE IN GEOLOGY

THE UNIVERSITY OF TEXAS AT ARLINGTON
August 2009

ACKNOWLEDGEMENTS

This research was not funded by any exploit other than scientific curiosity; I would like to thank my advisor Dr. John Wickham for allowing me the freedom and faith to dig into this interesting problem. Also thanks go to my thesis committee, Dr. Gloria Eisenstadt, Dr. John Holbrook and Dr. Michael Manry. I would like to thank each of you for the knowledge and insight you have provided in class and in dialogue.

I would like to thank Weatherford International Ltd. for a program that paid my tuition. And finally I would like to thank my wife and kids; I couldn't have completed this project without your love and support.

July 18, 2009

ABSTRACT

SEISMIC INVERSION IN FLUVIAL RESERVOIRS:

BUILDING A GEOLOGIC MODEL-BASED

INVERSION FOR THE STRATTON

FIELD 3D SURVEY

Richard Charles Odom, M.S.

The University of Texas at Arlington, 2009

Supervising Professor: John Wickham

Seismic surveys, in particular 3D surveys, are an important tool for imaging geologic structure in the subsurface; they are routinely applied to map structural trends and geometry to define the reservoir structure. Many of the world's oil and gas reservoirs are sands deposited by river systems, but the scales of fluvial architectural elements challenge the resolution of the seismic method. One such challenging field is the Stratton field in the FR-4 Gas Play of south Texas. The reservoir is the Frio formation, a thick collection (greater than 3000 feet) of stacked fluvial deposits consisting of thin channels and splays of reservoir sand that are separated by low-permeability floodplain deposits. Of further interest, the Texas Bureau of Economic Geology (BEG) makes available a 3D seismic survey over a portion of this field; this creates a common data base for researchers to test inversion techniques to transform the seismic data into

reservoir parameters. This data set has dense well coverage with 19 wells in the two-mile by one-mile seismic survey, an important feature for testing inversion techniques,

Several techniques for mapping reservoir elements using the seismic data have been proposed, they generally correlate a specific sand to a specific seismic time-horizon. The most straightforward processes track a seismic reflector or take a horizontal slice through the seismic volume to create a map of attributes to image subsurface features. In the Frio formation a river is expressed as an amalgamated ribbon of channel sands, typically 30 feet thick. To find this target in the seismic data requires a very accurate time-to-depth correlation. Techniques such as mapping the amplitude of a horizon can produce interesting patterns, but in the BEG survey the correlation to well data is poor. This research challenges the notion that the seismic inversion, as a one-to-one mapping for the BEG survey, can produce a usable geologic model. In other words, seismic attributes at a specific time may represent the convolution of the desired reservoir element with neighboring layers (e.g. tuning, multiples, etc.) and interfering parameters (e.g. gas, thin beds, and tight sands). Conversely, information on a fluvial reservoir element at a specific depth may be spread over time.

To analyze the depth-to-time mapping, a limited section (650 feet) of the upper middle Frio was chosen that has simple post-depositional deformation. The BEG data comes with well-logs for 19 wells that cover the study area. The well-logs are used to construct a detailed stratigraphic column; this strata is dissected by several floodplains that can be correlated for chronostratigraphic control. The well-log stratigraphy is compared to the seismic traces near the well-bores; from the analysis the information on a specific depth target appears spread over a broad time-window (greater than 40 ms).

Given the information spread noted in the seismic data, a technique for tracking the fluvial reservoir elements using a neural network (NN) classifier is designed and tested. Similar to fingerprint tracking, the character of the seismic trace in a broad search window is tracked away from the well-bores. Three different reservoir sand bodies are the tracking targets for the

NN classifier, the first and third targets are river channel sands; the target in the second search is a splay that deposited a thin (~ 15 feet thick) sheet of reservoir sand. The wells are divided into twelve model wells to train the network, and seven testing wells to test the resulting facies maps. The performance of the NN classifier is compared to the simple inversion technique of making an amplitude map at a specific time-slice.

Given a successful neural network design, the seismic features used for training are analyzed by a clustering and sub-setting algorithm. The NN training data are examples of the seismic trace near the well-bores that have been classified; for a 44 ms search window (with 2 ms resolution) the feature vector would be 22 points along the trace (time, amplitude). The sub-setting of the features ranks which time segments in the search window contain information on the target class. The most potent features, when viewed as amplitude time-slices, often show plausible shapes for fluvial elements; in particular, we often note a “phantom-thalweg” as a trough in the seismic and high amplitude patterns that correlate to splays. Fusing the images from the “best” time-slices and the NN classifier, a fluvial model is mapped that has good correlation to the well-bore stratigraphy.

TABLE OF CONTENTS

LIST OF ILLUSTRATIONS

Figure Page

LIST OF TABLES

CHAPTER 1

INTRODUCTION

1.1 Problem Statement

In fluvial reservoir sequences, such as the Frio formation of south Texas, important reservoir features are often poorly resolved by seismic surveys. The Frio formation has been extensively discussed in the literature owing to a rich history of gas production; the Stratton field has produced more than 2 Tcf of gas over the past five decades. Reservoir sands are amalgamated channel and splay deposits with typical channels depositing 30 +/- 15 feet thick sands (Galloway (1977), Kerr (1990), Ambrose (2000)). The early work by Widess (1973) was the basis for the rule of thumb for vertical resolution: the minimum resolvable bed is one-fourth the wavelength. This research will focus on the upper middle Frio (UMF); the dominant frequencies in the seismic over this interval are shown in Figure 1.1

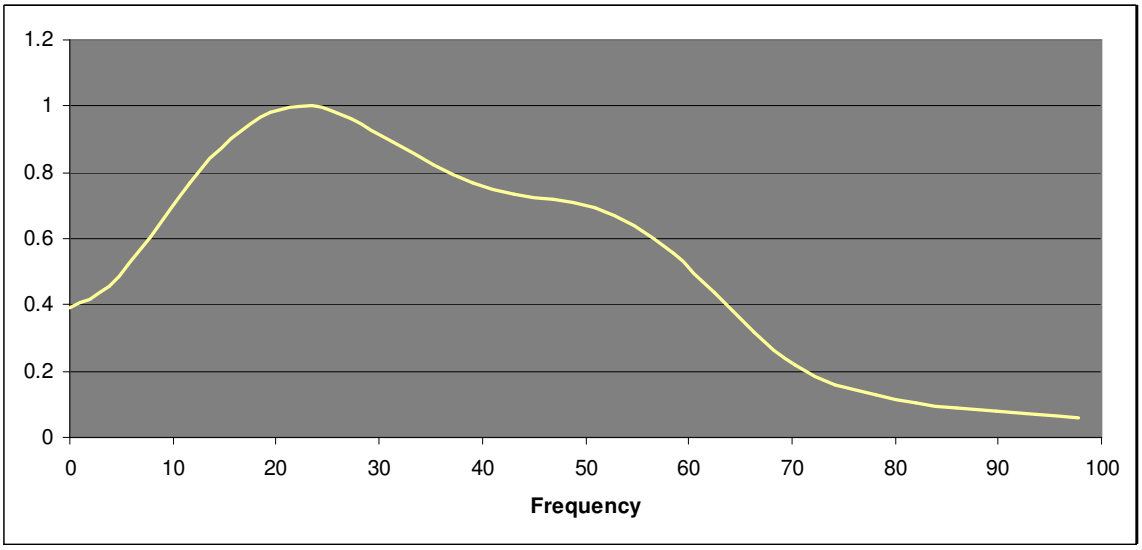

Figure 1.1 Frequency content for seismic signal in upper middle Frio sands (1.35 to 1.65 seconds)

The frequency content in Figure 1.1 is scaled relative to the dominant wavelet at 23.4 Hz and there is significant seismic energy up to 50 Hz. For these frequencies, the rule-of-thumb produces the results shown in Table 1.1. We would expect to resolve beds with a minimum thickness in the range 50 to 100 feet.

Table 1.1 Rule-of-thumb resolutions. Given an average interval velocity = 10093 ft/sec and the frequency content of Figure 1.1

Vertical resolution ~ ¼ wavelength	3D Horizontal resolution ~ ½ wavelength
@ 23.4 Hz = 108 ft	@ 23.4 Hz = 216 ft
@ 50 Hz = 50.5 ft	@ 50 Hz = 101 ft

Figure 1.2 is a plot of well logs and the Vertical Seismic Profile (VSP) data from well Stratton #9 (well 9) and a 5 traces from the 3D seismic that are near the well. The log response will be discussed in more detail in sections 1.6 and 1.7. For now this figure illustrates the scales of the Frio formation and the 3D seismic traces. In the figure, track one has the spontaneous potential SP curve, track two has the resistivity Rt. Reservoir sands have higher resistivity (Rt) and develop negative Spontaneous Potential (SP); the response at 5320 to 5340 feet is typical of river channel deposits. Track 3 is the acoustic impedance calculated from the well-log density and the VSP velocity and track 4 is the reflection trace from the VSP. Track 5 plots five traces from the 3D survey near the wellbore.

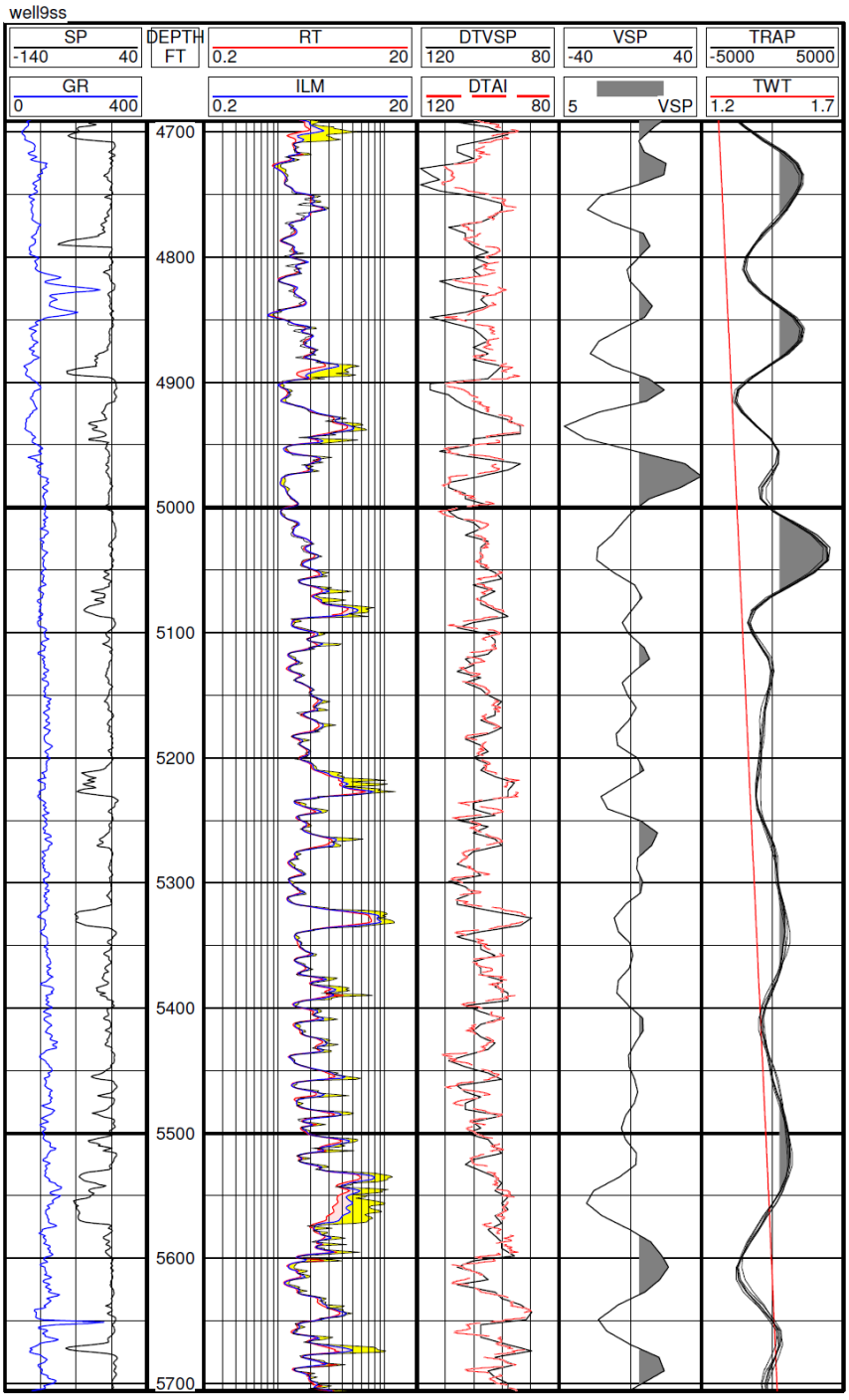

Figure 1.2 Well Stratton # 9 (well 9): well logs, acoustic impedance and VSP in well 9, in the fifth track are 5 seismic traces from the 3D survey.

Initial concerns for inversion:

1. Poor Resolution: In the upper middle Frio (UMF), most of the fluvial reservoir elements are less than 50 to 100 feet. In Figure 1.2 we note stacks of thin sands with typical reservoirs 30+/- 15 feet thick
2. Interference from non-reservoir formations: Reflections come from the interface between two layers with differing acoustic impedance; an interface where the top stratum is lower impedance has a positive reflection coefficient (and vise versa). If you differentiate the acoustic impedance (Figure 1.2) by eye it can be noted that there are many reflectors and not all are reservoir sands (In Section 1.4 is a discussion of the two types of sand facies).
3. Poor correlation with seismic: Finding fluvial reservoir elements will require very precise targeting of the time-based seismic signal tied to the depth-based geology. The correlation of acoustic impedance and the seismic trace is not straightforward from visual analysis of Figure 1.2. This poor correlation may be an indicator of noise or tuning artifacts in the seismic signal.
4. Gas saturation has potent effects on seismic and this is a gas producing field.
5. The study area is above the Vicksburg faulting but there has been significant post-depositional deformation; the appearance of plastic deformation is probably facilitated by sub-seismic faults and fractures which may add interference in searching for reservoirs.

Often in the literature a seismic inversion refers to mapping the seismic data into a stack of beds and solving for the acoustic impedance of the beds. In a geologic-based inversion the aim is to map the seismic data directly to a geologic model; this can be viewed more as a classification than a functional mapping. Hardage (1994) published one of the first geologic-based inversions for the Stratton field using a simple first-order technique; the recipe:

flatten the volume to remove post-depositional deformation, take a time-slice equivalent to a targeted depth that contains a fluvial reservoir element, and use the patterns seen in the amplitude time-slice and available well-logs to design a geologic model. Figure 1.3 is a diagram of this process for the F37 sand in the Stratton field. The left inset is Figure 12 from Hardage (1994); the seismic trace amplitude is plotted in a horizontal time-slice. Using the patterns in the time slice and data from nearby wells a model is drafted in the right inset (Figure 15 of Hardage) showing two river channels in dark gray and accompanying splays.

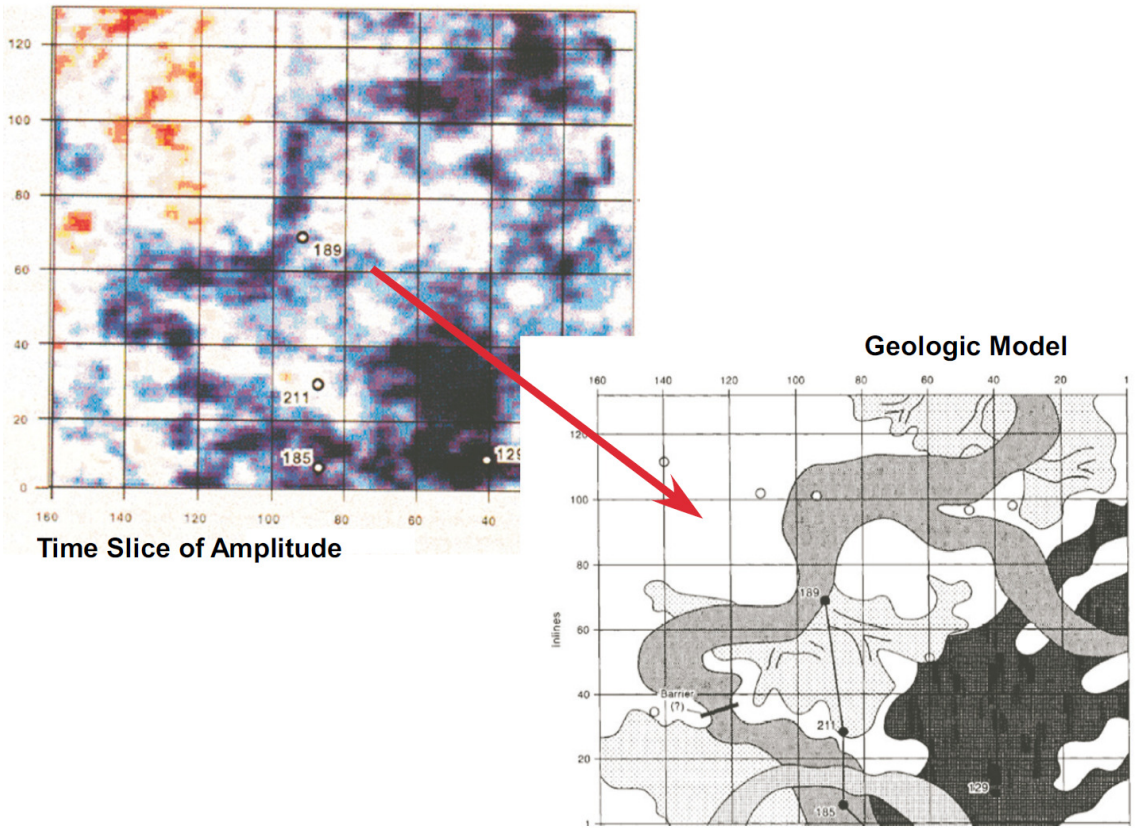

Figure 1.3 Geologic-based inversion by Hardage (1994) for the F37 sand

The simplicity of this inversion is attractive; however in practice (in the Stratton field) the patterns seen in the time slices have poor correlation to the geology derived from well logs. Pennington (2002) suggested an improvement to the recipe: Use a neural network to track a reflection horizon, make an amplitude plot of the tracked horizon, and then use patterns in amplitude plots as images of fluvial elements. Other methods have been proposed such as spectral decomposition (Sinha (2005)) or thin-bed reflectivity models (Chopra(2006)). To be effective, these inversion techniques require a precise time-to-depth tie and no interference; i.e. the seismic response at a specific time is a function of a formation interface at a specific depth.

Dorrington (2004) proposed a simple inversion solving for sand volume in a broad 42 ms window (equivalent to > 200 feet) using the well-log data as a reference datum. While this seems to be plausible given the seismic resolution, the broad window technique sacrifices information on the geometry of the reservoir units which is an important part of the puzzle in these highly compartmentalized reservoirs (Kerr (1990)).

1.2 Study Area

Figure 1.4 is a location map; the Stratton field is in Nueces County in southern Texas, near the city of Corpus Christi. The Stratton field is part of the prolific FR-4 gas play; thousands of wells have been drilled along this trend with most production coming from the middle and lower Frio sands.

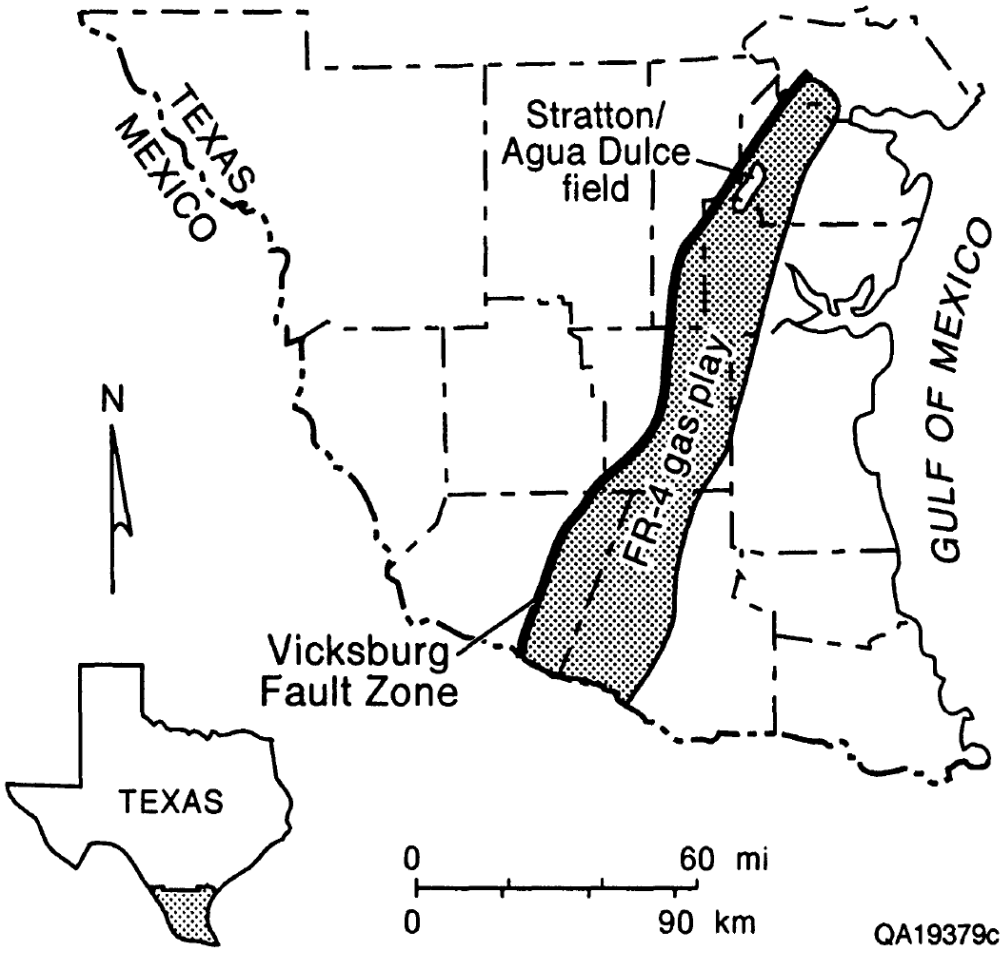

Figure 1.4 Location map of Stratton field in south Texas

1.3 Depositional Setting

At the location of the Stratton field, the Frio is part of the Gueydan fluvial system characterized by floodplains, channels and splay sands deposited at the ancient Rio Grande embayment. The Frio formed a thick progradational wedge deposited during a time with plentiful sediment supply and continued subsidence along the Gulf Coast; in the Stratton field the Frio deposits are approximately 3300 feet thick. Along with plentiful sediment, the river system was not well bounded by the coastal plain; this is expressed in the stratigraphic record

by long periods of floodplain aggradation cyclically interrupted by river channels and splays wandering through the field.

The depositional model shown in Figure 1.5 was originally drafted by Galloway (1977) and later updated by Kerr (1990) and Ambrose (2000). The channel-fill sands are typically 30 feet thick, often stacked and amalgamated laterally. These sands are bounded by silt and mud-rich floodplain deposits. The Frio in the FR-4 gas play has been extensively drilled and lateral bounds for the depositional model have been developed from the inter-well spacing. Kerr (1990) describes the channel-fill facies as relatively straight pathways with low sinuosity that are typically 30+/- 15 feet thick and 2500 +/- 500 feet wide. A single splay is modeled as fan shaped, but, because the splays are stacked, the changing depositional energy, accommodation space and crevasse location generate irregular shapes. Reservoir sands in the splay facies are thin and proximal to the channel; the splay complexes can be 20 +/- 10 feet thick and can extend 2 to 3 miles from the channel.

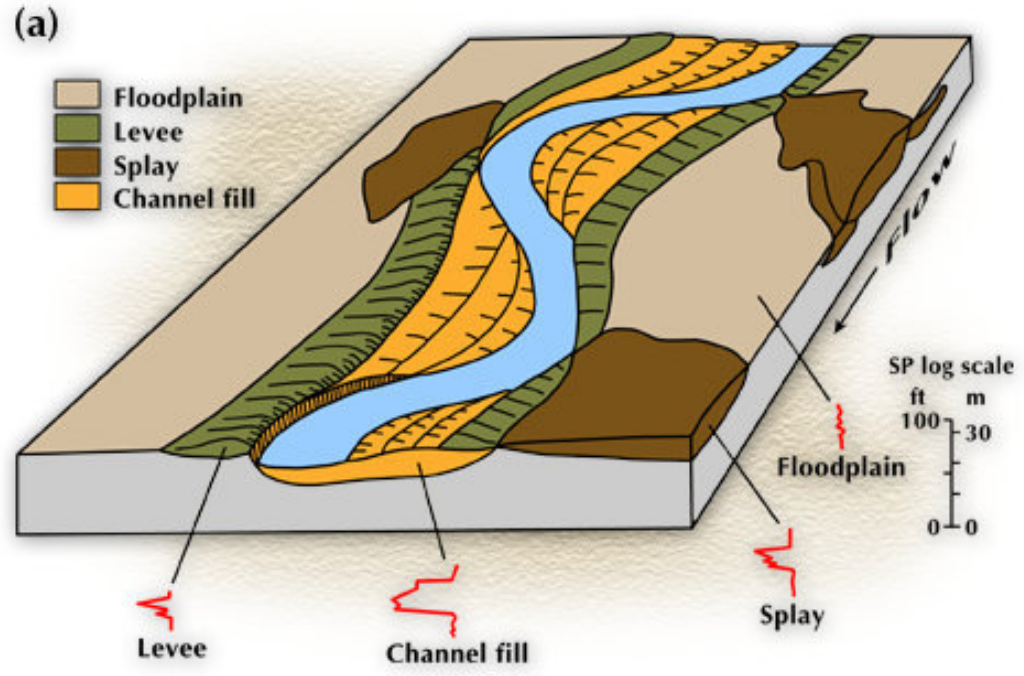

Figure 1.5 Depositional model for middle Frio

According to the Vail curve and fossil evidence (Galloway (1982)), the Frio was deposited during a sea level minimum during the Oligocene epoch, 30 to 32 MA. The continued subsidence of the coastal floodplain on the underlying Vicksburg faults, together with a regressive sea level, produced a wedge of sediments that thickens gulf-ward similar to the buttress fall model of Holbrook (2006). The low relief of the coastal plain did little to constrain lateral movements of the river systems; the combination of low relief and abundant sediment supply expressed shallow-incised river channels that stacked into multi-channel sheets.

Several horizons can be identified in the stratigraphy; the base of the Frio is the master sequence boundary noted by the change from the deltaic deposits of the Vicksburg formation. Further, the displacement and deposition along the Vicksburg faults suggest that the top of the Vicksburg is an unconformity. Within the Frio there is a period of high volcanic ash content in the sediment; the base (above the E41 sand) and the top (below the C18 sand) of the high volcanic ash sediments are interpreted as erosional surfaces. In the literature there is discussion on how to describe the Frio in terms of sequence stratigraphy (Edwards (2002)), but the limited study area of this research is not appropriate for the scale of sequence stratigraphy. For discussion purposes, the study area is dissected into parasequences, cycles when a river system is present in the study area, separated by periods of floodplain deposition.

In terms of chronostratigraphy the flood plain aggradation follows time. The river channel incises the floodplain, and the channel fill is laterally accreted so the base and top of the channel roughly tie in time to the floodplain at the top of a specific channel. The timing of deposition gets convoluted as the channel stacks and amalgamates laterally. The splays are vertically stacked and are interleaved with paleosols; these overlay the floodplains but have minimal erosion so the splay base is roughly tied to the chronostratigraphy of floodplain aggradation.

The Stratton field reservoir structure in the upper middle Frio is described as a dome-like portion of a rollover anticline. The anticline axis trends mostly north-south parallel to the Aqua Dulce fault immediately west of the study area; the deformation of the upper middle Frio is predominately post-depositional. The tectonic setting of the Stratton field and the underlying growth faults are discussed in a recent paper by El-Mowafy (2008).

1.4 Upper Middle Frio Facies

The facies in the upper middle Frio (UMF) can be described from two different approaches: they can be grouped by the rock fabric and reservoir properties, or alternately they can be grouped by their fluvial genesis (i.e. channel, floodplain, etc.). The choice of descriptive idiom is used based on the context of the analysis; for example, the interpretation of a single well log classifies the rocks by reservoir character, but tracking the reservoir geometry between wells is described in fluvial terms.

In the UMF strata there are three predominate facies with very similar mineralogical composition that includes 15 to 20% volcanic ash and glass (Kerr (1991)):

- Floodplain deposits: fine grained with paleosols, loess and lacustrine layers
- Tight sandstones: Feldspathic Litherenites, small grained, lithic glass fragments, clay cement
- Reservoir Sandstones: Feldspathic Litherenites, larger grained, lithic fragments are glass and carbonates, leached calcite cement.

The main distinctions between the facies are grain-size and diagenetic alteration (Grigsby (1991)). For example the reservoir sands are coarser-grained and the porosity/permeability of the reservoir sands has been enhanced by secondary leaching (Loucks (1977)).

1.5 The Texas Bureau of Economic Geology 3D Seismic Cube

A public domain seismic data set that covers the Frio formation in the Stratton field is available from The Texas Bureau of Economic Geology. This includes a 2 mile by 1 mile 3D

seismic survey, accompanying well logs and VSP data, and will be referred to as the BEG Cube.

Details on the seismic acquisition can be found in the distribution literature that is provided with the data set; details on the processing are discussed in Hardage (1994). The receivers were run east-west, and the vibrator sources were run north-south. This data was then processed and migrated as 100 east-west inlines and 200 north-south crosslines with a trace spacing of 55 feet. A Vertical Seismic Profile (VSP) was run in well Stratton #9 (well 9) and in Figure 1.6, a north-south seismic line that crosses well 9 is plotted with the VSP data and sand mnemonics.

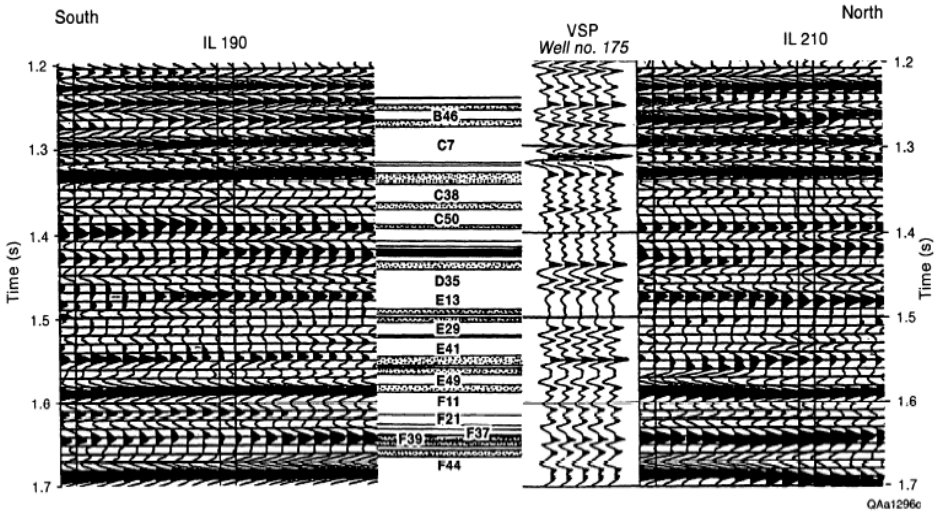

Figure 1.6 Seismic, VSP and sand units in the Frio section of Stratton field, south Texas (Figure 4 from Hardage (1994))

It is somewhat difficult to relate the BEG cube to previous work in the literature. The BEG cube is a small subset of a much larger 3D survey; for example the F37 channel from Hardage (1994) in Figure 1.3 is south of the BEG cube. Also the wells in the BEG data set use generic numbering 1 through 20; whereas the wells in the literature are referenced by the well name (e.g. BEG well 9 is Wardner 175). Cross-correlation of the well numbers can be

overcome using the Texas Railroad Commission maps, but other well data such as header information, drilling dates, production and pressure history are not included in the BEG data set.

1.6 Well-log Data Set

Nineteen wells cover the upper middle Frio study area in the BEG cube; the survey map is shown in Figure 1.7 with the well locations. Twelve of the wells have similar modern logging suites; these will be used to develop the geologic model and are marked as “model” wells on the survey map. Seven of the wells have older or limited data sets; these are marked as “testing” wells used to test the performance of the inversion techniques.

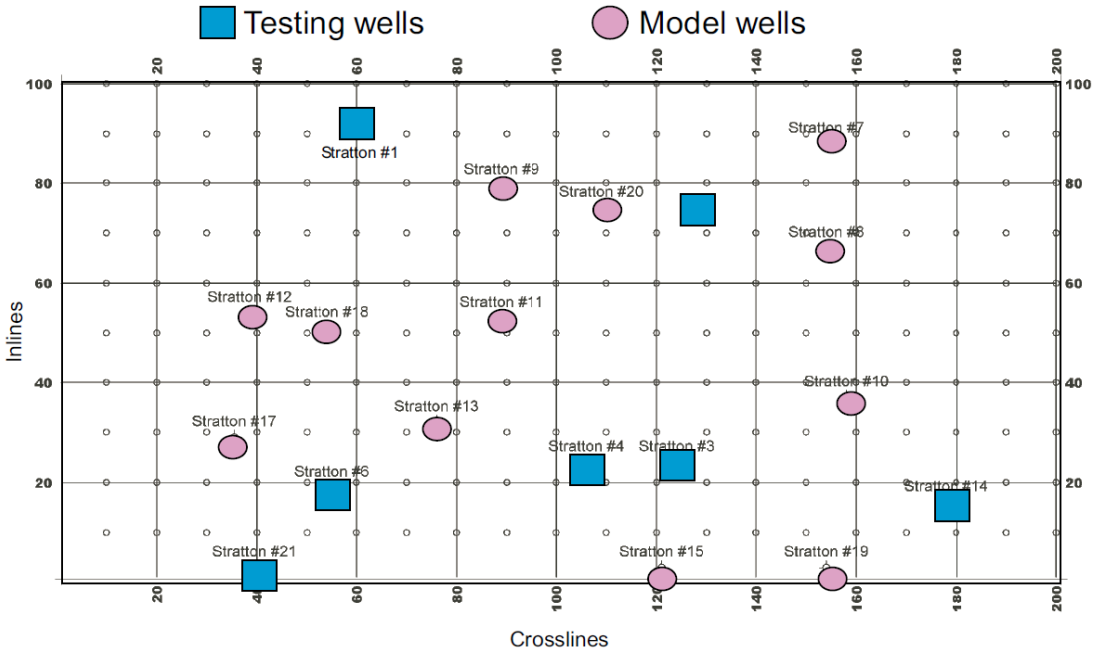

Figure 1.7 Map of well locations and classification (model or testing)

The typical logging suite for the model wells is shown in Figure 1.8; the model wells have a data set consisting of log Curves:

GR Natural gamma ray is typically used for sand/shale differentiation, however the high content of volcanic ash and glass obscure quartz/feldspar fractioning.

SP The change in salinity of the drilling fluid creates a voltage in formations with permeability (Spontaneous Potential).

Rt The deep resistivity of the formation is sensitive to grain size and fluid content.

ILM The medium-depth resistivity is used to map drilling fluid invasion (permeability).

SFL The shallow resistivity is used to map drilling fluid invasion (permeability).

RHOB The formation density is sensitive to rock matrix, porosity and gas content.

NPSS The neutron porosity is used with RHOB to derive the effective porosity (i.e. porosity of reservoir quality formations) and formation facies type.

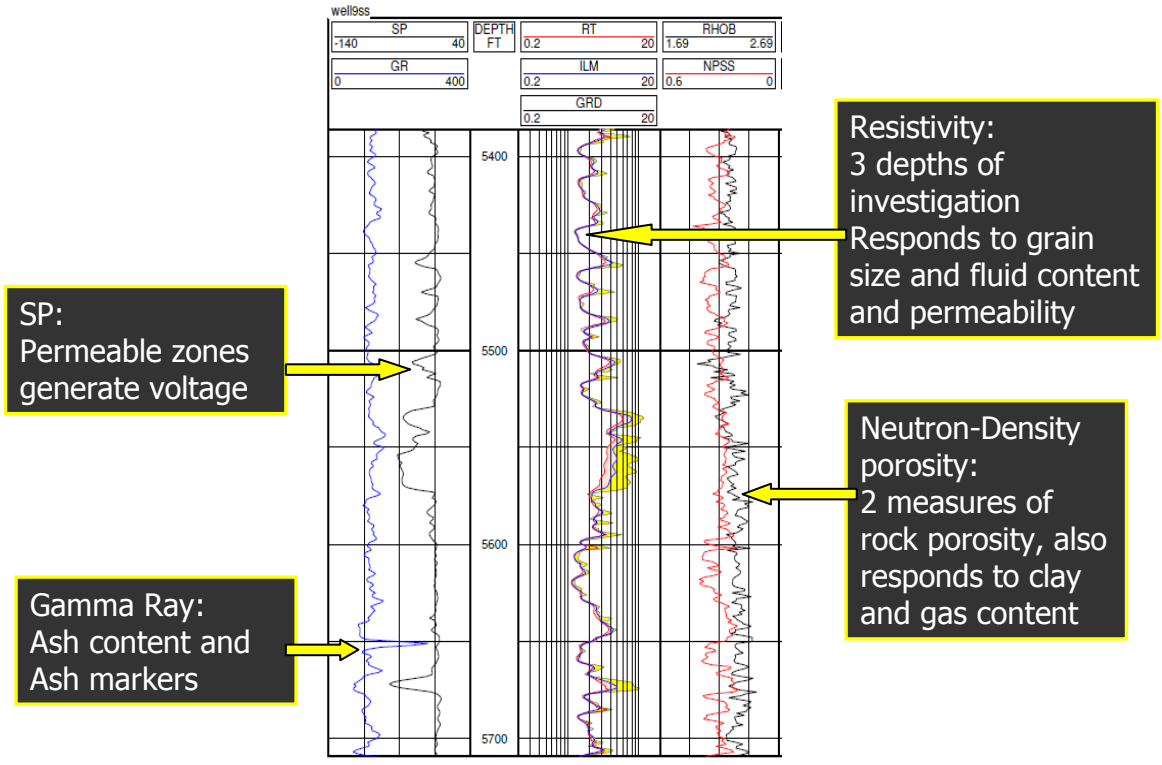

Figure 1.8 Well-log data set for the 12 model wells (model well 9)

The art of reading the logs and diagnosing the depositional environment is assumed to be heuristic and common knowledge of those trained in the art (i.e. it is hard to find basic

recipes in the literature). The fundamental aspects of the art are covered in Gilreath (1975). The logs respond to the rock fabric and fluids rather than the depositional genesis, but the sequence of rock facies can be interpreted for a depositional history. The insets of Figure 1.5 show the typical SP log responses for the Frio fluvial elements; in Figure 1.8 is more detail on log response for the model well logging suites. The well log response of the UMF facies is interpreted as:

Floodplains example at 5605 to 5625 feet has the typical response:

No SP response: No SP developed - very low permeability

Minimum Rt: very fine grained

maximum NPSS, higher density: porosity plus clay-bound water

Tight Sands example at 5630 to 5645 feet has the typical response:

SP response: No SP except tiny peaks from permeable streaks

Rt greater than 2 Ohm-m:

Median NPSS, with higher density: fine-grained, well-cemented sand

Reservoir Sands example at 5550 to 5570 feet has the typical response:

SP response: Thick sections (> 10 feet) of permeable sand

Rt greater than 2 Ohm-m:

Median NPSS, median density: low clay volume sand

Typically, channels are noted by blocky SP and Rt response and a neutron-density overlay that comes together indicating coarse sand content. Typical splay response is seen in the interval 5450 to 5500. Splays are often stacked and amalgamated sheets where the grain-size is fining upward creating exponential horns or bell-like shapes on the SP and Rt curves. Splays can have varying amounts of reservoir sand and often these layers can be thinner than the well log resolution and do not develop spontaneous potential. The tight sand at 5630 to 5645 feet and the reservoir sand at 5505 to 5515 feet can both be expressions of splays. This can create

some confusion in terms so for discussion purposes, the general linkage of the three main facies to the three main fluvial architectural elements is listed in Table 1.2.

Table 1.2 Facies composition of fluvial architectural elements in upper middle Frio.

Fluvial Architectural Element	**Facies Composition**
River Channel	Reservoir Sand
Floodplains	Floodplain Facie
Splays	layers of:
	Tight sand
	Reservoir sand
	Floodplain facie

1.7 Facies Classification from Well Logs

To aid the visual analysis of the well log data and to generate data on bed thickness, a stochastic model for facies classification was developed. Using the rules from the previous section, samples are selected from the well logs and used to train the artificial neural network diagrammed in Figure 1.9. The NuClass 7 software package from the Image Processing and Neural Network Laboratory (IPNNL (2004a)) was used to design a network with four inputs. The network is trained with multiple samples picked and classified from the well log data; then all of the model wells are processed through the automated facies classifier. The well logs, facies class and seismic traces near the wellbore are presented in Appendix E.

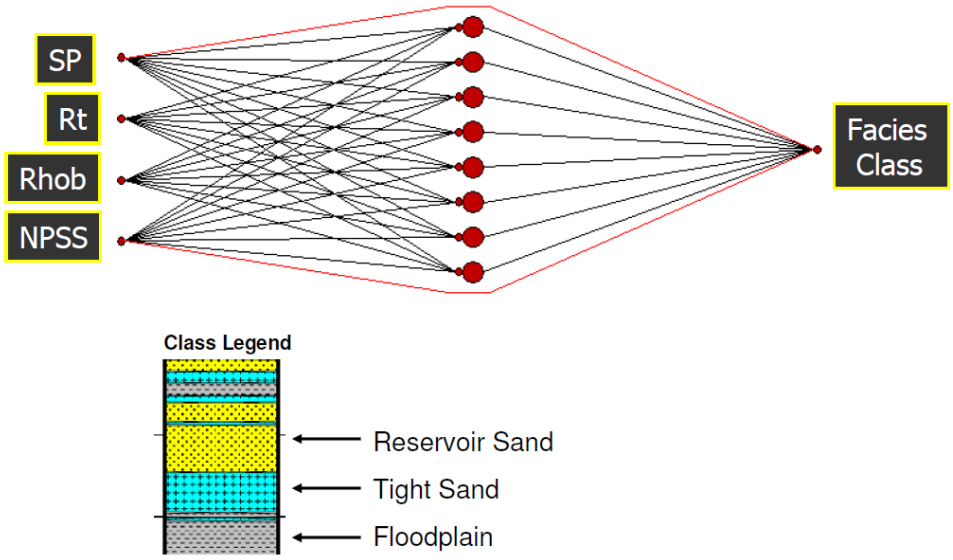

Figure 1.9 Artificial neural network classifier for automated facies discrimination.

1.8 Plan of Work

This research focuses on processes for identifying fluvial targets in the Stratton field 3D seismic survey. Because the coastal plains were nearly level during deposition, the search is best facilitated by a flattened data set. A limited section of the Frio formation with simple post-depositional structure was chosen from 5050 to 5700 feet subsea depth; this interval contains several area wide floodplains that serve as stratigraphic markers. The study area is bisected by a long period of floodplain deposition; the sub-intervals are referenced as geo-cell 1 (extent: 5050 to 5300 feet) and geo-cell 2 (extent: 5300 to 5700 feet). The two geo-cells are further dissected into individual parasequences, cycles when river channels and splays entered the study area bounded by periods of floodplain aggradation.

In Chapter 2 the match of the time-based seismic to the depth-based well log model is tested. To remove post-depositional deformation, the well logs and seismic data are connected to area-wide strata above the study interval. The well Stratton #9 (well 9) serves as the time-depth tie point, and the well logs and the seismic data are flattened to well 9 subsea depths and two-way time, respectively.

In Chapter 3 the synthetic seismic for the 12 model wells is used as a basis to analyze the seismic signal. By viewing the model well synthetics as ideal signals, the seismic is analyzed for noise and tuning artifacts.

The results of Chapters 2 and 3 are used to design a classifier for tracking a specific fluvial reservoir element. A neural network classifier uses a segment of the seismic trace as inputs (e.g. 22 time samples of the seismic trace at 2 ms per sample). The network coefficients are trained at the wellbore locations based on a class picked via well-log analysis. In Chapters 4, 5 and 6 “hunts” are described which track a specific reservoir sand body.

CHAPTER 2

TIME TO DEPTH TIE AND FLATTENING THE STUDY CUBE

To track targets at the scale of the fluvial reservoirs will require a very precise tie between the seismic time and the geologic depth (e.g. less than 20 foot error). With the BEG data set (and the SMT Kingdom Suite project) a Time-Depth (T-D) chart is provided based on the VSP in well Stratton #9 (well 9). Directly above the study area is the sequence of sands (C18 and above) that are continuous across the inter-well area and represent a change in depositional dynamics. Similarly, there are several bright reflectors that are associated with these sands, so this would be a good place to establish a match point and check the T-D chart precision.

When deposited, the coastal floodplains were close to level so searching for reservoir sand logically follows these paleo-surfaces. The field-wide match point will be used to flatten the well logs and seismic to remove post-depositional deformation at the top of the study area. As we descend into the cube, errors in the time-depth match will develop, so the study interval is limited to 650 feet. Variation in strata thickness is discussed at the end of this chapter, and the base of the study interval is tested using a chronostratigraphic marker in the well logs.

2.1 Initial Observations on the C38 Boomer

One of the first features noted on the seismic is a strong reflector that extends across the entire cube. It will be referenced as “C38 Boomer” owing to the proximity of the C38 sand. Shown in Figure 2.1, this reflection occurs at 1.332 seconds.

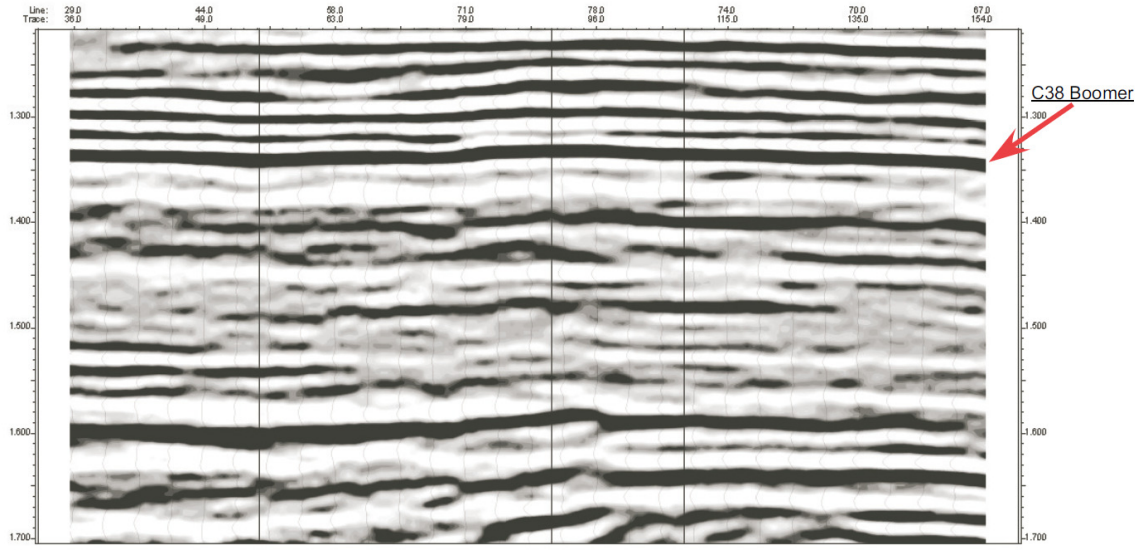

Figure 2.1 Seismic line through wells 17-18-9-20-8 (this cross-section is shown as the red line in map view of Figure 2.2)

The map view of the two-way travel time to the C38 Boomer correlates with the post-depositional structure of the field. The time map of Figure 2.2 correlates with the structure of the field where red is structural high; the time relief of 20 ms is equivalent to ~106 feet.

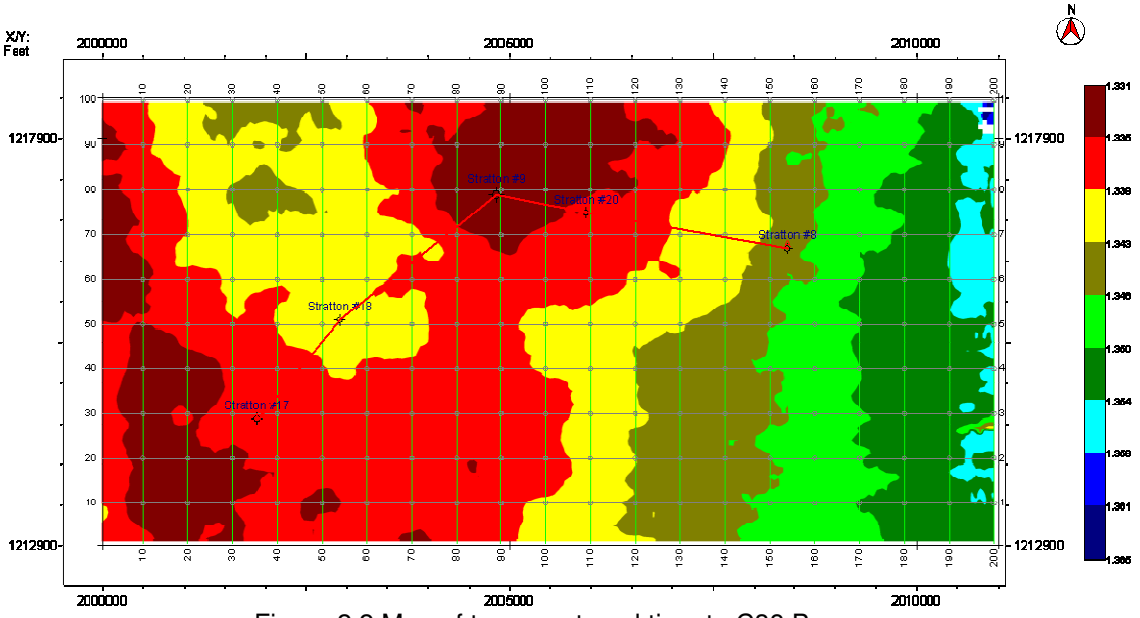

Figure 2.2 Map of two-way travel time to C38 Boomer

The C38 Boomer is the deepest peak in a set of strong reflectors; the seismic trace near well 9 is plotted in Figure 2.3. In the figure we note a distinct shift in the character of the seismic trace; above the C38 Boomer the trace is higher frequency and more coherent. This character suggests a strong resonant tuning emanating from the strata above the study area.

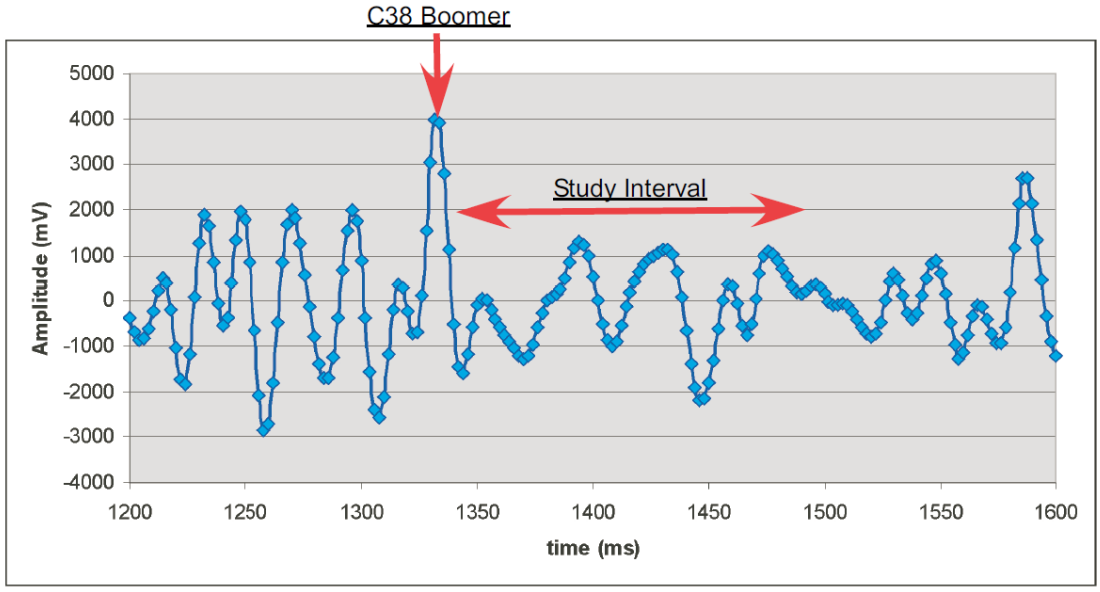

Figure 2.3 Trace from 3D seismic near well 9 shows character of the C38 boomer reflector compared to the upper middle Frio study area.

Figure 1.1 diagrammed the frequency content for the study area of the upper middle Frio. The frequency shown in this graph is often referenced as the dominant frequency of the zero-phased wavelet; it is calculated from the low frequency content of the seismic reflection trace. In Figure 2.4 the frequency content over the interval that contains the C38 Boomer (interval: 1.15 to 1.45 seconds) shows a noticeable shift to higher frequency content. In Figure 1.1 the attenuation of these higher frequencies is very effective at this depth so this is a good indicator of resonant tuning of a bed, where the bed thickness is an even multiple of the wavelength (e.g. ¼ wavelength resonance).

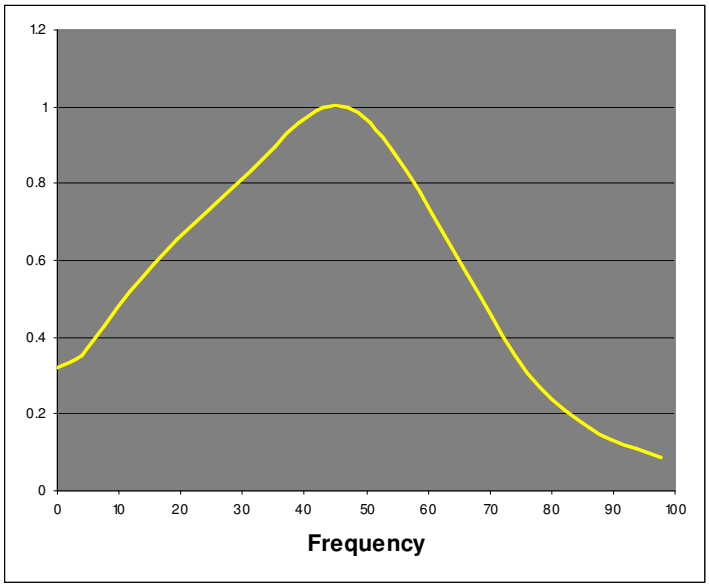

Figure 2.4 Seismic frequency content in the study cube over the interval 1.15 to 1.45 seconds

As discussed by Mundim (2006), the reflection trace has higher frequency content than the dominant frequency as a result of constructive/destructive interference as the dominant wavelet is convolved with reflectors. Thus, we can get more information about the tuning of the C38 Boomer by looking at the frequency content of the reflection traces. To zoom in on the segment of time with the C38 Boomer (1.25 to 1.35 seconds), a Finite Fourier Transform (FFT) is used to transform the trace into the frequency domain for traces near well 9, 11 and 13 and the well 9 Vertical Seismic Profile (VSP). In Figure 2.5 we note coherency at 48 and 60 Hz for the three wells and the VSP, again good evidence of a seismic tuning. For ¼ wavelength tuning this would correspond to bed thicknesses of 52 and 42 feet respectively (for average velocity = 10000 feet/second). Looking back at Figure 1.2 the sand below flooding surface 1 at 4914 feet has similar velocity and thickness to the tuning parameters, and also has a strong contrast in acoustic impedance. The base of this sand corresponds to the top of the high ash content sediments and is interpreted as an erosional unconformity.

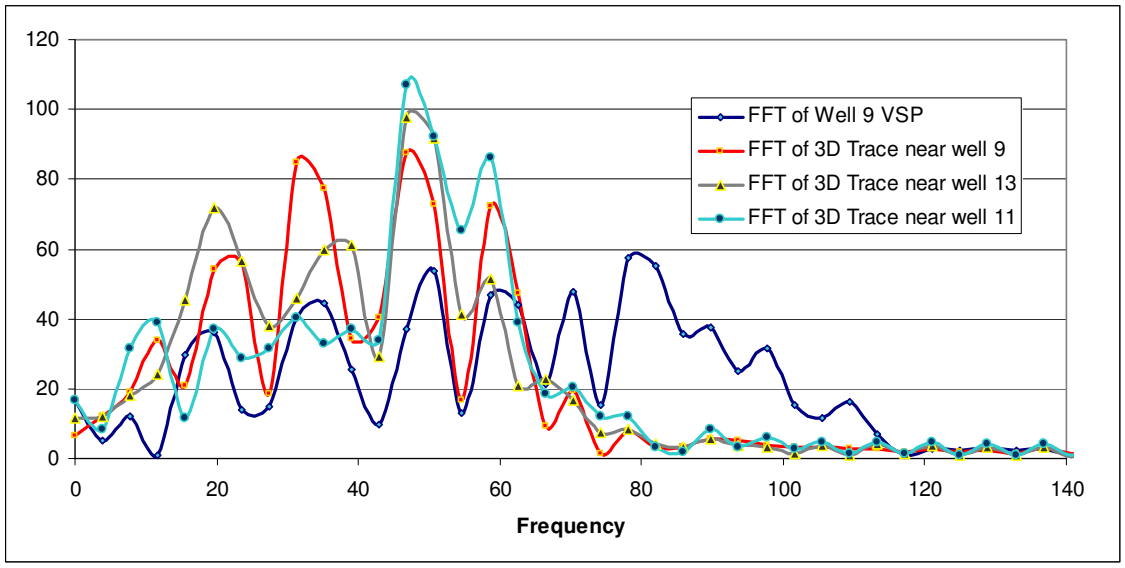

Figure 2.5 Finite Fourier Transform for 3D seismic traces from wells 9, 11 and 13 and the well 9 VSP survey, time interval: 1.25 to 1.35 seconds

Tuning can often be exploited to gain information in the subsurface. Similar to the guitar string, the harmonic content is the result of an exact set of parameters. Tuning for seismic occurs when the product of bed thickness and velocity are an even multiple of the frequency. Thus, the continuity of the C38 Boomer implies a continuous and consistent set of strata atop the study area that can be linked to the seismic signal to establish a time-depth match point.

2.2 Field-wide Strata – Flattening the Data Sets

From study of the model wells and literature (Ambrose (2000), Kerr (1990)) correlation of strata is best done beginning with the floodplains. By expression these are laterally continuous and represent periods of slow deposition when no river channel is present in the interval. Several floodplains can be correlated across the well log data sets in the interval above the C38 Boomer. Figure 2.6 is the overlay of the deep resistivity log Rt from the 12 model wells with the average value in heavy black. The seismic traces near the model wells are in track two with the average value in heavy black.

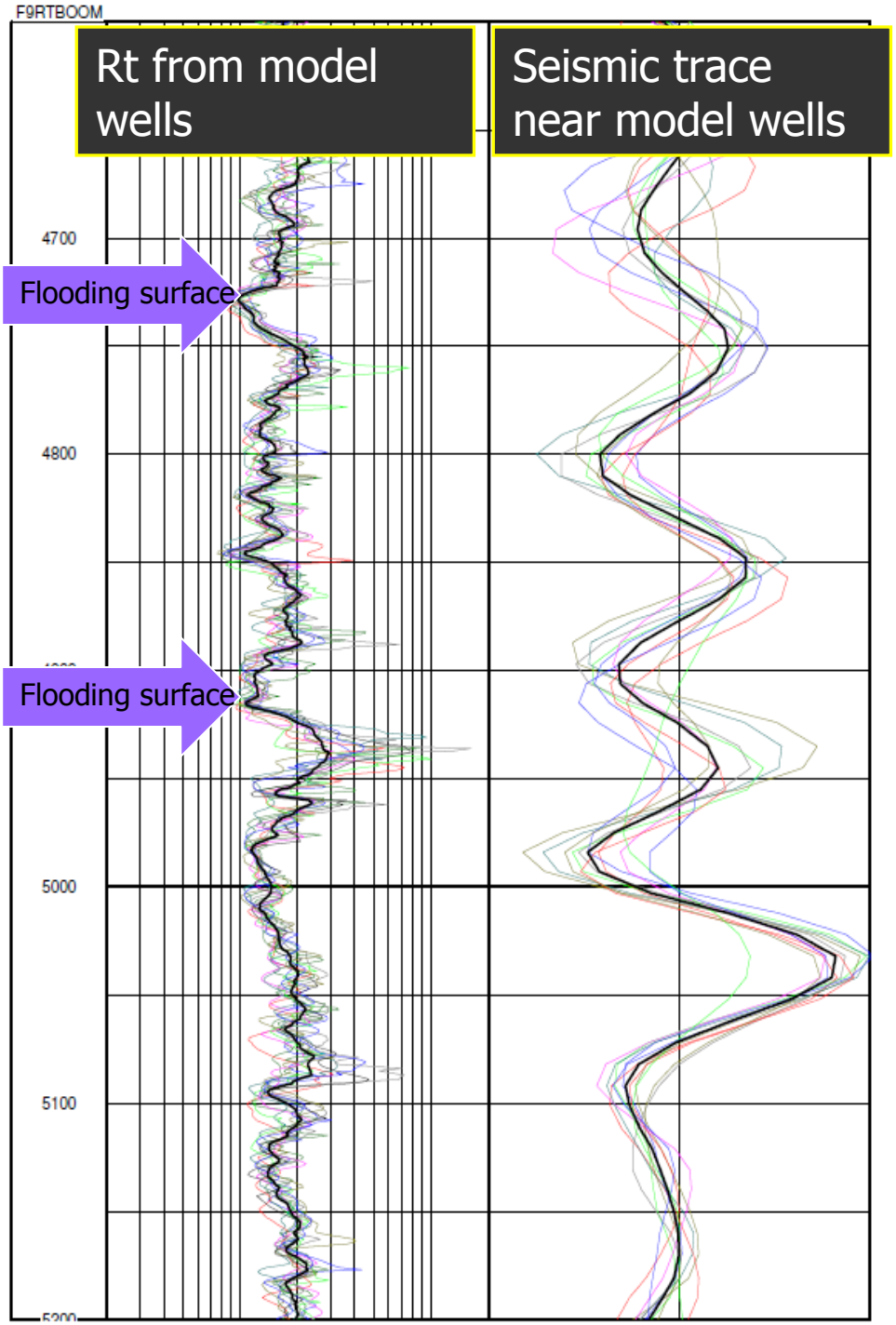

Figure 2.6 Overlay plots of resistivity, Rt, and the 3D seismic traces near the 12 model wells, the heavy black traces are the average value

On the Rt overlay, the floodplains are identified by low resistivity values near 1 Ohm-m for all the model wells; two floodplains are marked on Figure 2.6. These extensive floodplains are used to flatten the well log data set to the well 9 subsea datum. Similarly, the seismic traces have several peaks and troughs that appear continuous across the well volume; the C38 Boomer is the peak at 5031 feet. This horizon is tracked and used as a flattening reference.

2.3 Correlation of C38 Boomer to Strata

At this point we have two flattened data sets, but the mission of this chapter was to establish a point to tie seismic time to the geologic depth. The hypothesis that there are continuous strata means that the average values from the 12 model wells for resistivity Rt and seismic traces can be compared for features that are consistent across the intra-well volume. In Figure 2.7 we see a good correlation between average resistivity (Rt) and the seismic trace average, if we shift the seismic by associating the floodplain at 4914 feet to the C38 Boomer.

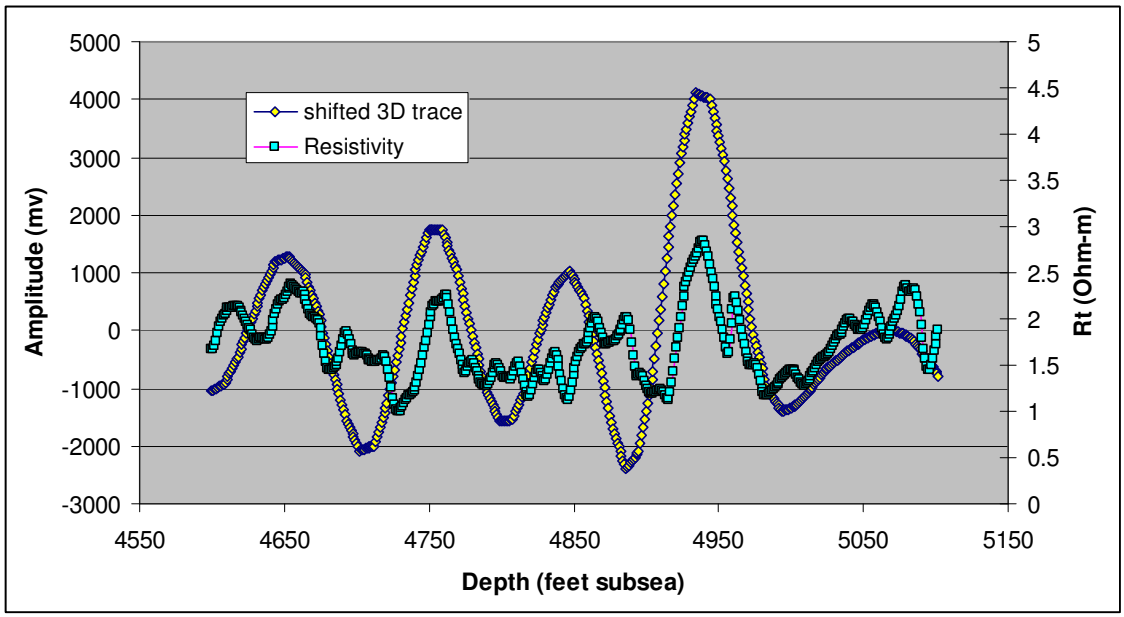

Figure 2.7 For the 12 model wells: the average seismic trace in gold squares is shifted for a visual match to Rt (resistivity) in turquoise squares

2.4 Time-Depth Match Integrity: Velocity Dispersion

Revisiting Figure 1.2 we note that the VSP trace leads the seismic trace similar to the geologic model, and the difference can be read directly from the log as 12 ms or 56 feet. This difference is troublesome for the time-depth accuracy considering the Time-Depth (T-D) chart provided with the BEG data set was based on the VSP survey.

The time-depth mismatch can be explained by research on velocity dispersion in thinly-bedded sequences. Rio (1996), presented data on modeling random stacks of thin beds that demonstrate the concept of frequency-dependent velocity dispersion. Figure 2.8 (Figure 1 from Rio, 1996) illustrates velocity dispersion for experiments using two frequencies and various stacks of plastic and steel. For very thin beds the velocity can be modeled as the slower effective media by poroelastic averaging (Backus averaging); for thick beds the effective velocity is faster and follows the ray theory limit (velocity averaging), and the transition between velocity models is dependent on the ratio of wavelength (λ) to bed-thickness (d).

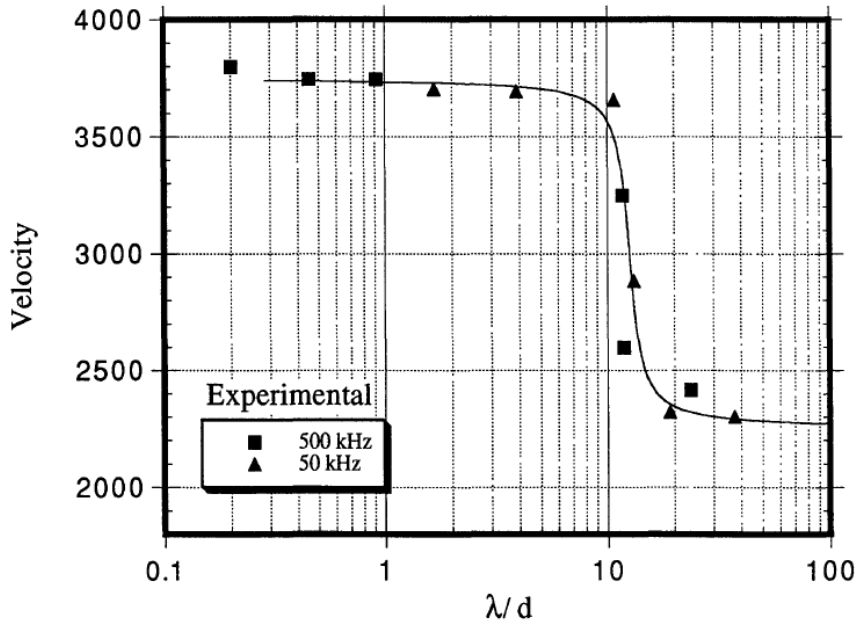

Figure 2.8 Figure 1 from Rio (1996) illustrates the concept of frequency-dependent velocity dispersion in thin-bedded sequences. The scale λ/d is the ratio of wavelength to bed thickness.

Figure 2.8 was from earlier work with even and alternating disks of plastic and steel; results for layered media with random thicknesses show a more linear transition between velocity models but a similar inflection point for bed thickness equal to one-tenth the wavelength. Revisiting Figure 2.5, the VSP trace is higher frequency (i.e. shorter wavelength) than the 3D seismic; given the thin beds of the Frio formation we would expect the VSP travel time to be less than the seismic. The other implication of a velocity dispersion model: the error in the T-D chart will continue to get worse as you go deeper.

2.5 Bed Thickness Distribution In Middle And Lower Frio

Log analysis of the model wells included the facies classifier described in Section 1.7. Data on facies classes from the twelve model wells was sorted by bed thickness for the middle and lower Frio (interval 4850 to 7150 feet subsea); the frequency distribution plotted in Figure 2.9. The frequency plot of bed-thickness is plotted on a dual scale since most of the beds are less than 10 feet.

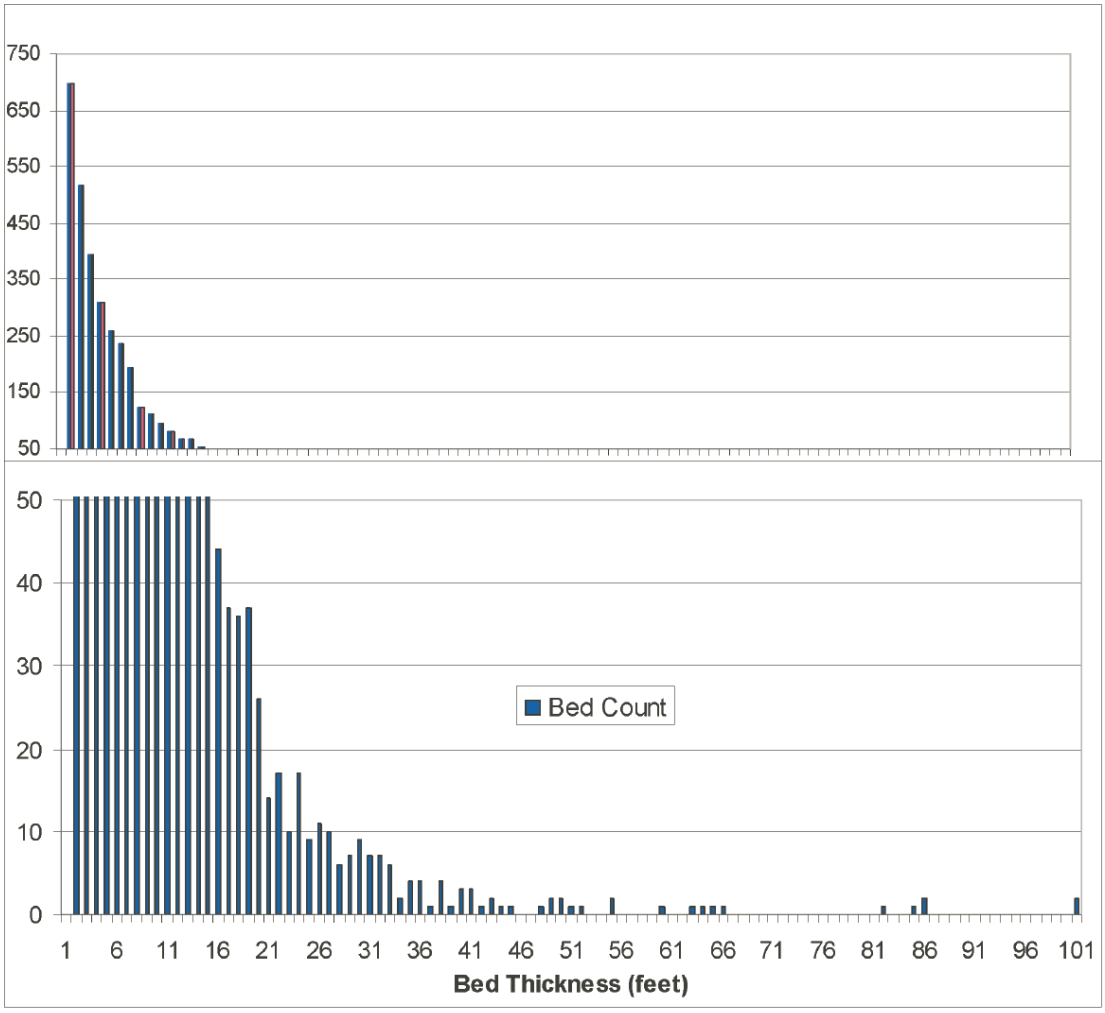

Figure 2.9 The count of beds of a specific thickness for the 12 model wells over the middle and lower Frio (depth interval 4850 to 7150 feet sub-sea)

Given the data on the bed thickness distribution, is velocity dispersion important? Figure 2.10 is a plot of the bed thickness count transformed to percent of the total interval. If say one-tenth the dominant 3D seismic wavelength is 40 feet and one-tenth the VSP wavelength is 20 feet, then about 16% of the total interval would have a frequency-dependent velocity model.

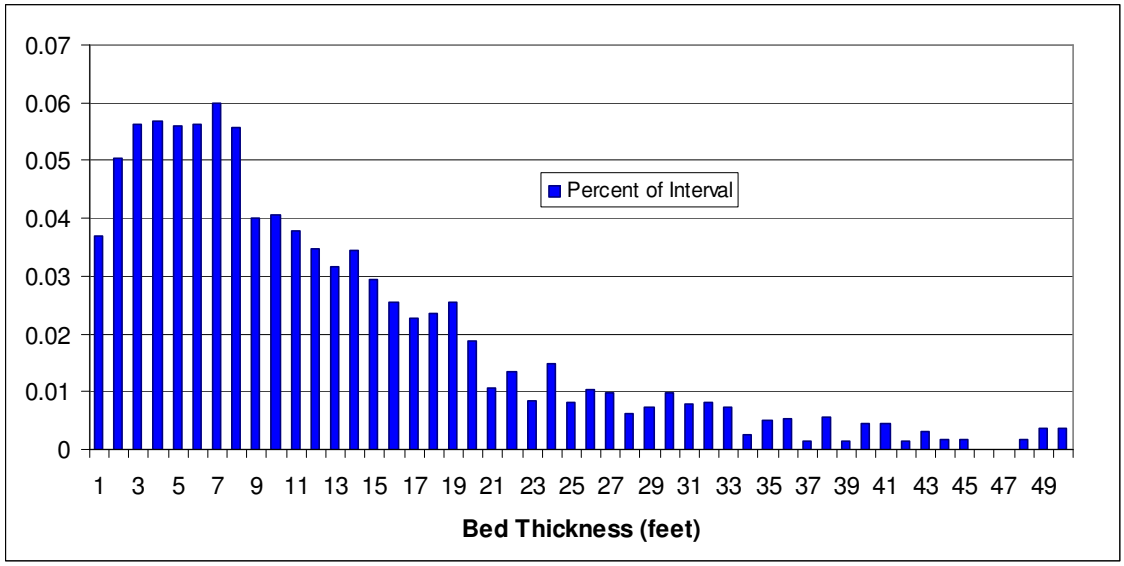

Figure 2.10 Beds of specific thickness as a percent of the total interval

2.6 Results of Chapter 2

The analysis of Chapter 2 indicates that the C38 Boomer is the result of seismic tuning. This has good and bad implications. The consistency of the C38 Boomer tuning indicates that reflecting strata are consistent across the seismic cube; this can establish a time-to-depth tie point. On the negative side: this strong signal may create artifacts in the time domain of the study area.

The accuracy of the T-D chart supplied with the survey is questionable, and there seems to be an offset of the 3D seismic to the VSP and the well model. The correlation of reflectors is not straightforward enough to establish a match point outside of the published T-D chart. So, based on the arguments above, the C38 boomer at 1.332 seconds (5031 feet on survey T-D chart) is will be matched to the flooding surface at 4914 feet in well 9. This will be the recipe for flattening the seismic and well-log data set at the top of the study cube, and the existing T-D chart will be used.

Research on velocity dispersion in thinly bedded sequences suggests that as we go deeper into the cube the time-depth match will get worse. Even more troubling than the T-D chart mismatch between the VSP and the 3D seismic, the thin-bed models predict a dual velocity model that is bed-thickness dependent. As we move deeper into the study cube we can expect increased interference from lateral heterogeneity above the target. In other words: lateral variations in bedding (e.g. other parasequences) above the target create lateral variations in the time-to-depth mapping; as we move deeper from the tie-point these variations are summed. Research by Gelinsky (1997) also shows that gas saturation in thin-beds can have dispersive effects.

The well logs are flattened to match well 9 subsea depth using 3 flooding surfaces above the study cube. There is also a chronostratigraphic marker at the base of the cube which will test the overall flatness of the study cube. Figure 1.8 shows a volcanic ash marker that occurs at 5651 feet in well 9 near the base of the study cube. This marker is a concentration of ash at the top of a floodplain that has heightened natural radiation (i.e. high gamma ray counts on the logs) and can be correlated in all the model wells. Figure 2.11 is the depth map of the ash marker after flattening the data-set. There is less than 11 feet of variation in the thickness of the study cube, which assures that fluvial targets will be at a constant depth in the flattened data-set (within error bounds).

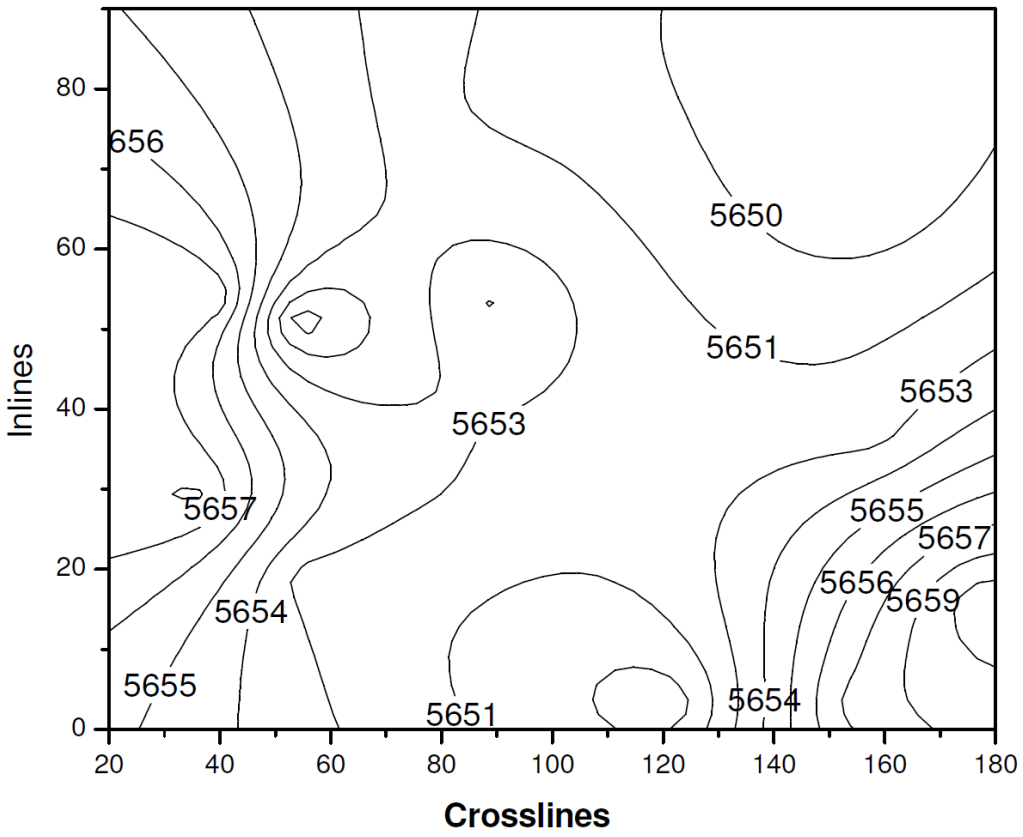

Figure 2.11 Contour map of ash marker at the base of study cube

CHAPTER 3

ANALYSIS OF SEISMIC SIGNAL FOR UPPER MIDDLE FRIO

In Chapter 2, a tie between the depth-based well log model and the seismic was developed at the top of the study cube. Next, we will try the Hardage recipe of taking an amplitude time slice that should correspond to a target channel. From the logs we note a large channel system at 5530 feet; from the T-D chart this corresponds to a time slice in the flattened seismic at 102 ms below the C38 time datum. In Chapter 2 it was noted that the VSP leads the 3D by approximately 12 ms, so, in Figure 3.1 the time slice 114 ms is also plotted. Figure 3.1 introduces the scoring template in the top frame; from well log analysis a class is assigned for each well at the target depth (see Appendix E), and the box on the template is colored by class, where:

red are thick-beds (>20 feet) of reservoir sand from channel deposits,

yellow are splay deposits, principally tight sands with few thin-layers (~2 feet) of reservoir sand,

and blue is floodplain.

The expectation that reservoir sands will be better reflectors is not verified by the wells template; the high trace amplitudes (yellow and red colors) on the time slice do not match template. For the time slice at 114 ms the negative correlation is a better fit (i.e. the channel corresponds to the blue, negative trace amplitude). The Hardage (1994) recipe swings both ways, in the F37 sand model (Figure 1.3) the channel is image with the amplitudes (i.e. the trough). In the D11 sand model (revisited in Chapter 6) the recipe uses positive amplitudes (i.e. peak).

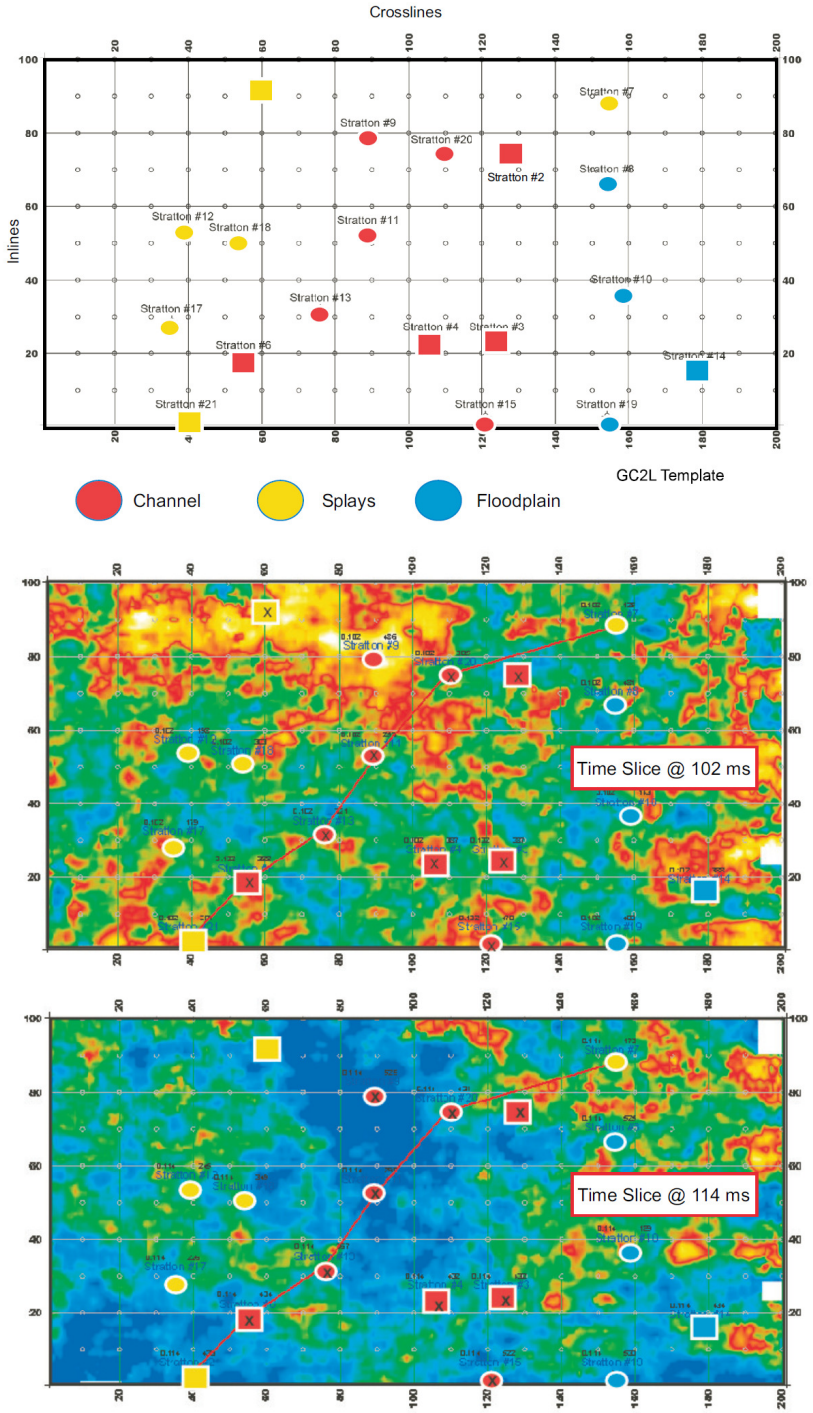

Figure 3.1 The well class template and time slices at 102 ms and 114 ms below the C38 time datum (time-slice color bar: red is high positive amplitude (peak), to blue is high negative amplitude (trough))

In the time-slice at 102 ms, in middle of the cube are neighboring wells 9, 20, and 11; well 9 has high trace amplitude and well 20 and 11 have mid-scale trace amplitude. From the overlays of Rt and SP in Figure 3.2 (left log), well 9 and 11 appear to have the same channel at 5530 to 5570 feet but the higher resistivity in well 9 indicates higher gas saturation. Looking back to Figure 2.2, well 9 is near the structural high of the field and all of the sands show higher gas saturation than well 11. Skopec (1994) discusses that gas can have significant effects on both shear and compressional velocities.

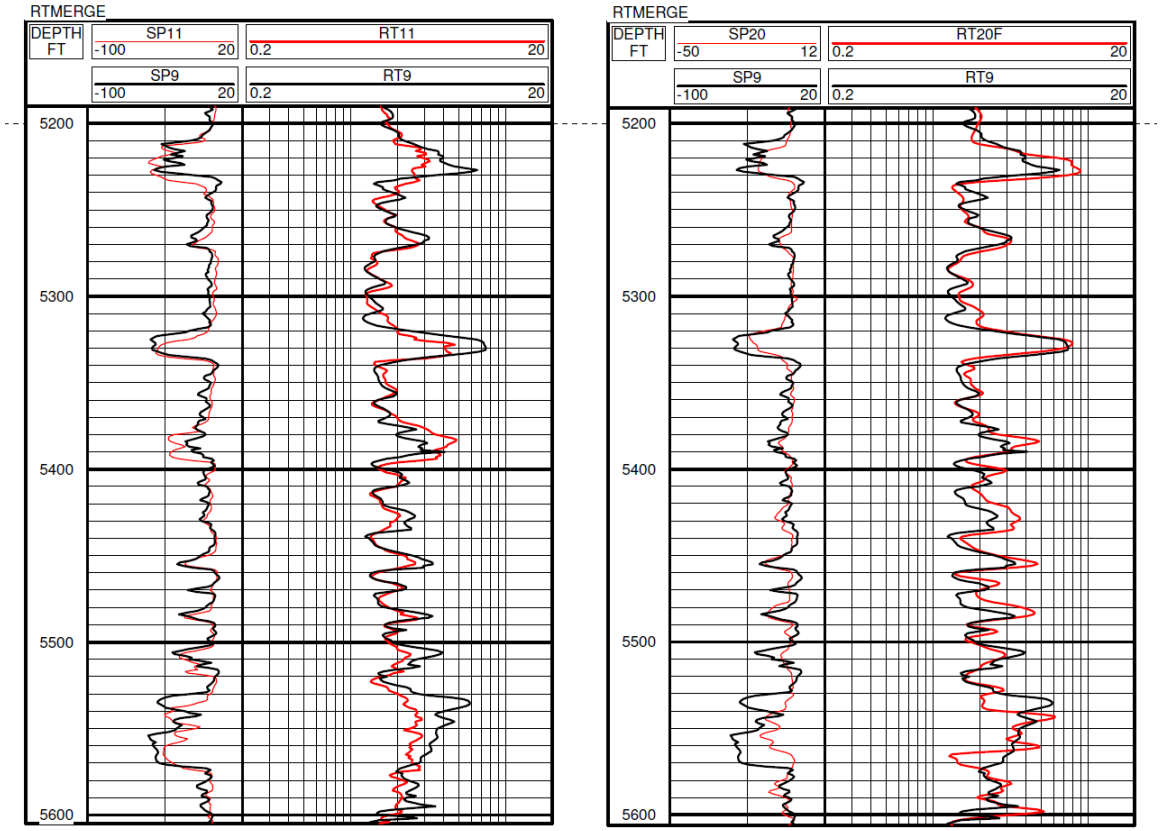

Figure 3.2 Well log comparison between well 9 (black)) and well 11 (red) in left inset. Well log comparison of well 9 (black) and well 20 (red) in right inset. The target channel sands are at 5550 feet.

Comparing well 9 to well 20 (Figure 3.2 , right log), the channel in well 20 is about 20 feet thinner and has a more levee/splay character (i.e. more thinly bedded than well 9) but has more gas than well 9.

Similar to Chapter 2 concerns on thin-bed effects on velocity, variation in gas content between the flattening surface and the target will cause variation in velocity. In hydrocarbon exploration this effect, termed “velocity push-down,” is exploited, but, for geologic inversion it creates interference. Pennington (2002) suggested an improvement on the Hardage recipe by having a neural network track a horizon at the offset depth, then making an amplitude map of the horizon to identify the channel. Figure 3.3 is a vertical seismic slice through well 9 and well 18 and several horizons are manually tracked with colored pens. The time-relief seen in Figure 3.3 would be equivalent to greater than 50 feet of relief. Given the number of wells it might be possible, but highly improbable, that 50 foot structures would not show up at any of the wells. So the Pennington recipe suffers similar to the time-slice technique; there is not a deterministic link between reflection horizons in the seismic and strata from the depth-based well model.

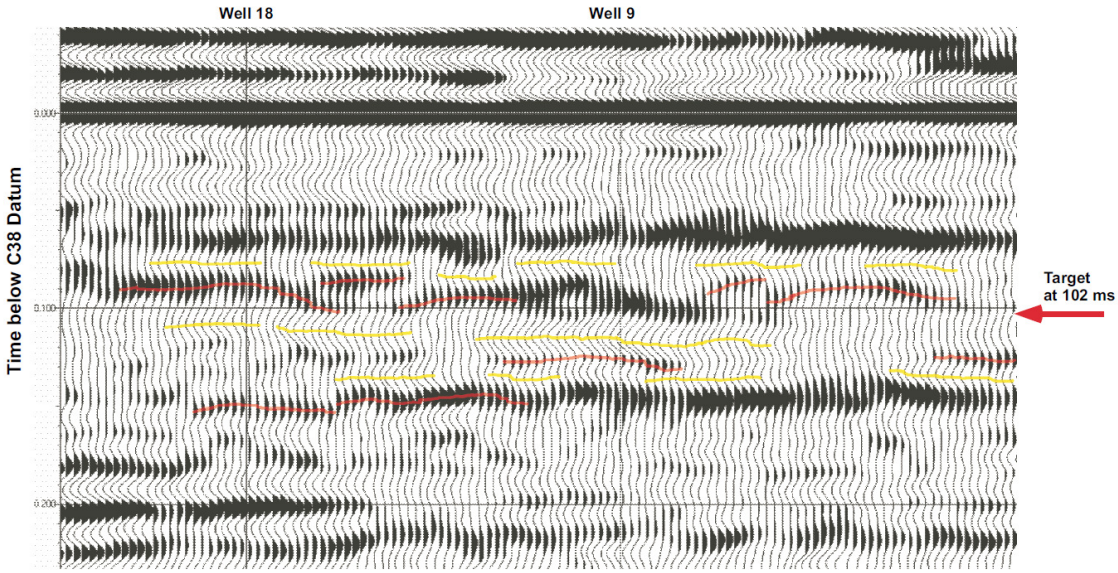

Figure 3.3 Seismic line through well 9 and well18 with some hand-picked horizons near the target.

3.1 Synthetic Seismic and RC Series

One of the first steps in the traditional seismic workflow is to generate a synthetic seismic from well logs. The preferred method: use the density and the sonic log to calculate acoustic impedance, differentiate the acoustic impedance to generate the reflection coefficient (RC) series, and convolve a wavelet with the RC series to create a synthetic seismic trace. To generate the synthetic seismic trace for well 9, the density log, RHOB, and the velocity from the VSP are used to make acoustic impedance. Figure 3.4 is the Seismic Micro Technology SynPak user interface for processing the synthetic; the first four tracks show the inputs used in synthetic process. The fifth track is the acoustic impedance; changes in acoustic impedance are the source of reflections (and refractions), and the RC series in the sixth track are the reflection coefficients. SynPak offers several choices for wavelets; this synthetic is generated using a zero-phased wavelet with frequency content extracted from the seismic interval (1.35 to 1.65 seconds)diagrammed in the seventh track. The two rightmost tracks are the synthetic seismic (track 8), and a comparison seismic trace (track 9) from near well 9. As we noted in the initial observations, the correlation of the seismic to geologic model is poor, the correlation coefficient (R) is 0.378.

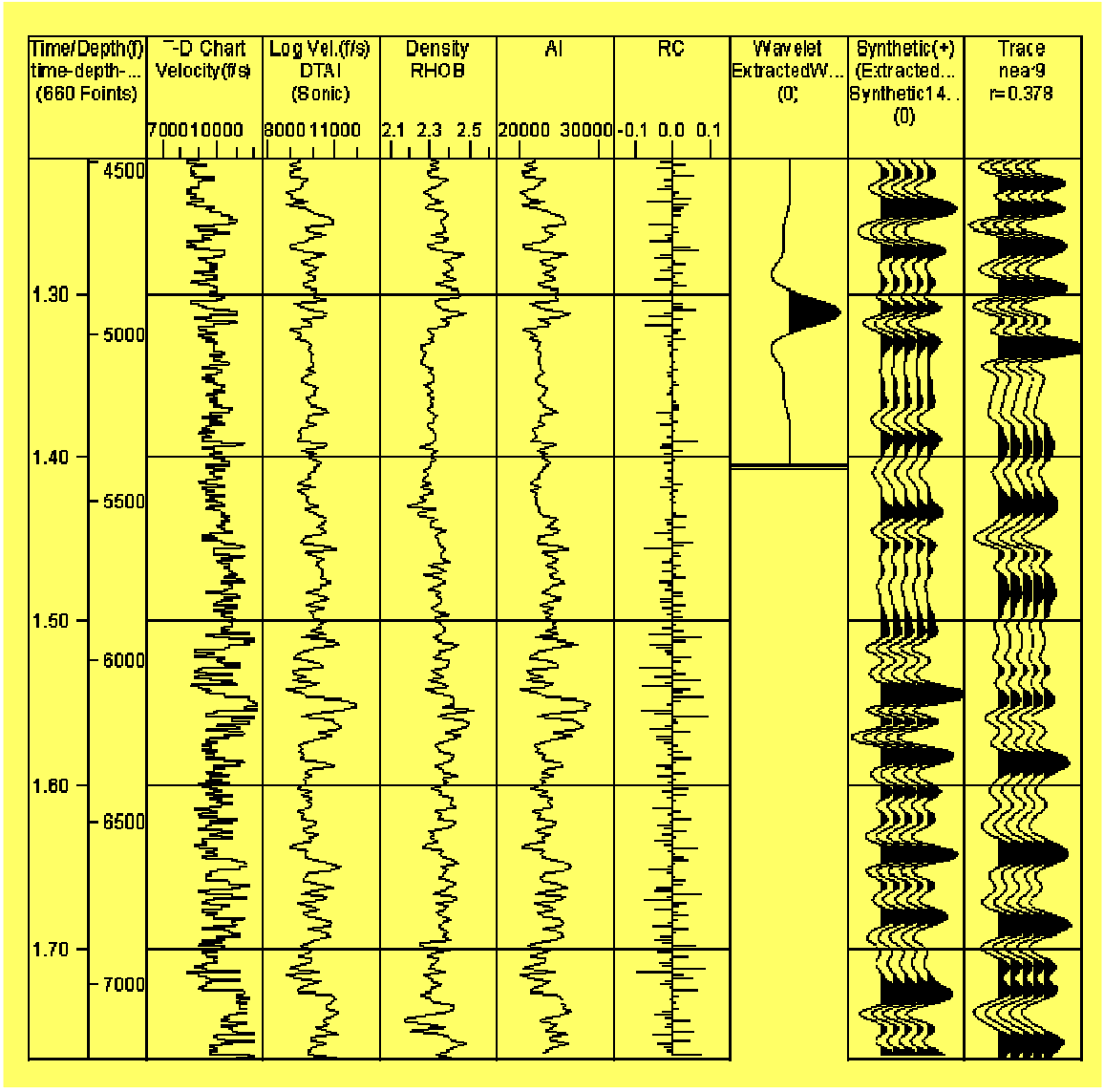

Figure 3.4 User interface from the Seismic Micro Technology SynPak software for generating synthetic seismic

The typical seismic workflow offers options of wavelet and phases to force a match with the synthetic seismic; this allows the interpreter to tie a seismic horizon to a geologic horizon. With this match the seismic is used to track structural trends similar to using the map of the C38 Boomer (Figure 2.2) to describe the post depositional deformation in the field. One of the analysis tools available in the SynPak module of SMT is to extract a Wiener-Levinson (W-L)

wavelet. This method uses the Wiener-Levinson filter (Wiener (1949)) to predict a wavelet that when convolved with the reflection coefficients from the well log will produce a synthetic that matches the example trace. The W-L wavelet extracted from the middle and lower Frio (depths 4500 to 7000 feet) is shown in Figure 3.5. The extracted W-L wavelet presents a similar convoluted result for the T-D match with information spread over a significant time period. The largest peak is shown trailing the strata at 42 ms after the zero-time depth, and a trough at 12 ms following the positive reflection.

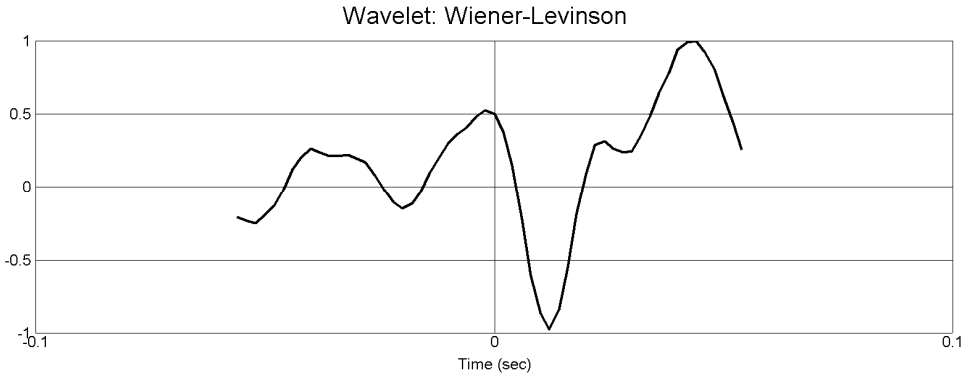

Figure 3.5 W-L wavelet extracted from the seismic trace in well 9

Fluvial reservoir targets are sub-wavelength and will require very accurate time-targeting but the W-L wavelet in well 9 shows information spread from +/- 40 ms; this is equivalent to several hundred feet. Further, there is expectation that the information spread will get worse as we consider the whole study cube (Figure 3.5 is for well 9). The likely causes of information spread:

1. gas saturation,
2. time-to-depth mapping inaccuracies, and
3. thin-bed anomalies.

Cause 1 has been extensively covered in the literature. Cause 2 for the information spread relates to heterogeneity in the time-depth match as discussed in Chapter 2. As well as velocity

dispersion, research on thin bed models by Liu (2003) and Imhof (2003) demonstrate that the reflectivity of thin-beds can have anomalous behavior.

3.2 Generating Synthetic Seismic for the 12 Model Wells

In this chapter the synthetic seismic from the 12 model wells are used to analyze the seismic near the wells to get a more detailed look at where the reservoir target is presented in the seismic trace.

The synthetic seismic for well 9 (Figure 3.4) uses as input the "slowness" calculated from the VSP velocity. An alternate input for velocity is the "slowness" from wellbore sonic logs, termed Delta-T. The slowness is scaled in microseconds per foot. The model wells do not have sonic logs so Delta-T for the 12 model wells is generated by the neural network diagrammed in Figure 3.6.

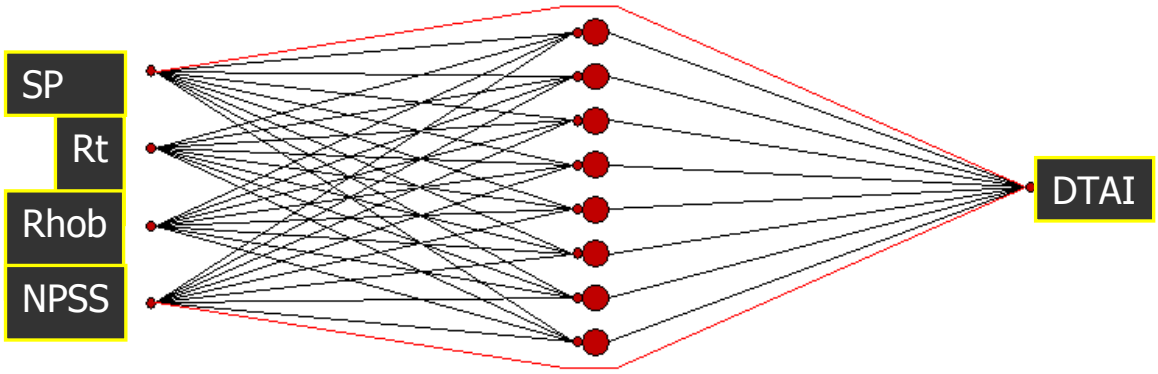

Figure 3.6 Diagram of neural network used to generate Delta-T for model wells

The mapping software NuMap 7.1 (IPNNL (2004b)) facilitated the training and processing of the network. Four well log inputs {spontaneous potential (SP), resistivity (Rt), density (RHOB), and neutron porosity (NPSS)} are applied to a Multi-Layer Perceptron (MLP) network. The VSP slowness in well 9 is used to train the network coefficients. The fit of the mapping in well 9 is shown in Figure 1.2 where DTVSP is the VSP slowness and DTAI is the

network output. The trained network generated Delta-T for the 12 model wells, and these were input to SMT SynPak software to generate synthetic seismic for the model wells.

3.3 Analysis of Synthetic Seismic from Model Wells

Evidence in the previous discussions suggests that the signal from a specific bed is spread or shifted in time within the seismic trace. A simple model for this information spread/shift would be a linear convolution of an ideal signal at different time shifts (also termed phase shifts). Using the formalism proposed by Weiner (1949), we can assume the synthetic is a noise-free signal and use it to isolate the phases present in the seismic signal. We can express a mixed-phase additive noise model as

$$\mathbf{Y}(t) = G_1 * \mathbf{Z}(t + s_1) + G_2 * \mathbf{Z}(t + s_2) + \ldots + G_n * \mathbf{Z}(t + s_n)$$

Where: $\mathbf{Y}(t)$ is the seismic trace
G_n is the gain of the n^{th} phase shift
s_n is the time shift of n^{th} phase
$\mathbf{Z}(t)$ is the synthetic trace

This is a linear statistical model as described in texts such as Box (1987); in matrix form we have n samples and k phase shifts.

$$\mathbf{Y(t)} = \begin{vmatrix} Y1 \\ Y2 \\ Y3 \\ . \\ . \\ . \\ Yn \end{vmatrix} \qquad \mathbf{Z_k(t)} = \begin{vmatrix} Z11 & Z21 & \ldots & Zk1 \\ Z12 & & & . \\ . & & & . \\ . & & & . \\ . & & & \\ . & & & . \\ \mathbf{Z1n} & & & \mathbf{Zkn} \end{vmatrix} \qquad \mathbf{G_k} = \begin{vmatrix} G1 \\ G2 \\ . \\ . \\ . \\ Gk \end{vmatrix}$$

And the solution for the phase gains G_k is

$$\underline{\mathbf{g}} = (\mathbf{Z'Z})^{-1}\mathbf{Z'}\underline{\mathbf{y}}$$

This is obviously a very simple model but it should be noted that our aim is not to devise a deconvolution but rather to dissect the seismic trace to find where information about the depth

target is in time. A plot of the gains versus the phase shifts is used where higher gains point to time shifts that have information.

Figure 3.7 plots the synthetic seismic (SS11) and the seismic trace (trace 11) from well 11 that will serve as inputs to the convolution. The first experiment uses 16 phase shifts (8 positive shifts, 8 negative shifts) of the synthetic by 4 ms for a 64 ms window. The convolution window was performed over the upper middle Frio in the 12 model wells.

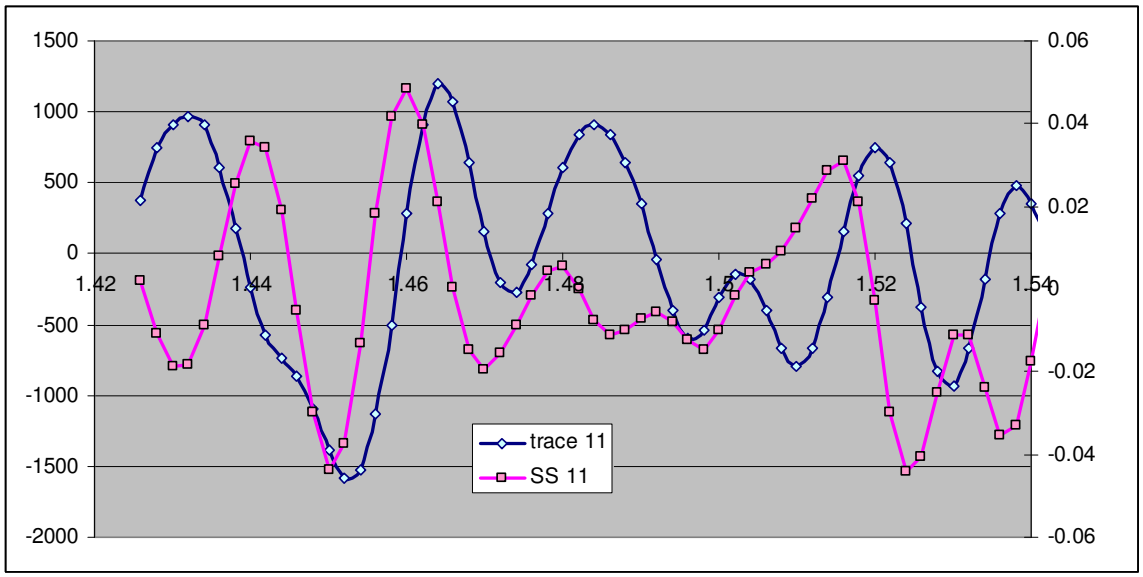

Figure 3.7 Example of synthetic seismic (SS11) and 3D seismic trace (trace 11) for well 11

As described above, gains for each of the phase shifts were solved; the gains and phases are then convolved, and the output is a good fit with the seismic trace, plotted in Figure 3.8.

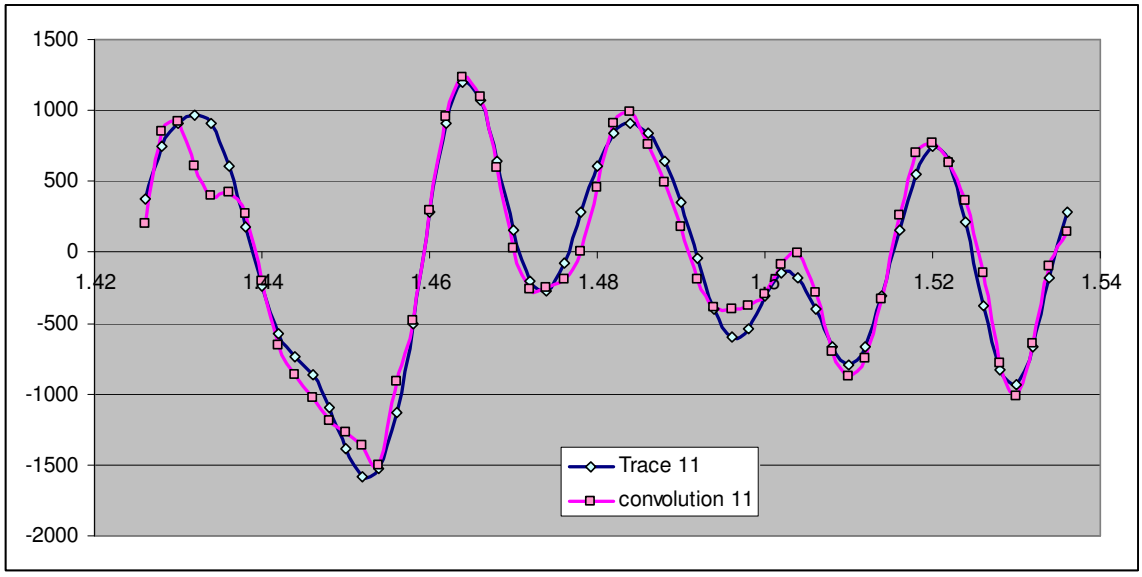

Figure 3.8 Comparison of 3D seismic trace (trace 11) to the convolution of synthetics (convolution 11) in the first experiment for well 11

The fit in some of the more western wells (e.g. well 12 and well 17) was not as good as well 11. This prompted a second experiment with even a wider window, still with 8 shifts positive and 8 shifts negative but covering a window of 96 ms. In Figure 3.9 are the results for well 12 for the first and second experiments.

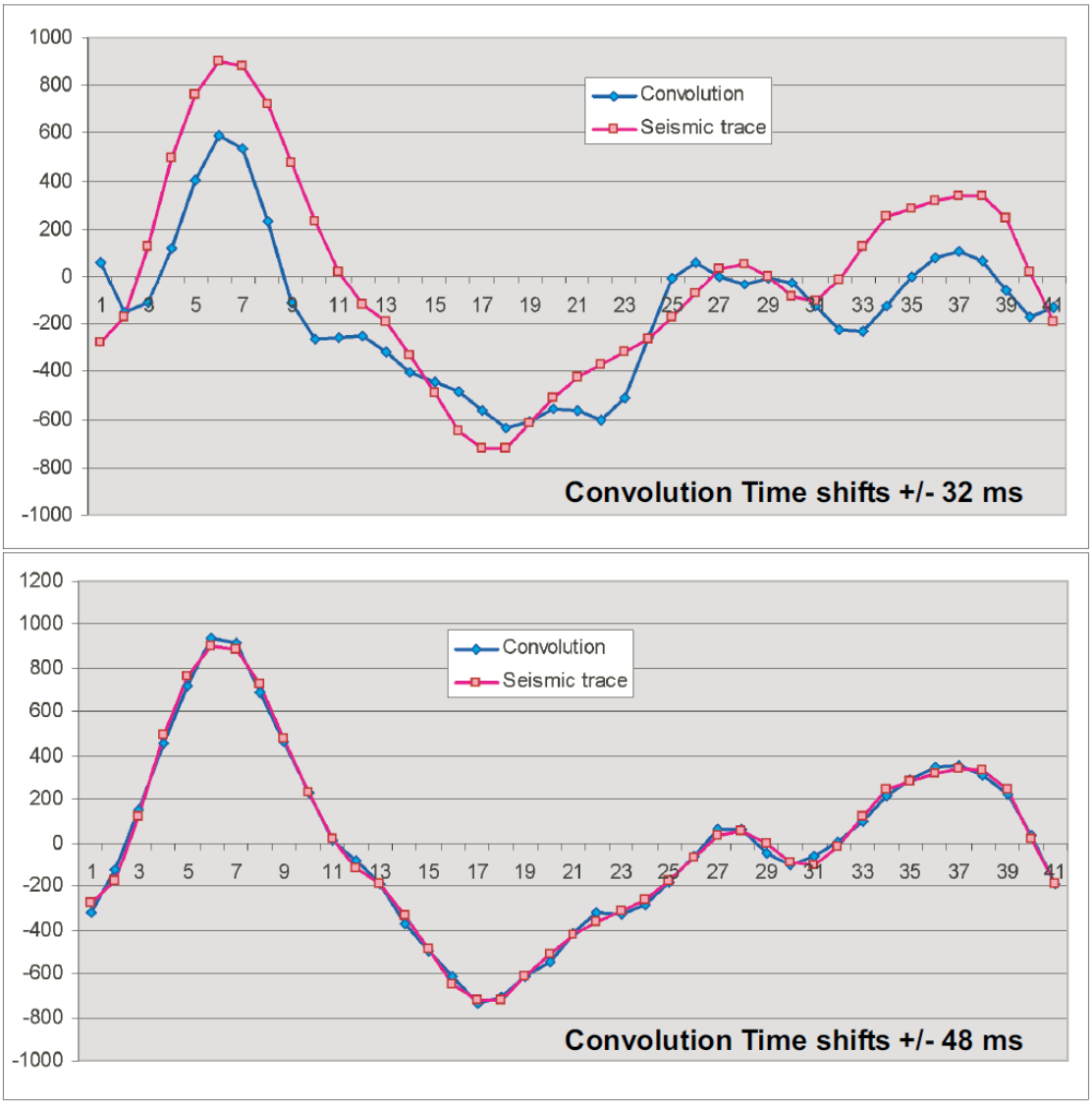

Figure 3.9 Comparison of the 3D seismic trace to the convolution in experiments #1 (top inset) and experiment #2 (bottom inset) for well 12.

Gains were solved in experiment #2 for each of the 12 model wells and were averaged; the results are plotted in Figure 3.10. The top pane in the graph is the phase-gain plot for the upper middle Frio in experiment #2. The bottom pane is the Weiner-Levinson wavelet from SynPak (Figure 2.9) from well 9 for the entire middle Frio. Note that compared to Figure 3.5 the time scale for the W-L wavelet has been reversed for the graphic comparison. In SynPak we

were looking for a wavelet to shift the synthetic; in this experiment we are looking for the time shift from the synthetic to the information in the seismic trace. From the figure, note that the information spread is not as bad in the study cube as are compared to the entire middle Frio that includes the C38 Boomer and the lower middle Frio; but they are similar.

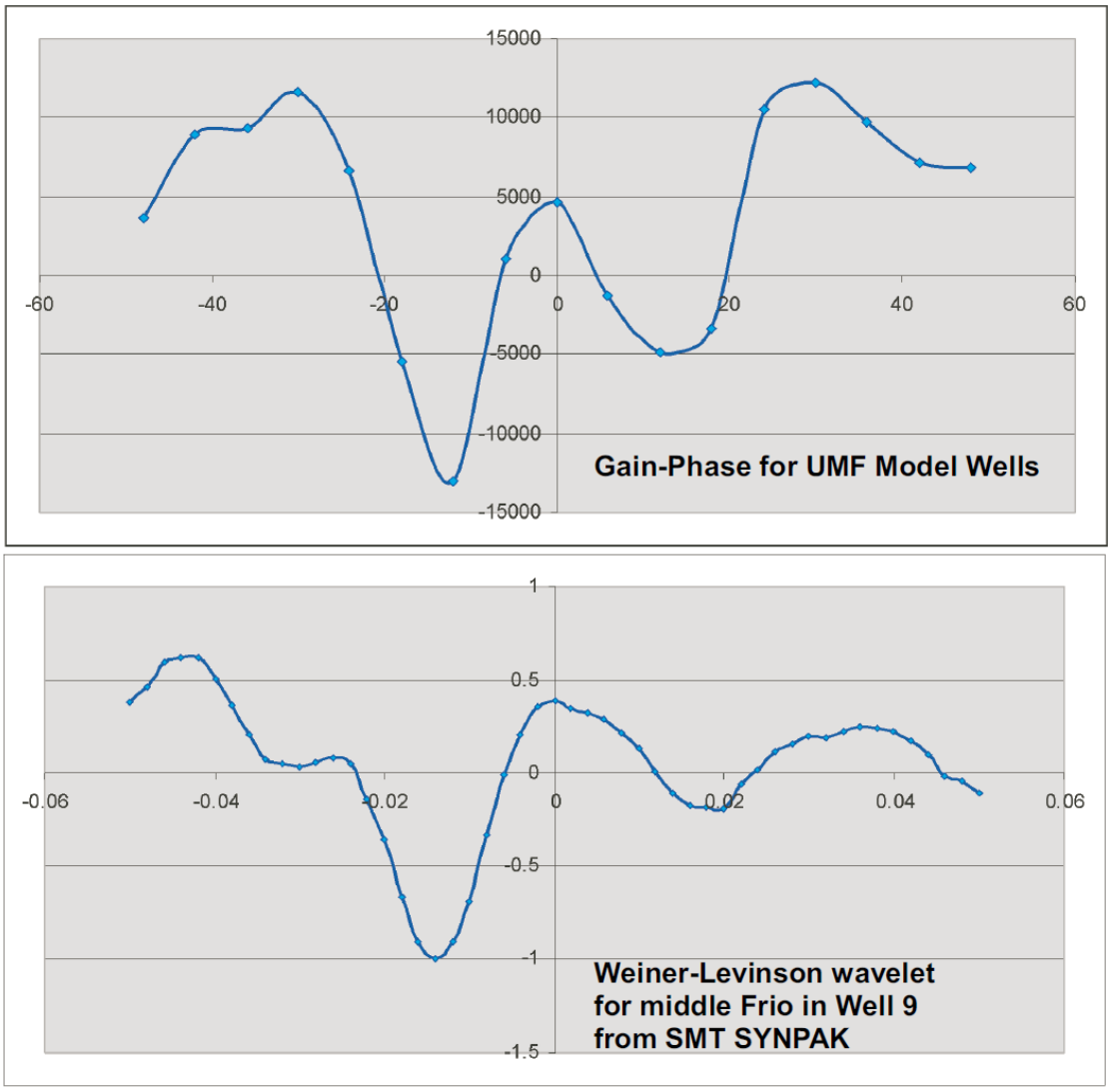

Figure 3.10 Gain-Phase plot (upper inset) for the 12 model wells over the upper middle Frio compared to W-L wavelet for middle and lower Frio in well 9.

3.4 Results of Chapter 3

In this chapter we used the synthetic seismic from the 12 model wells to analyze the seismic for noise and information spread. Instead of just a shift caused by an inaccurate T-D chart, the seismic appears to have information spread over a wide window (e.g. 40 ms). It should be noted that this analysis was cube-wide and represents an average noise over time and lateral extent. By noise, I am referring to interference in applying the assumption that a formation at a specific depth creates a seismic signal at a specific time and these are connected via the T-D chart. The time to depth match at the C38 boomer has the 3D seismic trailing the geologic model, and velocity dispersion from thin beds and gas are predicted to worsen this match as we move away from the tie-point. This would represent time-dependent noise in targeting the reservoir because of T-D chart inaccuracies. Lateral heterogeneities in bedding and gas saturation cause a second type of information spread; the time to a specific formation at one location may be different than the time to the formation at another location. The transit time to the specific formation is the convolution of the beds between the target and the time datum. This effect is seen in the exaggerated time-relief noted in Figure 3.3.

CHAPTER 4

CLASSIFIER HUNT GC2L

Section 4.1 gives details on the Neural Network classifier design and the three searches termed Hunt GC2L (Chapter 4), Hunt GC1U (Chapter 5) and Hunt GC2U (Chapter 6). For each hunt a well template, as shown in the top inset of Figure 3.1, is determined from well log analysis for the target depth. This template is used to score the performance of the NN classifier as well as time-slices in the search window (i.e. the Hardage recipe).

4.1 Detail on the Hunts and Processing

The thick floodplains at 5000, 5300 and 5610 feet subsea divide the study cube into two reservoir cells, referenced GC1 (5000 to 5300 feet) and GC2 (5300 to 5700 feet). The first experiment on tracking a fluvial reservoir element is referenced as Hunt GC2L, as the target is a river channel in the lower half of Geo-cell 2. A cross-section through wells 17, 18, 9, 20, and 8 (Figure 4.1) gives a sub-surface view of the study cube in Figures 4.2 and 4.3.

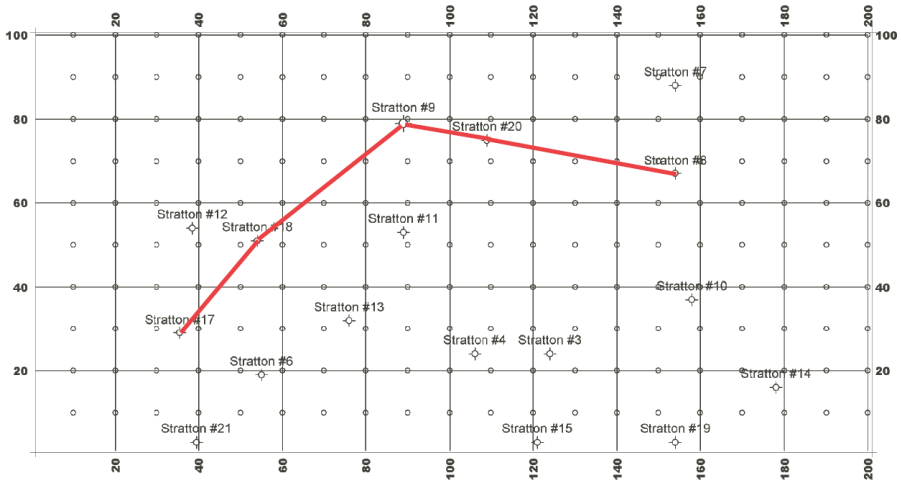

Figure 4.1 Map view of cross-section through wells 17-18-9-20-8

The floodplains that are continuous throughout the well data are marked in Figure 4.2 in green; the ash-marker described in Section 2.6 is shown in blue. In cross-section (after flattening) the study cube is basically flat with a slight drop (~10 feet) and syndepositional growth in well 17. Wireline depth errors are typically 20 to 30 feet relative to a subsea datum (Loermans (1999)) from a variety of causes. In the well data set, however, we have tied the depths of strata to well 9 which, in a relative sense, should have the precision that is close to the 1 foot in 5000 feet specification of wireline vendors.

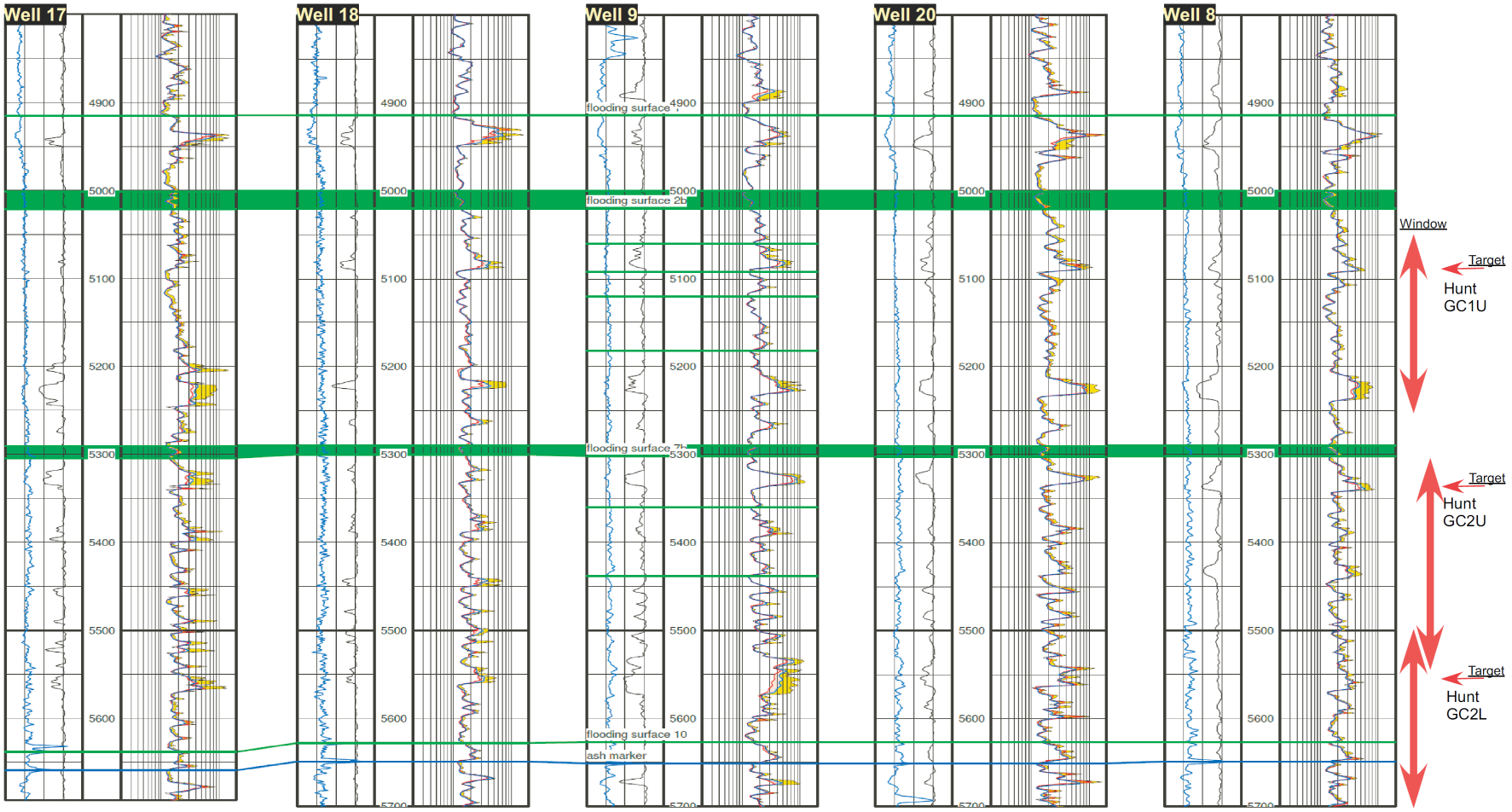

Figure 4.2 Well log cross-section of wells 17-18-9-20-8 after flattening to flooding surfaces in well 9, the red arrows on the right edge mark the search intervals for Hunt GC1U, Hunt GC2U, and Hunt GC2L. Several of the flooding surfaces are marked in green and the ash marker (Section 2.4) is marked in blue.

As discussed in Chapters 2 and 3, the information in the seismic signal appears trailing the well-based geological model, and the information is spread over approximately 40 ms. Thus, the design of the search process will use search windows on the order of 44 to 54 ms; these are marked with red arrows on the right edge of Figures 4.2 and 4.3. From the T-D chart this is equivalent to a search window of approximately 200 feet. In each of the hunts, one fluvial reservoir element is the target, but the search window contains several parasequences (i.e. fluvial elements at other depths in the search window). For discussion purposes, time is measured as the two-way-time with respect to the C38 time datum.

Hunt GC2L: Depth: 5500 to 5700 feet, Time: 94 ms to 138 ms
Target: Channel sand @ 5550 (t= 102 ms, depth =5535 feet)
Hunt GC1U: Depth: 5140 to 5240 feet, Time: 14 ms to 54 ms
Target: Basal Reservoir sands in C38 (t=10 ms, depth = 5080 feet)
Hunt GC2U: Depth: 5300 to 5566 feet, Time: 54 ms to 108 ms
Target: D11 Channel sand at 5328 (t=60 ms, depth = 5328 feet)

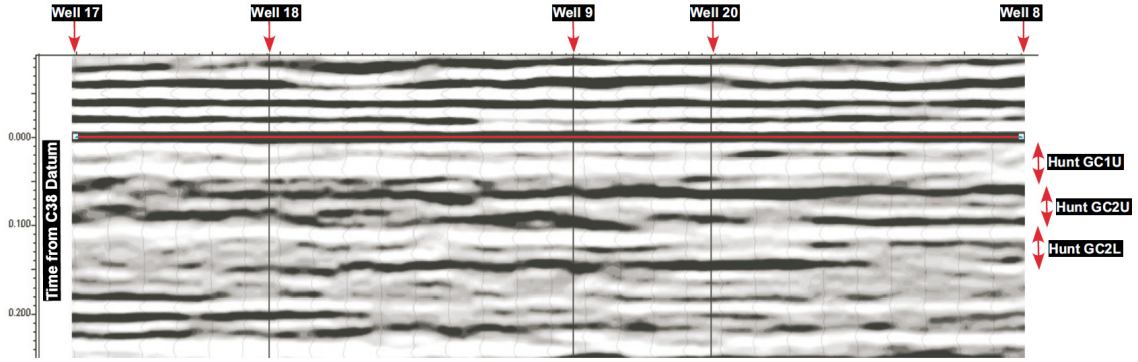

Figure 4.3 Seismic line in C38 flattened cube through wells 17-18-9-20-8, the red arrows on the right edge mark the search intervals for Hunt GC1U, Hunt GC2U, and Hunt GC2L

So what is left is more akin to the forensic science of fingerprinting: tracking the reservoir sand via a characteristic signature that is embedded in the seismic trace. Given that we are looking at less than a wavelength, and a model that is relational rather than functional, the confidence in tracking results is limited as we extrapolate away from the well-bores.

A neural network classifier is used to track the target away from the well bore; the seismic trace data (time, amplitude) are the inputs to this classifier. Details on the processing

workflow can be found in Appendix A. At each model well the analyst determines a class based on the presence/absence of the reservoir element (e.g. channel, splay, and floodplain) at the target depth. Seismic trace segments near the model wells are merged with the assigned class to form the training data set for the neural network. The trained network is then used to process the entire 3D cube (20K traces) to produce facies maps. The seven testing wells are also classified by the analyst, and these are used to score the network classifier performance. The seismic amplitude time-slices are scored in a similar manner although the discrimination is binary: reservoir sand at the target depth should have peak colors (e.g. yellow to orange); no reservoir sand should have trough colors (e.g. green to blue). The visual scoring is based on the predominate class (NN classifier) or color (time-slices) in a 200-foot diameter circle centered on the well location (i.e. most common color on the perimeter of the well marker on the template). Since this scoring scheme is subjective the scoring details are presented in Appendix B, C and D for hunts GC2L, GC1U and GC2U respectively.

On the subject of classifying the model and test wells, the logs and geologic model are plotted in Appendix E. The classification is somewhat subjective; for example, in this hunt well 20 is classified as channel since it has nearly 30 feet of reservoir sand, but it is thinly bedded, more typical of splays and levee deposits. This level of detail is addressed in Section 4.7 where the well logs are revisited for sequence timing and drafting a fluvial model from the facies map.

The neural network classifier used was a mapping Multi-level Perceptron (MLP) network from the software package NuMap 7.1 (IPNNL (2006b)). The class selection is put in a formatted style where class 3 would be:

network output # 1 = 0

network output # 2 = 0

network output # 3 = 1.

I chose a mapping network rather than a classifying network to test whether a confidence indicator could be developed. For example, a good output might be {0.067, -0.0058, 0.94}, a low confidence output might look like {0.5, -.59, 1.09}. Using a form:

Class = Maximum Output

then,

Confidence = (Max Output)/ (Sum of Absolute Value of outputs)

and,

An ideal classification has confidence = 1.

In the case of the good example the confidence is 0.93, and for the low confidence example the confidence is 0.5.

Five traces near each borehole were chosen for the first training set: the trace nearest the well and the adjacent traces to the north, south, east and west. This yields a training set with 60 feature vectors. With this small training set the network can memorize the patterns, and the network trains to a zero error at the well bores. To obtain a more generalized search, the wells are analyzed to pick similar neighbors to augment the training data, this augmented set classifies 400 to 600 neighboring traces (out of the 20000 traces in the study cube) for the second network training.

4.2 Hunt GC2L

A thick river channel complex in the lower half of Geo-Cell 2 was chosen as a first experiment since it had several favorable factors:

1. At the target depth is a parasequence with one river system that stayed in the cube long enough to produce a thick (>40 feet) channel sand complex. Given the slow aggradation of the floodplain and typical channel depths of 10 feet, these deposits represent an extended period where the river stayed fairly stationary in the study cube.
2. Above the target sand (e.g 5530 to 5250 feet) are several continuous flood plains and short-lived river systems. Below the target depth (e.g. 5570 to 5610 feet) all the

wells show splays and floodplains. The lower half of the search window contains two parasequences that are consistent across the model wells. In simpler words: the main lateral changes in this search volume are at the target depth.

This hunt will create a map with three facies classes: A typical member for each class is diagrammed in Figures 4.4, 4.5 and 4.6. For the model wells there are five wells with channel class, four wells with splay class, and three wells with floodplain class. The Channel Class is the reservoir sand of the channel complex. Well 9 in Figure 4.4 is a typical member with channel sands stacked to approximately 40+feet in thickness.

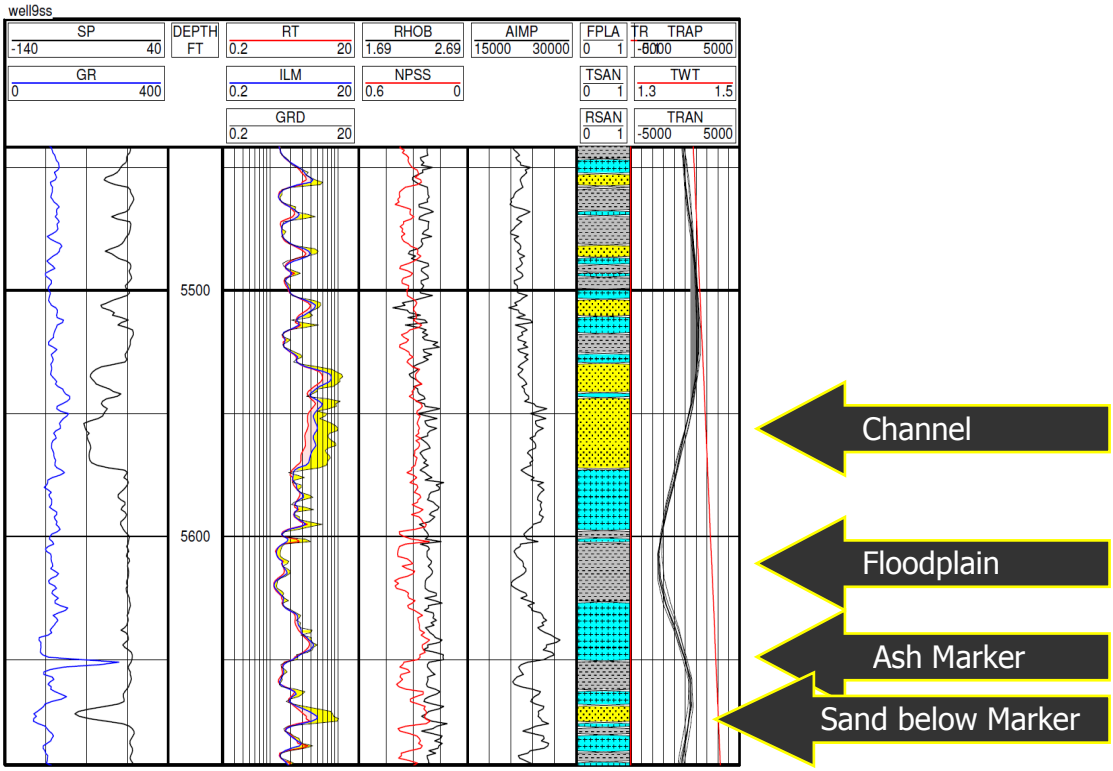

Figure 4.4 Well 9 is a typical Channel Class member, well logs, geologic model and seismic traces

A typical member for the Splay Class is well 18 shown in Figure 4.5. This class has several stacked splays at the target depth; some are close enough to the channel to be coarse-

grained. It should be noted that is hard to distinguish splay from levee deposits (or a mixture), but splays typically have greater lateral extent.

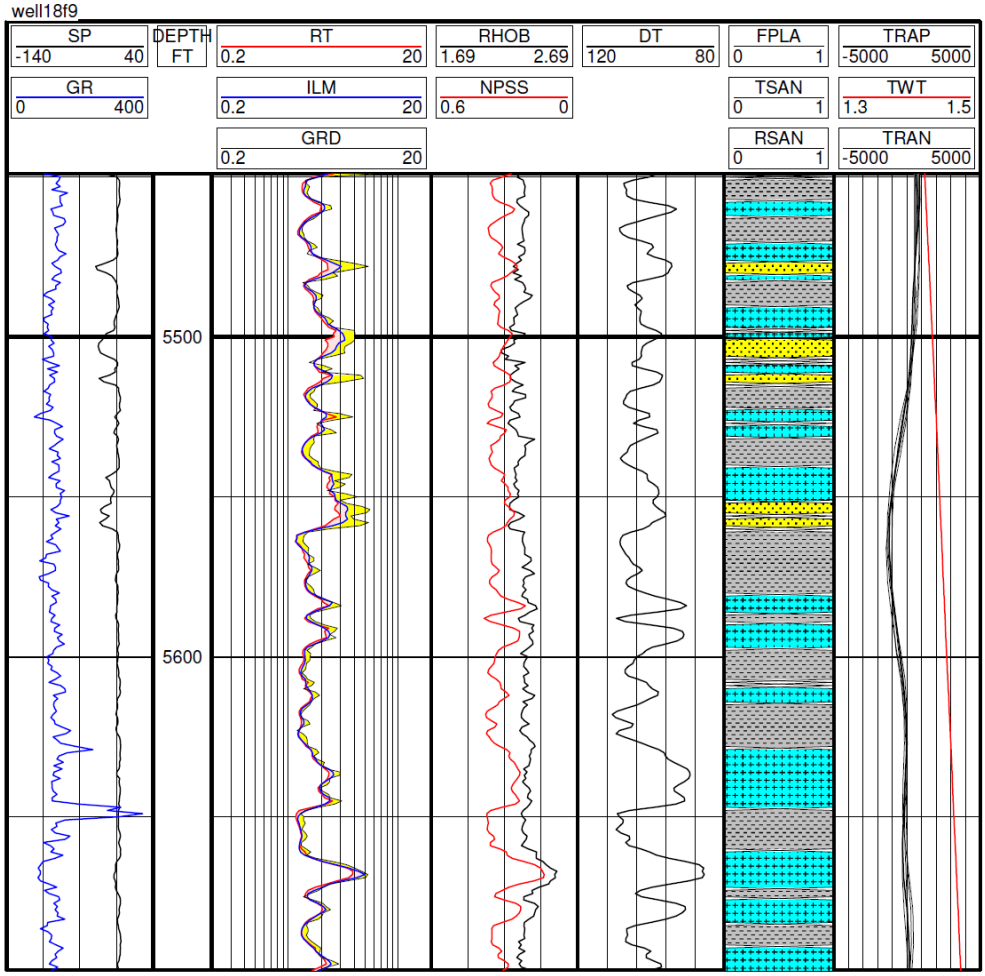

Figure 4.5 Well 18 is a typical Splay Class member: well logs, geologic model and seismic traces

A typical Floodplain Class member is well 8 of Figure 4.6. At the target depth there are some sand deposits from splays and flooding but these deposits are fine grained and finely bedded (i.e not reservoir quality).

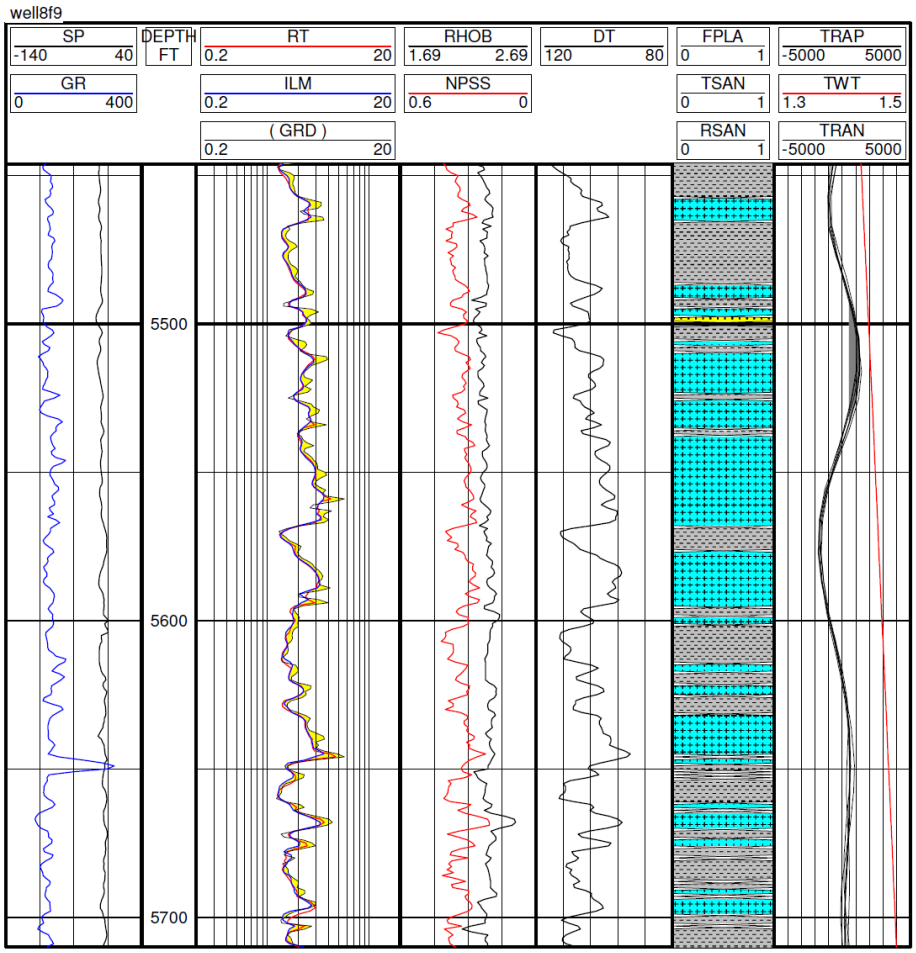

Figure 4.6 Well 8 is a typical Floodplain Class member: well logs, geologic model and seismic trace

4.3 Training the Neural Network Classifier Local to Wells

In the first training, five traces nearest to the model wells are used: the closest trace, one north, one south, one east and one west. With a trace spacing of 55 feet this is well within the horizontal resolution shown in Table 1.1. The facies map from the classifier is Figure 4.7. The coding is as follows: red is Channel class, yellow is Splay class, and blue is Floodplain. The scoring template uses the same color scheme with model wells (circles) and testing wells (squares) filled with red, yellow or blue depending on class.

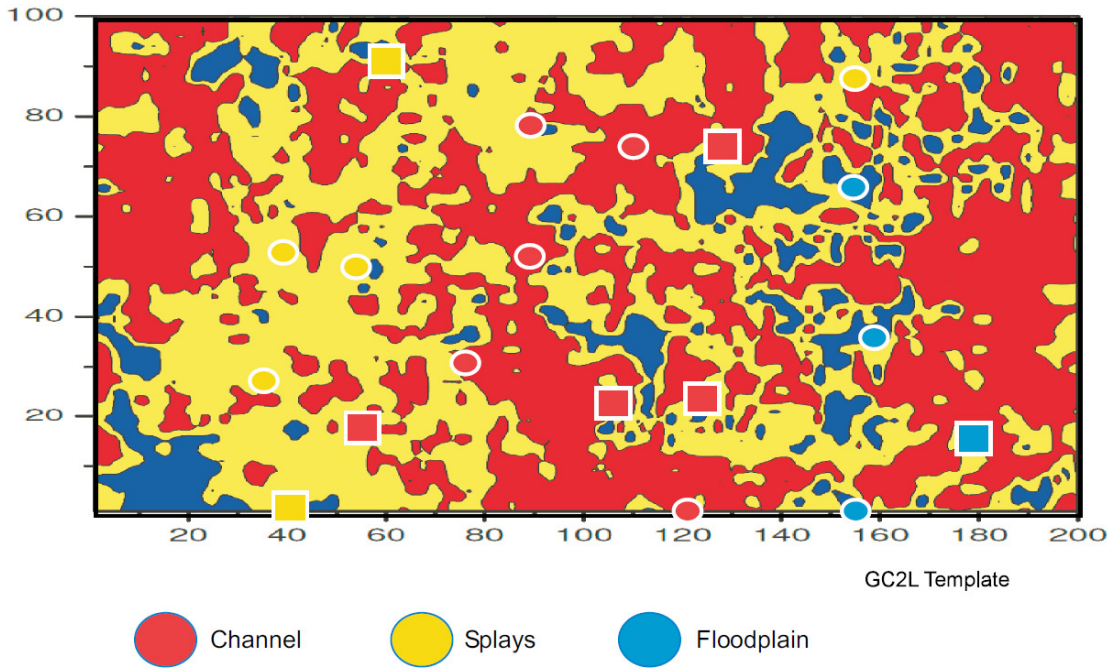

Figure 4.7 Class map from first training of Neural Network classifier for Hunt GC2L.

Figure 4.8 is the confidence map, the legend is inset where red coding is high confidence and blue coding is low confidence. For this minimal training set the network can memorize the all of the traces such that high confidence means a close match to the seismic trace of a particular well. Much of the confidence map is magenta (i.e. confidence of 04. to 0.6) which is low confidence and there are some blue areas where the match was very poor.

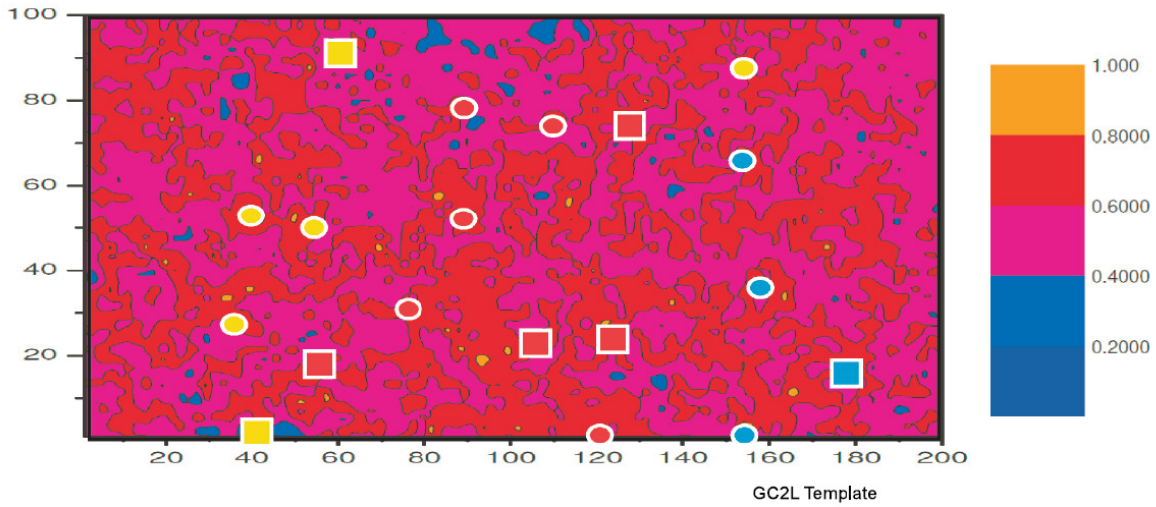

Figure 4.8 Confidence map from first training of NN classifier for Hunt GC2L

4.4 Training the Neural Network Classifier with an Augmented Training Data Set

Assuming lateral continuity of fluvial deposits between neighboring wells with the same classification, the training data set can be augmented using the inter-well traces. Figure 4.9 maps the location of these augmenting segments. The augmented training set for this hunt contains 459 of the 20,000 traces.

With this larger training set the network no longer memorizes the traces and must develop a relational mapping of trace characteristics into class membership; this is indicated by the training error no longer going to zero.

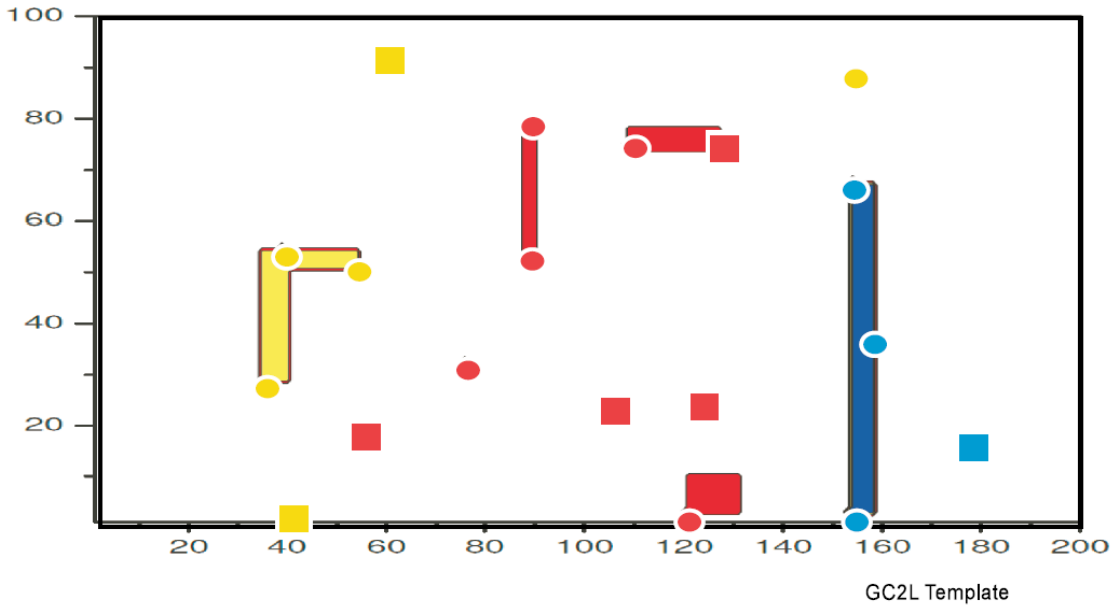

Figure 4.9 Map of augmenting segments used in second training data set

The facies map from the augmented network is Figure 4.10. The network misclassified testing well 1 and testing well 21 of the seven testing wells; these are marked “X” on the template of Figure 4.10. The confidence map in Figure 4.11 shows lower confidence in the classification near wells 1 and 21. In both cases the map showed these wells on the edge between classes; reviewing the well-logs in Appendix E, both of these wells have a good bit (>10 feet) of reservoir sand at the target depth in splay-like deposits. Of note here, for objective scoring follow the scoring rule, but practical application may need to be more subjective.

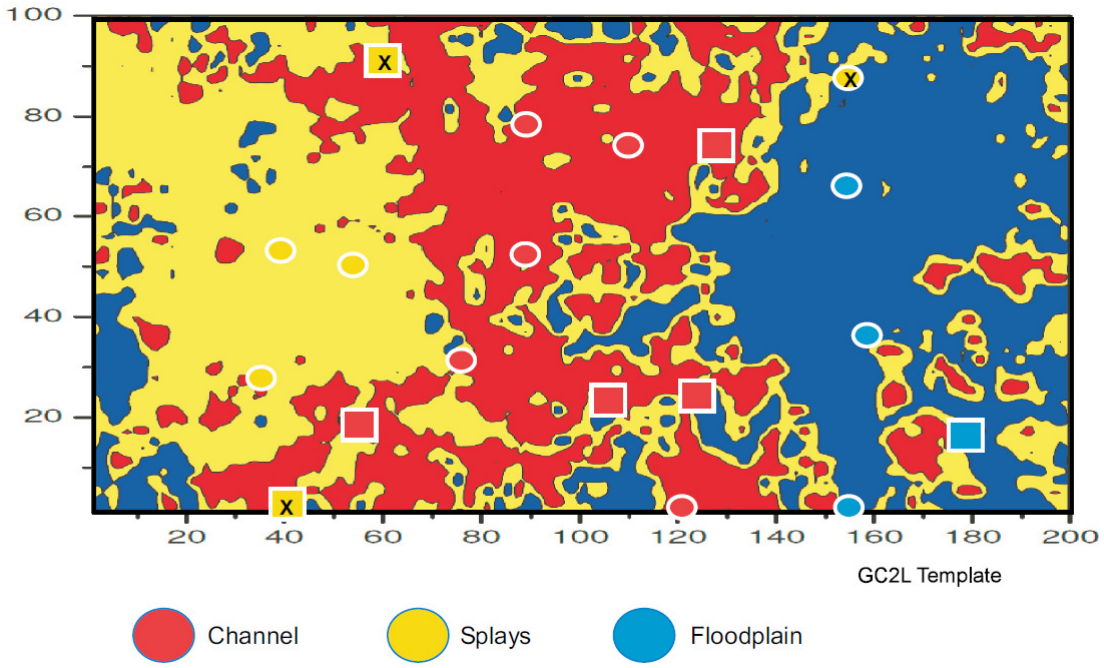

Figure 4.10 Class map for NN classifier trained with augmented training data.

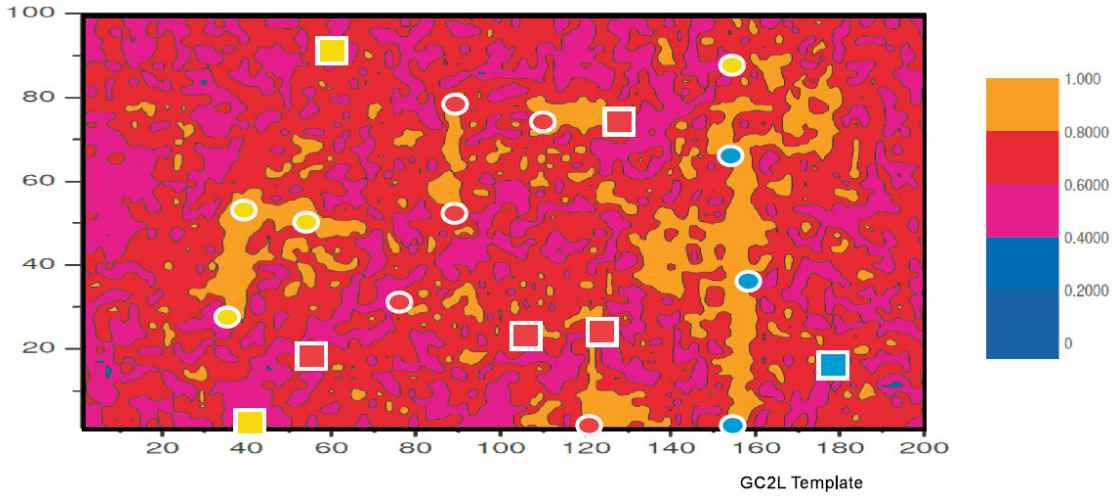

Figure 4.11 Confidence map for NN classifier trained with augmented training data

4.5 Analysis of the Training Data Using a Sub-Setting Algorithm

In the classification literature the inputs are referenced as features; in this classifier network the inputs, or features, are a segment of the seismic trace. Often in classifier refinement, the designer would pick a subset of the features, possibly fusing some inputs, possibly transforming some of the inputs to make a simpler yet effective classifier. This process of sub-setting serves our aim in a different manner: an effective network that uses fewer inputs must be using parts of the seismic time segment that contain information on the target. Again, the aim here is not to devise a simpler feature vector but rather to answer the overall question: where in this time series is information about the targeted fluvial reservoir element? In this search we used a trace segment with 22 points sampled at 2 ms. Manual testing all of the permutations of sub-sets would produce a multitude of evaluations. For example, if we wanted to find the two most potent features, from the binomial theorem the number of subsets we would have to evaluate is:

$$\begin{bmatrix} 22 \\ 2 \end{bmatrix} = \frac{22!}{(22-2)!(2!)} = 231 \text{ evaluations,}$$

The number of evaluations continues to grow as we consider subsets of 1 to 21 features.

The GIGO software (Li (2006a and 2006b)) from the Image Processing and Neural Networks Lab at University of Texas at Arlington, performs the sub-setting and evaluations of the training data automatically. The training data is segregated into clusters, and the error calculation for a given subset uses the corresponding rows and columns of the auto- and cross-correlation matrices for each cluster. The choice of subsets is done via a Floating Search algorithm which is faster than, but not as exhaustive as the Branch and Bound algorithm described by Fukunaga (1990). A Piecewise Linear Network is designed for each subset to evaluate performance and the most potent set of features for each subset size is ranked.

The results from the GIGO analysis of the training data for Hunt GC2L are shown in Table 4.1; we note that the most potent features are time steps 5, 22, 13 and 21. This search window starts 94 ms after the C38 time datum so these features correspond to times-slices 102, 136, 118 and 134 ms in the flattened cube.

Table 4.1 Results of sub-setting the training data with GIGO software

Predicted Error	Subset Size		Subset Members
0.142946	1		{ 5, }
0.119171	2		{ 5, 22, }
0.105213	3		{ 5, 22, 13, }
0.091866	4		{ 5, 22, 13, 21, }
0.081279	5		{ 5, 22, 13, 21, 4, }
0.072833	6		{ 5, 22, 13, 21, 1, 2, }
0.063898	7		{ 5, 22, 13, 21, 1, 2, 16, }
0.057335	8		{ 5, 22, 13, 21, 1, 2, 16, 9, }
0.051743	9		{ 5, 22, 13, 21, 1, 2, 16, 9, 19, }
0.047878	10		{ 5, 22, 13, 21, 1, 7, 17, 8, 11, 3, }

For our classifier we are using a segment of the seismic trace as input. This simple set is over-sampled when we consider that the trace is continuous; it can be argued that at least half of the inputs are not linearly-independent, and thus, have limited potency in discriminating class membership. This is seen in the predicted error column (Table 4.1) that adding a tenth input has little effect on error improvement. Note that using a mapping network, the reported error is the error in the three outputs in a least-squares sense, which is related to, but not the same as the classification error. But again, our aim is not to build a more efficient network; rather use the GIGO scan of the inputs to analyze where in time-based search window is information on the depth-based target.

4.6 Scoring Time-Slices and NN Classifier Results

As discussed above, the scoring of the network map and time-slices was done on a visual basis by placing a 200-foot lens around the well and estimating the class. Since this is a

subjective process, Appendix B shows the NN classifier facies map and the time-slices overlain with the GC2L scoring template. The template is based on well-log analysis; the logs are presented in Appendix E with annotations on target classes for each hunt.

The scores are listed in Table 4.2; it can be noted that even with the subjective uncertainty of the scoring, the time-slices have poor correlation with the well-based geologic model as compared to the NN classifier. In viewing the results in Table 4.2, the worst fit can be viewed as the best fit for inverted data. In other words, the trough in the amplitude map (blues and greens) may correlate to the reservoir sand.

Of interest is the comparison of the scoring results to the GIGO results: In second place and fourth place in the GIGO rankings are times equivalent to time-slices 136 ms and 134 ms, respectively. In scoring results time-slice 134 was the “best-of-the–worst”, and both of these slices show a plausible shape for the river channel as a trough in the seismic.

Table 4.2 Scorecard for Hunt GC2L

Slice	Model wells	Testing wells	Total
ms	% correct	% correct	%correct
NN Classifier	100.00%	71.43%	89.47%
102	66.67%	28.57%	52.63%
104	66.67%	28.57%	52.63%
106	66.67%	42.86%	57.89%
108	66.67%	42.86%	57.89%
110	58.33%	42.86%	52.63%
112	58.33%	42.86%	52.63%
114	58.33%	42.86%	52.63%
116	50.00%	42.86%	47.37%
118	41.67%	71.43%	52.63%
120	25.00%	57.14%	36.84%
122	41.67%	71.43%	52.63%
124	50.00%	71.43%	57.89%
126	41.67%	71.43%	52.63%
128	58.33%	71.43%	63.16%
130	66.67%	42.86%	57.89%
132	41.67%	42.86%	42.11%
134	25.00%	28.57%	26.32%
136	58.33%	28.57%	47.37%
138	75.00%	57.14%	68.42%
140	66.67%	57.14%	63.16%

. Time-slice 136 is plotted in Figure 4.11 the channel shape in blue-green seems to agree with the NN classifier map. In the figure the wells marked with X are deemed to be the incorrect class by the scoring rule: reservoir sands are high amplitude (reds and yellows).

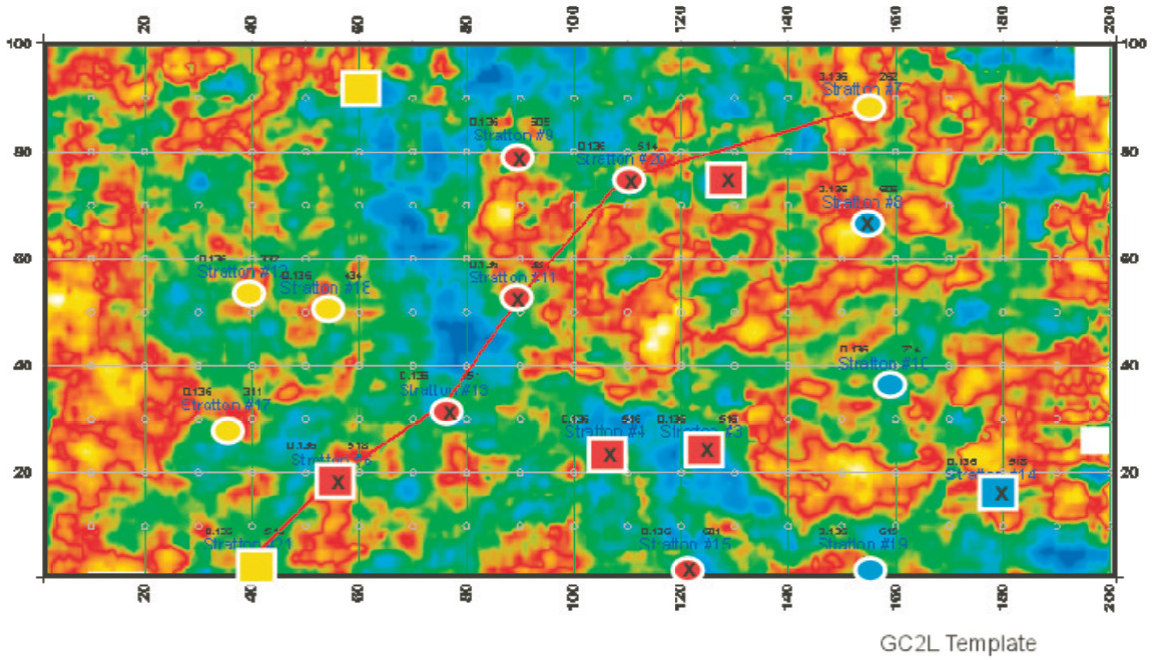

Figure 4.12 Time-slice 136 ms (color bar: red is high positive amplitude (peak) to blue is high negative amplitude (trough))

Of interest to the aim of the research, the GIGO results from successful network training and the scoring of the time slices both confirm the initial analysis that the information in the seismic is spread over a window trailing the depth-based geologic model. In the design of a neural network classifier there is concern of forced results, indeed we could get a facies map that would match the well-bores using a network trained to somewhat random data. The relation of the NN facies map and the GIGO results to the time-slice scoring gives a sense that:

1. The neural network, trained at the wellbores, is functionally connected to the study cube,
2. The NN facies map is a better match than any specific time-slice, so we will use it in construction of a fluvial model, and,
3. Identifying the most potent time-slices may illustrate how the Hardage recipe could be improved; this has value since this recipe is widely accessible to seismic interpreters.

4.7 Sequence Timing and Refinement of the Fluvial Model

The lateral continuity of splays can be use to set some bounds on the river-way. Figure 4.13 is a cross-section going east of well 9 with wells 20, 2 and 7. The river seen in well 9 created several splaying events that can be tracked. The channel sand complex in well 9 is marked with a red block in Figure 4.3; two splays that correlate between wells 20, 2 and 7 are marked with yellow bars along with a floodplains marked with a green bar. Similarly, splays in the western wells can be tracked to establish a western bound.

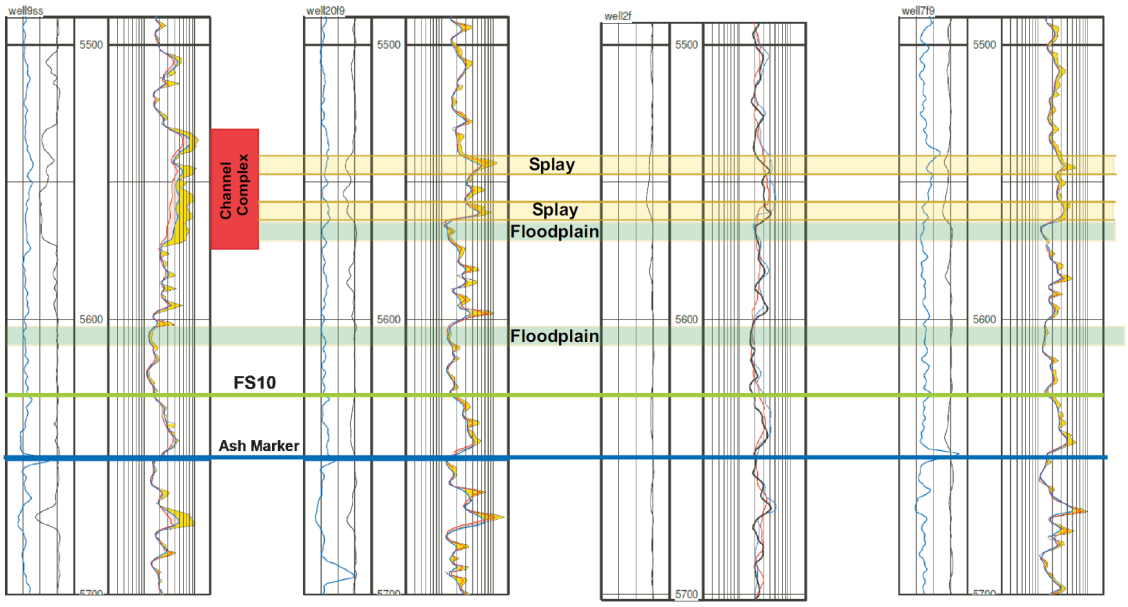

Figure 4.13 Well-log cross-section of wells 9-20-2-7 (left to right).
Splays correlate eastward from the channel in well 9 are marked with yellow bars.

In Figure 4.14 the cross-section of wells 6, 13, 4, and 15 gives a west-to-east look at the timing of the river-way across the base of the study area. In this cross-section we note that the older part of the channel was in the east in wells 15 and 4, the younger part of the channel moved west through wells 13 and 6. Also the displacement seen in the ash marker (blue line in Figure 4.14) to the west indicates syndepositional growth. This channel sand complex is stacked vertically over a long period; a fault that is synthetic to the Aqua Dulce fault is proposed

by Mowafy, continued subsidence may helped constrain the river-way. Kerr (1990) proposes that vertical stacking is more likely in the middle Frio during high periods of floodplain aggradation.

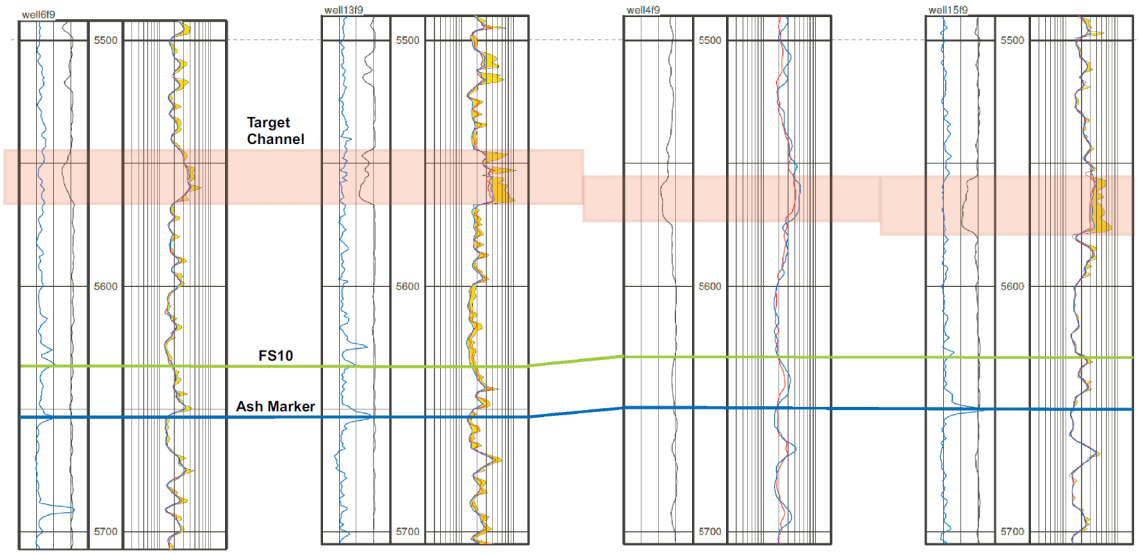

Figure 4.14 West to east cross-section through wells 6-13-4-15 (left to right), The channel sand complex is marked with a pink bar.

A fluvial model is drafted in Figure 4.15 using the following assumptions:

1. The river channel was bounded on the west by coarse-grained splays and levees, layered with the tight sand facie. East of the river channel are coarse-grained splays in the north, near well 7. Most of the east bank is layered with tight sand and floodplain facies.
2. The time-slice at 136 ms has a channel-like pattern bounded by higher trace amplitude that correlate with the splays,
3. and, as the river channels stacked vertically they migrated to the west at the base of the study cube with the oldest channel exiting near well 15.

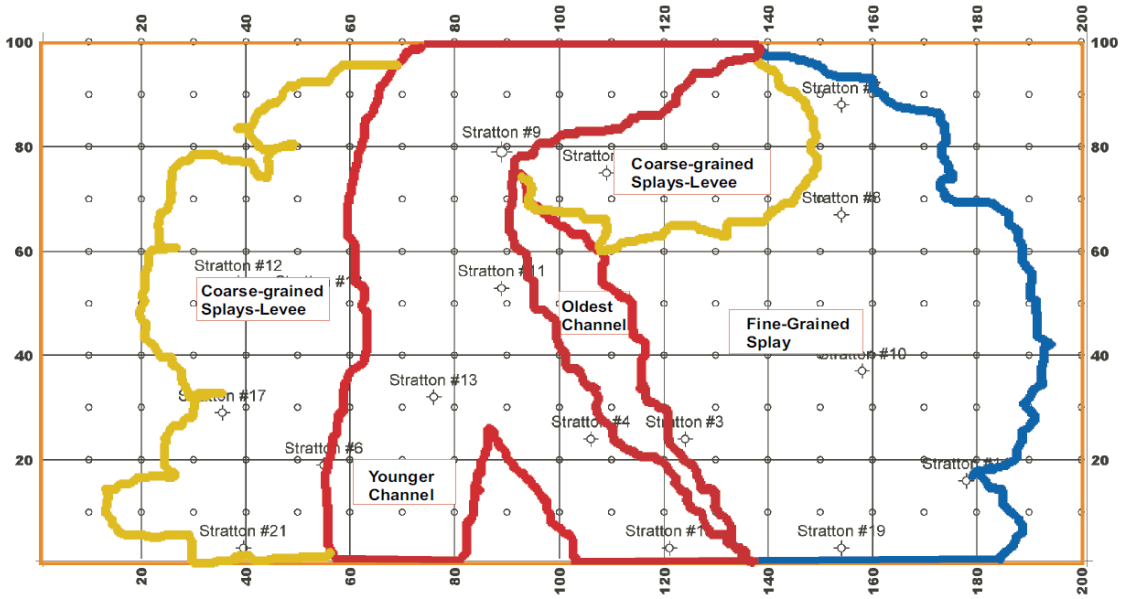

Figure 4.15 Fluvial model for the target depth in Hunt GC2L

CHAPTER 5

HUNT GC1U

The target in this hunt is the reservoir sand at the base of the C38 sand, shown in Figure 5.1 at the depths 5080 to 5090 feet. The C38 sand is a thick splay complex comprised of thin layers of tight sand and reservoir sand. There is a coarse-grained portion of at the base of the C38 sand where several splays deposited thin sheets of reservoir sand that are laterally extensive. In well 9 (Figure 5.1) the sheets are stacked, and the base shows a weak channel-like pattern (e.g. ramping base on the SP curve and a reworked channel depth of 10 feet).

In the previous hunt the targets were fluvial architectural elements, where: Channel class was reservoir sand, Splay class was tight sand with some thin layers of reservoir sand and Floodplain class was comprised of layers of tight sand and floodplain facies. This hunt has two classes: splay class has >10 feet of reservoir sand, no splay class has tight sand and floodplain facies at the base of the C38 sand. The challenge of this hunt is a minimal thickness target that is proximal to the C38 Boomer tuning. In the rightmost track of Figure 5.1 is the 3D seismic trace, the big peak at 5031 feet is the C38 Boomer, and the target is in the trailing trough. If target information is offset in time we can use an offset search window to eliminate interference from the C38 Boomer. This hunt will use a search window in the seismic from 5100 to 5300 feet (14 to 58 ms). Below the target, in the lower half of geo-cell 1, is a parasequence containing a vertically stacked river channel complex seen at 5210 feet in well 9 (Figure 5.1).

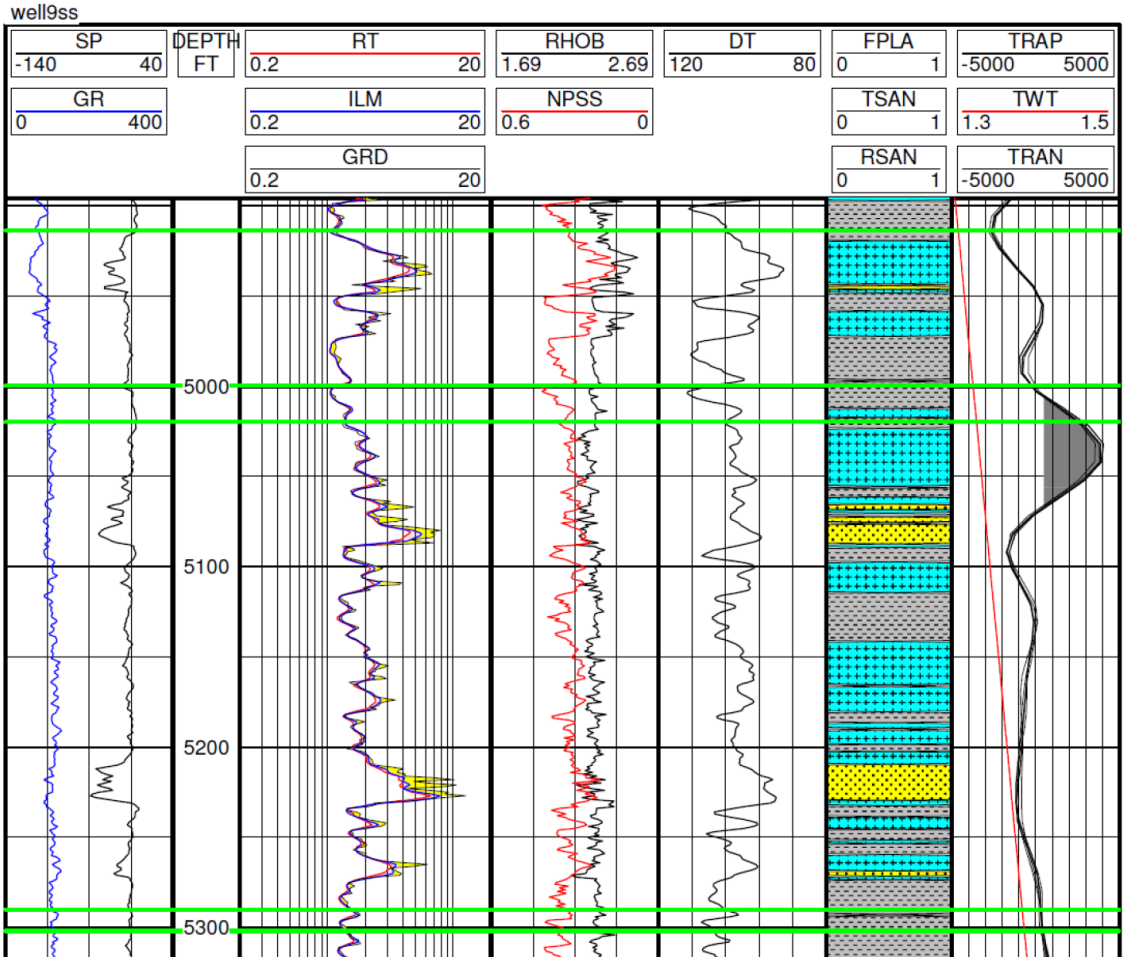

Figure 5.1 Logs and seismic trace from well 9. The target is the reservoir sand at the base of C38 sand at 5080 to 5090 feet.

5.1 Classes for the Neural Network Classifier

In this hunt the class discriminant is whether the wellbore intersected more than ten feet of reservoir sand. To provide a bit more specific information to the classifier, the network was trained with six output classes based on the class discriminant and the character of deposits in the lower parasequences. The model wells are plotted by class in Figure 5.2.

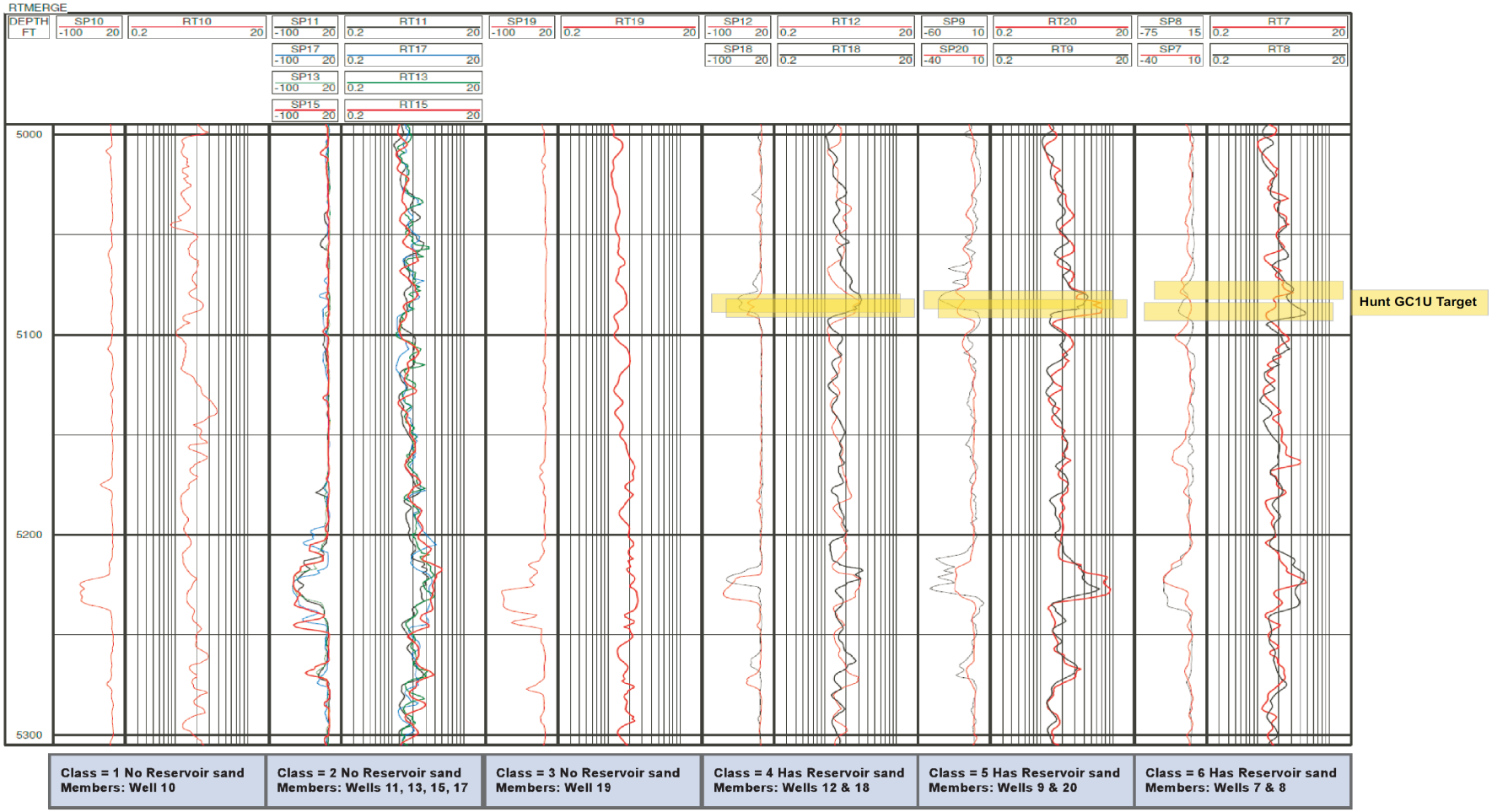

Figure 5.2 The model wells are grouped into classes by character. Classes 1, 2 and 3 do not have reservoir sand, classes 4, 5 and 6 have reservoir sand. The sorting of classes is also based on the character of the lower parasequence at 5200 to 5250 feet.

5.2 Training the Neural Network with an Augmented Training Data Set

Similar to the process outlined in Chapter 4 the network training set was augmented by adding traces between neighboring wells. Using the augmented data, the training set classified 445 traces of the 20000 traces in the cube. The facies map from the NN classifier is plotted in Figure 5.3 with red as Splay class (reservoir sand) and blue as No Splay class. The classifier was correct on six of the seven testing wells, missing well 6 (marked with an "X").

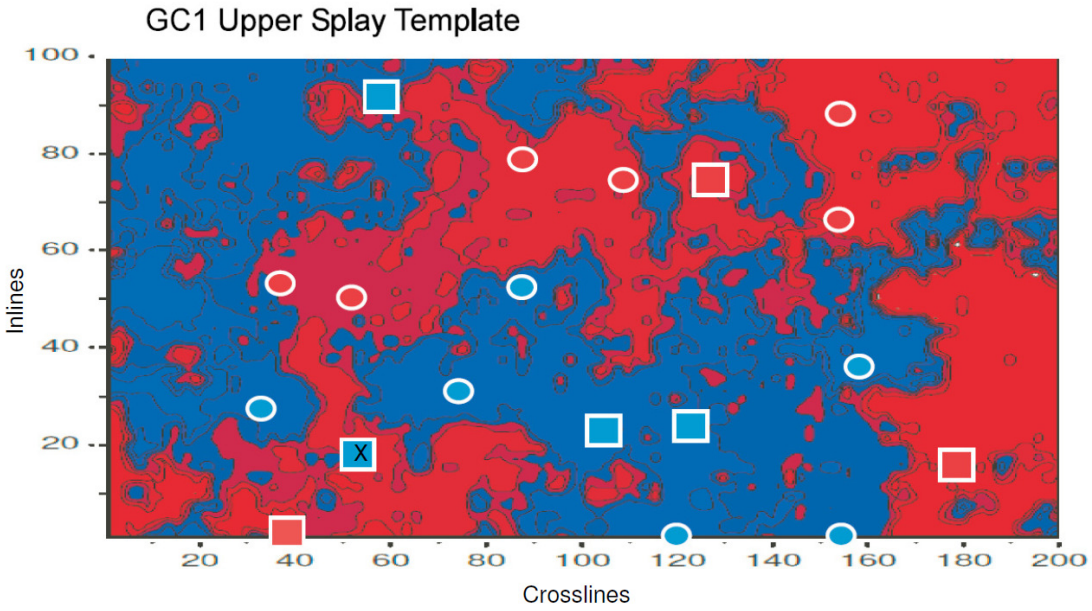

Figure 5.3 Class map for NN classifier using augmented training data, red indicates basal reservoir sand, blue indicates tight sand splays or flood plains at the target depth.

The NN classifier confidence map is Figure 5.4. We can note a lower confidence in this hunt compared to Chapter 4, part of this lowered confidence can be linked to having six classes rather than three.

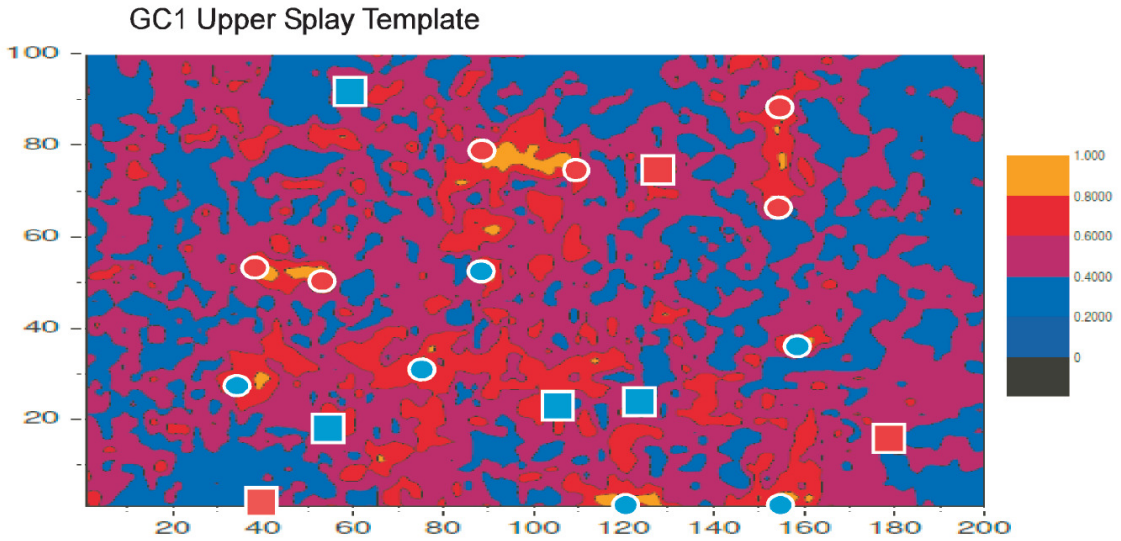

Figure 5.4 Confidence map for NN classifier in Hunt GC1U

5.3 Analysis of the Training Data Using a Sub-Setting Algorithm

As discussed in Chapter 4, the training data is analyzed using the GIGO software to determine which times in the search window are important in discriminating the reservoir sand. The results in Table 5.1 suggest the ordinal importance of time slices at 40 ms, 24 ms, 32 ms and 48 ms (indexed as 2 ms steps starting at 14 ms).

Table 5.1 Results of sub-setting the training data with GIGO software

Predicted Error	**Subset Size**		**Subset Members**
0.258457	1		{ 13, }
0.2347	2		{ 13, 5, }
0.213225	3		{ 13, 9, 17, }
0.193565	4		{ 13, 9, 17, 21, }
0.177893	5		{ 13, 9, 17, 21, 2, }
0.162917	6		{ 13, 9, 17, 21, 2, 6, }
0.154704	7		{ 13, 9, 17, 21, 2, 6, 12, }
0.147831	8		{ 13, 9, 17, 20, 2, 6, 12, 22, }
0.14227	9		{ 13, 9, 17, 20, 2, 6, 12, 22, 1, }

5.4 Scoring time-slices and NN classifier results

The neural network classifier and time-slices in the search window are scored in Appendix C; the results are presented below in Table 5.2. The NN classifier picked the correct class in six of the seven testing wells; well 6 was misclassified but did not show particularly low confidence. In general the time-slices scored poorly with most results around 50%, similar to the broken clock that is correct twice a day, with a roughly 50/50 mix of classes even an all-trough time slice (e.g. time slice at 40 ms) can score 50%.

Table 5.2 Scorecard for Hunt GC1U

Slice	Model wells	Testing wells	Total
ms	% correct	% correct	%correct
NN Classifier	100.00%	85.71%	94.74%
10	N/A - all Trough		
13	N/A - all Trough		
16	N/A - all Trough		
18	58.33%	57.14%	57.89%
20	66.67%	42.86%	57.89%
22	75.00%	42.86%	63.16%
24	58.33%	28.57%	47.37%
26	58.33%	42.86%	52.63%
28	50.00%	85.71%	63.16%
30	58.33%	71.43%	63.16%
32	41.67%	85.71%	57.89%
34	50.00%	71.43%	57.89%
36	N/A - all Trough		
40	N/A - all Trough		

Of interest in the scoring is the time slice at 24 ms has the worst score and was ranked by GIGO as the second most potent discriminator. This slice is picked as the most potent time–slice and is plotted in Figure 5.7, the patterns of this slice are used in developing the fluvial model of Section 5.4.

5.5 Improving Classifier Results

The analysis of well 6 yields some insight on how the network performs and how to improve the results. Figure 5.5 plots the NN classifier output with all six classes. Well 6 is part of a continuous shape that was classified as class 5, class members are well 9 and well 20, but well 6 does not have the basal reservoir sand.

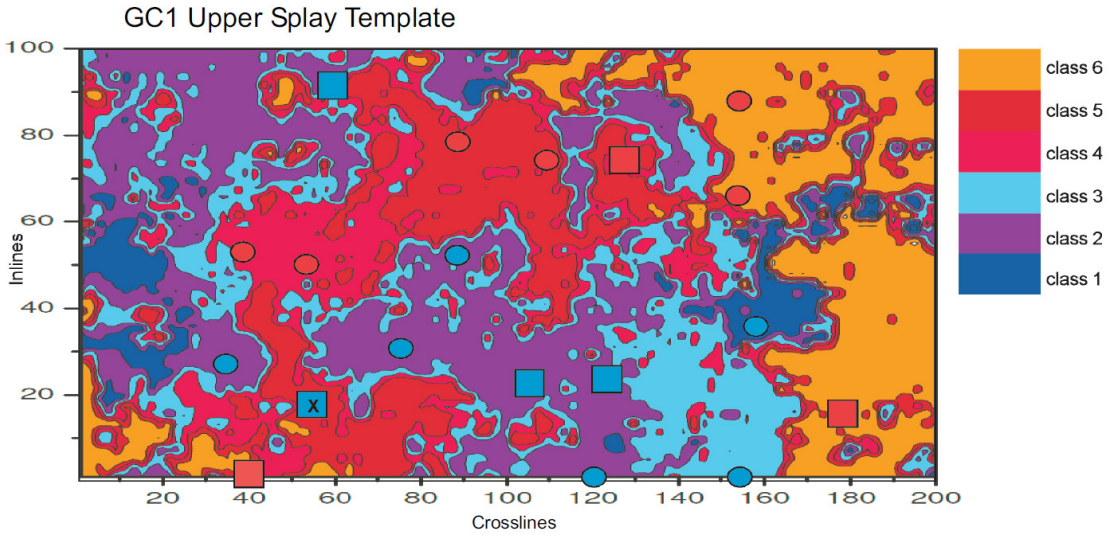

Figure 5.5 Well 6 is miss-classified as Class 5 (marked with "X")

Figure 5.6 provides more details on well 6 and Class 5 member well 9; in the figure the well logs and the 3D seismic traces near each well are plotted. The seismic traces from the two wells are similar over the search window. On Figure 5.6 the red cross bars represent the three most potent time-slices from the GIGO processing. Analysis of the training data established these three times as potent class discriminators, but well 6 and well 9 are very similar at these points.

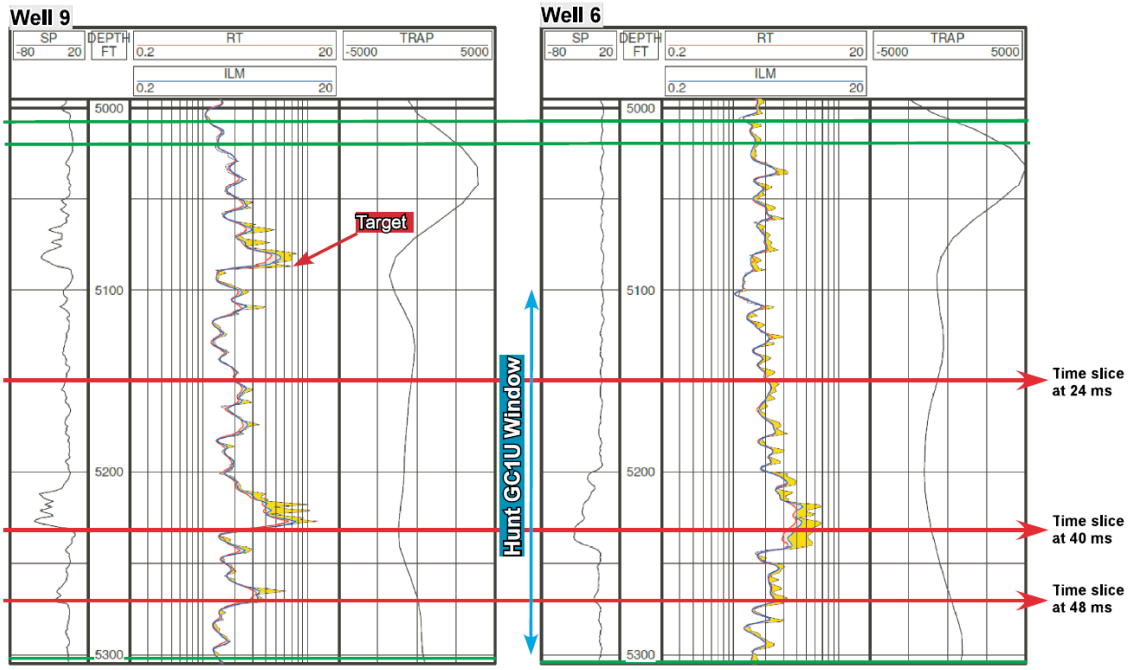

Figure 5.6 Well-logs and 3D seismic traces for well 6 and well 9

This case might be referenced as a training class outlier, a group of traces having similar traits to an identified class but belonging to an unidentified class. How can we improve results in this case?

1. Traces near well 6 (and the other testing wells) could be added to the training data, then retrain a NN classifier with improved results.
2. Even in the map view of Figure 5.5, the traces around well 6 formed a visual outlier. A filter could be developed to exclude disjoint groups of traces. Requiring a continuous extrapolation away from the well bore will be important in surveys with less well coverage than the BEG cube.

5.6 Sequence Timing and Refinement of the Fluvial Model

This very-thin target challenges the depth control of the well-based stratigraphy; as discussed in Chapter 4, the depth uncertainty in the well logs and deformation is on the order of ten feet (the target thickness). So the assumption on timing is the reservoir sands are coeval

splays that deposited in thin sheets with some minor channel-like structures. Using the high amplitude (reds and yellows) in the time-slice at 24 ms as tight splays and floodplains, and the low amplitudes (blues and greens) as the reservoir sands; this information is fused with the neural network facies map to draft the fluvial model shown in Figure 5.5.

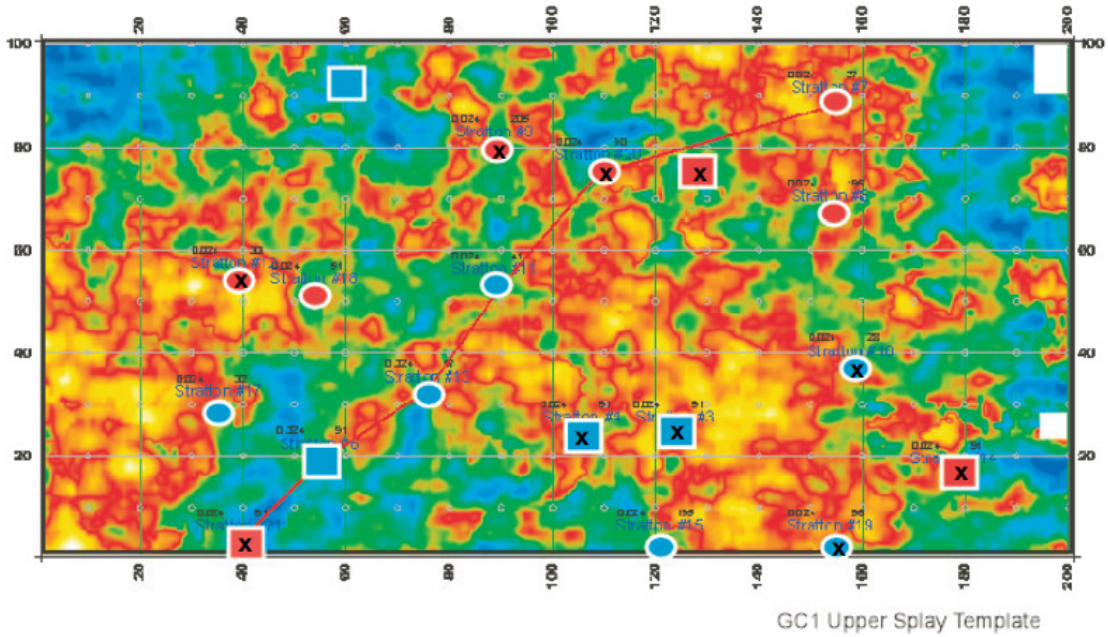

Figure 5.7 Time slice at 24 ms below C38 time-datum (color bar: red is high positive amplitude (peak) to blue is high negative amplitude (trough))

The reservoir sand seen in well 9 (Figure 5.1) showed some possible channel reworking; in the model this is a coarse-grained dendritic tongue that carries the fine sediment and flood water to the extent of the splays. In the eastern portion of the model there is a single sheet of reservoir sand as seen in well 8 and well 14 with lesser thickness in the south. Given the depositional model, it is inferred that the crevasse in the river levee was nearby and north-northeast of the study cube.

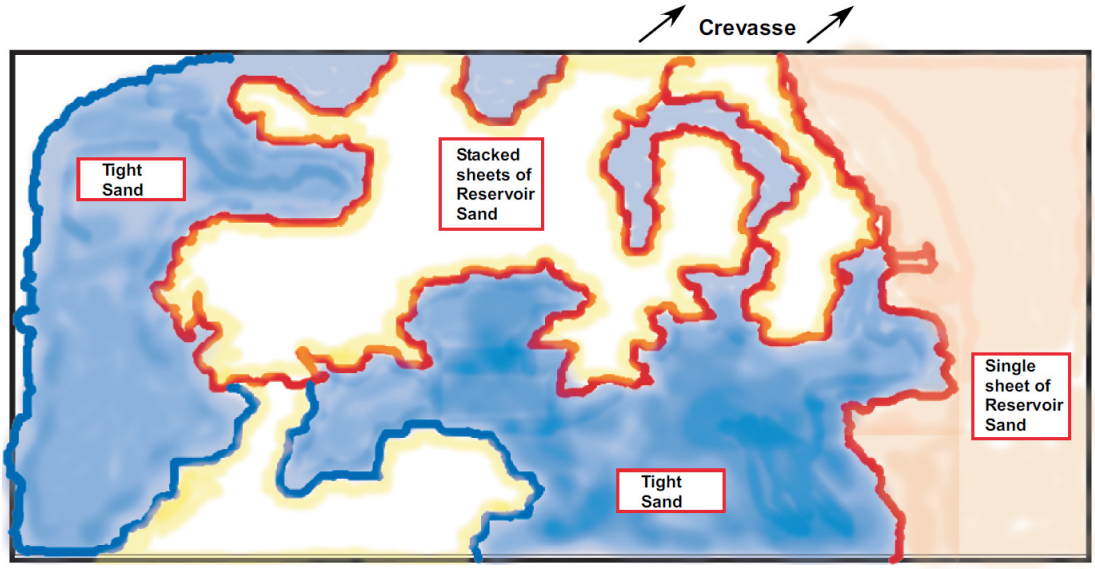

Figure 5.8 Map of reservoir sands at target depth. The sand distribution suggests the crevasse in the river levee was north-northeast of the study cube.

CHAPTER 6

HUNT GC2U

This hunt is particularly challenging from the standpoint of interference from neighboring sequences. The hunt window for GC2U has six different parasequences and the target, the D11 sand, is in the topmost. Of further interest, this hunt also covers part of the survey used by Hardage (1994) for a D11 sand model so we can compare results.

6.1 Parasequences in Hunt GC2U

Hunt GC2U will use a 54 ms window covering depths 5300 to 5566 feet. On the cross-section of Figure 6.1 six parasequences are diagrammed:

Parasequence 1 contains the target D11 sand. The expression on the logs indicates a powerful river channel with channel turbidation depths of 15 feet. Timing from the well logs indicate north to south flow with an early channel in the eastern portion (wells 7, 8, and 10) moving central (wells 9, 11 and 13).

Parasequence 2 contains another deep river channel but the timing and expression in the well-logs is unique. The channel goes through well 13 (and well 2) and there is evidence of splay/levee in a few wells, but the footprint is much narrower which would indicate it came into the area and left suddenly before building extensive splays or laterally accreting channel sands.

Parasequence 3 contains a shallower channel with depths on the order of 10 feet.

Parasequence 4+ and 5: The + on 4+ indicates that there are more than one parasequence; in general these are much lower-energy river systems with channel depths less than 10 ft, slowly moving from well to well.

Parasequence 6+: again several sequences from a powerful river system as evidenced by extensive splays. No channels were noted crossing the well locations.

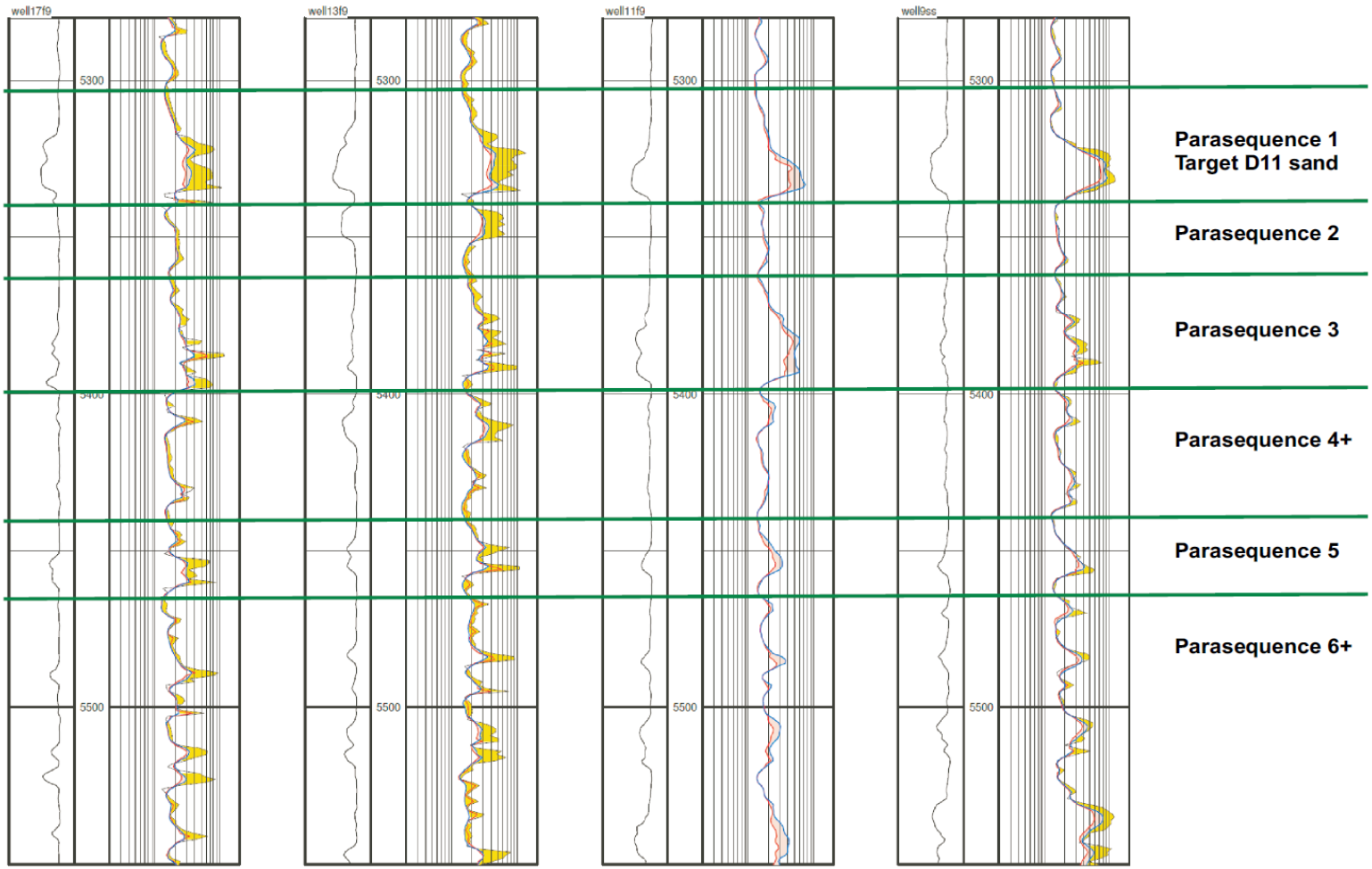

Figure 6.1 Parasequences in the Hunt GC2U window seen in well log cross-section of wells 17-13-11-9

6.2 Training the Neural Network Classifier with an Augmented Data Set

Using the same process outlined in the previous hunts (Chapters 4 and 5), the traces local to the well-bores plus some augmenting segments between like neighbors were used to train the NN classifier. The augmented training set contained 624 of the 20,000 traces. The trained network was used to generate the class map is shown in Figure 6.2. Since none of the wells had the floodplain class at the target depth, traces with confidence factors less than 0.7 are shown in black.

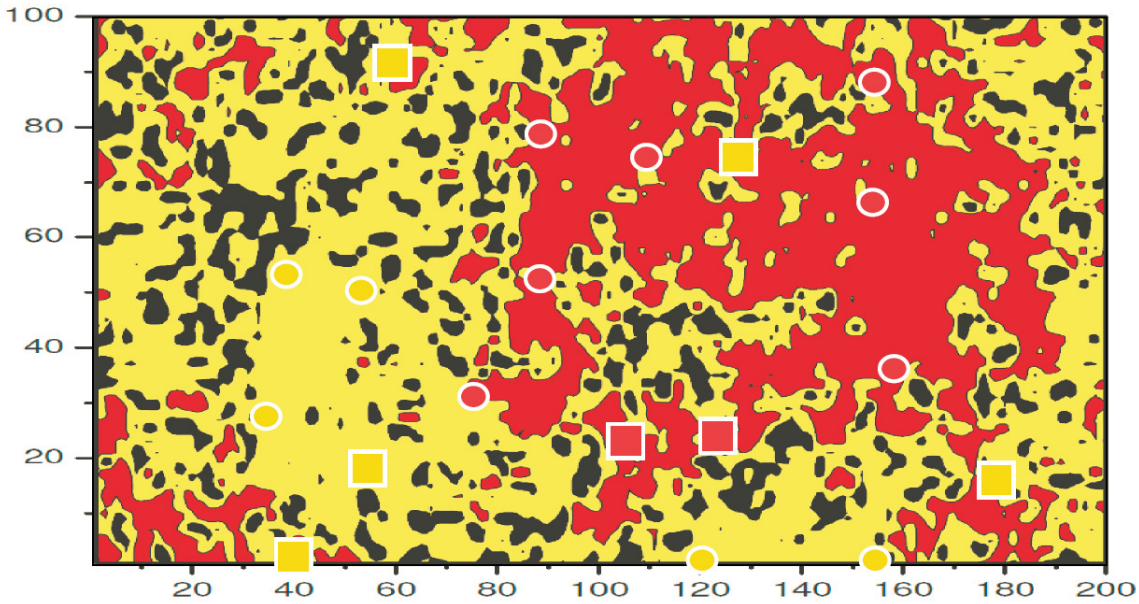

Figure 6.2 Class Map from NN classifier, red is channel, yellow is splays, black is low confidence

6.3 Analysis of the Training Data Using a Sub-Setting Algorithm

As discussed in Chapter 4, the training data is analyzed using the GIGO software to determine which times in the search window are important in discriminating the reservoir sand. The results in Table 6.1 suggest the ordinal importance of time slices at 90 ms, 80 ms, 86 ms and 68 ms (indexed as 2 ms steps starting at 54 ms).

Table 6.1 Results of sub-setting the training data with GIGO software

Predicted Error	Subset Size		Subset Members
0.08197	1		{ 19, }
0.070761	2		{ 19, 14, }
0.064013	3		{ 19, 14, 18, }
0.059022	4		{ 19, 14, 18, 7, }
0.056597	5		{ 19, 14, 18, 7, 1, }
0.054283	6		{ 19, 14, 18, 7, 1, 27, }
0.053084	7		{ 19, 14, 18, 7, 1, 27, 10, }
0.051466	8		{ 19, 14, 18, 7, 1, 26, 4, 2, }
0.049844	9		{ 19, 14, 25, 6, 1, 26, 20, 2, 27, }
0.048677	10		{ 19, 14, 25, 6, 1, 26, 20, 2, 27, 24, }

Analysis of the Training vectors using the GIGO program is discussed in Section 4.5.

6.4 Scoring Time-slices and NN Classifier Results

The scores are listed in Table 6.2; it can be noted that even with the subjective uncertainty of the scoring the time-slices have poor correlation with the geologic-model as compared to the NN classifier. GIGO ranked time-slice 90 as the most potent input, in the scoring it is in a four-way tie for second place for positive scoring. GIGO ranked time-slice 68 as fourth place; this was first place in positive scoring. Compared to Hunt GC2L the time-slice scores are generally lower, and the best-of-the worst are still the best scores. Ironically the worst scores at slices 56 and 58 are at the target time.

Table 6.2 Scorecard for Hunt GC2U

Slice	Model wells	Testing wells	Total
ms	% correct	% correct	%correct
NN Classifier	91.67%	85.71%	89.47%
50	41.67%	71.43%	52.63%
52	58.33%	57.14%	57.89%
54	41.67%	28.57%	36.84%
56	41.67%	0.00%	26.32%
58	58.33%	0.00%	36.84%
60	58.33%	14.29%	42.11%
62	N/A - all peak		
64	N/A - all peak		
66	58.33%	42.86%	52.63%
68	66.67%	57.14%	63.16%
70	58.33%	28.57%	47.37%
72	41.67%	42.86%	42.11%
74	66.67%	28.57%	52.63%
76	41.67%	14.29%	31.58%
78	41.67%	42.86%	42.11%
80	16.67%	57.14%	31.58%
82	25.00%	71.43%	42.11%
84	16.67%	71.43%	36.84%
86	25.00%	71.43%	42.11%
88	50.00%	57.14%	52.63%
90	58.33%	42.86%	52.63%

In a visual analysis of the time-slices, none have an image that is faithful to the model from the well-logs with the older channel going through wells 7-8-10 amalgamated to a younger channel going through wells 20-9-11-13. Time-slices at 76, 78 and 80 have a plausible younger channel shape, time slice 80 scored second place and all three have low scores. For these reasons, the time-slice at 80 ms is selected as most potent.

6.5 Comparing to Hardage Model for D11 Sand

In Hardage (1994) a model for the D11 sand was proposed. The BEG 3D survey is a subset of a much bigger survey and the D11 model of Hardage is based on a section that

overlaps the northeastern portion of the BEG survey. In Figure 6.3 the match point of Hardage Figure 16 and the BEG survey is diagrammed; well 156 is referenced as well 7 in the BEG survey.

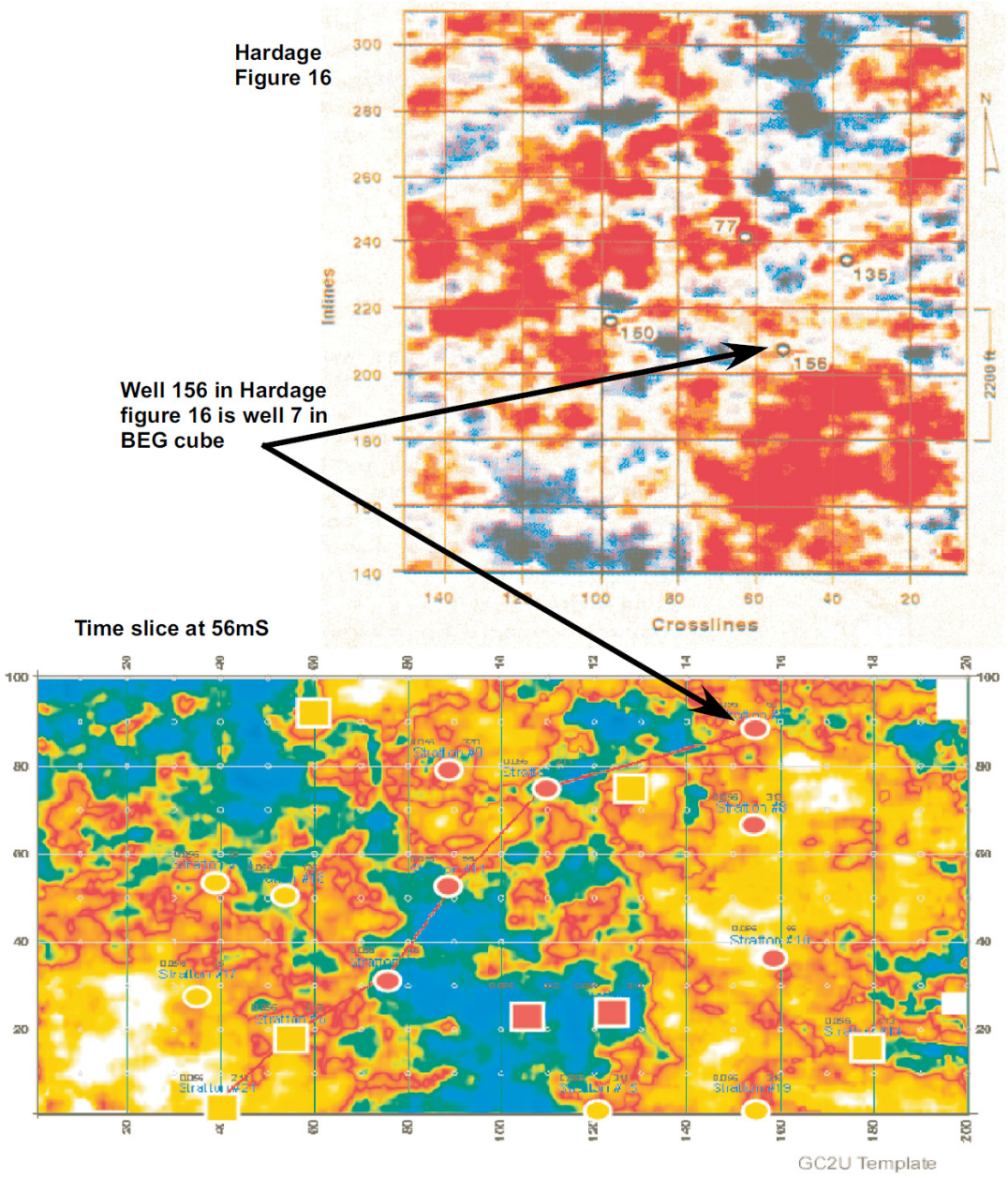

Figure 6.3 Hardage (1994) Figure 16 and time-slice at 56 ms, the well tie-point for the two images is marked.

Using the image for D11 from the time-slice at 56 ms, Hardage proposed the geologic model in Figure 6.4. This model was refined to include an older and a younger channel based on well pressure test data. In Figure 6.4, the geologic model of Hardage's is overlain with the GC2U scoring template. "Channel B" in this model corresponds to the targeted D11 channel sand, but the model does not score well. Still this look northeast of the BEG cube will help in the next section in construction of a fluvial model in the BEG survey.

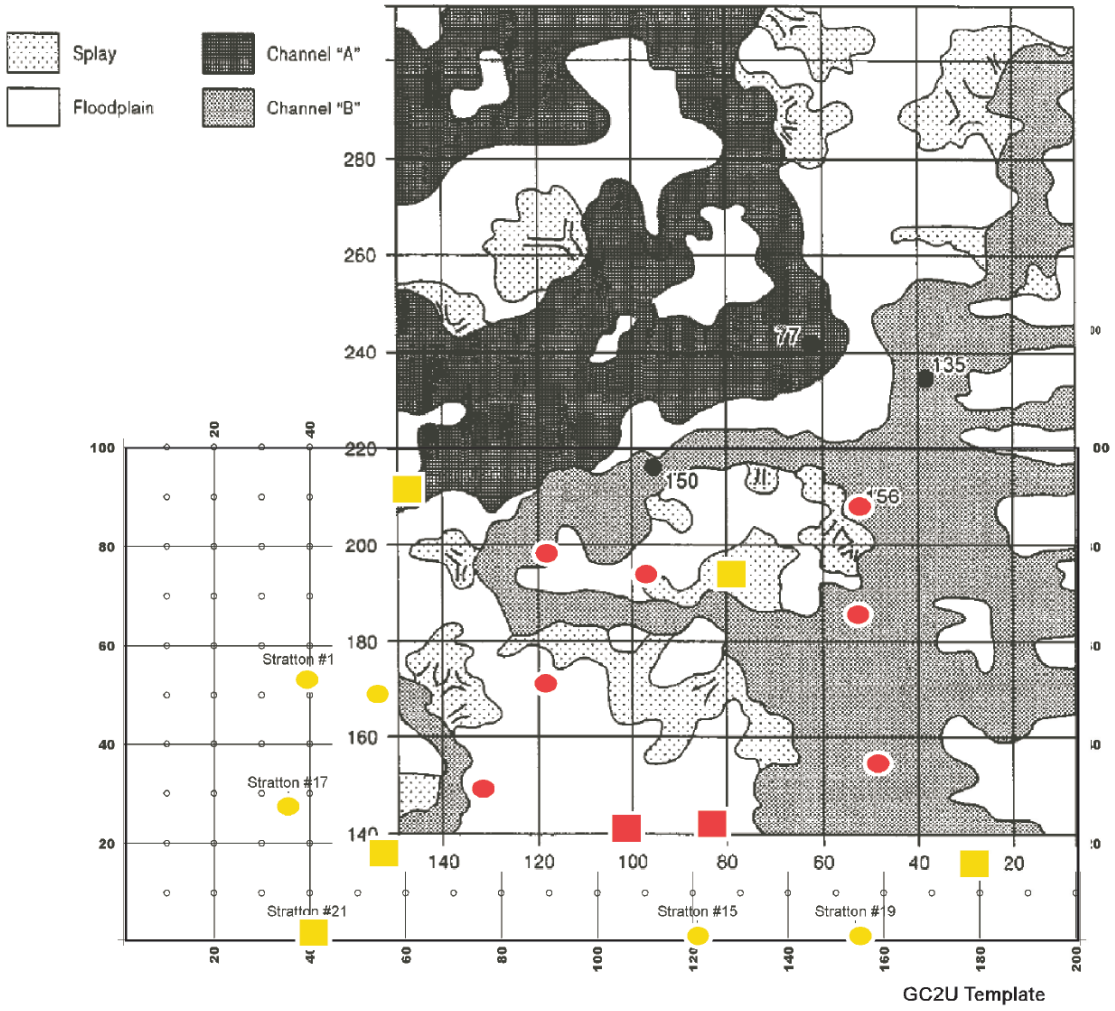

Figure 6.4 Overlay of Hardage (1994), Figure 18 with GC2U scoring template

6.6 Sequence Timing and Fluvial Model Refinement

From the Hardage model and from the model wells of this study, we begin with an image of a river trending north-northeast to south-southwest. A cross-section perpendicular to the river-way through wells 9, 20 and 8 is shown in Figure 6.5. In the cross-section well 8 seems to have some displacement that relates to either geology or wireline depth measurement. As the channel sands amalgamated westward, an extensive splay caps the well 8 channel sands; this splay that can be tracked to the south extending to wells 14 and 19.

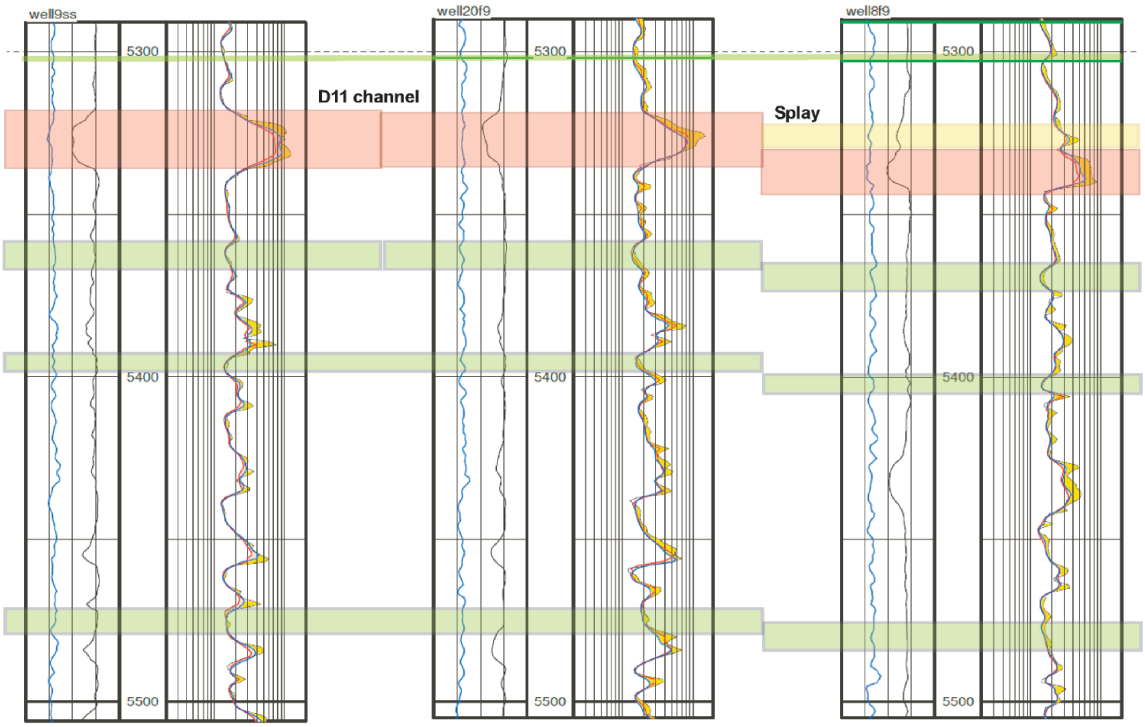

Figure 6.5 Well log cross-section through wells 9, 20 and 8

To predict an exit point for the river-way we can correlate splaying events: west of the hypothetical river-way, wells 12, 18, 17, 6 and 21 have stacks of coarse grained splays occur and several splays can be correlated between these wells. In the eastern area of wells 15, 19 and 14 we can correlate several extensive splays. The eastern splays do not correlate well with the western splays: the eastern splays start earlier and are thin (e.g. ~10 feet) extensive splays,

while the western deposits have a more mixed/levee character with limited extent. This east-west difference suggests that the river exited the study area between well 15 and well 21.

Given the assumptions above a fluvial model is interpreted using the recipe:

1. the class map from the NN classifier can outline the river-way using the channel class,
2. the river-way is inferred to enter the study area from the northeast side of the top and exit the base of the study area between well 15 and 21,
3. and, the high amplitude patterns in the time-slice at 80 ms corresponds to splays.

Given these assumptions a map-view of the fluvial model interpretation is drafted in Figure 6.6.

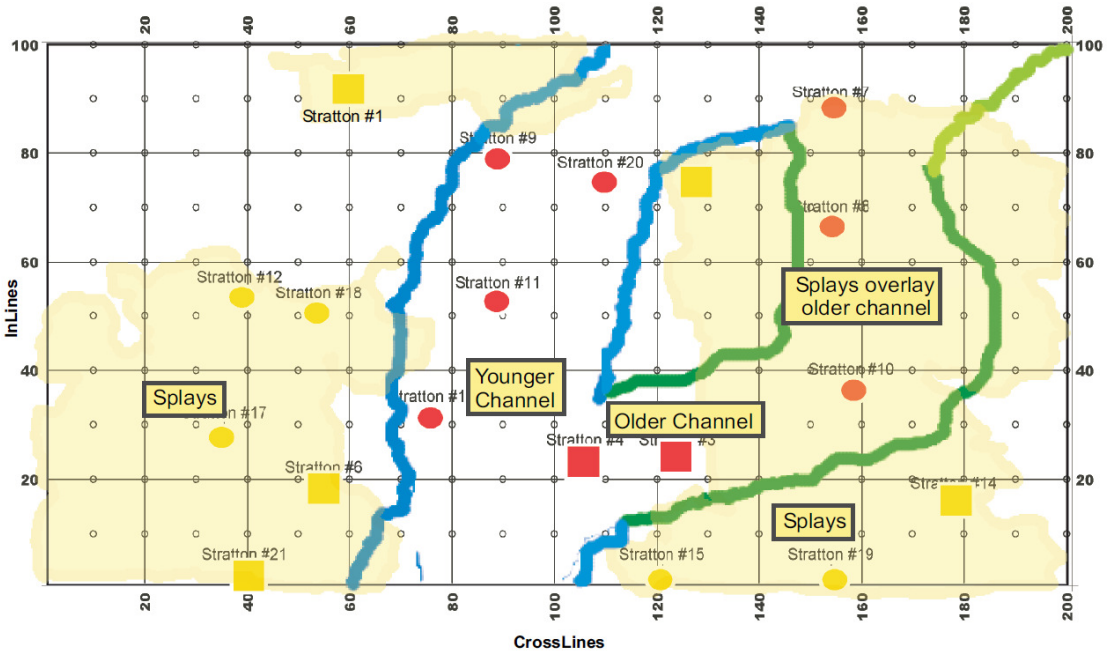

Figure 6.6 Interpreted fluvial model from wells and seismic

CHAPTER 7

CONCLUSIONS AND RECOMMENDATIONS FOR FUTURE RESEARCH

The study cube of this research offers a unique data set for testing inversion techniques in fluvial reservoirs. The dense well coverage in the 2-mile by 1-mile survey is used to develop twelve high-resolution, high quality stratigraphs and seven lesser-quality stratigraphs for testing inversion performance. Further, a set of continuous strata atop of the study area creates a seismic tuning response, this is exploited to establish a tie-point between the time-based seismic and the depth-based stratigraphic model from the well logs.

In Chapter 2, the time-to-depth analysis shows that using the T-D chart derived from the Vertical Seismic Profile (VSP) of well 9 (provided with the BEG data set) results in a 12 ms offset between the VSP and the 3D trace at the tie-point (C38 Boomer). Further, research on velocity dispersion in thin-bed models would suggest that the mismatch between the VSP (T-D chart) and the 3D seismic will worsen with depth.

The analysis in Chapter 3 used the synthetic seismic from the 12 model wellbores as ideal signals; these are compared to the proximal seismic traces to examine the spread of information. In conclusion these results may be overly pessimistic since the analysis was conducted over the entire study cube. The information spread at a specific point in the study cube is the combination of the T-D chart inaccuracies and lateral heterogeneities in the velocity model.

Given the concerns of Chapters 2 and 3, an artificial neural network classifier was designed and trained using a broad segment of the seismic trace near the wellbore locations; these segments were then assigned a class based on well log analysis. To test this process, three “hunts” were described in Chapters 4, 5, and 6 that track a reservoir sand body. Using the

trained network, all 20,000 traces in the study cube were processed to generate a facies-class map of the 3D survey for the search target.

The time-slices in the search window were scored and tabulated for each hunt, similar to the original Hardage (1994) recipe. The network design was effective and scored better than any time-slice in the search window at matching the stratigraphic model at the wellbores. Given an effective network design the training data was analyzed by a sub-setting program to identify the most potent time-slice in class discrimination. Using the neural network classifier map, the most potent time-slice, and well log data, a fluvial model was drafted for each of the three hunts.

In utilizing neural networks there is an obvious concern of forced results or memorization, but the linkage of the time-slice scoring, the sub-setting of the training data, and the wellbore models suggests the network has established a relationship to the scattered information. In the traditional seismic workflow the synthetic seismic is used to tie a specific formation to a specific seismic horizon. However, in the BEG cube this tie is not straightforward. By establishing a wellbore geologic model and then using the neural network to sort through a broad aperture we achieve a tie between the depth-based target and the time-based seismic information. The NN classifier achieves better results than a single time-slice by incorporate some of the interfering effects such as lateral heterogeneity in the training. The T-D chart is typically used as an average time-to-depth mapping for the entire seismic cube; similarly, the most potent time-slice demonstrates which time best matches the target depth as a lateral average. In the results of the search processes is time targeting information that can be exploited to improve the T-D chart. Consider the graph of the time difference between the target and the most potent time-slice in Figure 7.1

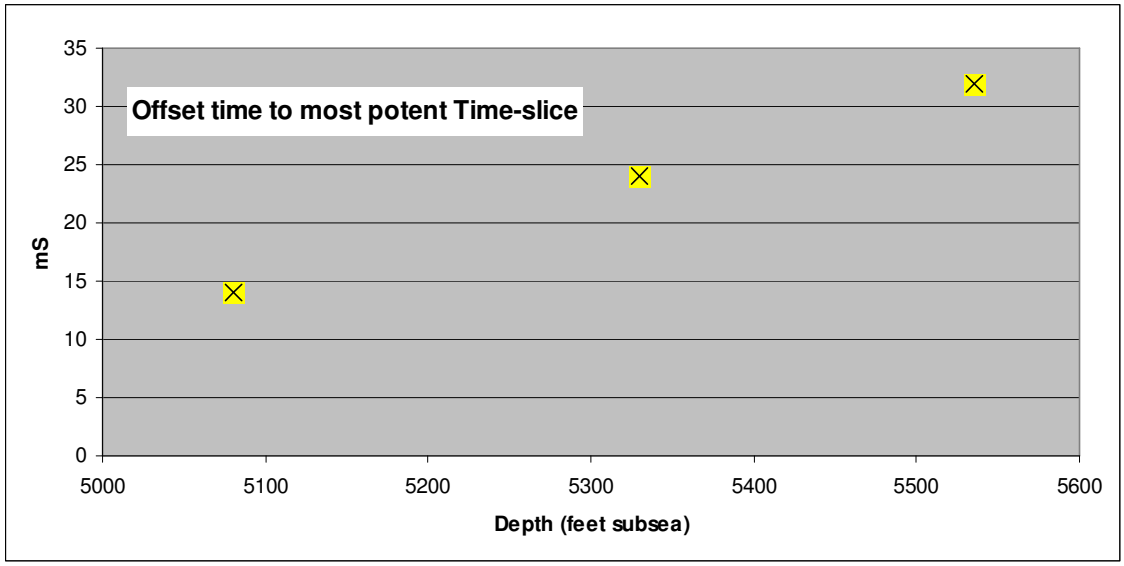

Figure 7.1 The offset between the targeted time (T-D chart) to the most potent time-slice found in the three Hunts.

Hunt GC1U is 50 feet below the tie-point and the most potent slice is 14 ms below the target, similar to the mismatch noted at the tie-point. Hunt GC2L (Chapter 4) was the deepest target and the most potent time-slice is offset by 32 ms. Given this data, a more accurate T-D chart could be determined to account for velocity dispersion. With better T-D chart accuracy we can expect better results using the Hardage or Pennington recipes. This has broad appeal since processing the attributes of time-slices or horizons are available with seismic processing platforms such as Seismic Micro Technology Kingdom Suite.

Another interesting result of this research: In the three hunts of Chapters 4, 5, and 6, the reservoir sands are best identified in the time-slices as “phantom thalwegs” where the reservoir sand is a trough rather than a peak in the seismic. Possible causes for this response:

- The seismic is inverted.
- The peak is subject to more interference than the trough, so we see the trailing trough more clearly.

- The channel has a higher degree of anisotropy than the flat-laying floodplains and splays and thus is a poor reflector.
- The finely layered floodplains and splays respond as a low-permeability, thick-bed in the effective media model (Backus Averaging) where the channel sand complex responds as a solitary thin bed with permeability.

7.1 Recommendations for Future Research

1. To test if these results are specific to the BEG cube, the processes could be refined and tested on a different seismic survey. Of particular interest: development of paradigms for surveys with sparse well coverage, and, application to other Frio 3D surveys.
2. In Figure 3.3, the exaggerated time-relief of horizons was questioned given the assumption of flattened strata. Lateral heterogeneities in bed thicknesses and gas saturation cause lateral uncertainty in time-targeting. Figure 7.2 plots the flattened seismic through five wells. Plotted on the seismic line at the well locations are the tops of the E41 sand and the base of the high ash content based on the project T-D chart. Similar to the sand associated with the C38 Boomer, this surface is interpreted as an erosional unconformity. The data in Figure 7.1 would predict that a target at 210 ms will appear in 3D seismic 54 ms later. So a useful hypothesis is: the strong reflection at 260 ms is the E41 sand. What is the utility of proving this hypothesis? If gas saturation and/or thin-beds can be functionally linked to this time-relief, maps of this “velocity push-down” could be developed as an exploration tool.

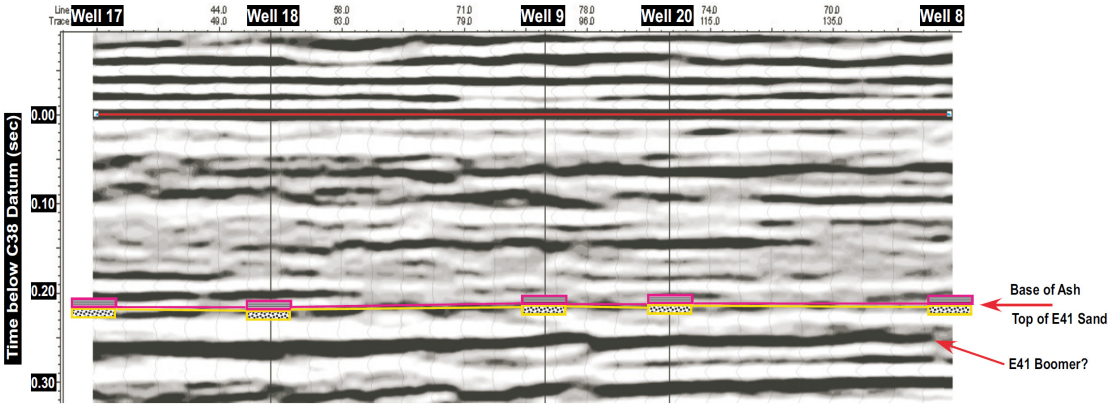

Figure 7.2 Flattened seismic line through wells 17-18-9-20-8 with the E41 sand and the base of the high ash content marked at well locations

3. Better understanding of the "phantom thalweg" response is important, particularly as applied to other fluvial reservoirs and seismic data sets. Using Frio-like parameters for geometry and elastic properties, a simple inductive model for the reflectivity of a channel could be developed. This reflectivity model could be used to test parameters such as thin-beds, anisotropy, permeability, and gas saturation to see if the response is deterministic and can be applied to other seismic surveys in fluvial reservoirs.

APPENDIX A

DETAILS ON PROCESSING WORKFLOW

Details on Processing Workflow

The BEG Stratton field data set comes on a distribution CD with the SEG-Y seismic file and text files for the well-logs, VSP data and documentation. This project is also loaded in the Seismic-Micro Technology, Kingdom Suite as a demo project. Seismic data management and plotting of seismic vertical and time-slices are done with the Kingdom Suite package. Fugro-Jason Power-Log was used for Data management and plotting for the well logs.

For each of the NN classifier hunts a subset of the flattened seismic is extracted for processing as diagrammed in Figure A.1. The seismic is flattened to the C38 Boomer horizon as discussed in chapter 2, this horizon is tracked and mapped in Figure 2.2, and the Kingdom suite can flatten the seismic volume and make plots and time-slices. Similar to the time-map of Figure 2.2 the C38 horizon time map can be exported, the grid spacing is set to match the seismic trace spacing and a text file of the horizon is output as C38B Grid File shown in Figure A.1 contains data {X, Y, TWT to the C38 Boomer}. To extract the trace segments a specific-purpose program was written; the user inputs the well 9 start-time and segment length to the program rdSEGY, using the grid file and the user input, trace segments are extracted from the SEGY file. The rdSEGY extracts segments referenced in time to the C38 Horizon by using the grid file for the trace flattening offset; this program also translates the SEG-Y format into textx format. The data in SEG-Y format is written in various archaic computer tape formats, in the case of the Stratton field the traces are in IBM 32-bit floating point, so the rdSEGY must bit-decode and translate the traces. The output from the rdSEGY program is a text file that is formatted as: X, Y, Trace(start time)….Trace(end time) where X and Y are the 200 by 100 trace locations (i.e. 20,000 trace segments). Individual traces from the flattened seismic can be exported as text from the kingdom suite, these were used as quality checks of the processing.

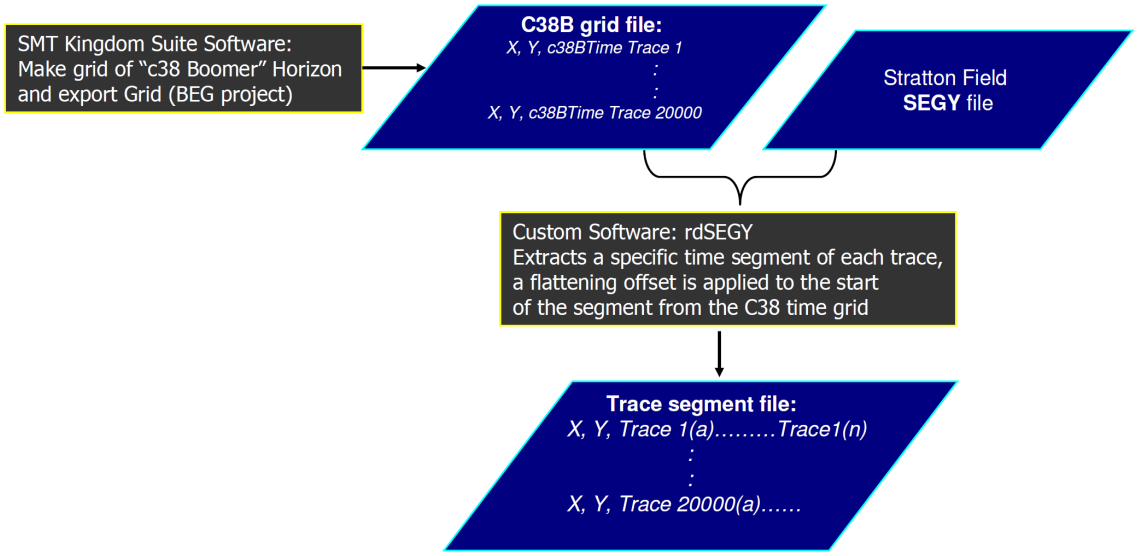

Figure A.1 Extracting Trace segments from the flattened seismic volume

The next step involves training the NN Classifier. The Trace Segment File is imported to Microsoft Excel as shown in Figure A.2 and trace segments adjacent to the well bores are sorted into a network training file. For the specific target of the hunt, each well bore is assigned a class by log-analysis/human-discretion and this class is assigned to seismic traces proximal to the wellbore. The samples of seismic trace segments with assigned classes are used to train a

MLP mapping network using the NuMap7.1 software package refR$. In the Hunts a first network was trained with 5 traces around the 12 model wells (i.e. 60 training vectors), a second network was trained using traces between similar neighboring wells, this augmented training set consisted of 400 to 600 of the 20,000 traces. The network topology and coefficients of the trained network are stored in the Network Weights File as diagrammed in Figure A.2.

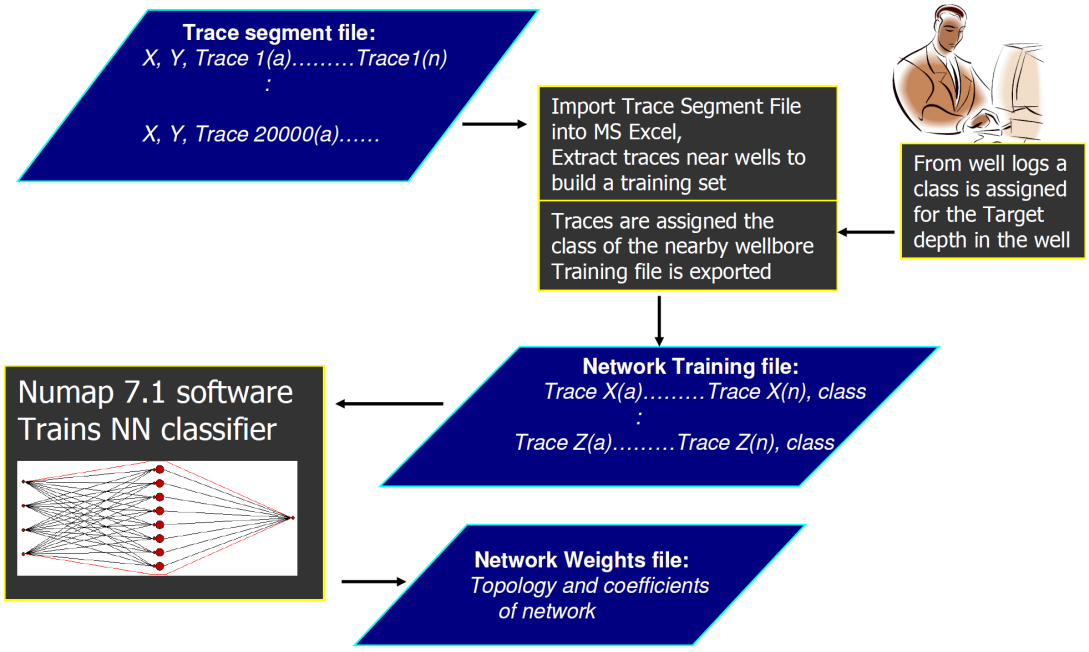

Figure A.2 Training the Neural Network Classifier

Using the trained network the entire Trace Segment File is processed as shown in Figure A.3. The networks outputs a class for each of the 20K trace segments and a class map is plotted. The Network output is imported to a 3-D graphing package (MicroCal Origin) for color contouring; the network output is also processed to generate the confidence maps.

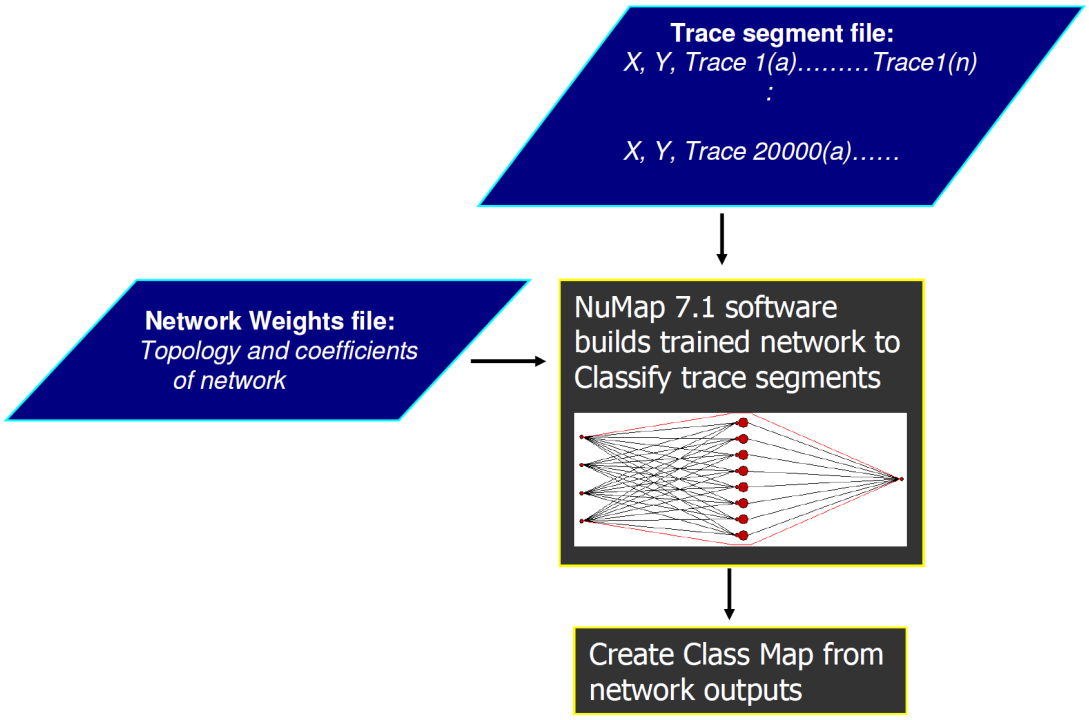

Figure A.3 Processing the Traces to generate facies (class) map

APPENDIX B

GC2L SCORE CARD

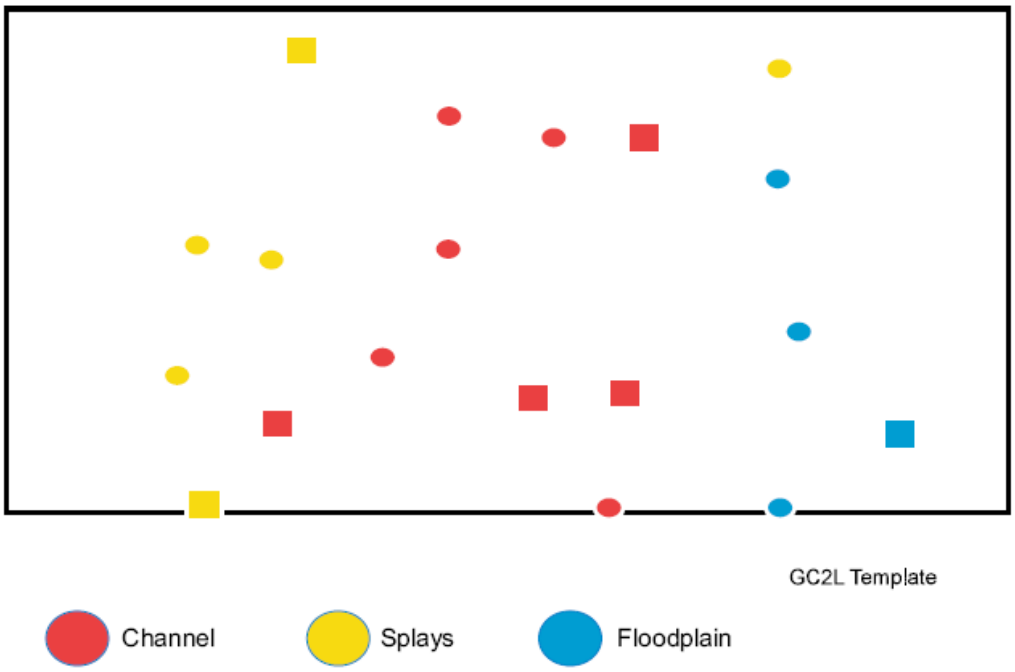

Figure B.1 Scoring Template for channel class in GC2L

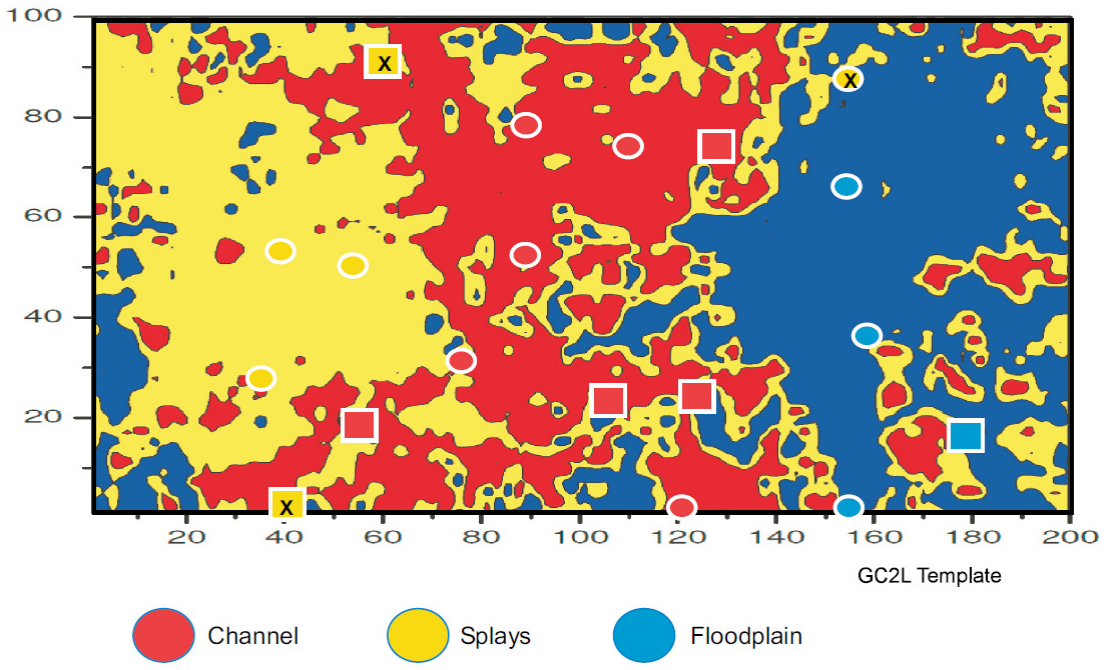

Figure B.2 Map From Neural Network Classifier: Model Wells 12/12, Test Wells 5/7

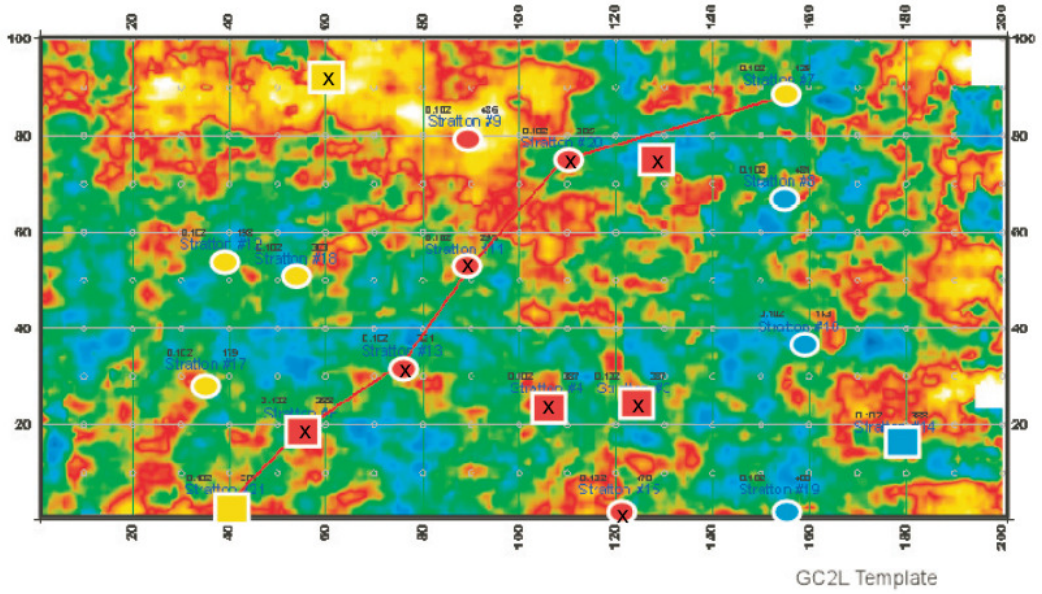

Figure B.3 Seismic Slice at 102 ms: Model Wells 8/12, Test Wells 2/7

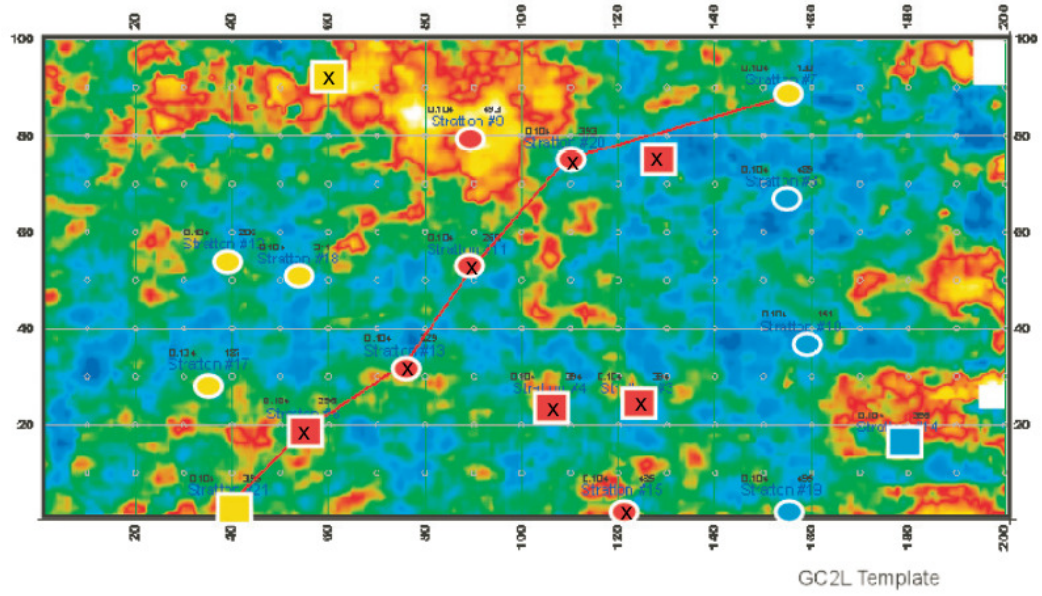

Figure B.4 Seismic Slice at 104 ms: Model Wells 8/12, Test Wells 2/7

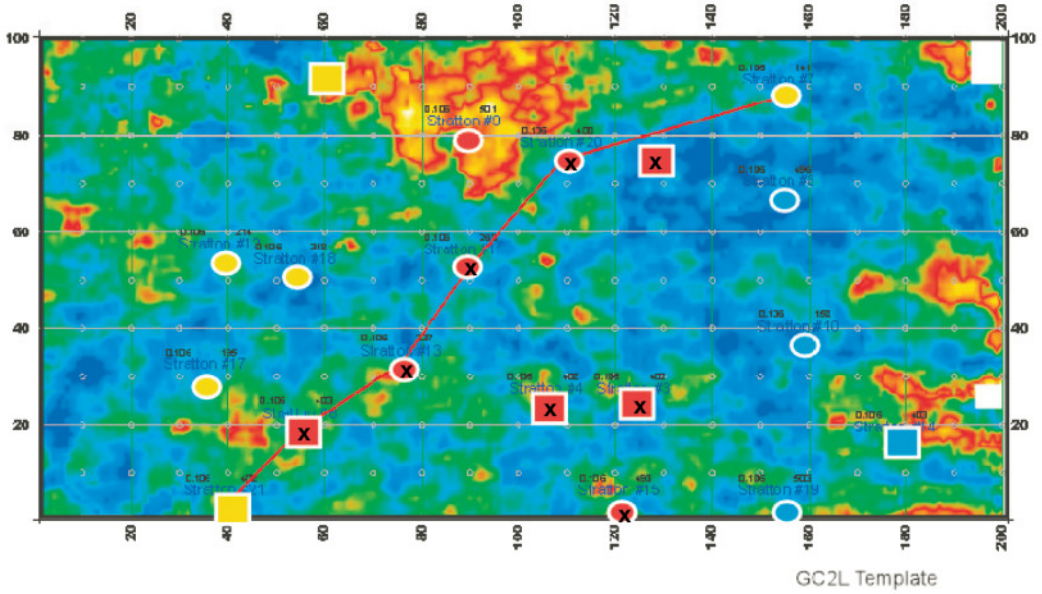

Figure B.5 Seismic Slice at 106 ms: Model Wells 8/12, Test Wells 3/7

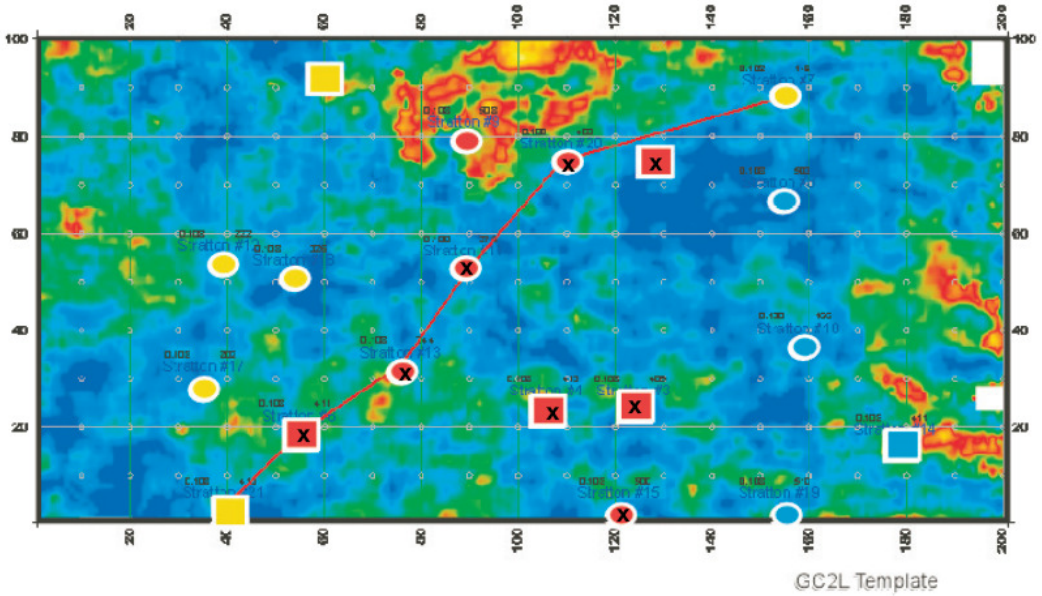

Figure B.6 Seismic Slice at 108 ms: Model Wells 8/12, Test Wells 3/7

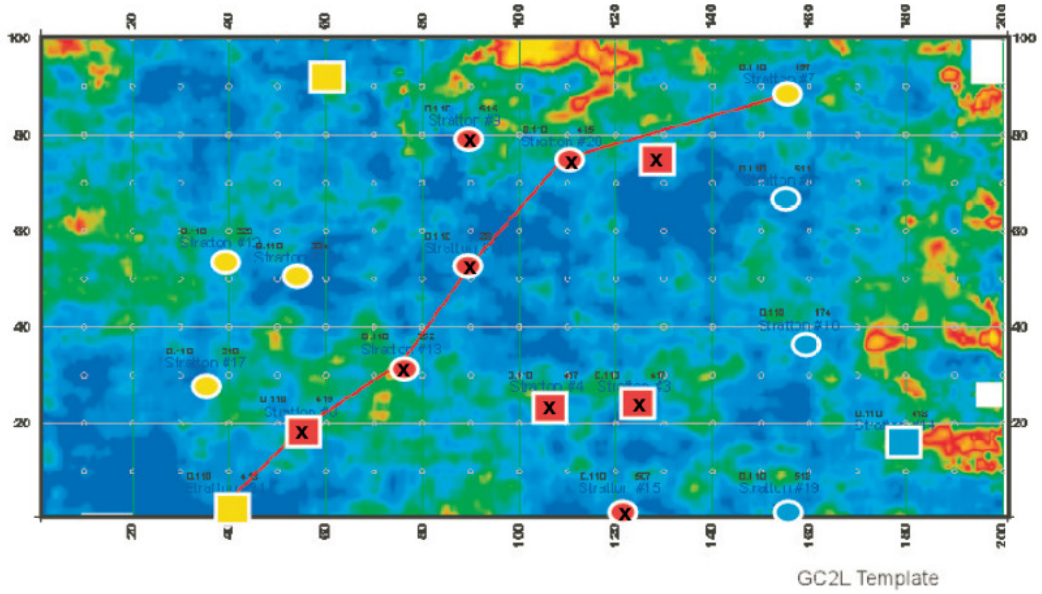

Figure B.7 Seismic Slice at 110 ms: Model Wells 7/12, Test Wells 3/7

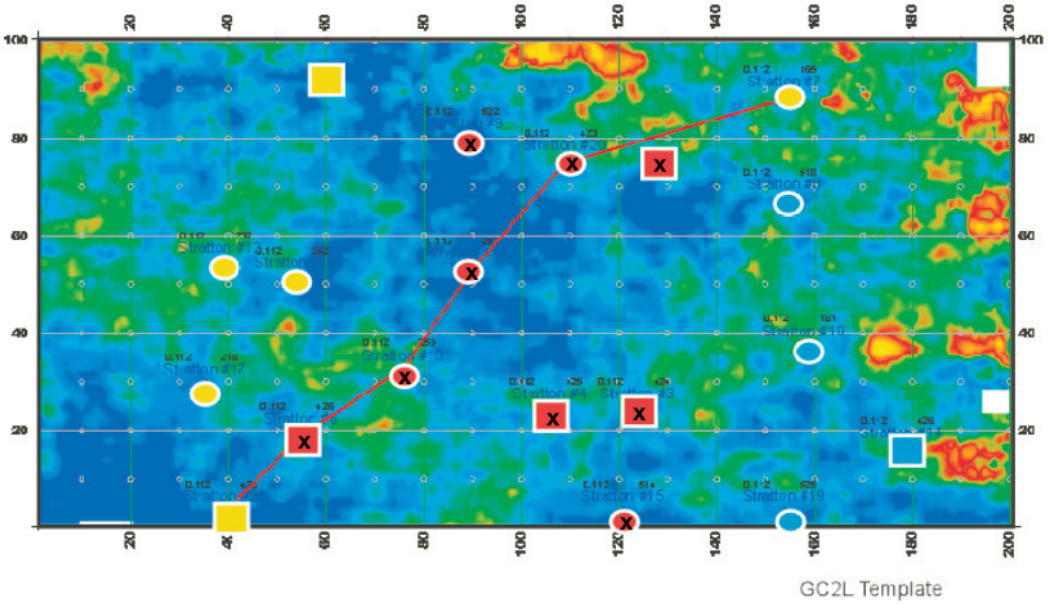

Figure B.8 Seismic Slice at 112 ms: Model Wells 7/12, Test Wells 3/7

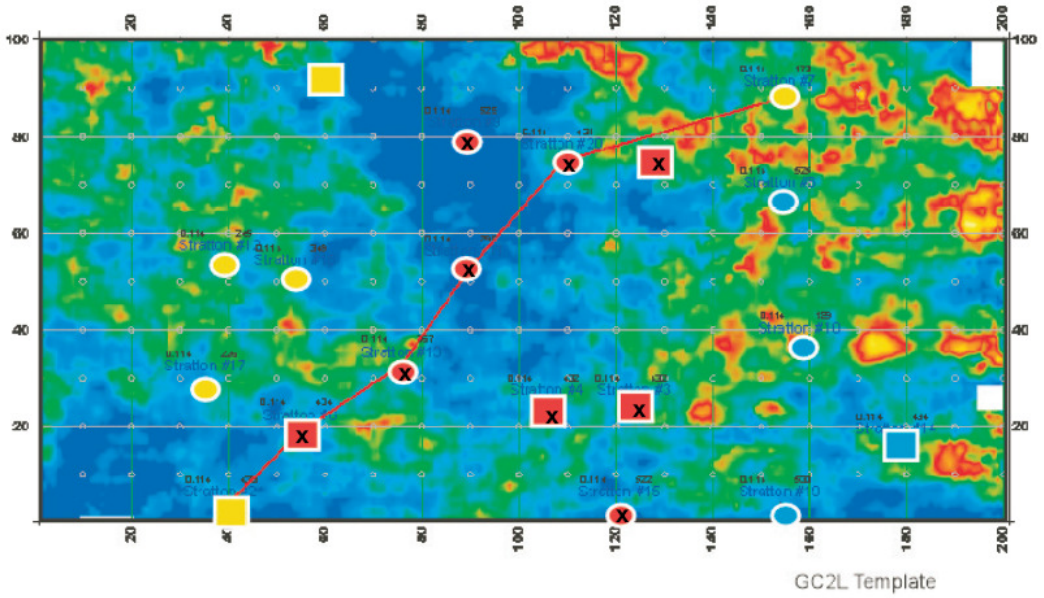

Figure B.9 Seismic Slice at 114 ms: Model Wells 7/12, Test Wells 3/7

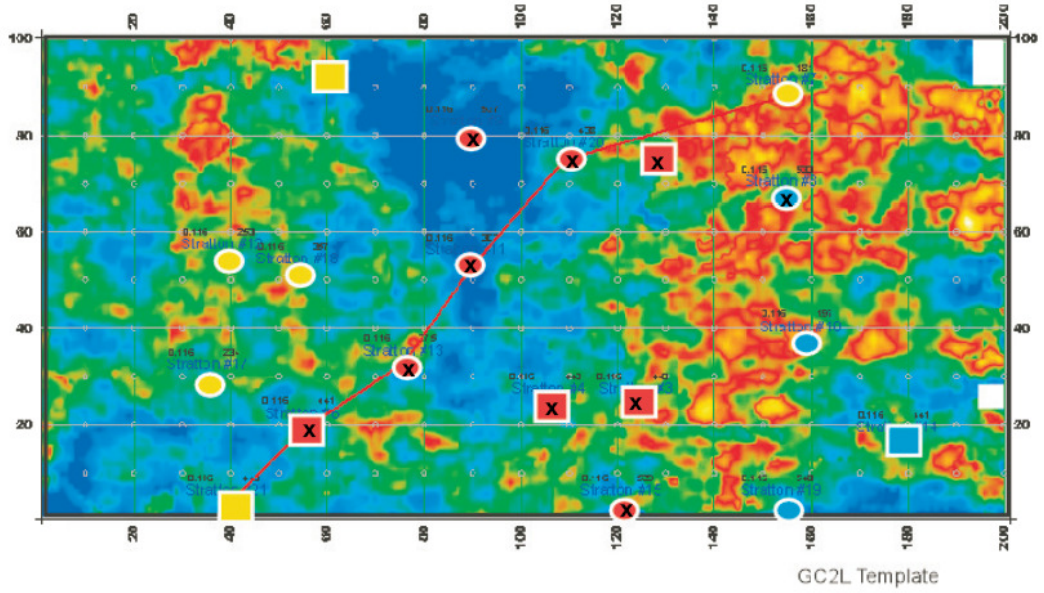

Figure B.10 Seismic Slice at 116 ms: Model Wells 6/12, Test Wells 3/7

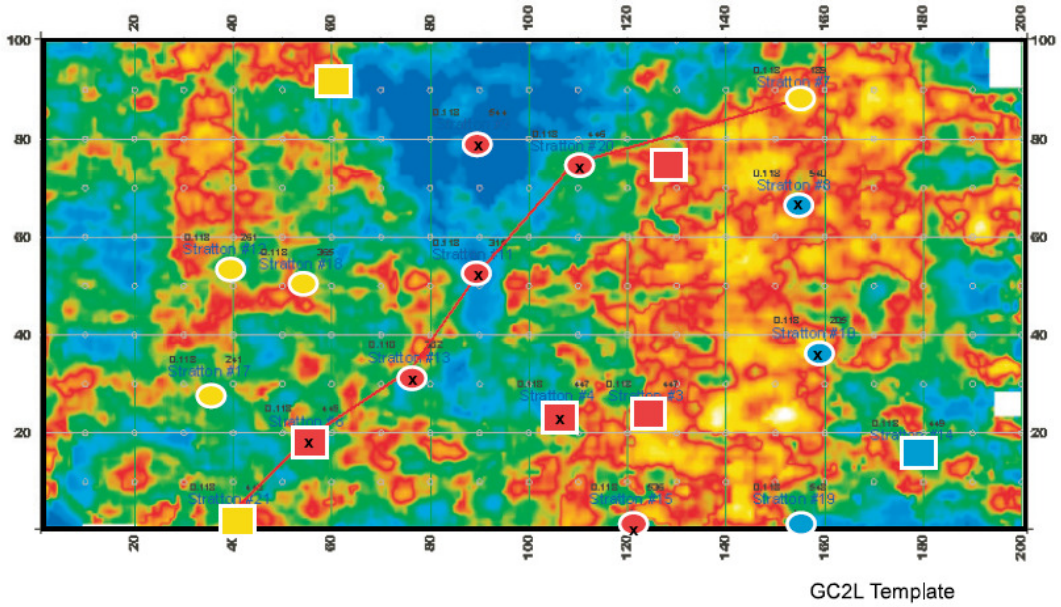

Figure B.11 Seismic Slice at 118 ms: Model Wells 5/12, Test Wells 5/7

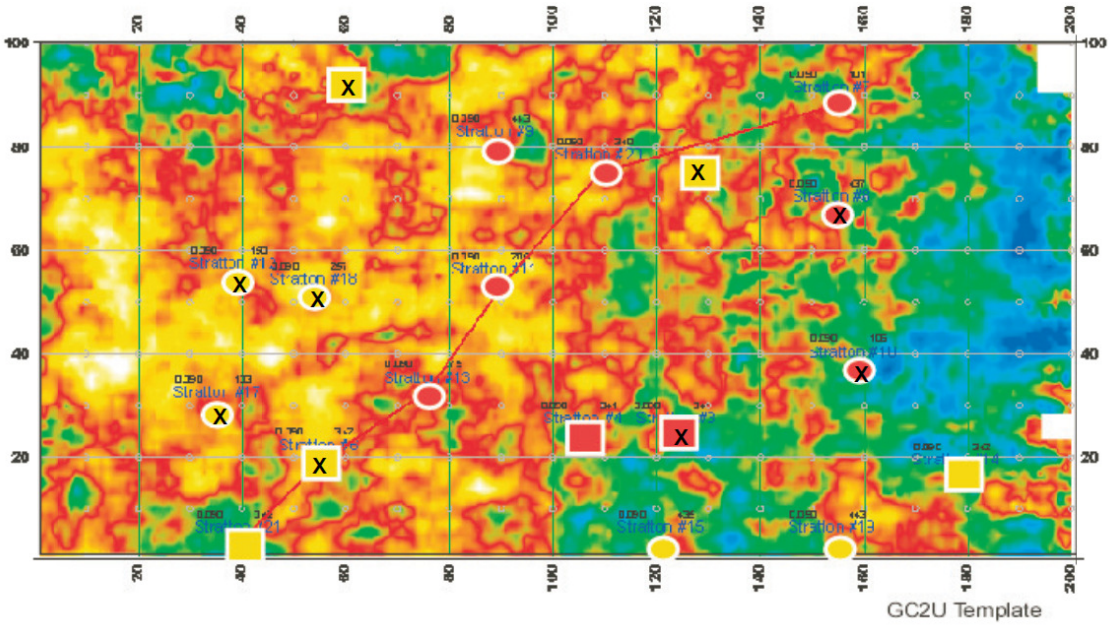

Figure B.12 Seismic Slice at 120 ms: Model Wells 3/12, Test Wells 4/7

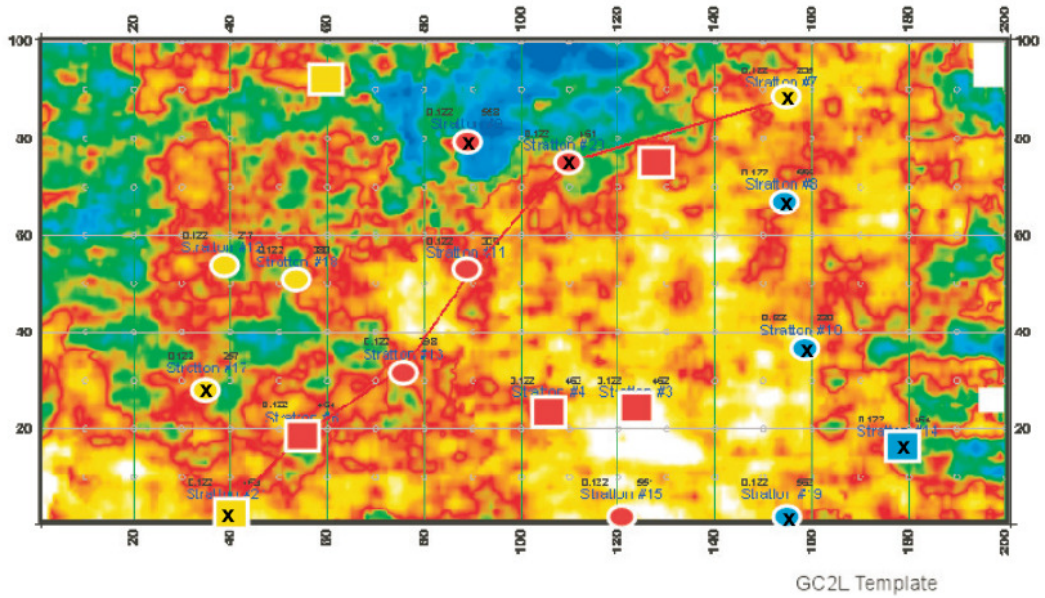

Figure B.13 Seismic Slice at 122 ms: Model Wells 5/12, Test Wells 5/7

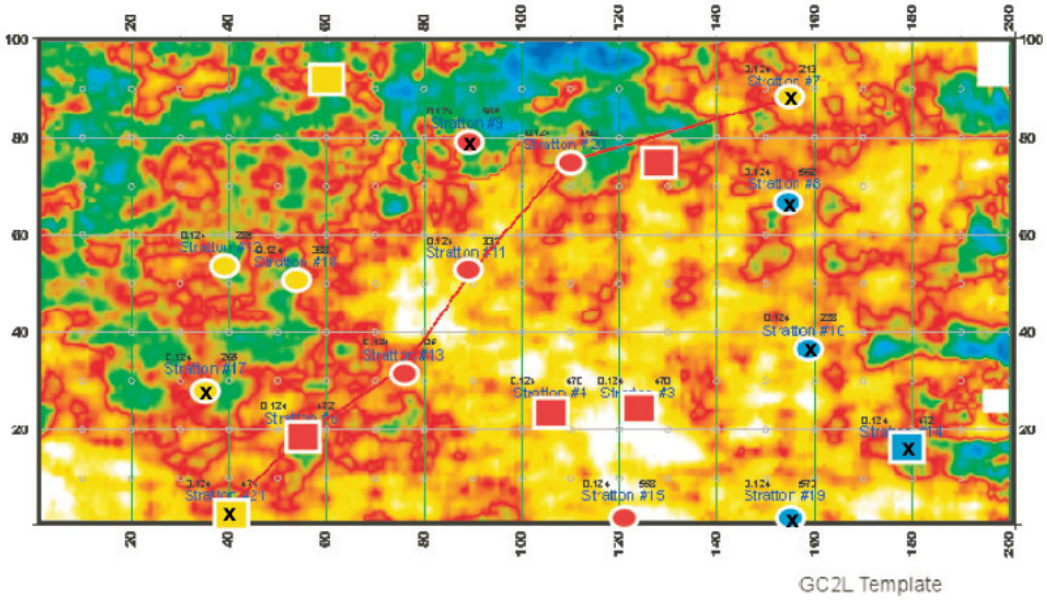

Figure B.14 Seismic Slice at 124 ms: Model Wells 6/12, Test Wells 5/7

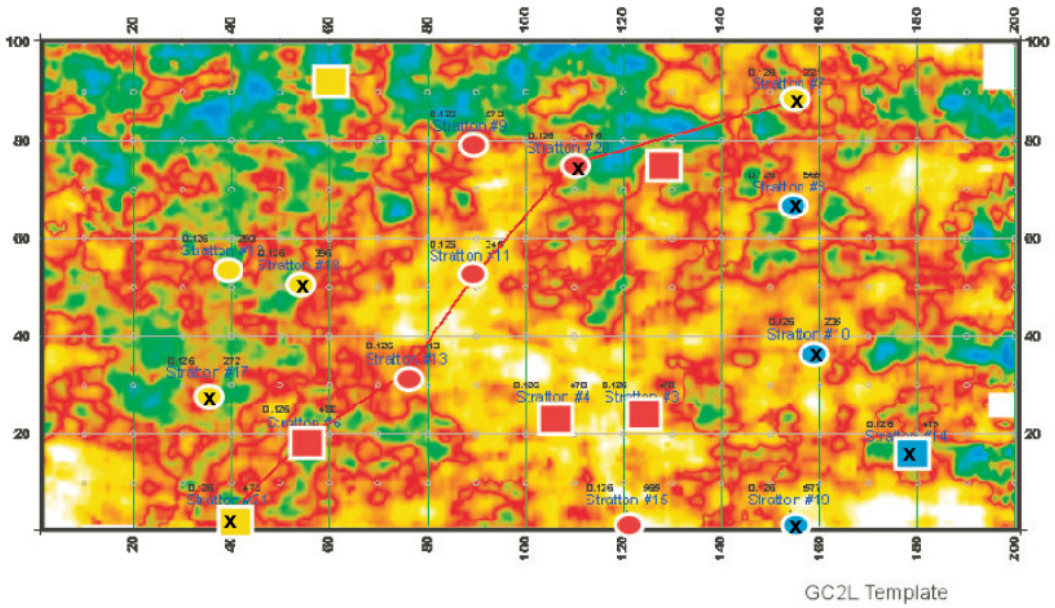

Figure B.15 Seismic Slice at 126 ms: Model Wells 5/12, Test Wells 5/7

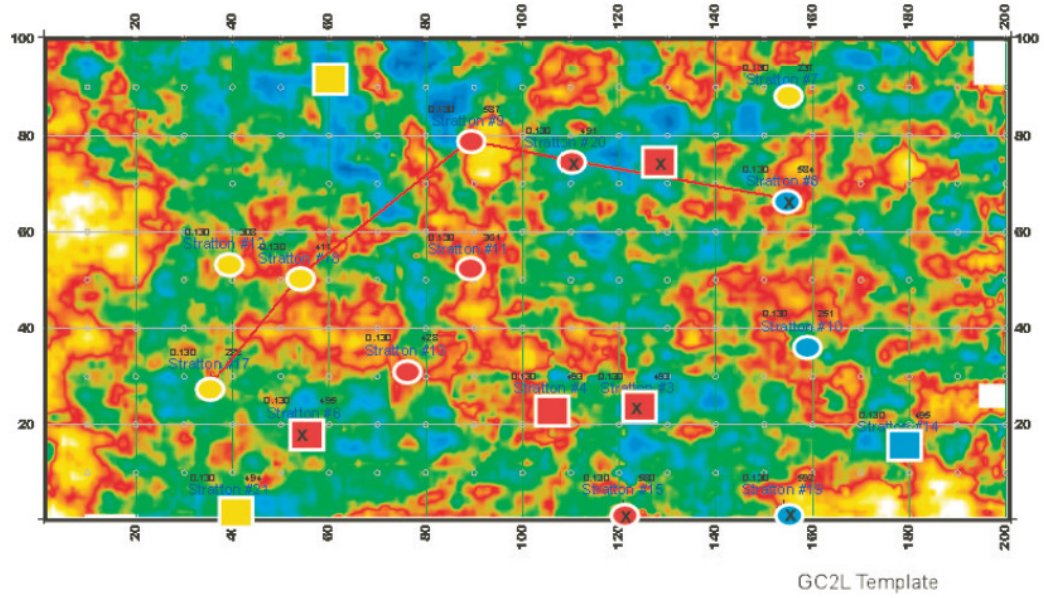

Figure B.16 Seismic Slice at 128 ms: Model Wells 7/12, Test Wells 4/7

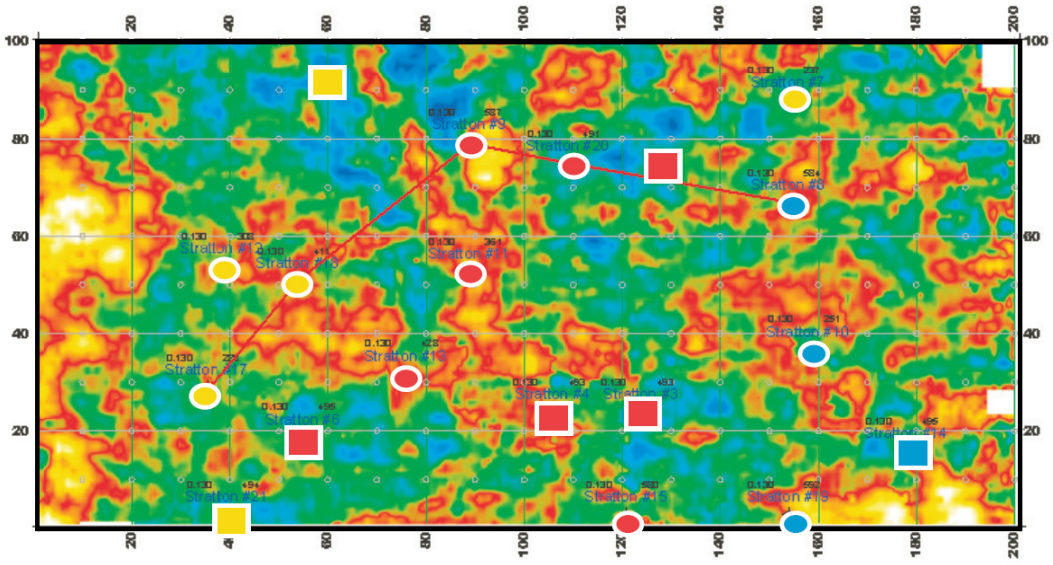

Figure B.17 Seismic Slice at 130 ms: Model Wells 8/12, Test Wells 3/7

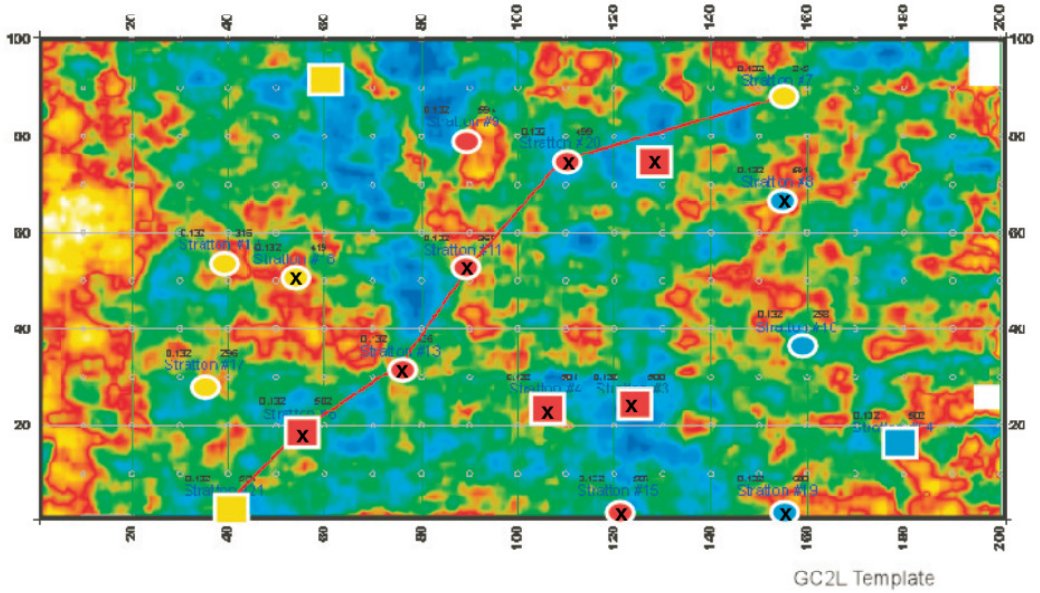

Figure B.18 Seismic Slice at 132 ms: Model Wells 5/12, Test Wells 3/7

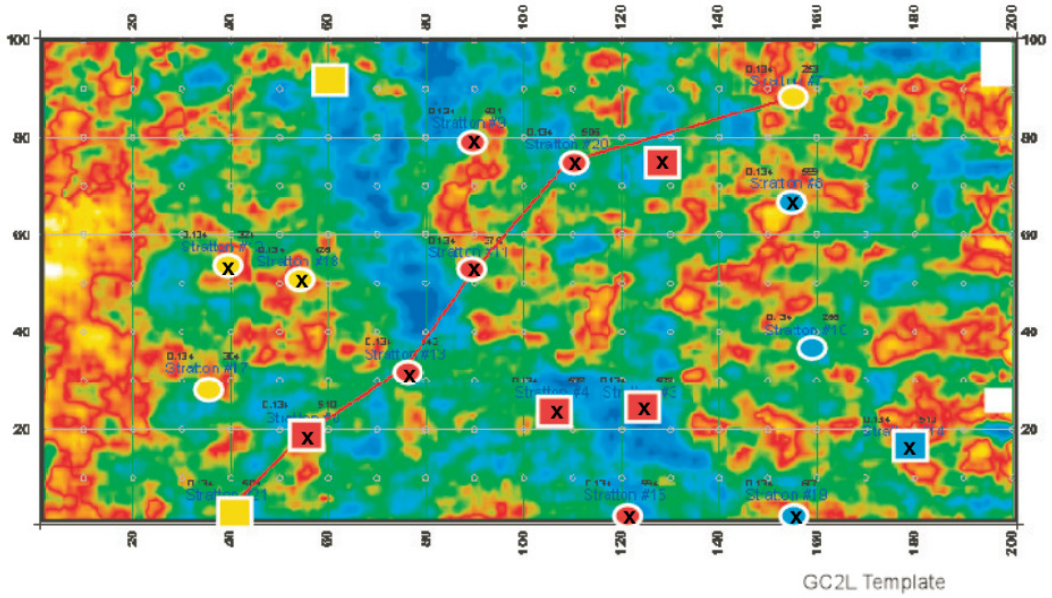

Figure B.19 Seismic Slice at 134 ms: Model Wells 3/12, Test Wells 2/7

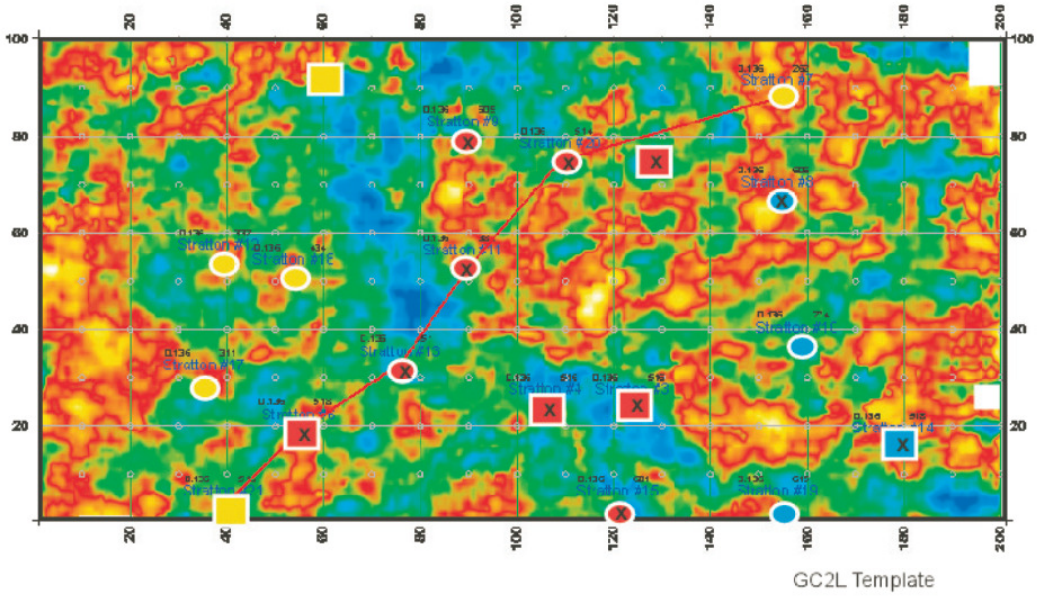

Figure B.20 Seismic Slice at 136 ms: Model Wells 6/12, Test Wells 2/7

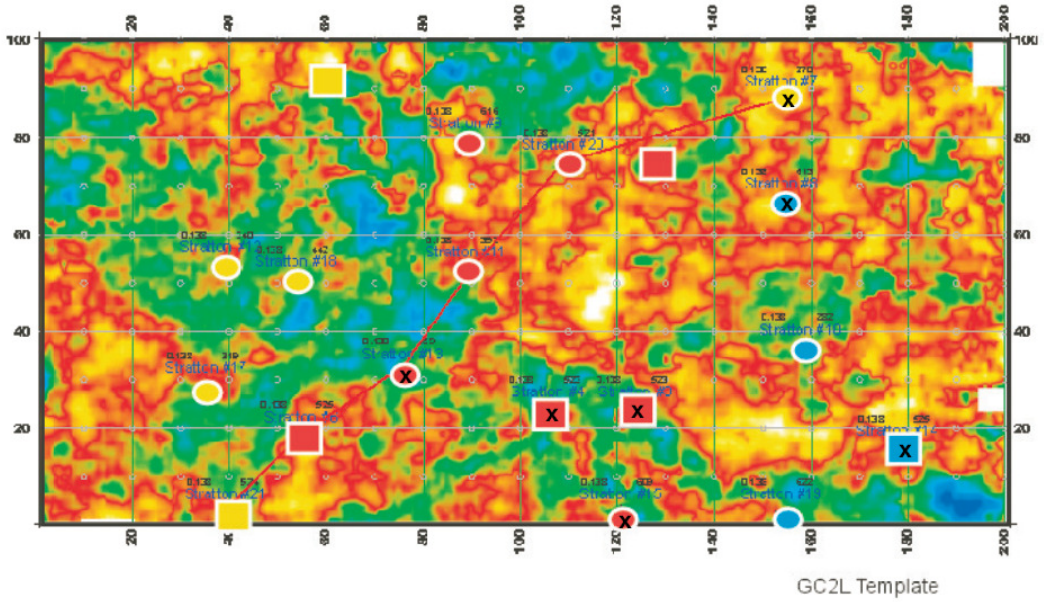

Figure B.21 Seismic Slice at 138 ms: Model Wells 9/12, Test Wells 4/7

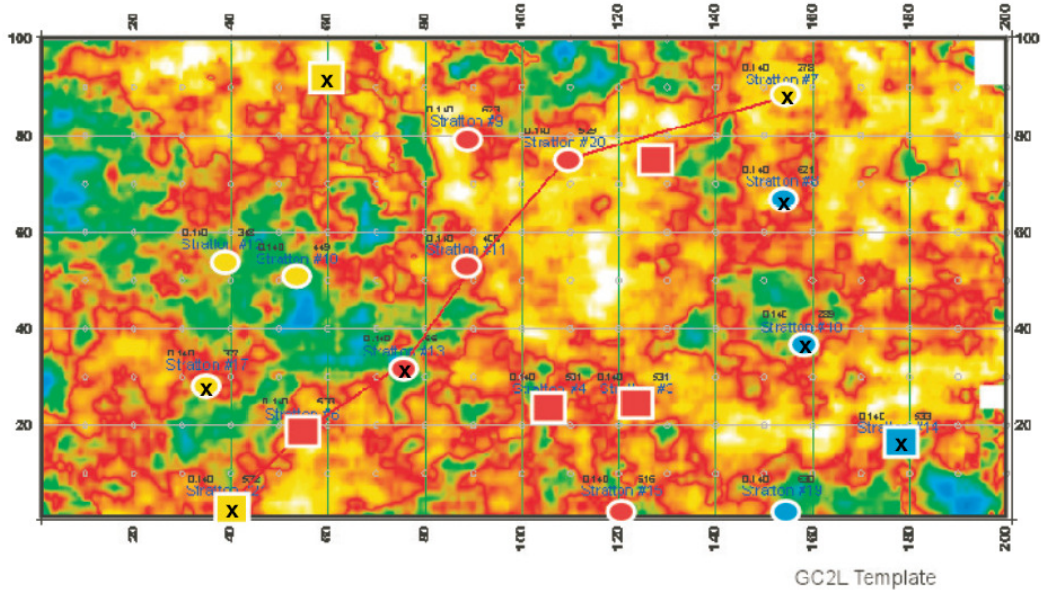

Figure B.22 Seismic Slice at 140 ms: Model Wells 8/12, Test Wells 4/7

APPENDIX C

GC1U SCORE CARD

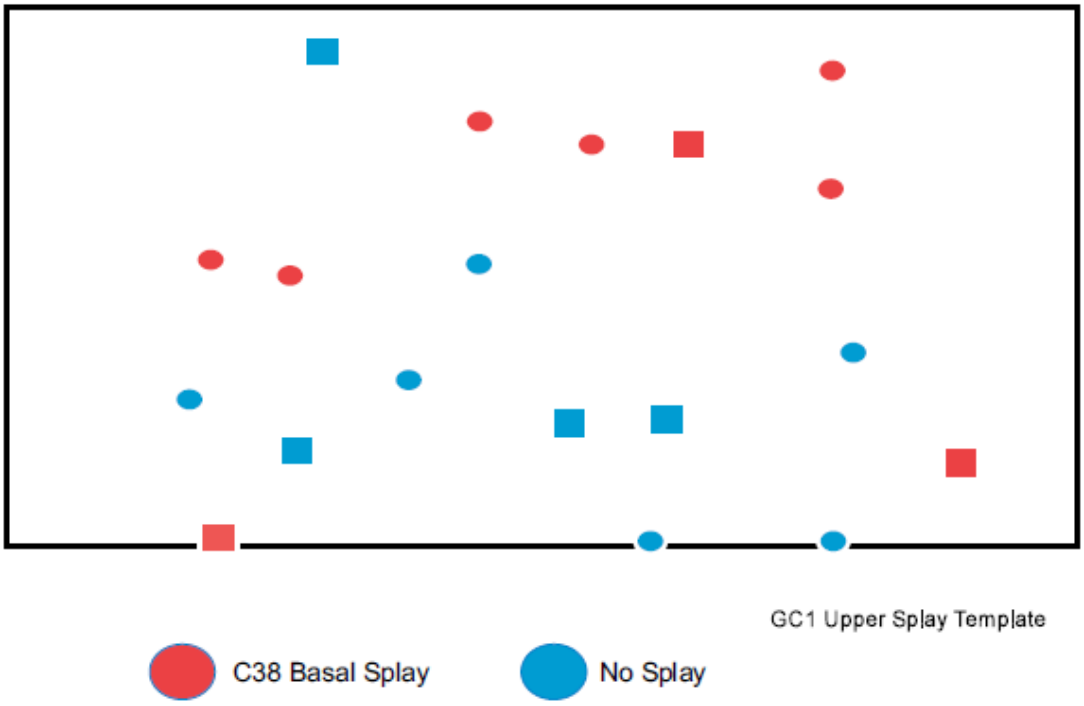

Figure C.1 Scoring Template for Basal splay In GC1U

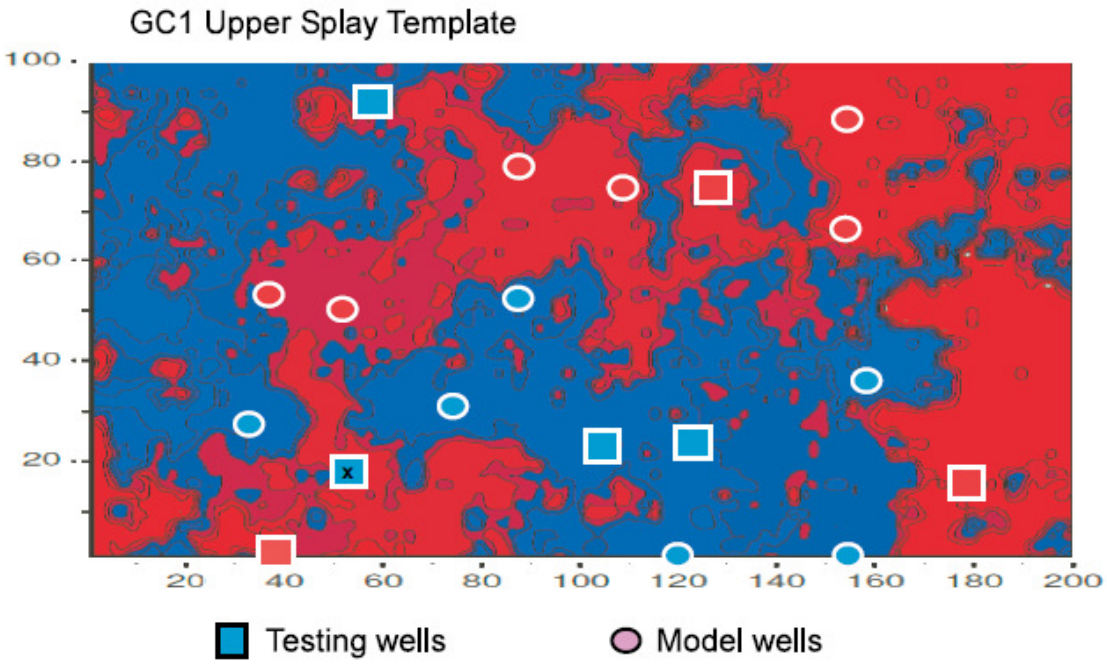

Figure C.2 Map From Neural Network Classifier: Model Wells 12/12, Test Wells 6/7

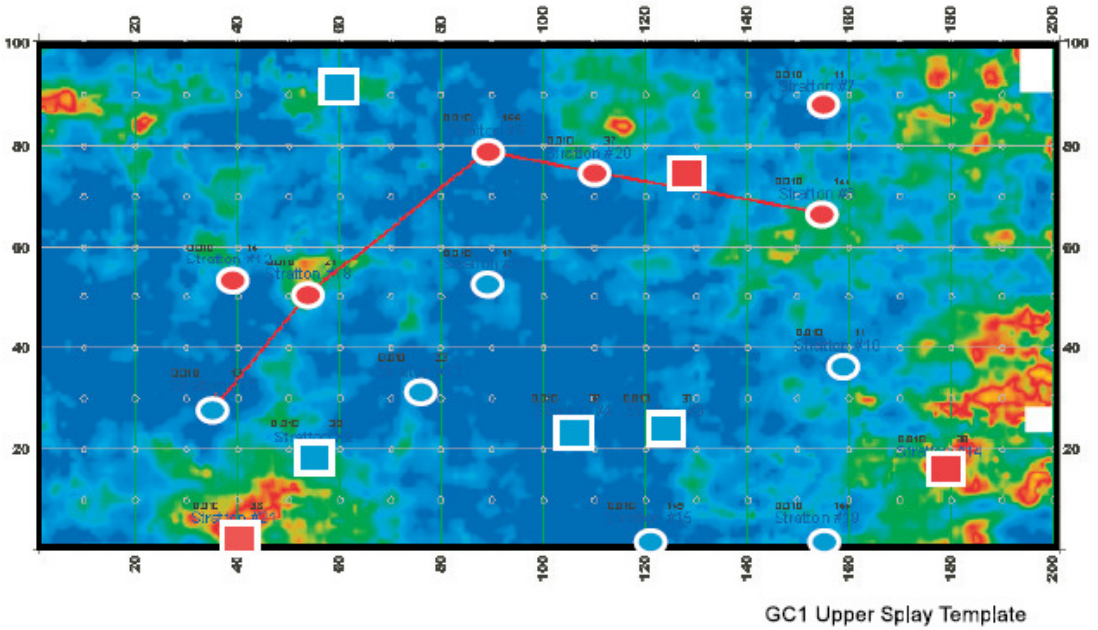

Figure C.3 Seismic Slice at 10 ms: Not scored, all trough

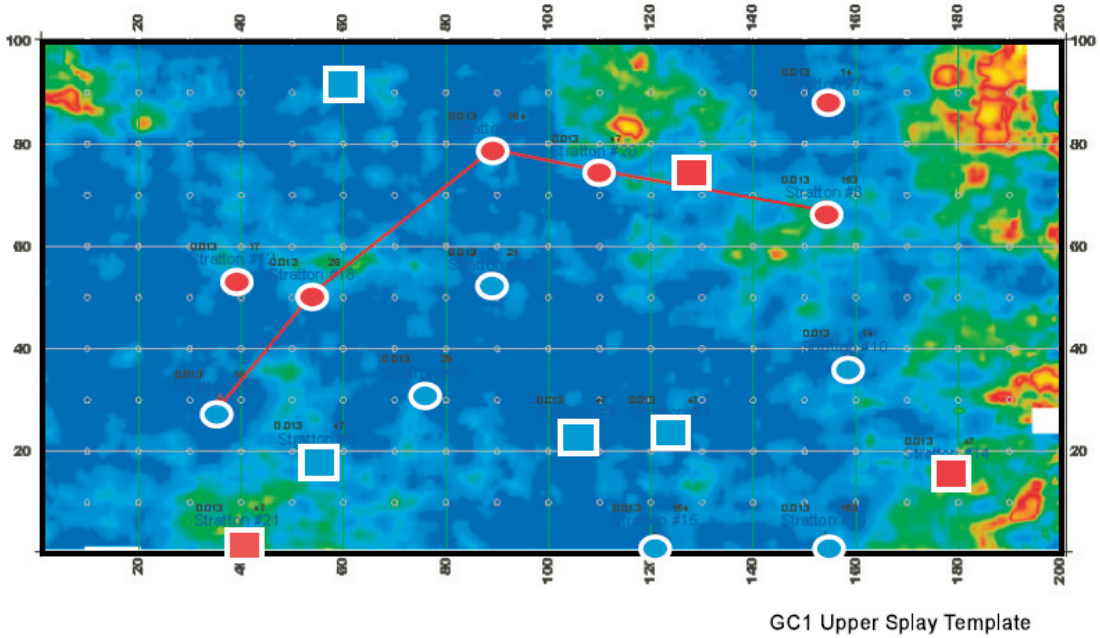

Figure C.4 Seismic Slice at 13 ms: Not scored, all trough

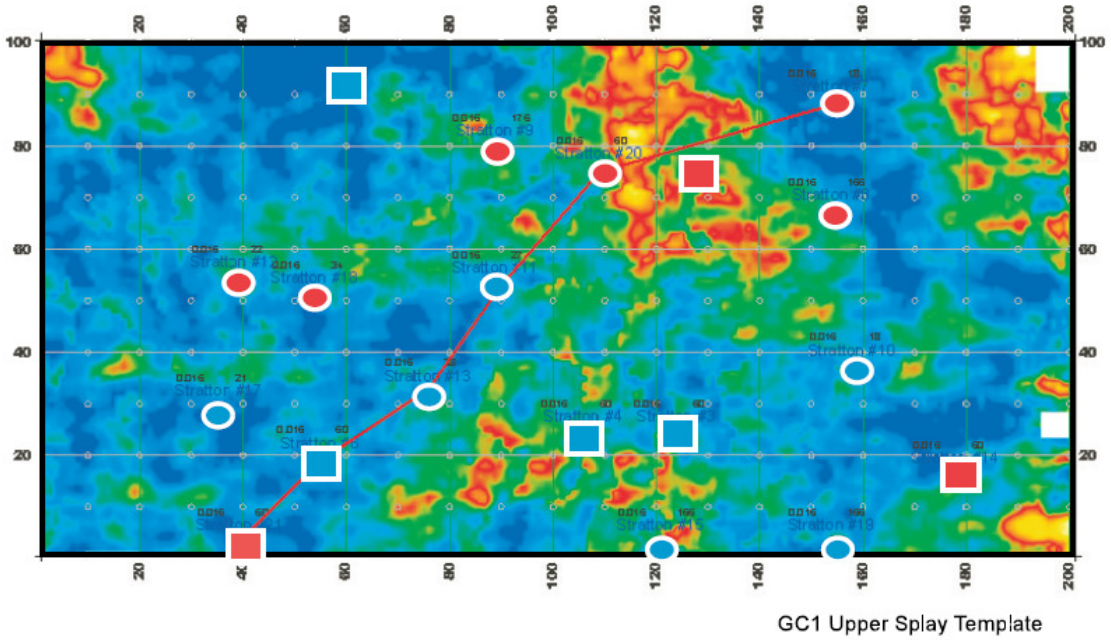

Figure C.5 Seismic Slice at 16 ms: Not scored, all trough

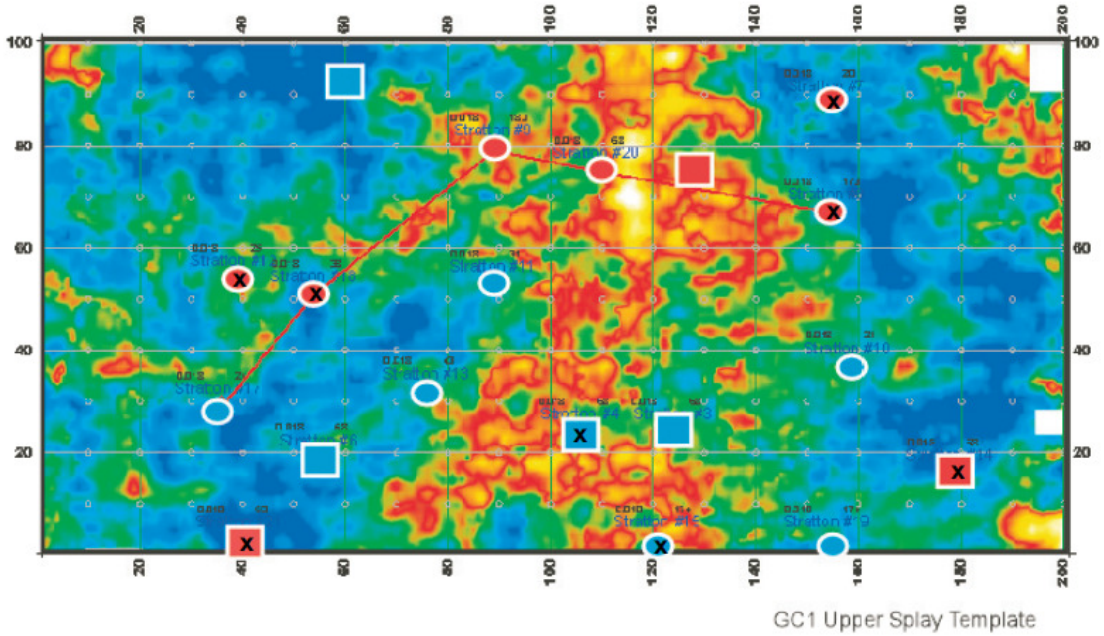

Figure C.6 Seismic Slice at 18 ms: Model Wells 7/12, Test Wells 4 /7

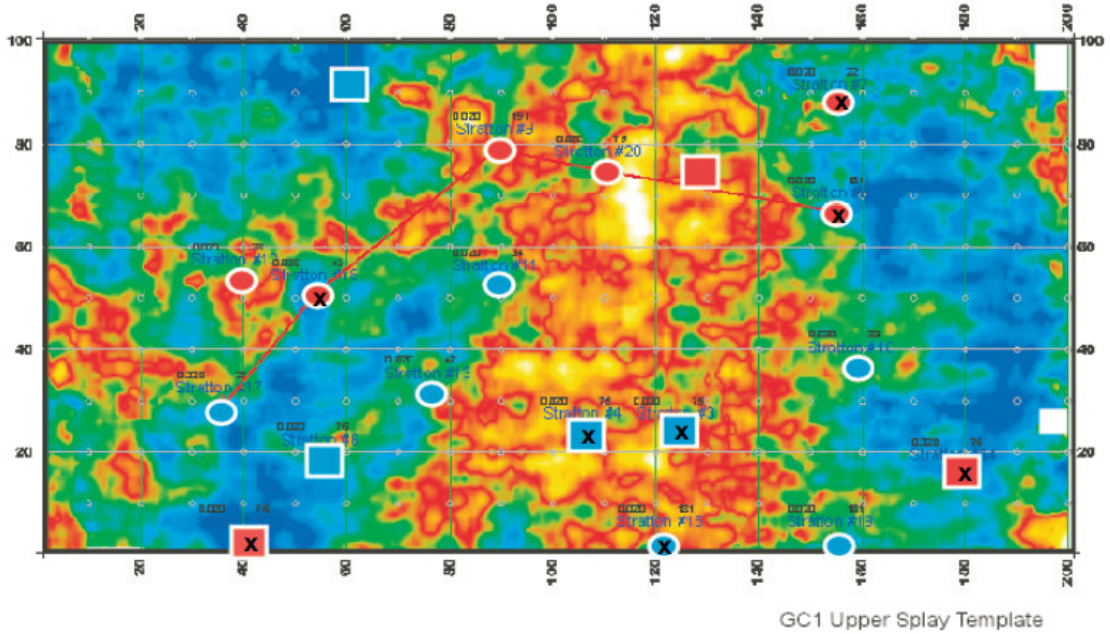

Figure C.7 Seismic Slice at 20 ms: Model Wells 8 /12, Test Wells 3/7

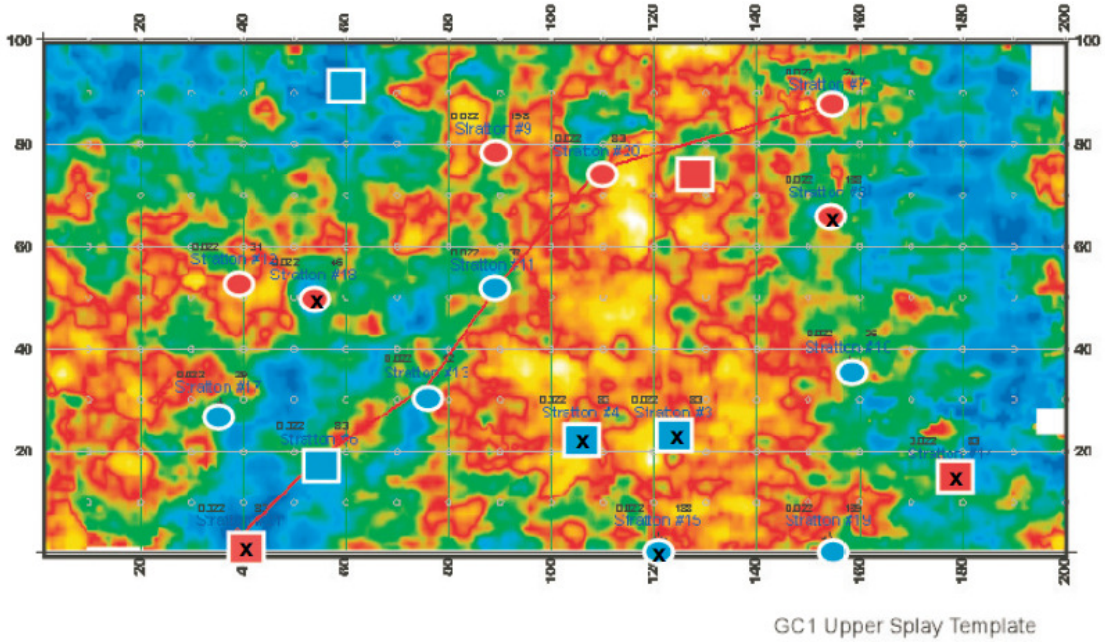

Figure C.8 Seismic Slice at 22 ms: Model Wells 9/12, Test Wells 3/7

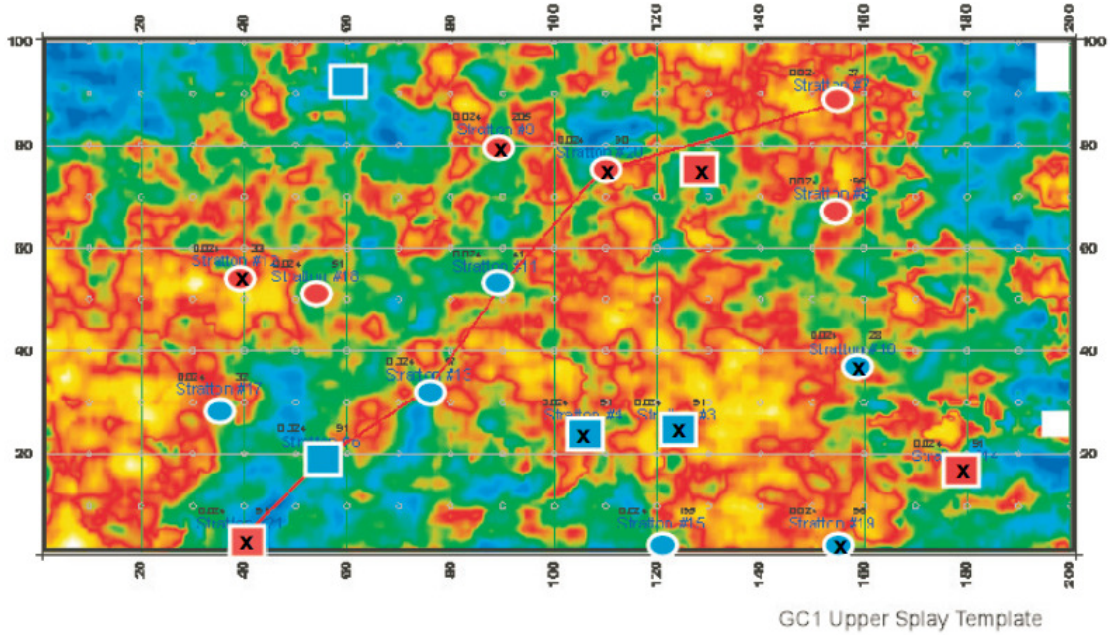

Figure C.9 Seismic Slice at 24 ms: Model Wells 7/12, Test Wells 2/7

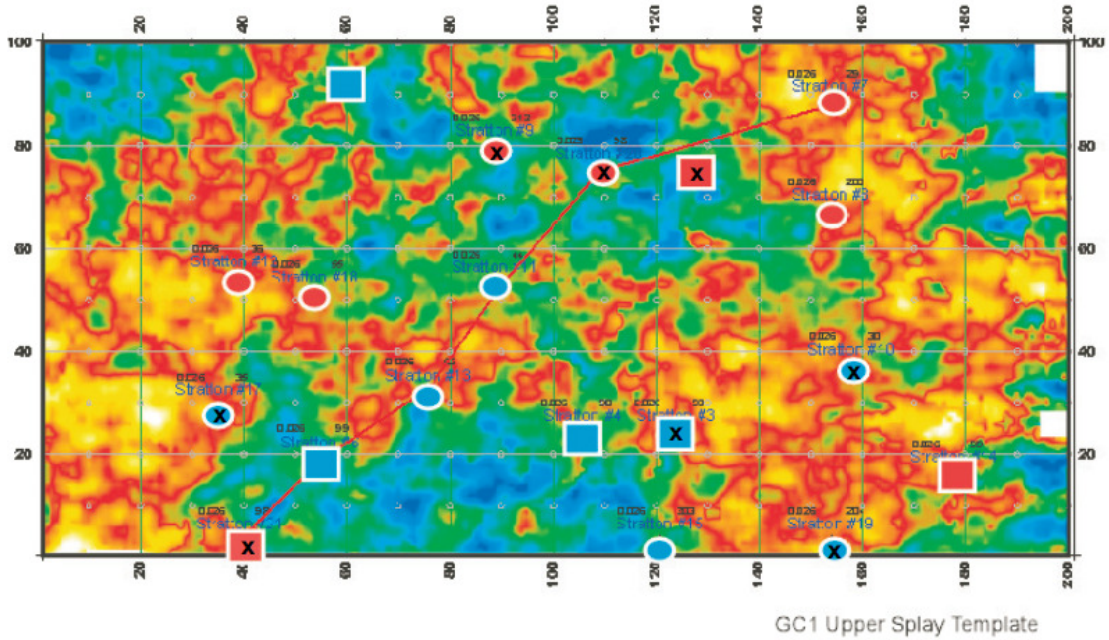

Figure C.10 Seismic Slice at 26 ms: Model Wells 7/12, Test Wells 3/7

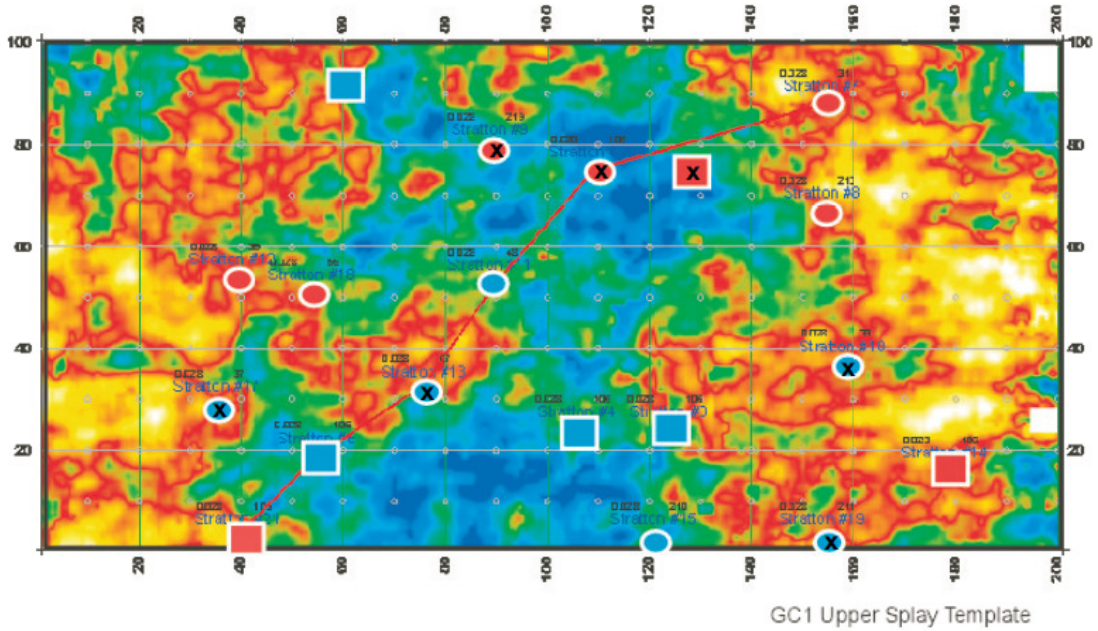

Figure C.11 Seismic Slice at 28 ms: Model Wells 6/12, Test Wells 6/7

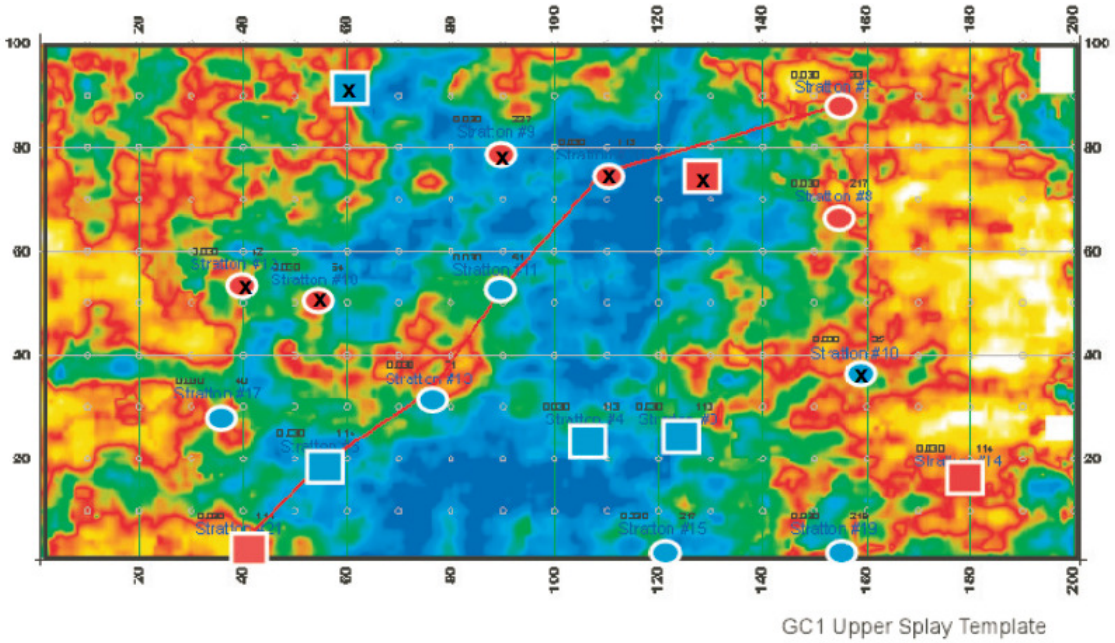

Figure C.12 Seismic Slice at 30 ms: Model Wells 7/12, Test Wells 5/7

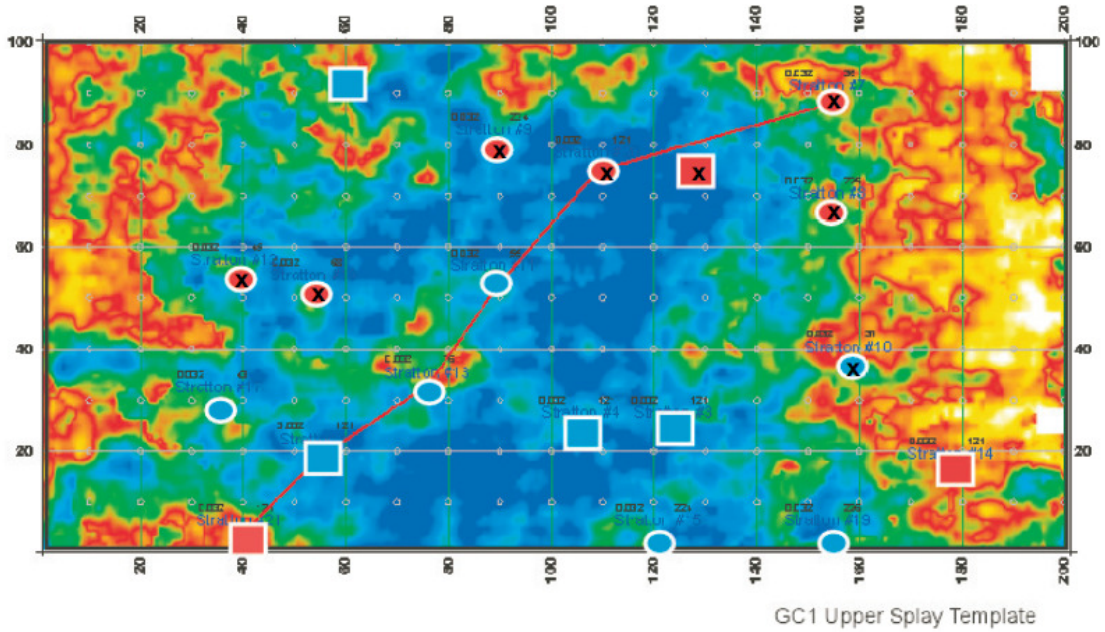

Figure C.13 Seismic Slice at 32 ms: Model Wells 5/12, Test Wells 6/7

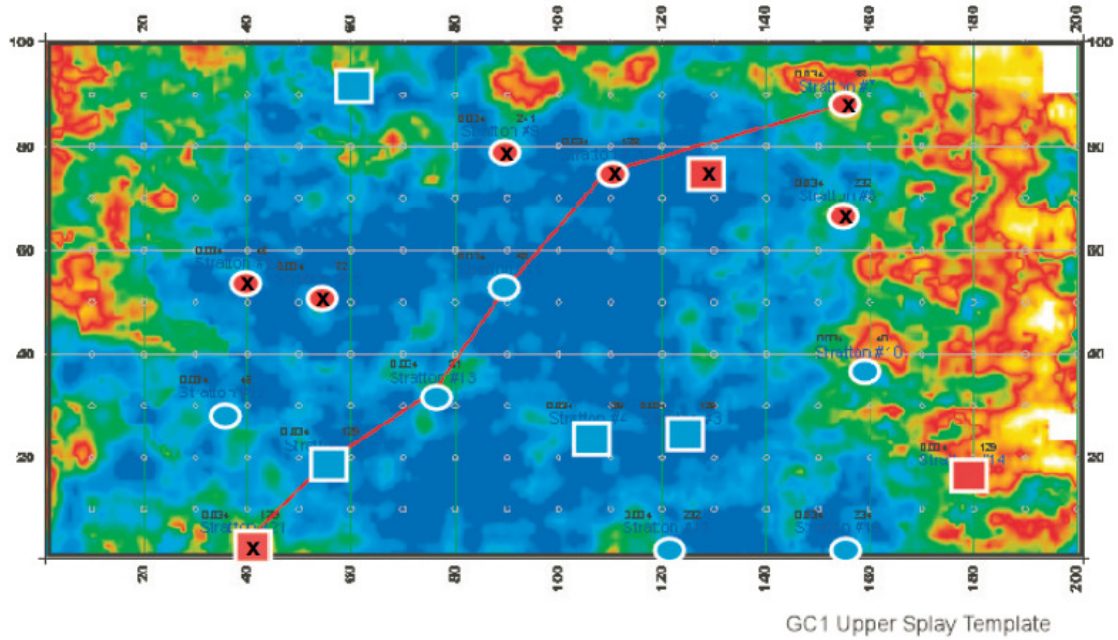

Figure C.14 Seismic Slice at 34 ms: Model Wells 6/12, Test Wells 5/7

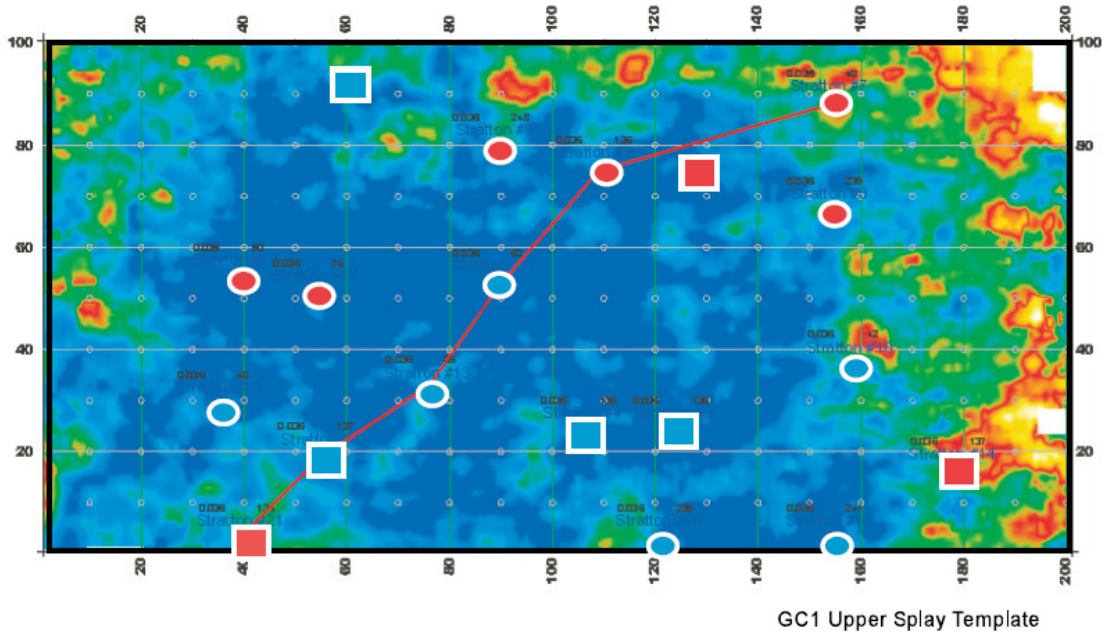

Figure C.15 Seismic Slice at 36 ms: Not scored, all trough

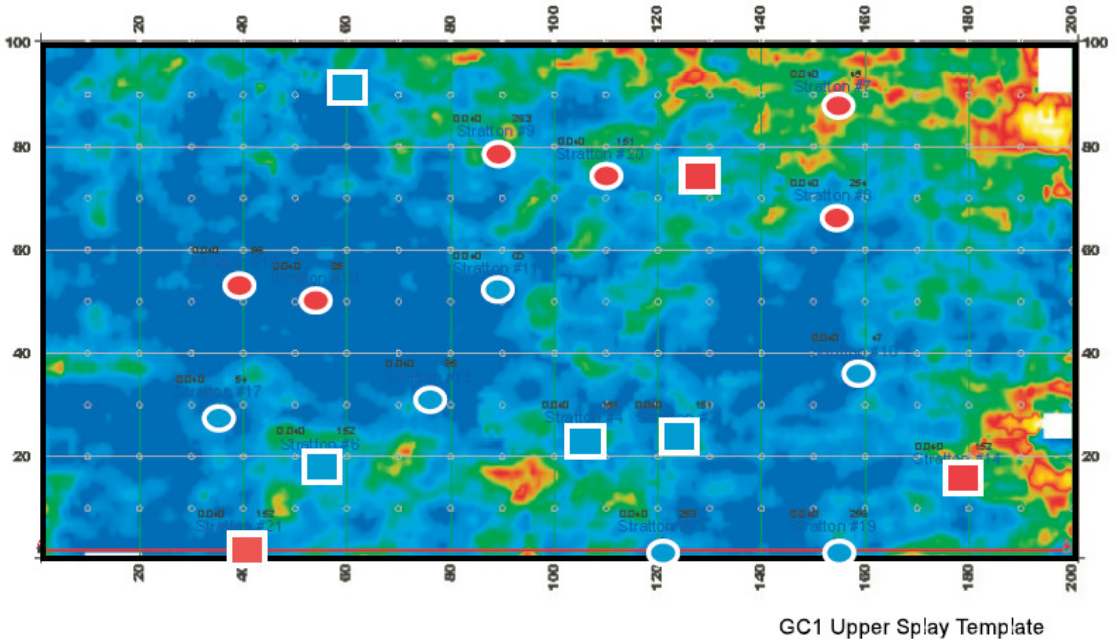

Figure C.16 Seismic Slice at 40 ms: Not scored, all trough

APPENDIX D

GC2U SCORE CARD

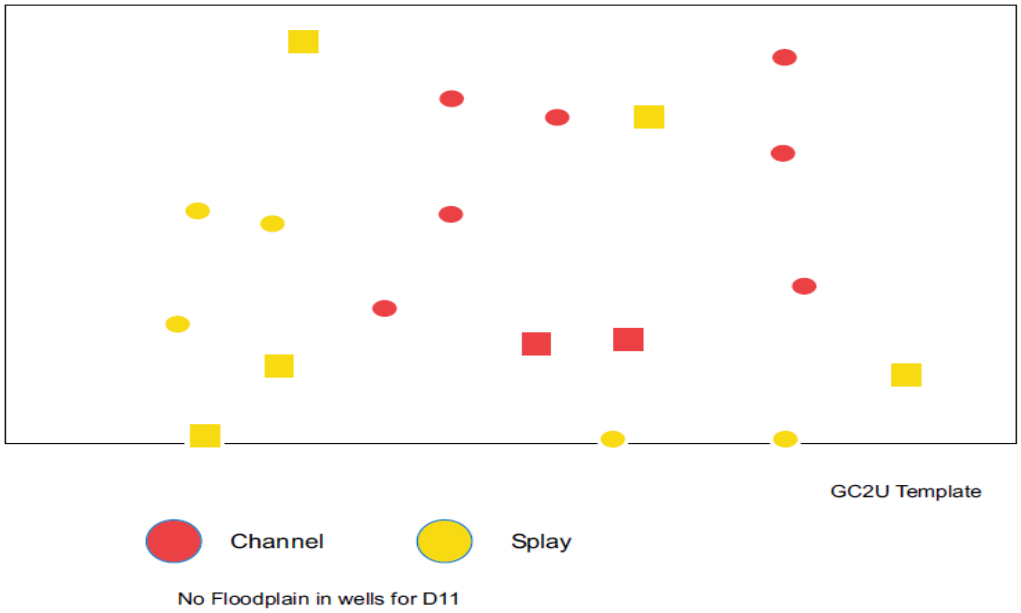

Figure D.1 Scoring Template for D11 Channel In GC2U

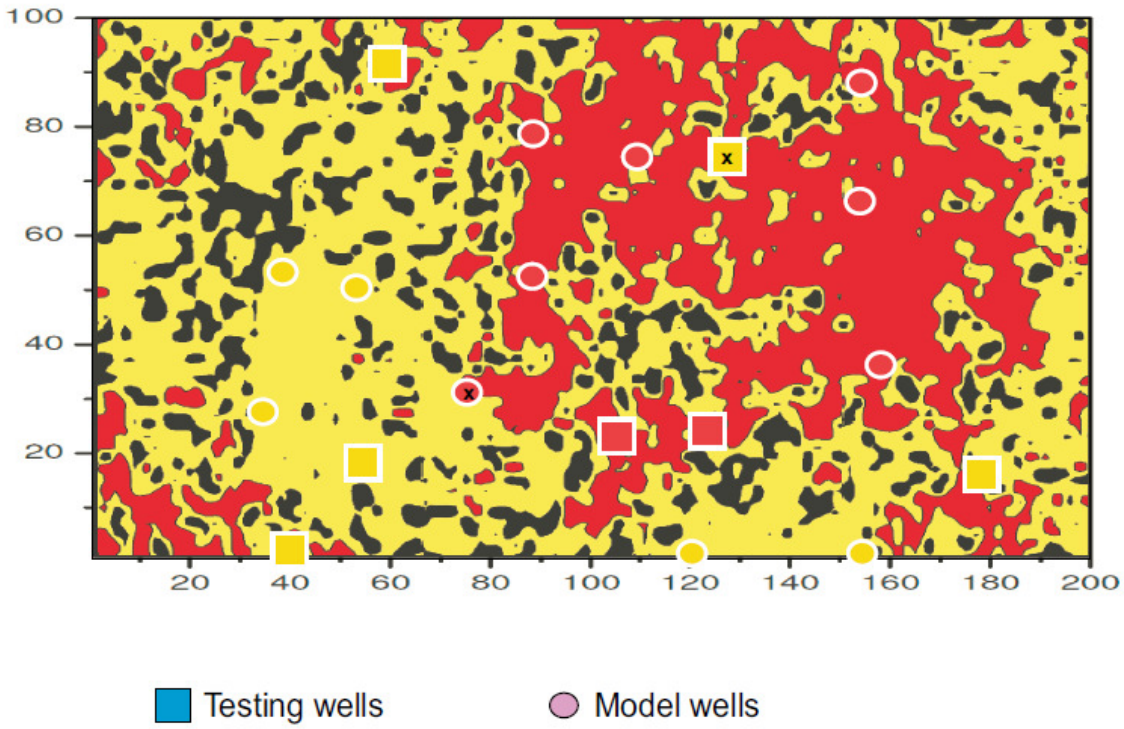

Figure D.2 Map From Neural Network Classifier: Model Wells 11/12, Test Wells 6/7

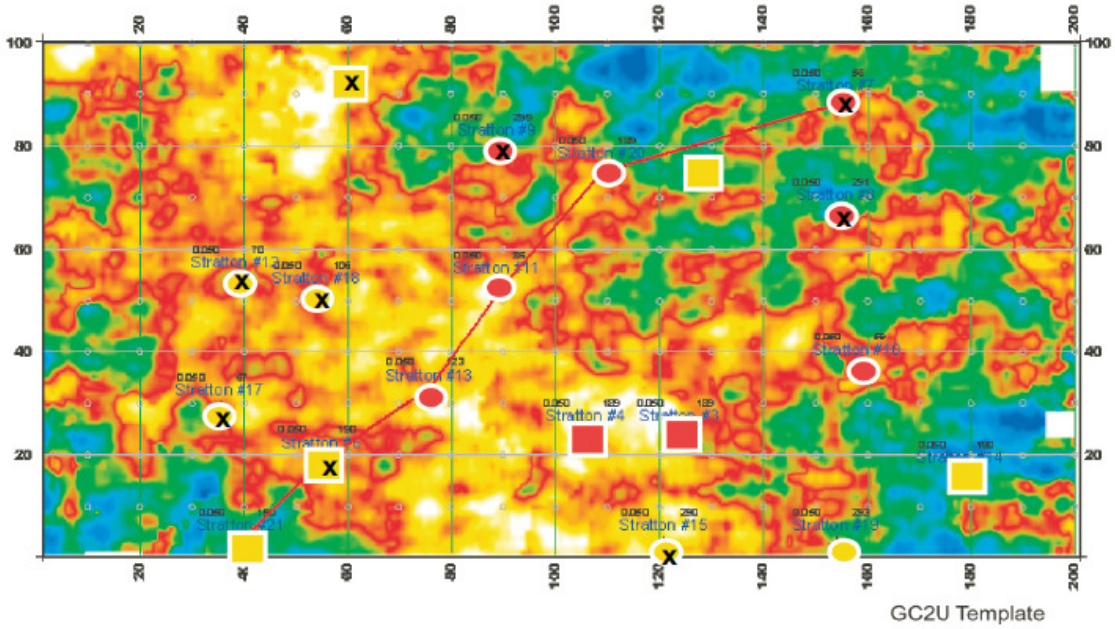

Figure D.3 Seismic Slice at 50 ms: Model Wells 5/12, Test Wells 5/7

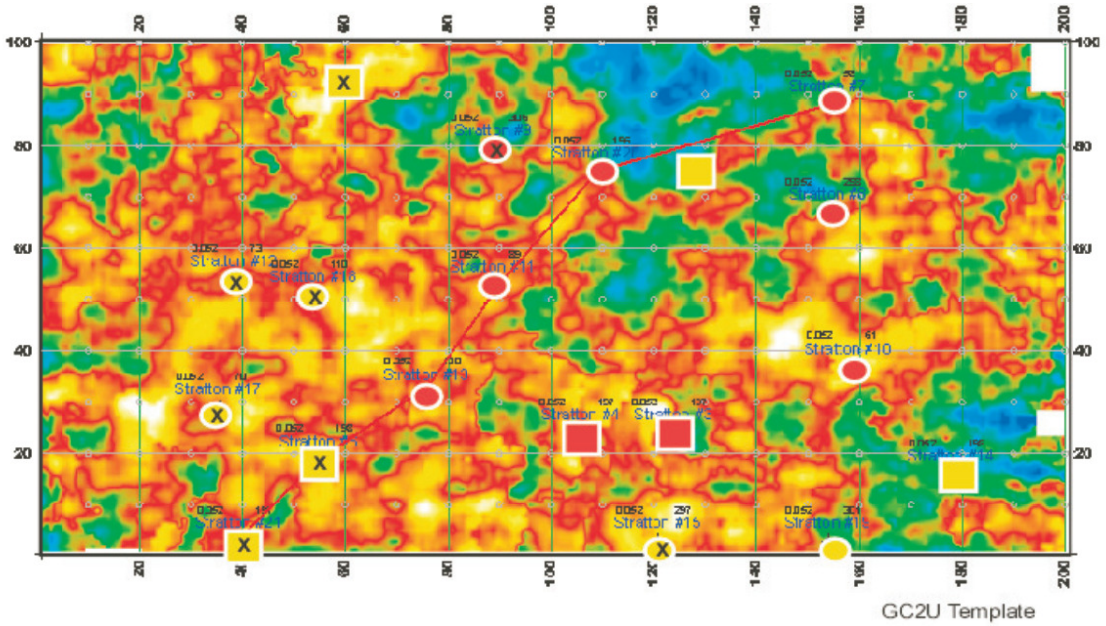

Figure D.4 Seismic Slice at 52 ms: Model Wells 7/12, Test Wells 5/7

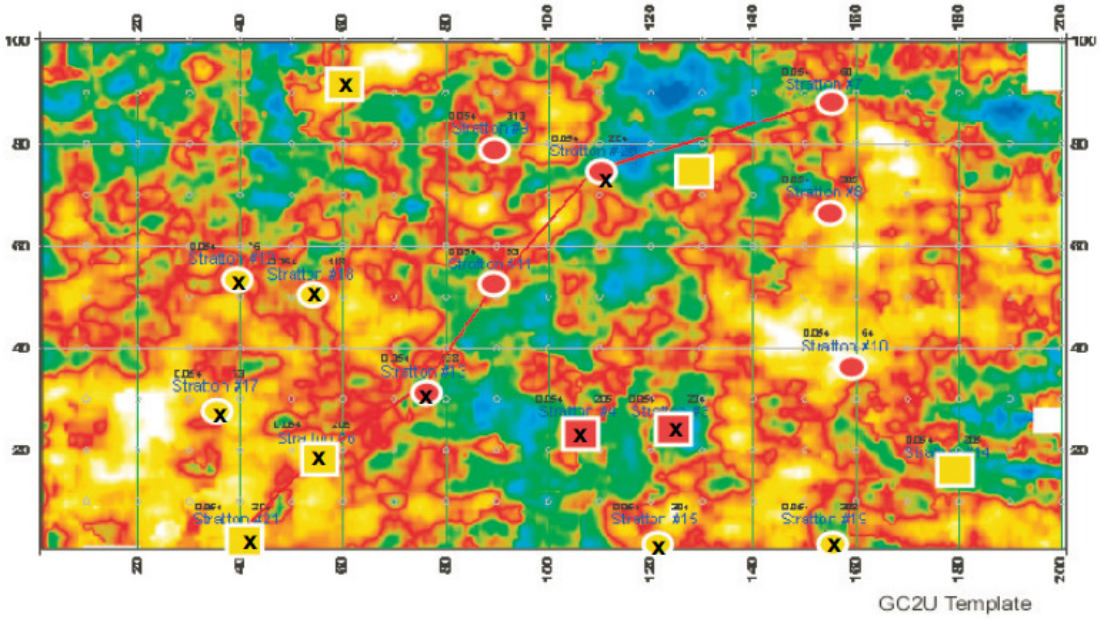

Figure D.5 Seismic Slice at 54 ms: Model Wells 5/12, Test Wells 2/7

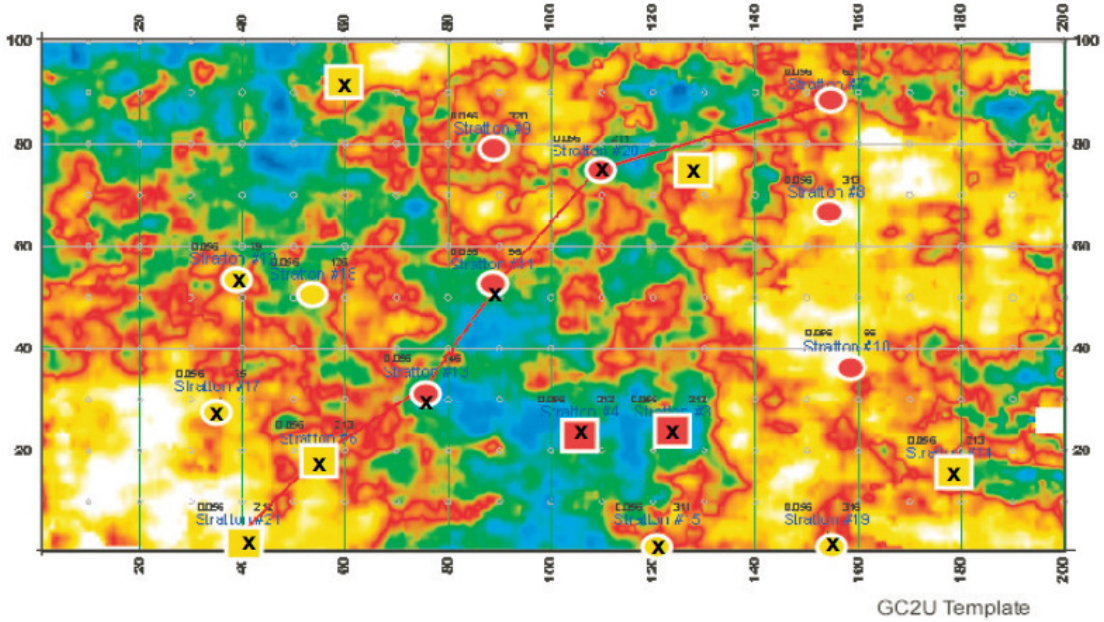

Figure D.6 Seismic Slice at 56 ms: Model Wells 5/12, Test Wells 0/7

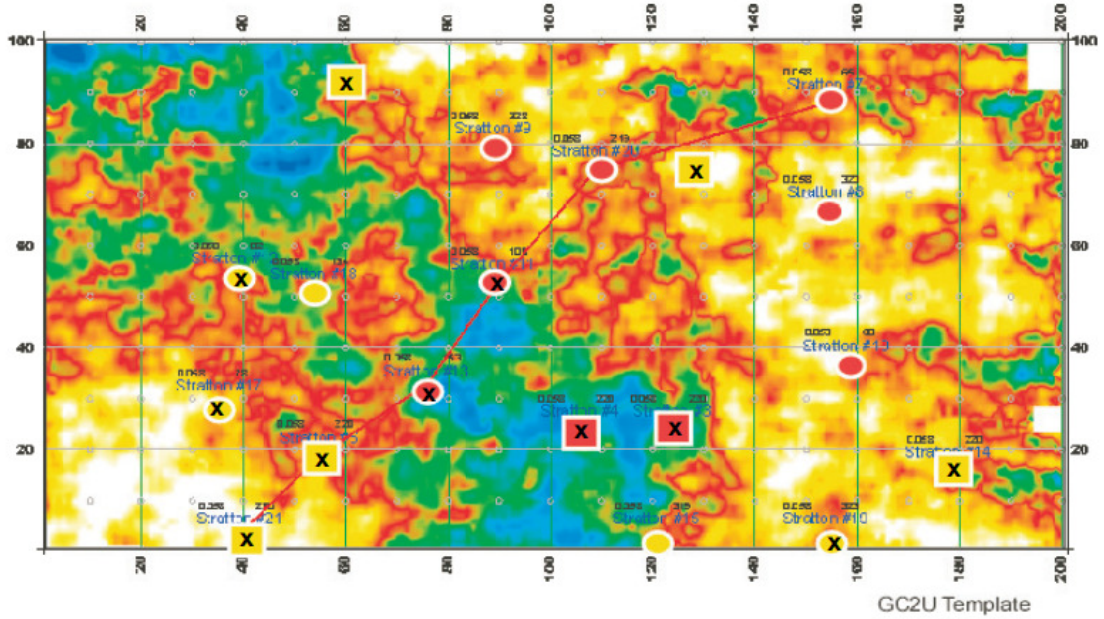

Figure D.7 Seismic Slice at 58 ms: Model Wells 7/12, Test Wells 0/7

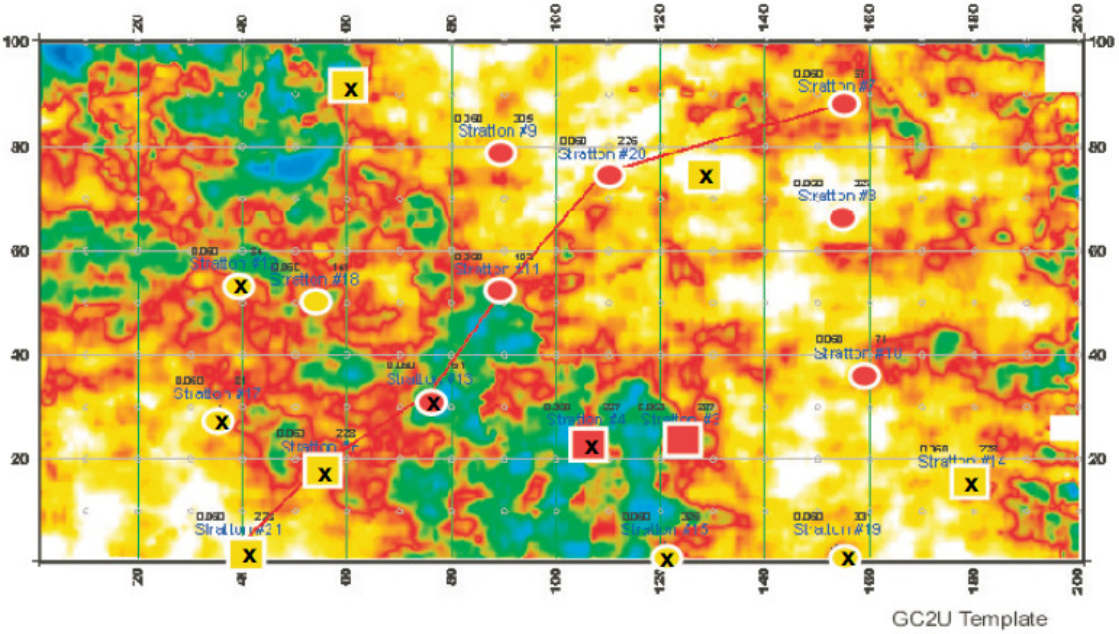

Figure D.8 Seismic Slice at 60 ms: Model Wells 7/12, Test Wells 1/7

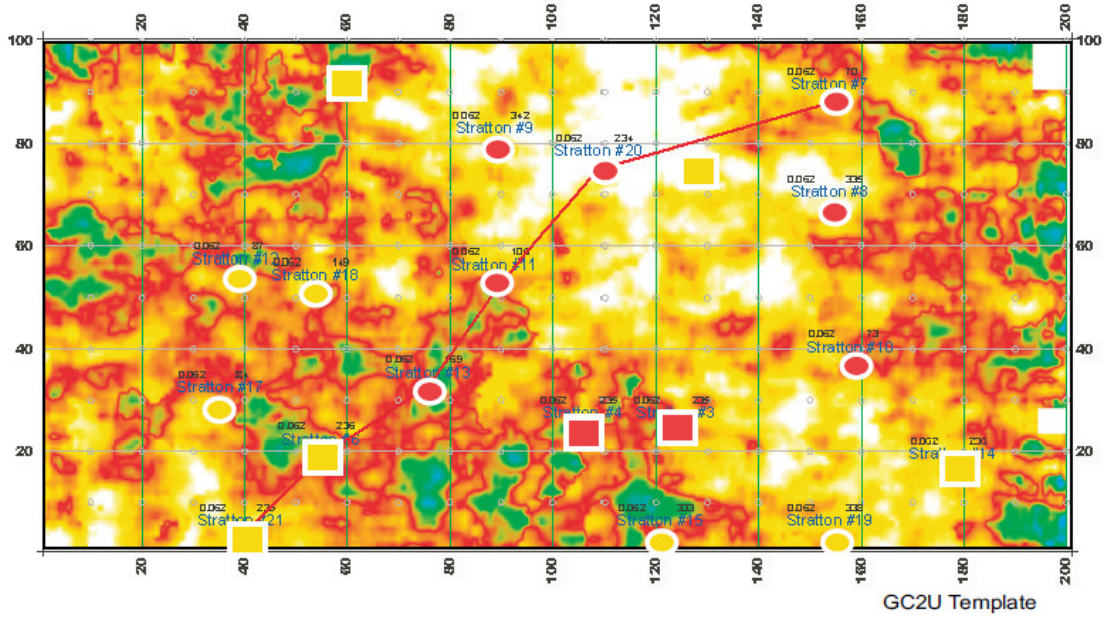

Figure D.9 Seismic Slice at 62 ms: Not scored, all peak

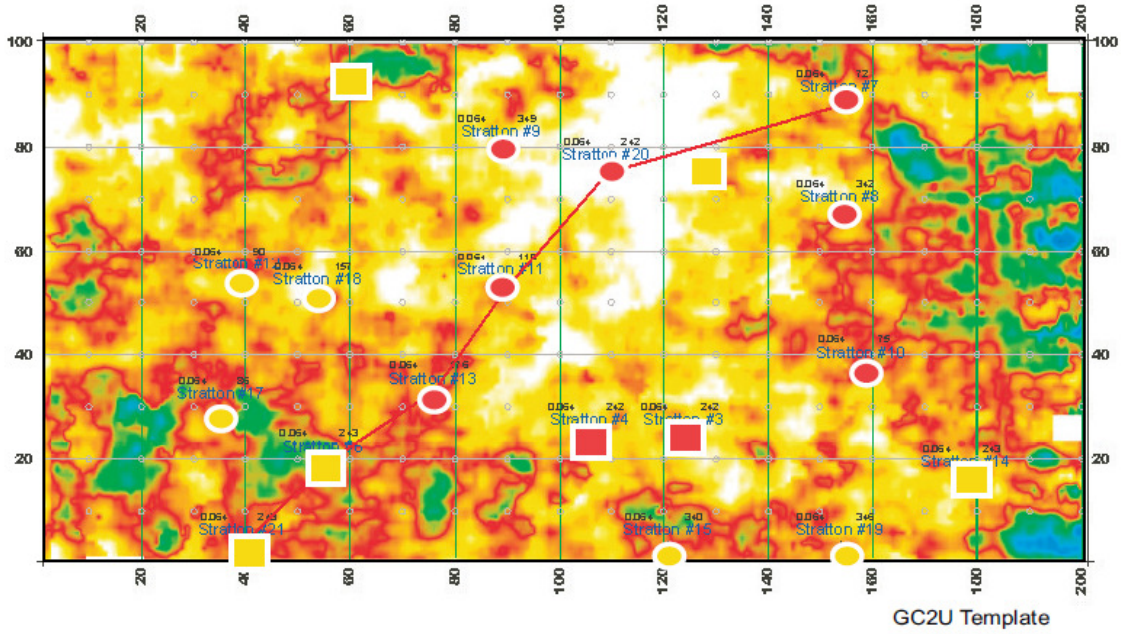

Figure D.10 Seismic Slice at 64 ms: Not scored, all peak

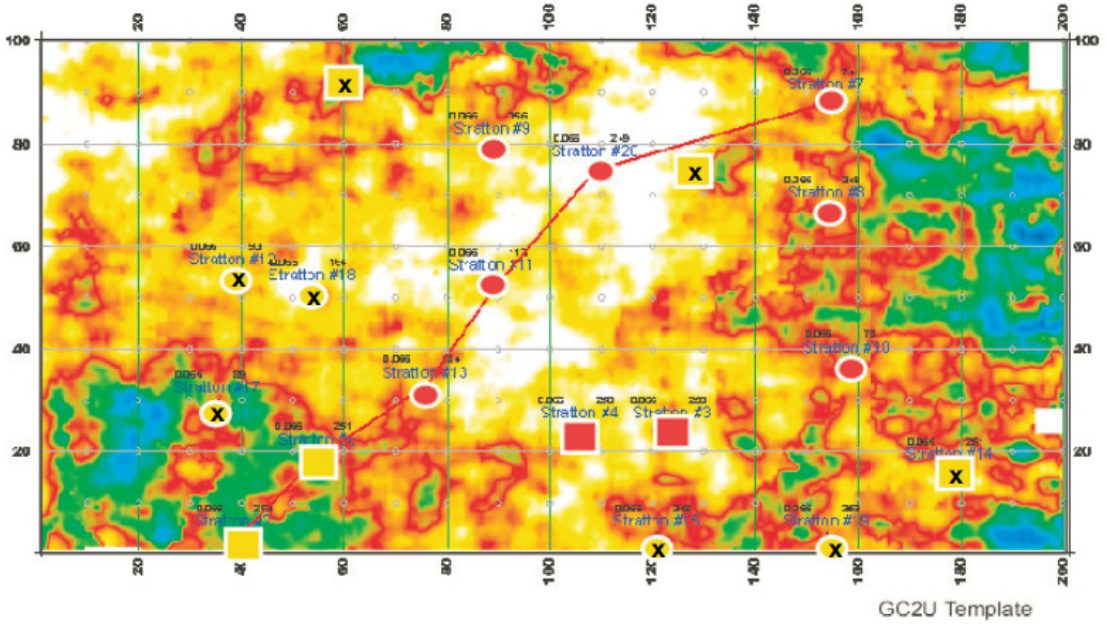

Figure D.11 Seismic Slice at 66 ms: Model Wells 7/12, Test Wells 4/7

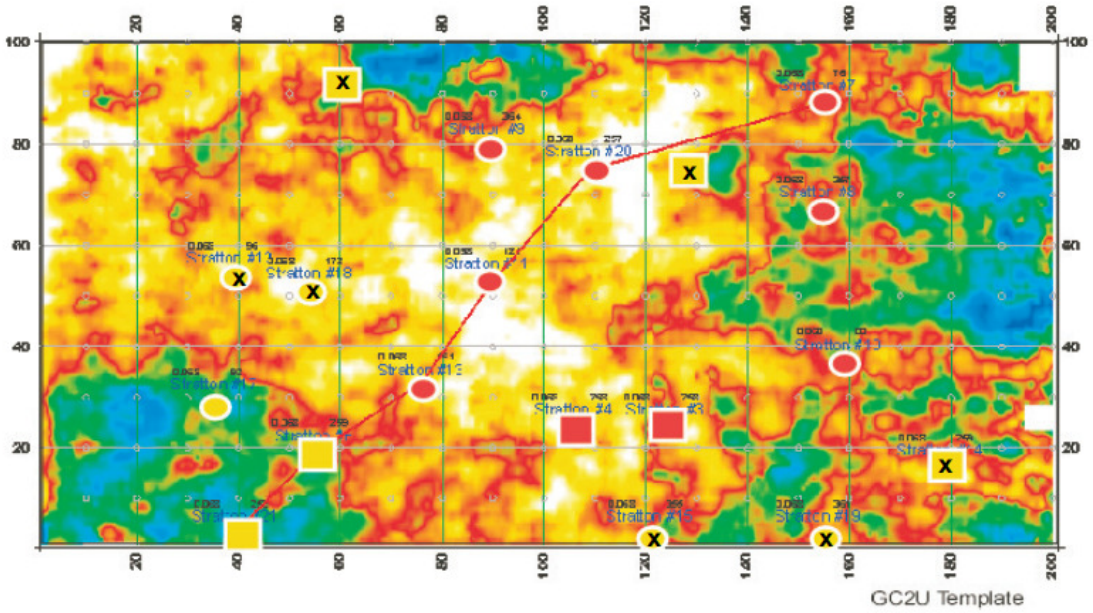

Figure D.12 Seismic Slice at 68 ms: Model Wells 8/12, Test Wells 4/7

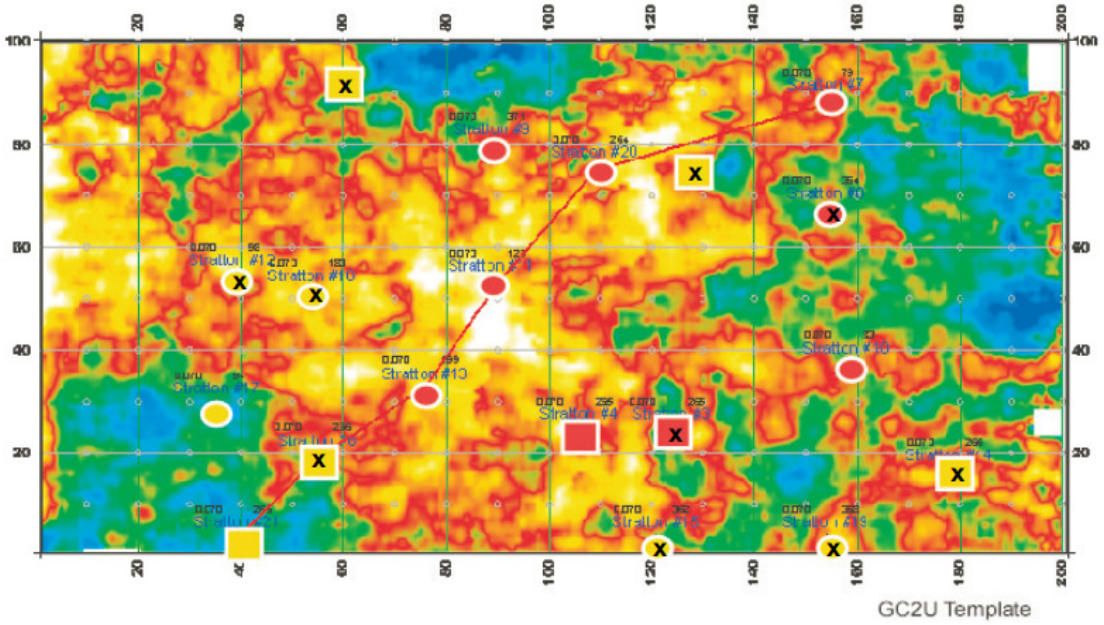

Figure D.13 Seismic Slice at 70 ms: Model Wells 7/12, Test Wells 2/7

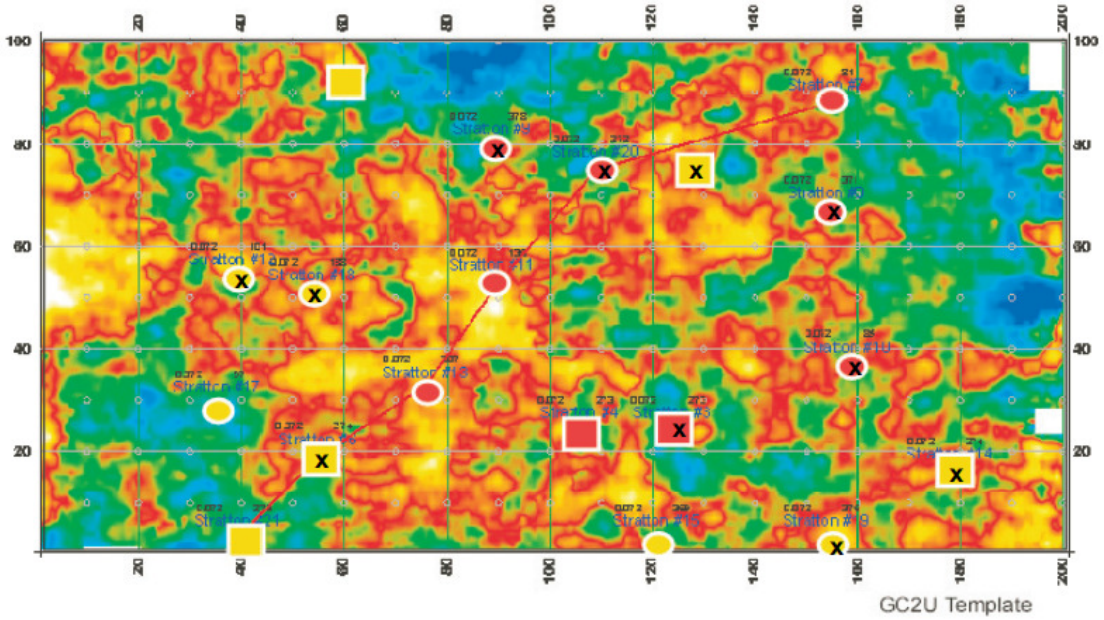

Figure D.14 Seismic Slice at 72 ms: Model Wells 5/12, Test Wells 3/7

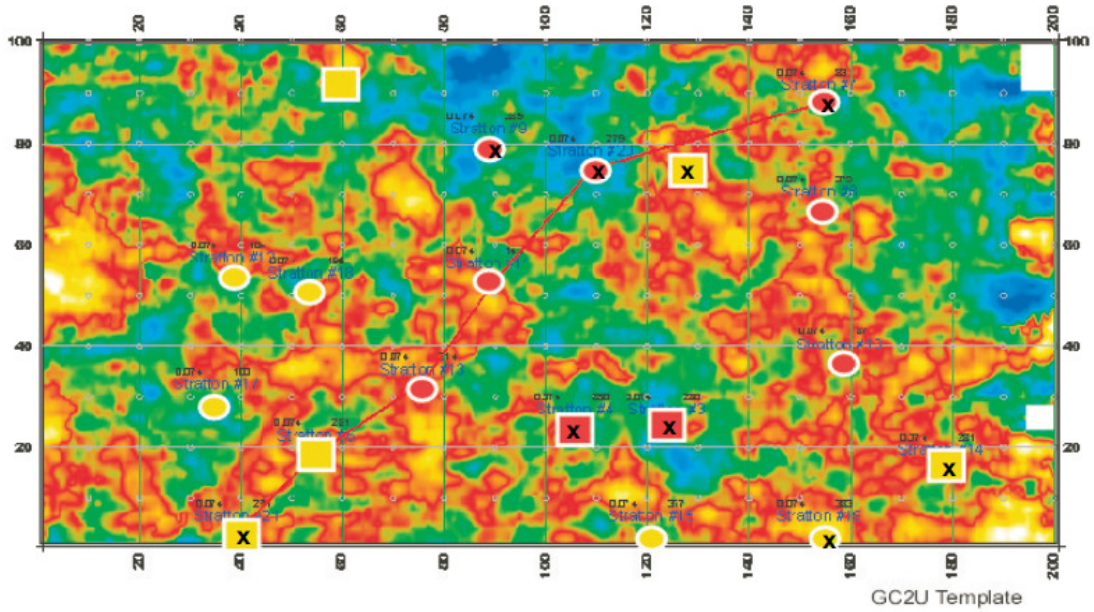

Figure D.15 Seismic Slice at 74 ms: Model Wells 8/12, Test Wells 2/7

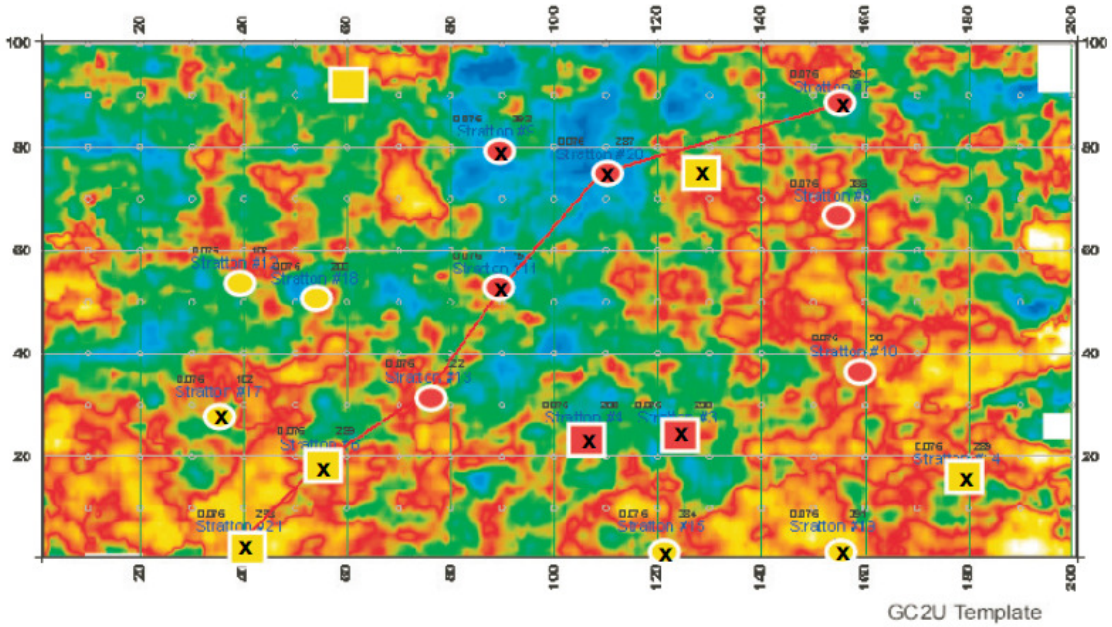

Figure D.16 Seismic Slice at 76 ms: Model Wells 5/12, Test Wells 1/7

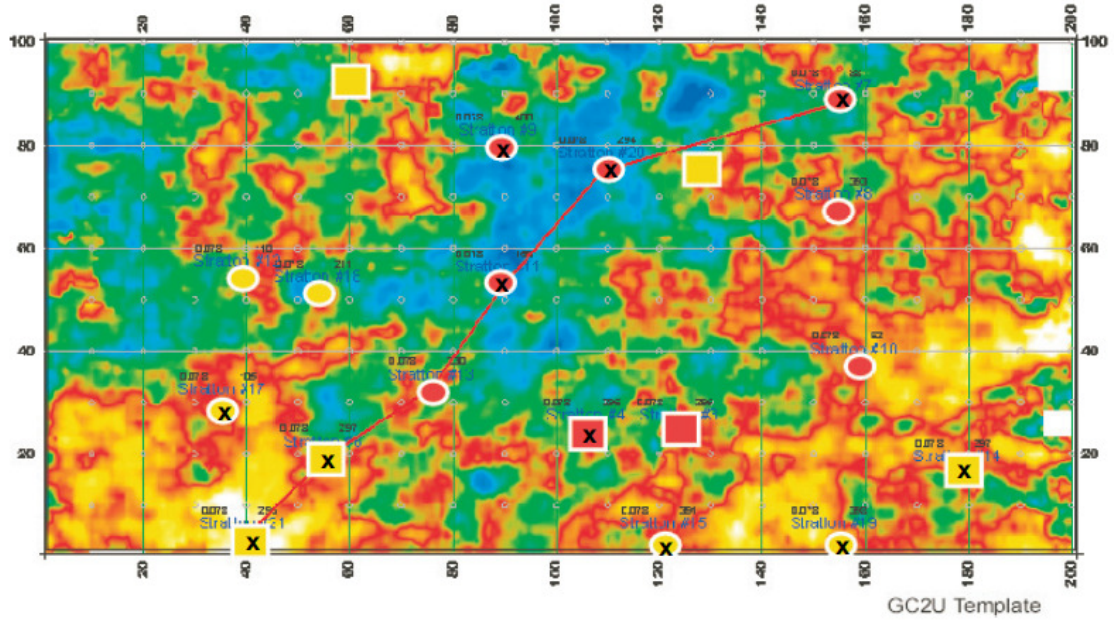

Figure D.17 Seismic Slice at 78 ms: Model Wells 5/12, Test Wells 3/7

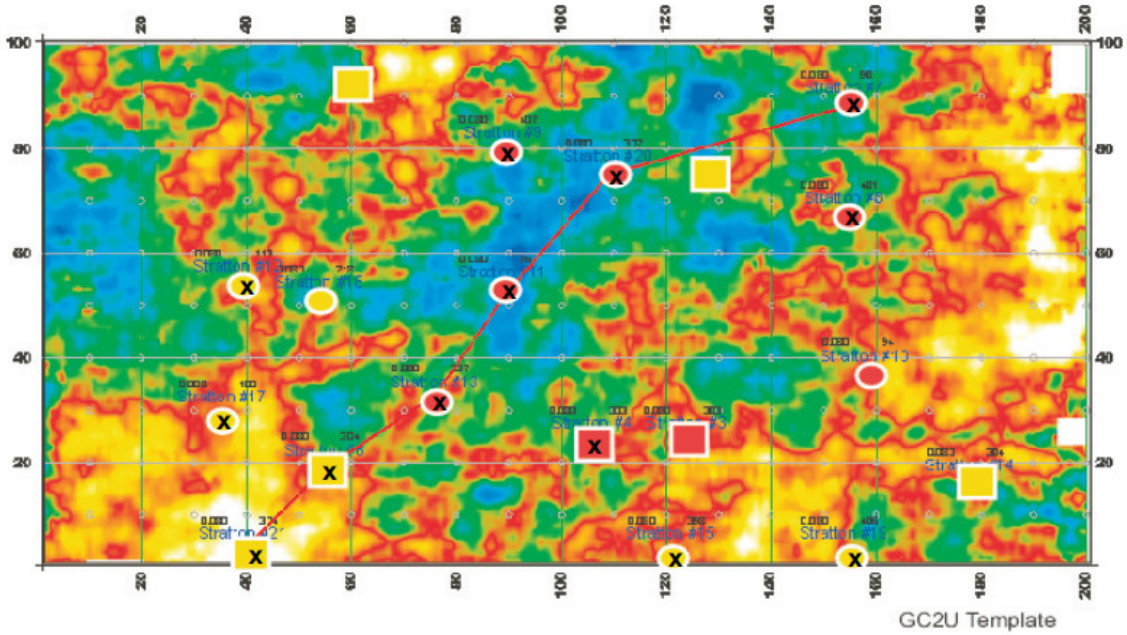

Figure D.18 Seismic Slice at 80 ms: Model Wells 2/12, Test Wells 4/7

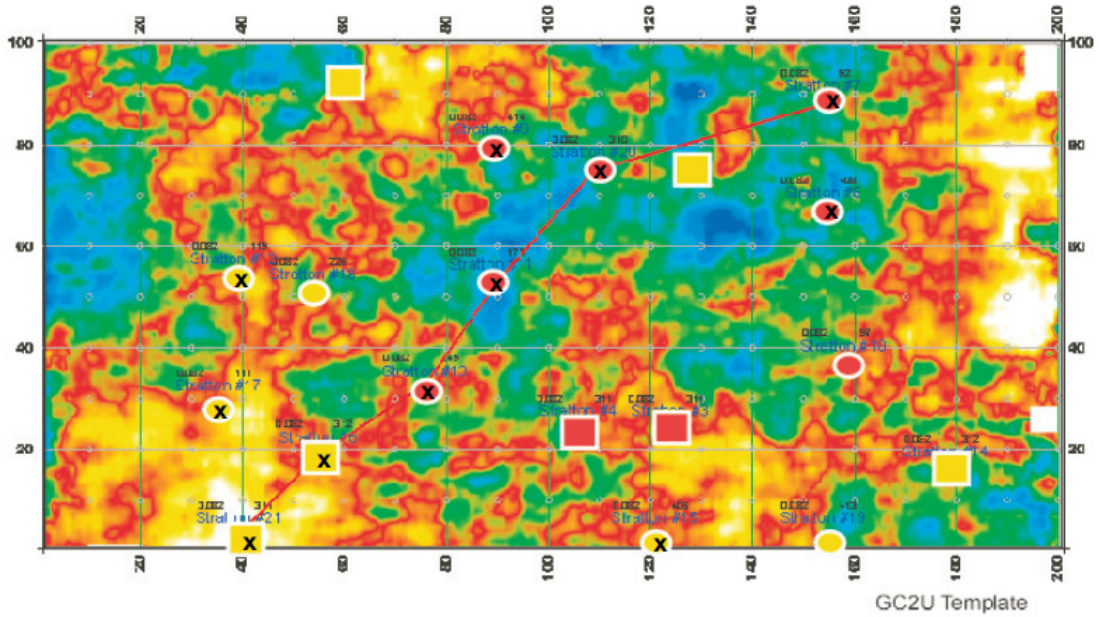

Figure D.19 Seismic Slice at 82 ms: Model Wells 3/12, Test Wells 5/7

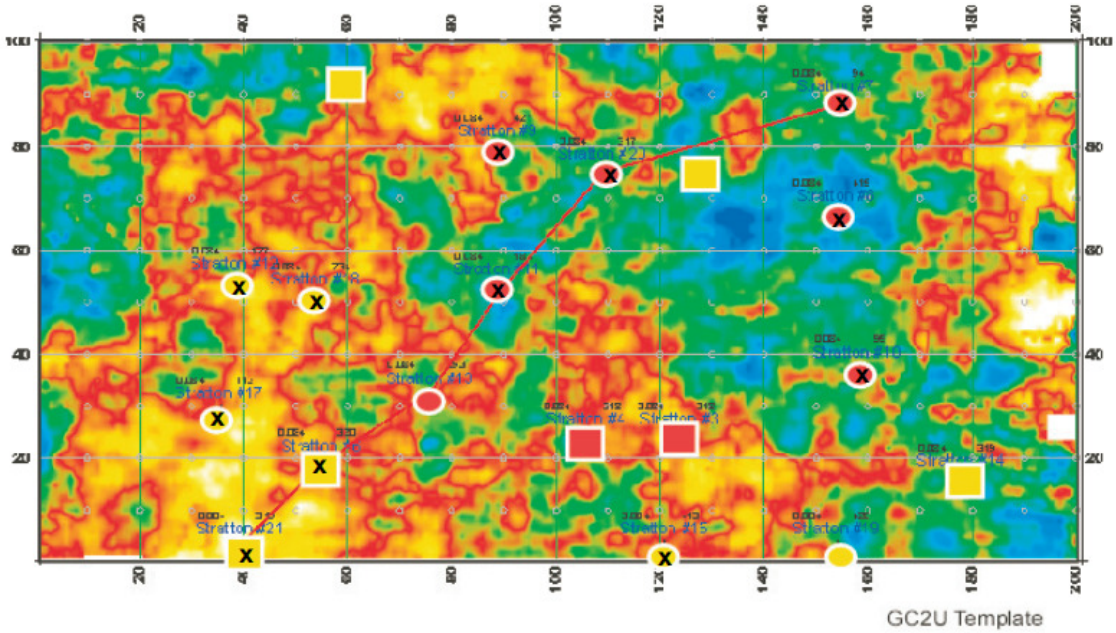

Figure D.20 Seismic Slice at 84 ms: Model Wells 2/12, Test Wells 5/7

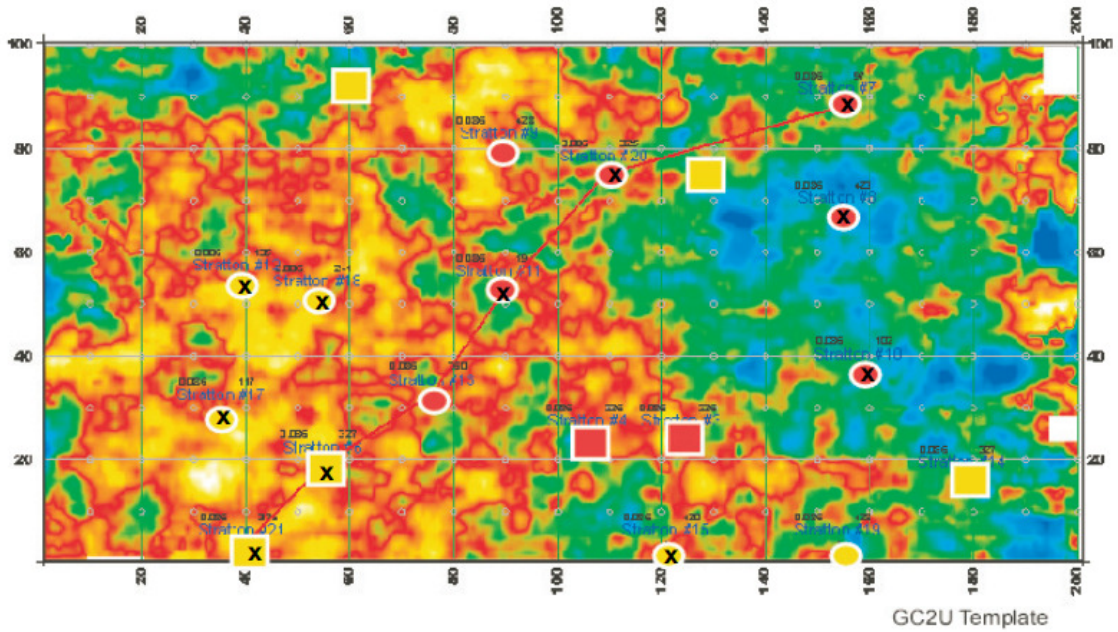

Figure D.21 Seismic Slice at 86 ms: Model Wells 3/12, Test Wells 5/7

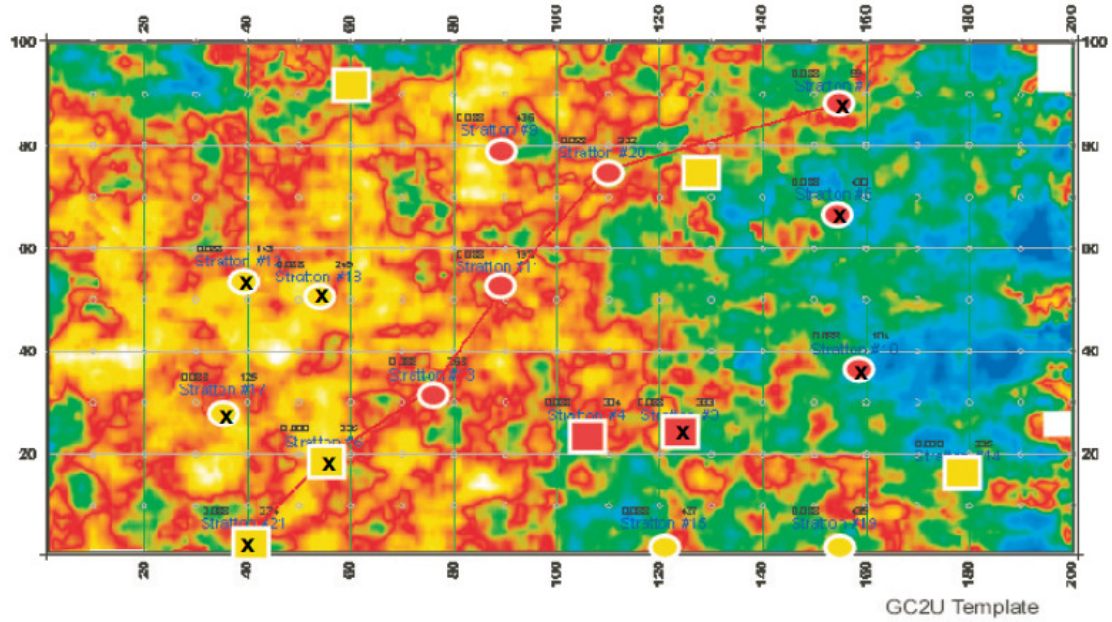

Figure D.22 Seismic Slice at 88 ms: Model Wells 6/12, Test Wells 4/7

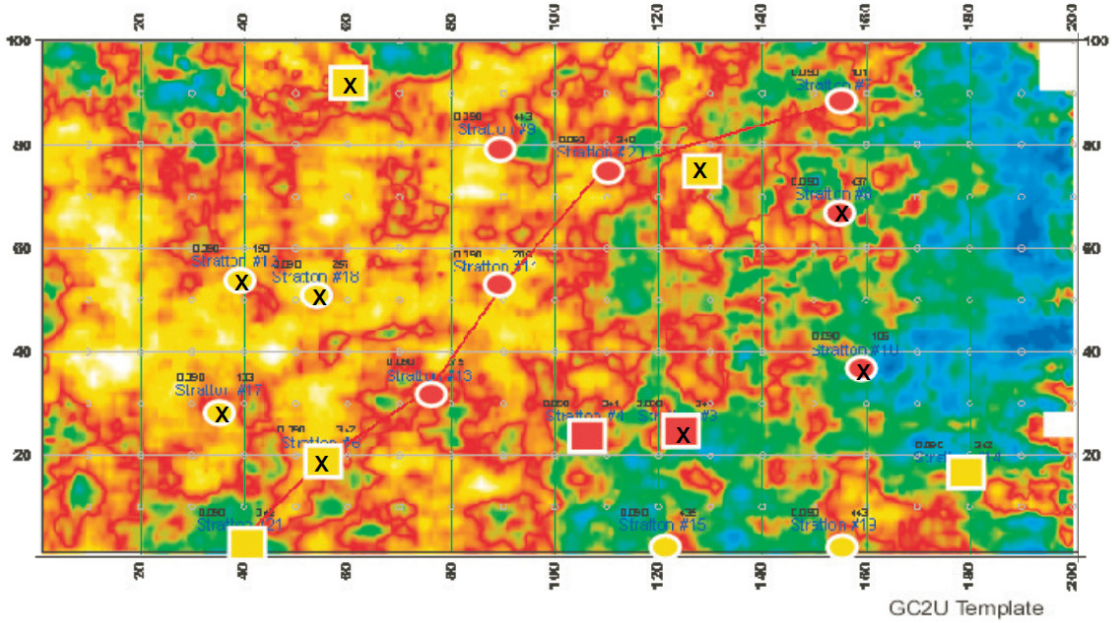

Figure D.23 Seismic Slice at 90 ms: Model Wells 7/12, Test Wells 3/7

APPENDIX E

WELL LOGS AND CLASS PICKS

Well Logs and Target Classification

The well logs are flattened to flooding surface 1 in well 9 (subsea depth of 4914 feet)

The classification of the target is based on visual-analysis of the well logs and human discretion of class. This is a subjective process so in this appendix the well logs are presented along with annotations specific to the classification of the three targets:

Hunt GC2L Target is a Channel sand complex at 5530 to 5370
Hunt GC1U Target is the Basal Reservoir sands in C38 at 5080 feet
Hunt GC2U Target is the D11 Channel sand at 5330

Well 9 is presented first as this was the tie point for flattening the data sets, then the other eleven model wells, then the 7 testing wells. Flooding surfaces are marked with green bars and the volcanic ash maker is marked in blue. The wells have been flattened to well 9 depths using flooding surfaces above the study area, Flooding Surface 1 is shown at 4914 feet

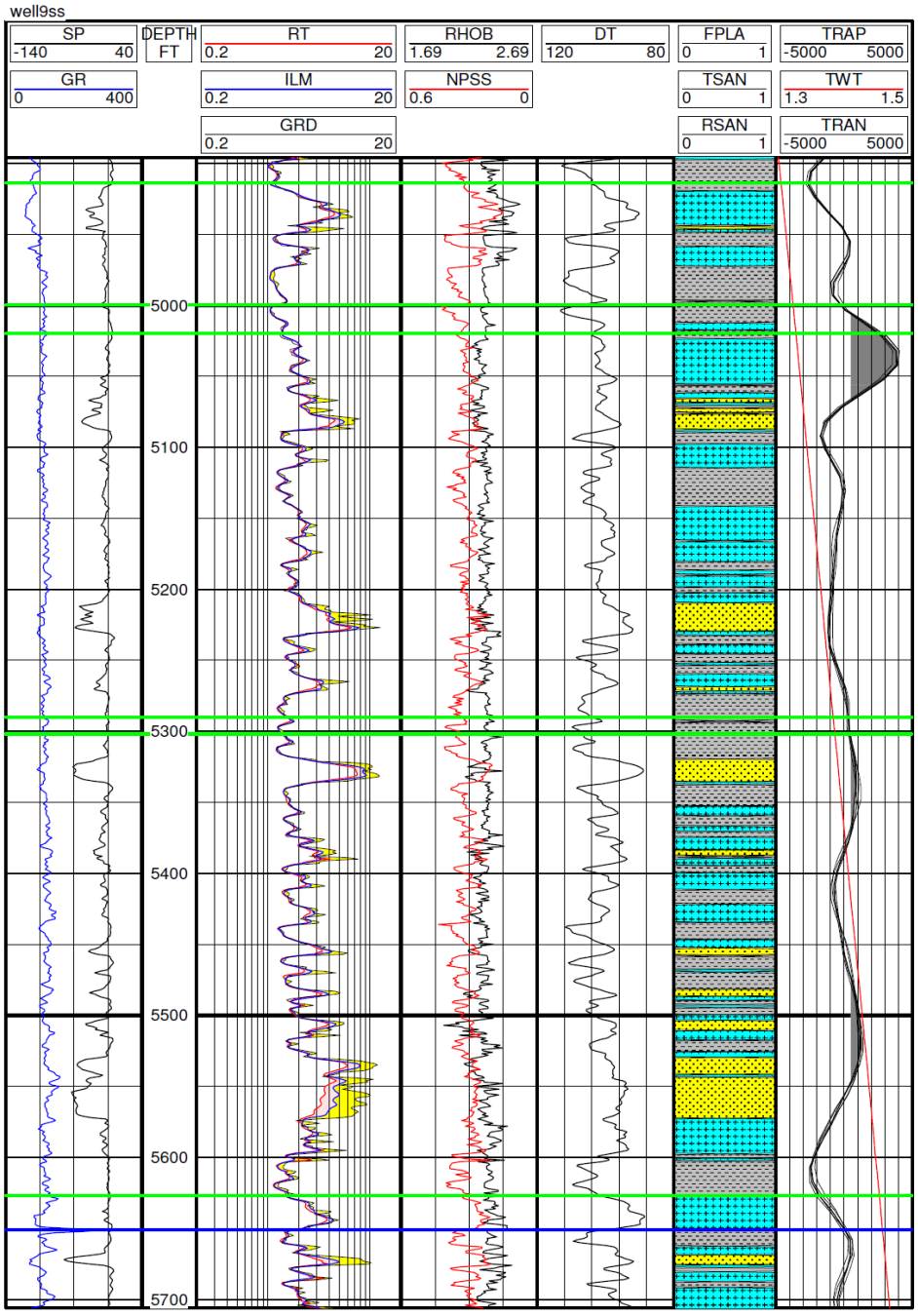

Figure E.1 Model Well 9ss (subsea depth)

GC2L Target: Channel Class, Thick reservoir sand from 5530 to 5575, resistivity profile indicates transition in water saturation with gas on top (when the well was drilled).
GC1U Target: has C38 Basal Reservoir sands, thick bottom lobe at 5080 feet
GC2U Target: D11 Channel class, reservoir sand at 5330

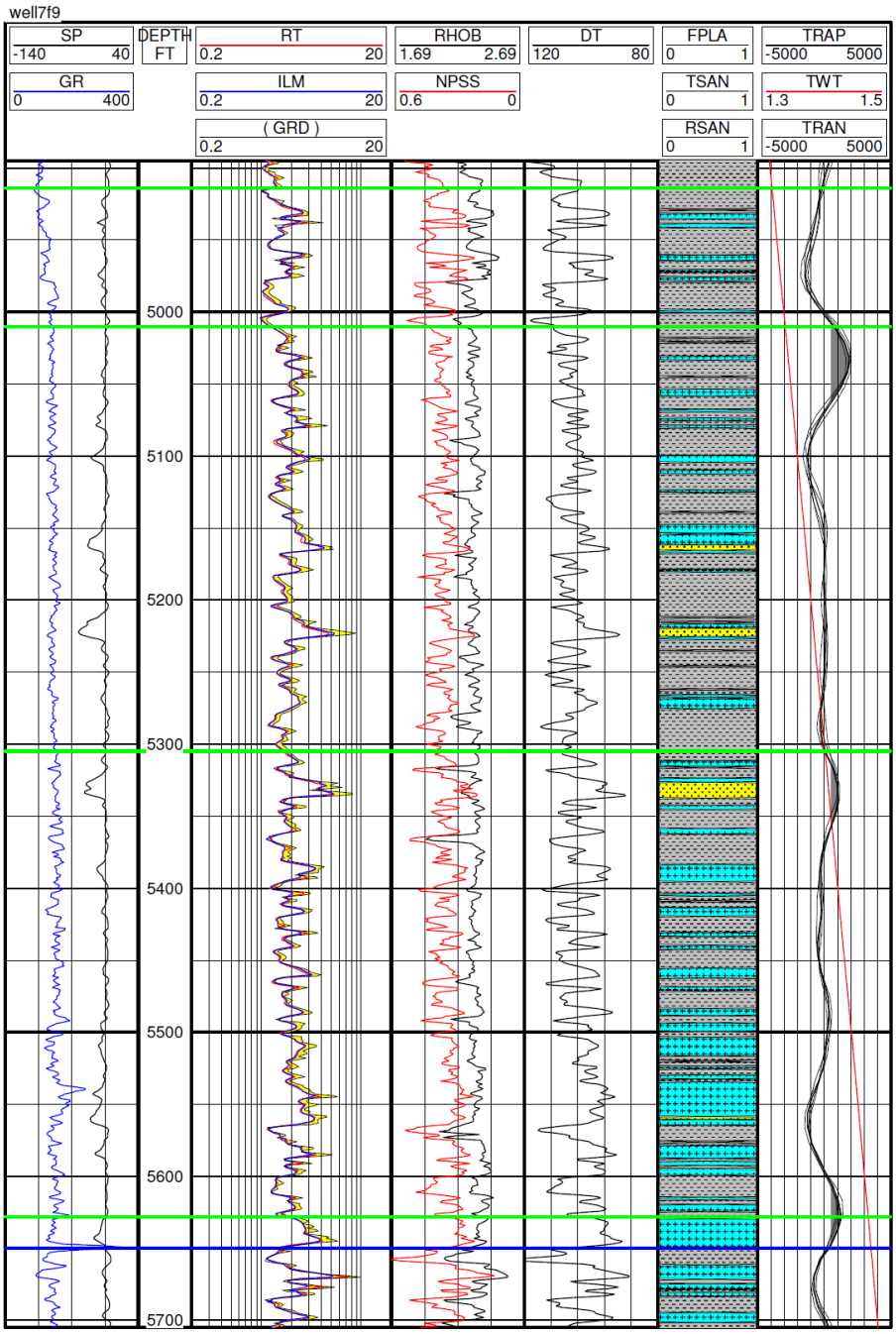

Figure E.2 Model Well 7 (flattened to well 9)

GC2L Target: Floodplain Class, some tight splays, no reservoir sand
GC1U Target: No C38 Basal Reservoir Class
GC2U Target: D11 Channel class, channel/levee character at target

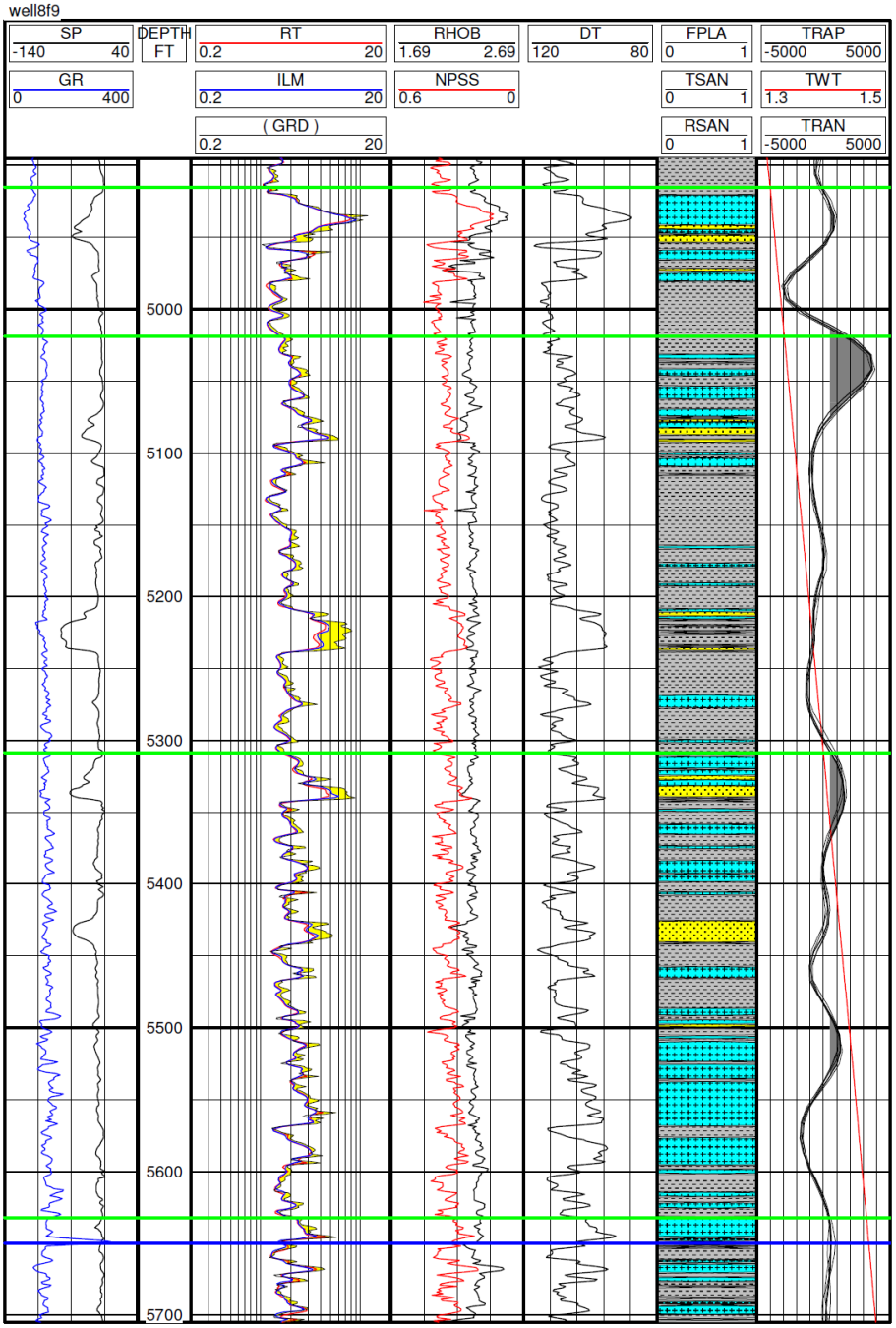

Figure E.3 Model Well 8 (flattened to well 9)

GC2L Target: Floodplain Class, some tight splays, no reservoir sand
GC1U Target: Has C38 Basal Reservoir Class
GC2U Target: D11 Channel class, channel character at target

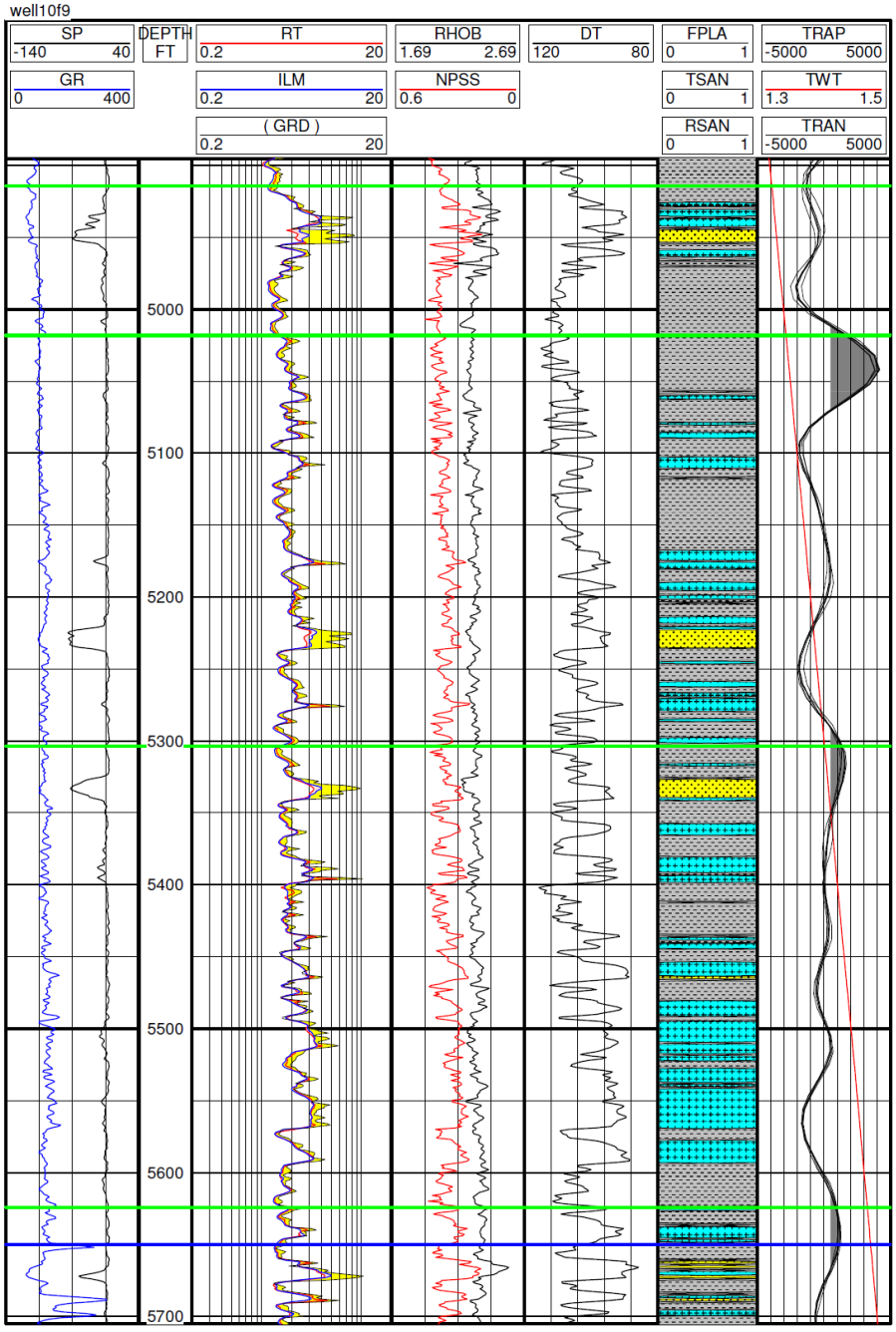

Figure E.4 Model Well 10 (flattened to well 9)

GC2L Target: Floodplain Class, some tight splays, no reservoir sand
GC1U Target: No C38 Basal Reservoir Class
GC2U Target: D11 Channel class, channel character at target

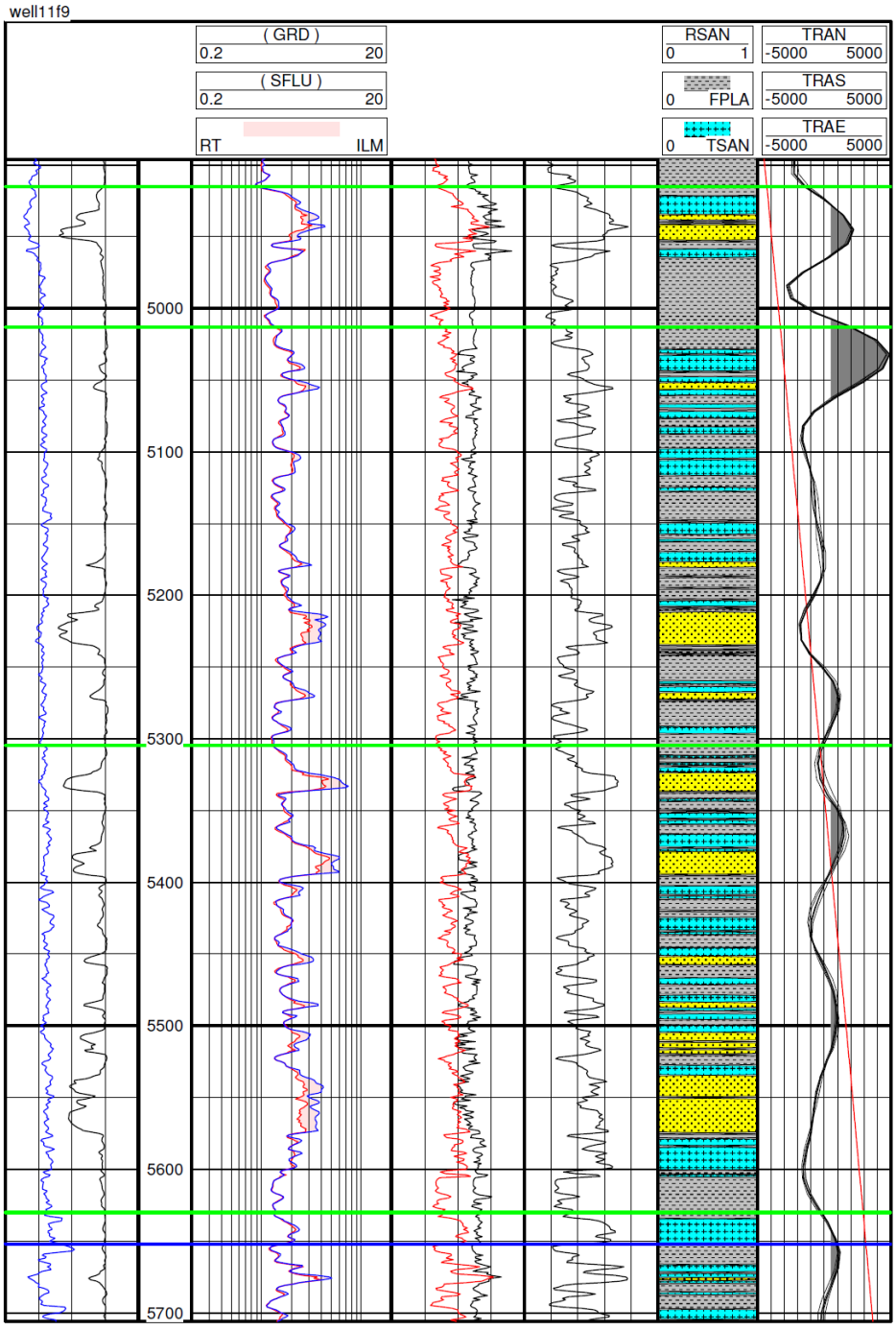

Figure E.5 Model Well 11 (flattened to well 9)

GC2L Target: Channel Class, thick reservoir sand 5535 to 5575
GC1U Target: No C38 Basal Reservoir Class, flood plains at target
GC2U Target: D11 Channel class, channel character at target

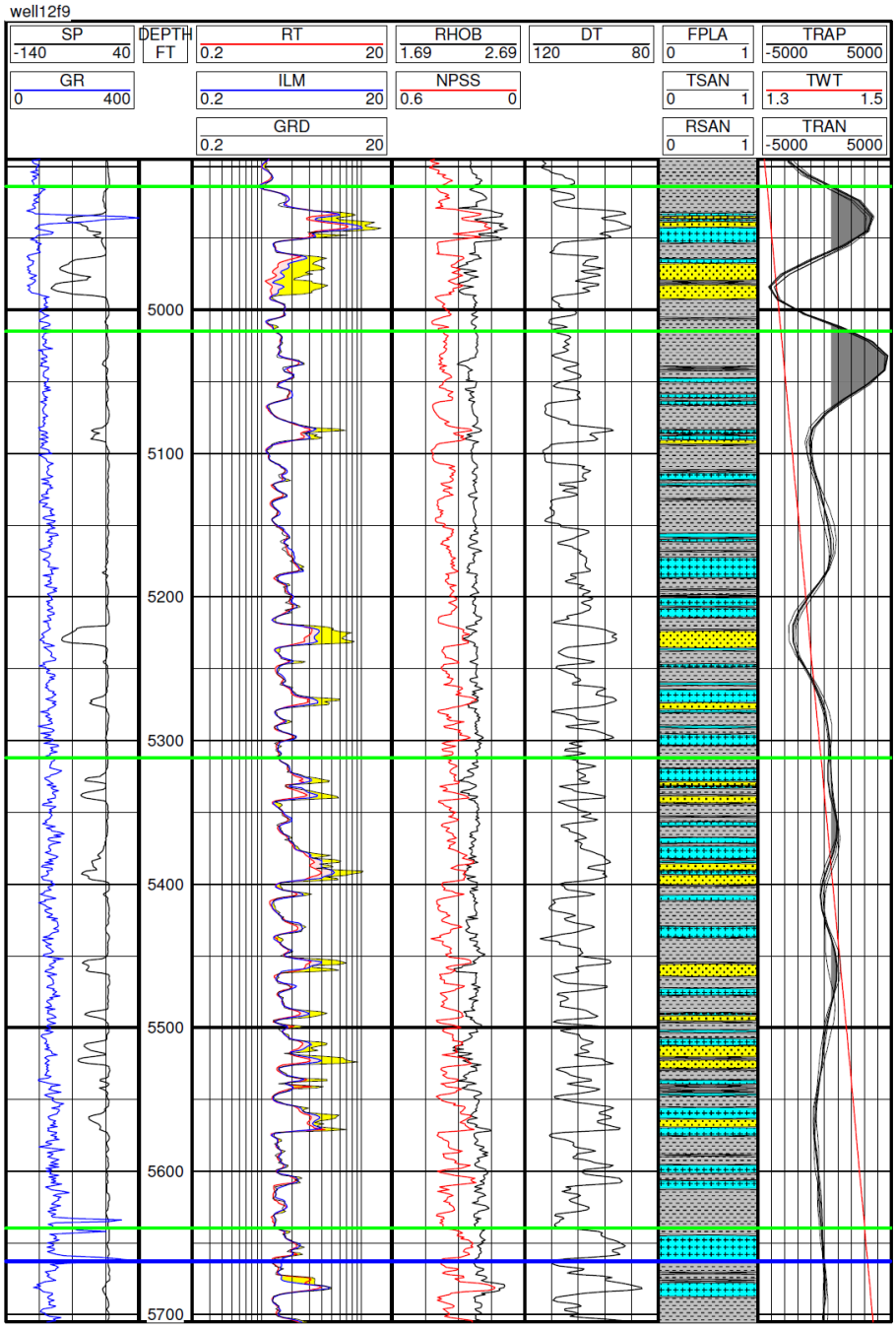

Figure E.6 Model Well 12 (flattened to well 9)

GC2L Target: Splays Class, several coarse grained splays from 5535 to 5575
GC1U Target: Has C38 Basal Reservoir Class, 2 splays at target depth
GC2U Target: D11 Splay Class, Thick splay/levee character at target

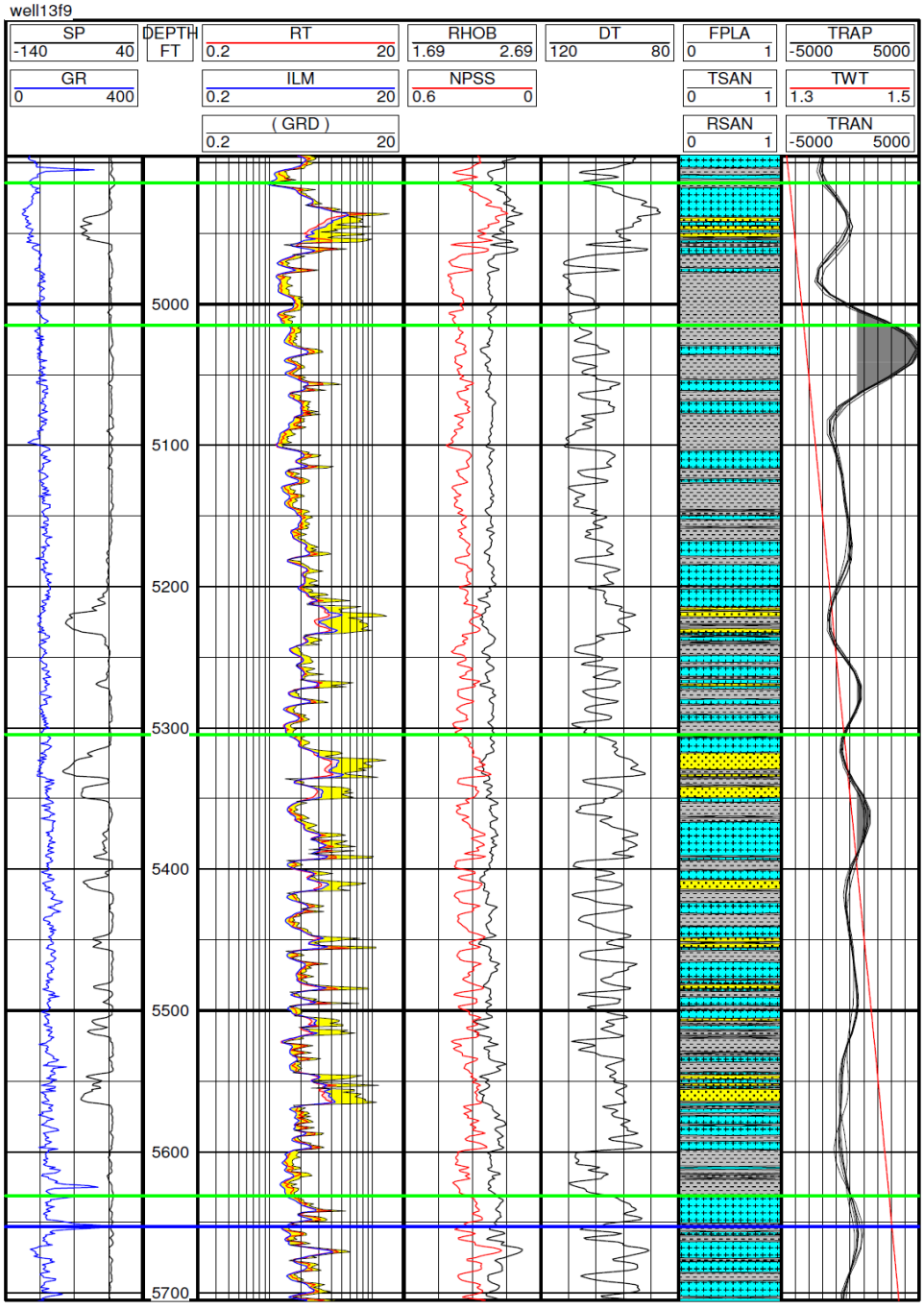

Figure E.7 Model Well 13 (flattened to well 9)

GC2L Target: Channel Class, several coarse grained splay/levee sands and basal channel sand from 5545 to 5575
GC1U Target: No C38 Basal Reservoir Class, tight splays at target depth
GC2U Target: D11 Channel Class

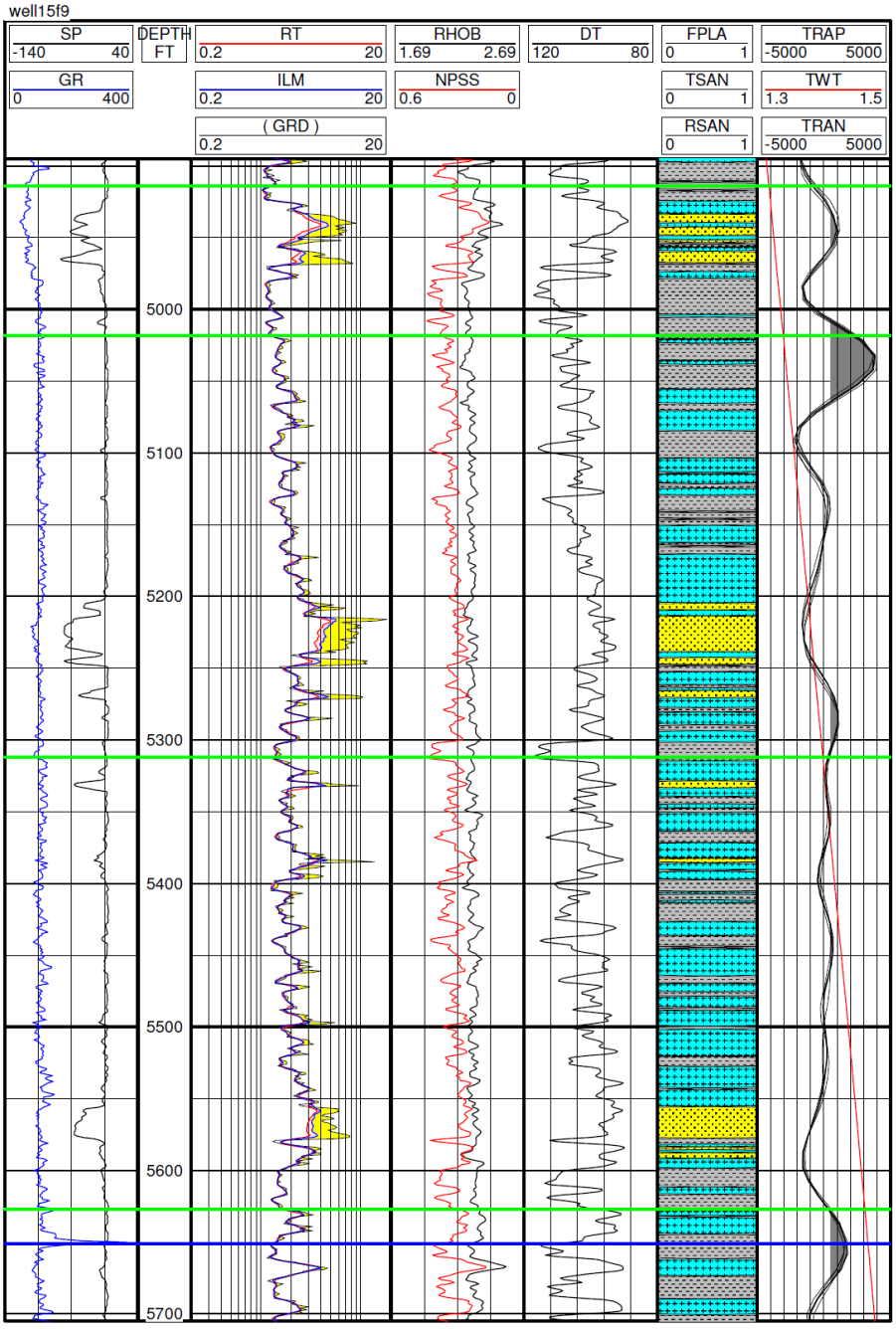

Figure E.8 Model Well 15 (flattened to well 9)

GC2L Target: Channel Class, earlier channel sand from 5555 to 5575
GC1U Target: No C38 Basal Reservoir Class, tight splays and floodplain at target depth
GC2U Target: D11 Splay Class, two splays at 5330 to 5340

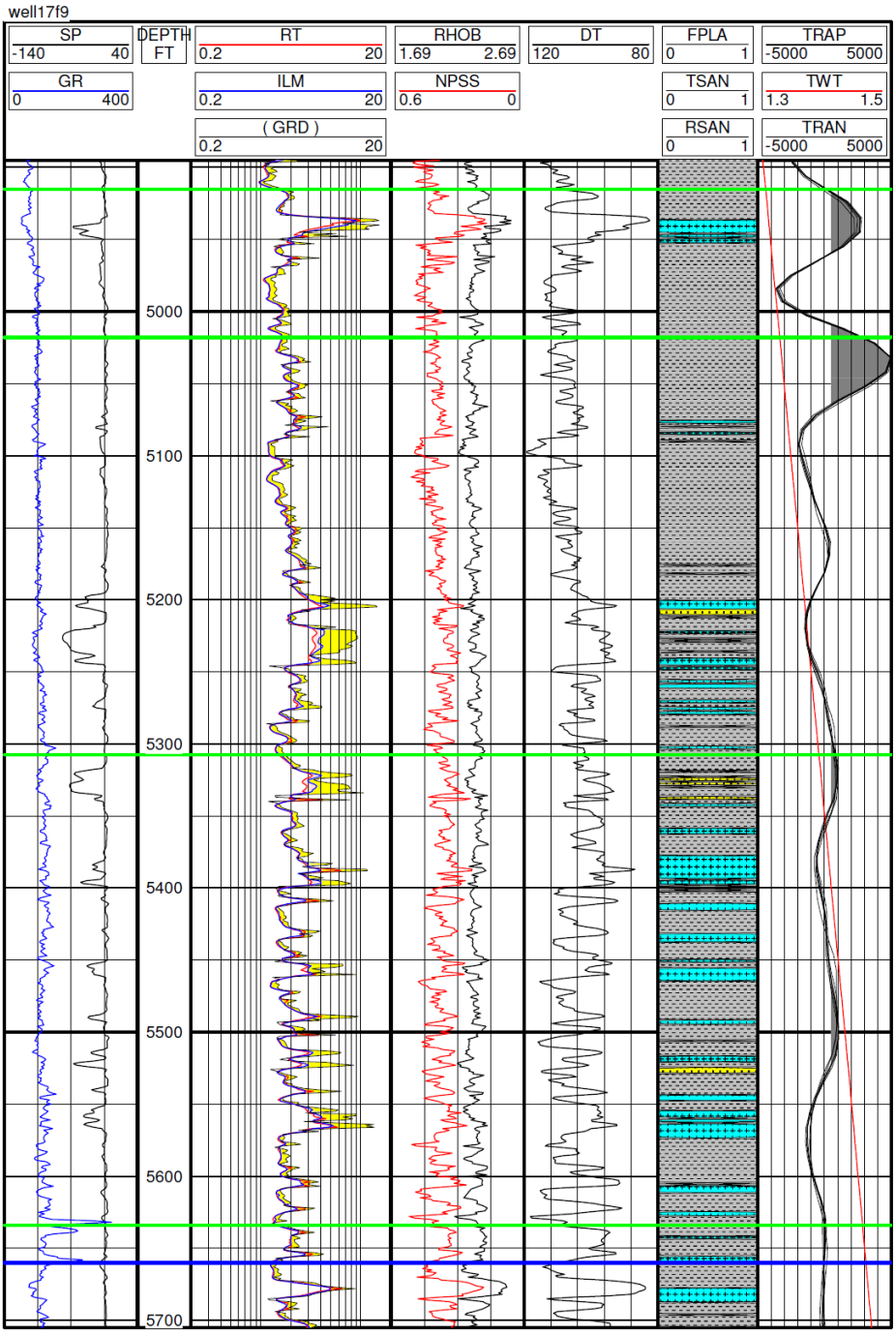

Figure E.9 Model Well 17 (flattened to well 9)

GC2L Target: Splay Class, splay/levee character from 5535 to 5575
GC1U Target: No C38 Basal Reservoir Class, tight splays and floodplain at target depth
GC2U Target: D11 Splay Class, stacked splay/levee sands at 5330 to 5340

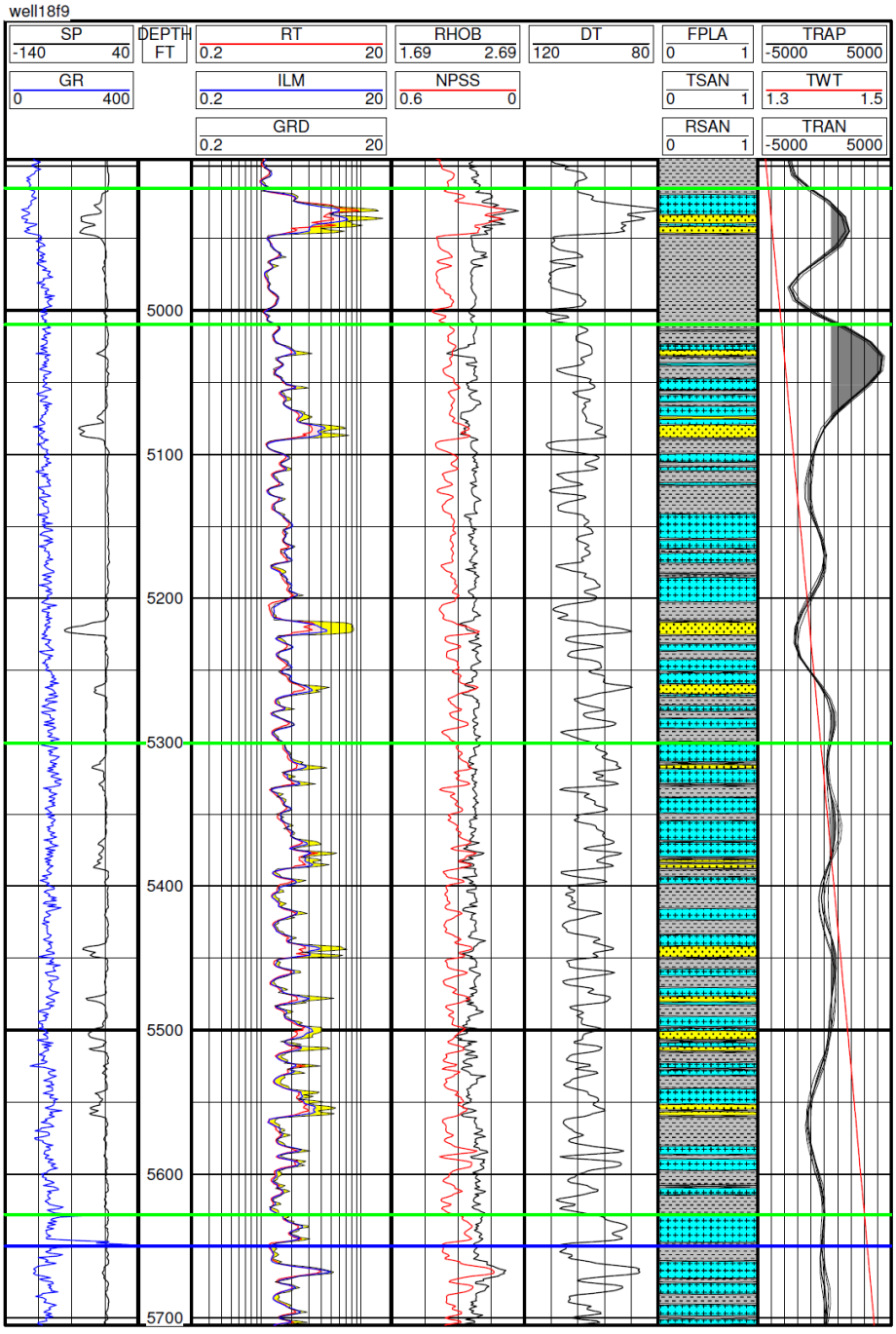

Figure E.10 Model Well 18 (flattened to well 9)

GC2L Target: Splay Class, splay/levee character from 5535 to 5575
GC1U Target: Has C38 Basal Reservoir Class
GC2U Target: D11 Splay Class, single splay at 5320

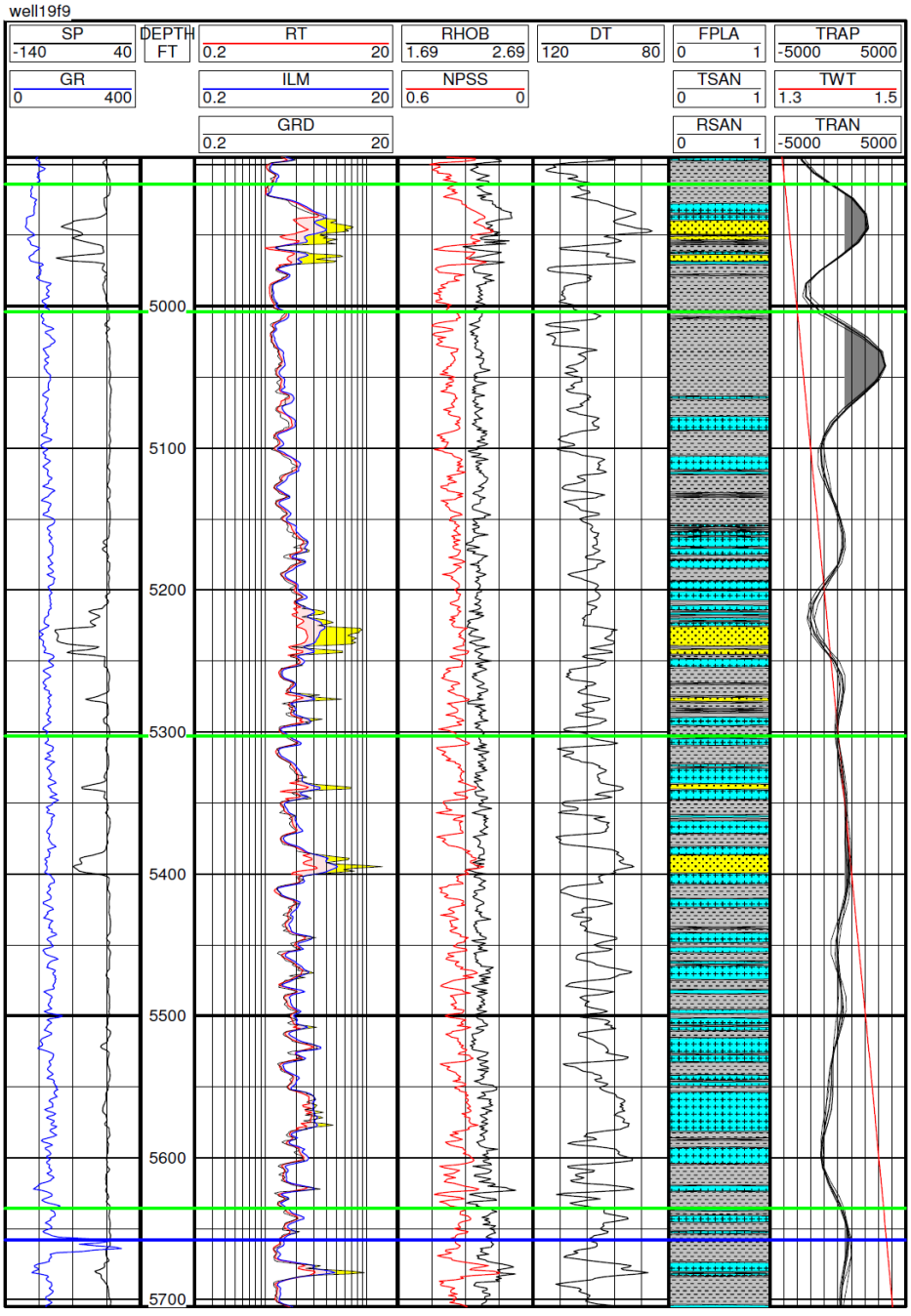

Figure E.11 Model Well 19 (flattened to well 9)

GC2L Target: Floodplain Class, a few tight splays, no reservoir sand
GC1U Target: No C38 Basal Reservoir Class at 5080
GC2U Target: D11 Splay Class, splays and tight sands at target depth

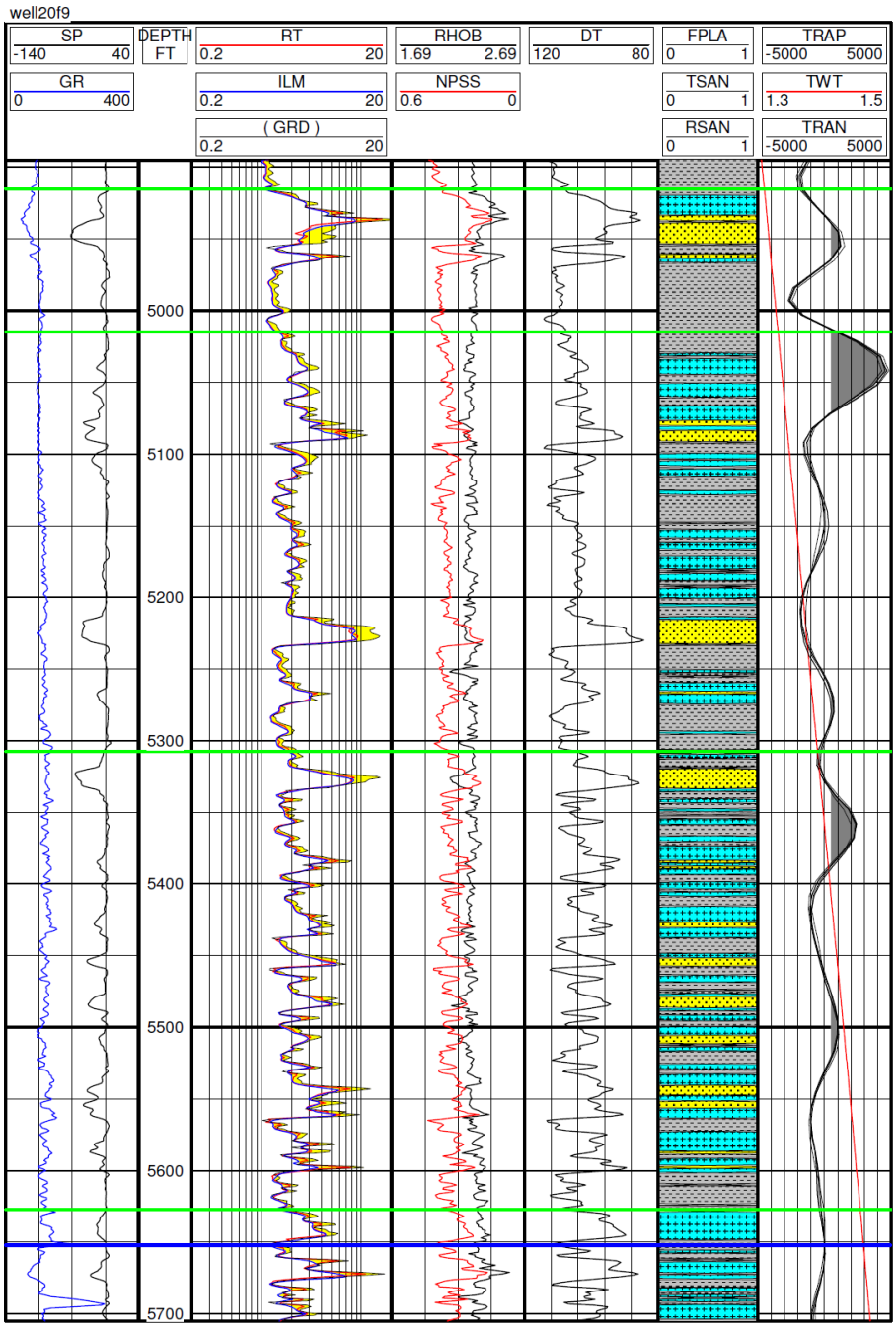

Figure E.12 Model Well 20 (flattened to well 9)

GC2L Target: Channel Class, splays/levee character with thick reservoir sand
GC1U Target: Has C38 Basal Reservoir Class at 5080
GC2U Target: D11 Channel Class

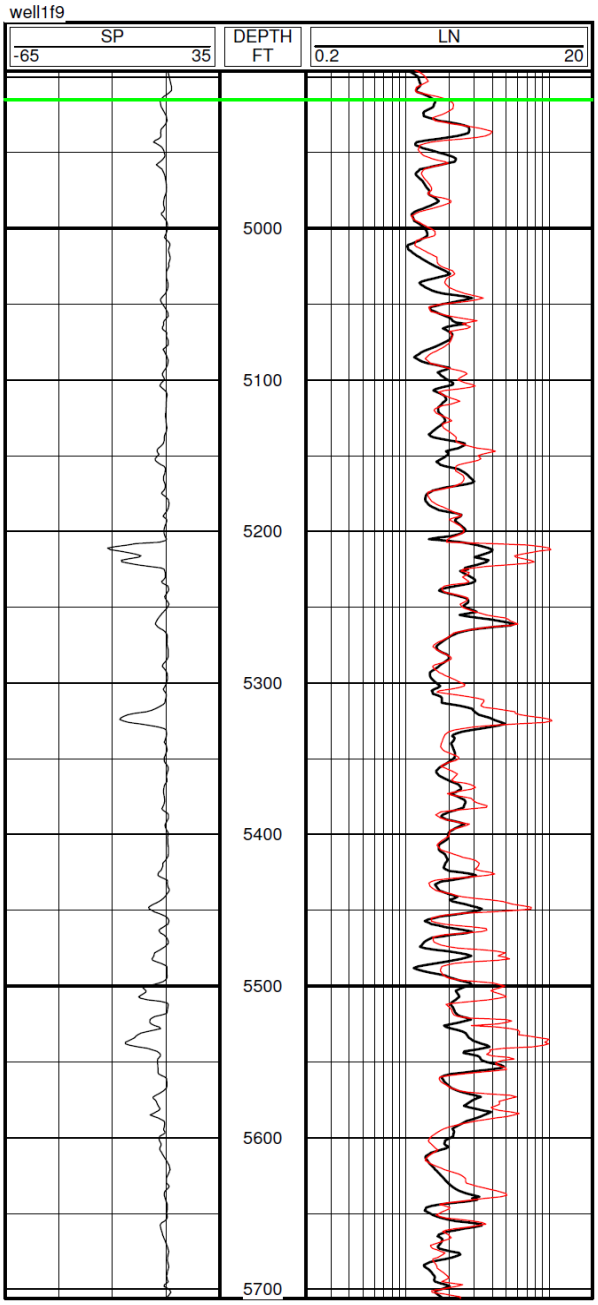

Figure E.13 Testing Well 1 (flattened to well 9), Note: this is the poorest data set, a very old E-log from the 1950's

GC2L Target: Splay Class, splays/levee character 5530 to 5545 some reservoir sand
GC1U Target: No C38 Basal Reservoir Class at 5080
GC2U Target: D11 Splay Class, a single splay at 5320

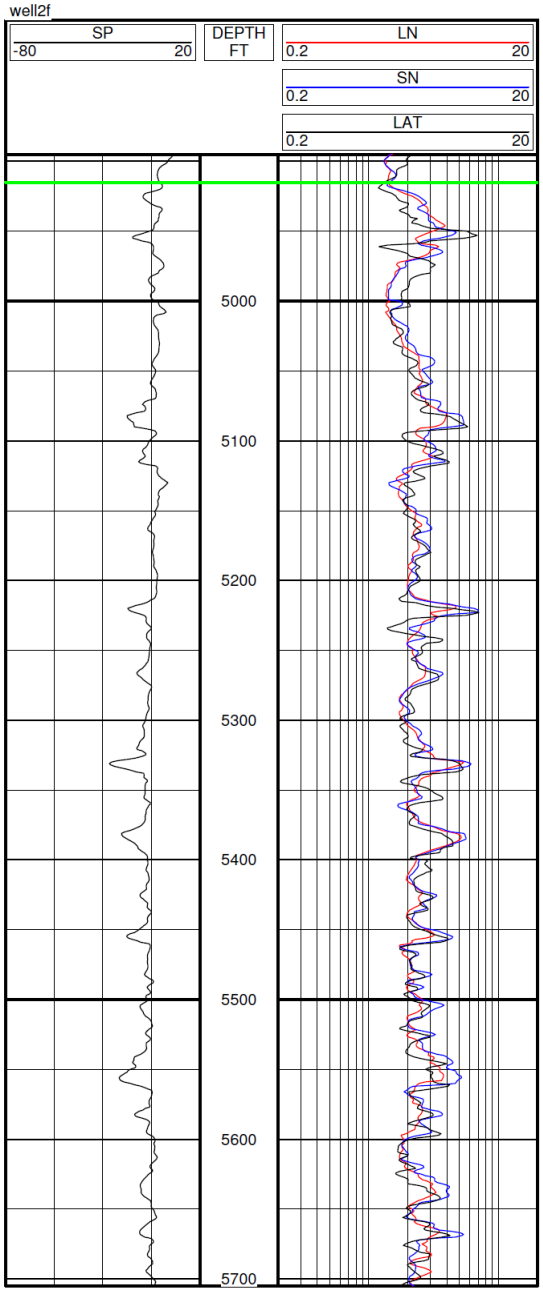

Figure E.14 Testing Well 2 (flattened to well 9), Note: another older E-log data set

GC2L Target: Channel Class, channel/levee character 5530 to 5565
GC1U Target: Has C38 Basal Reservoir Class at 5080
GC2U Target: D11 Splay Class, a single splay at 5330

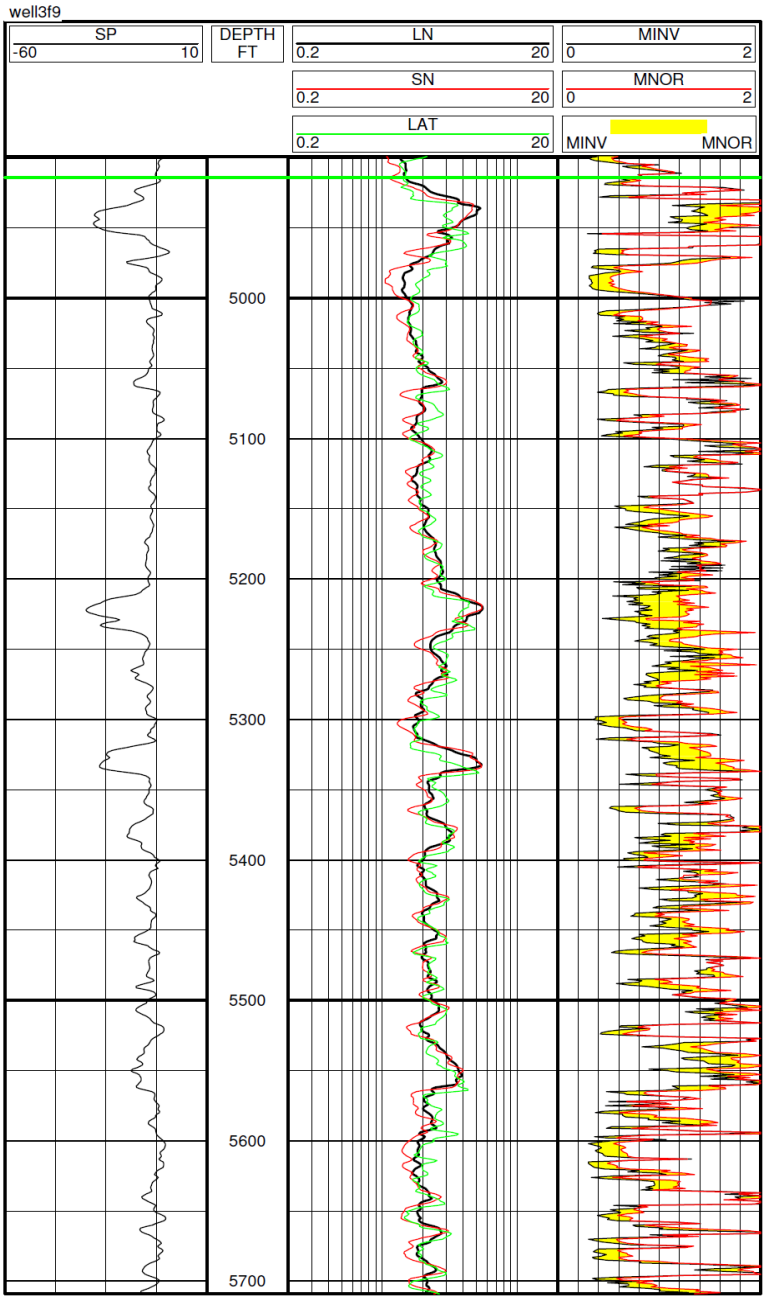

Figure E.15 Testing Well 3 (flattened to well 9), Note: older E-log data set with micro-resistivity data

GC2L Target: Channel Class, channel/levee character 5530 to 5565
GC1U Target: No C38 Basal Reservoir Class at 5080
GC2U Target: D11 Channel Class

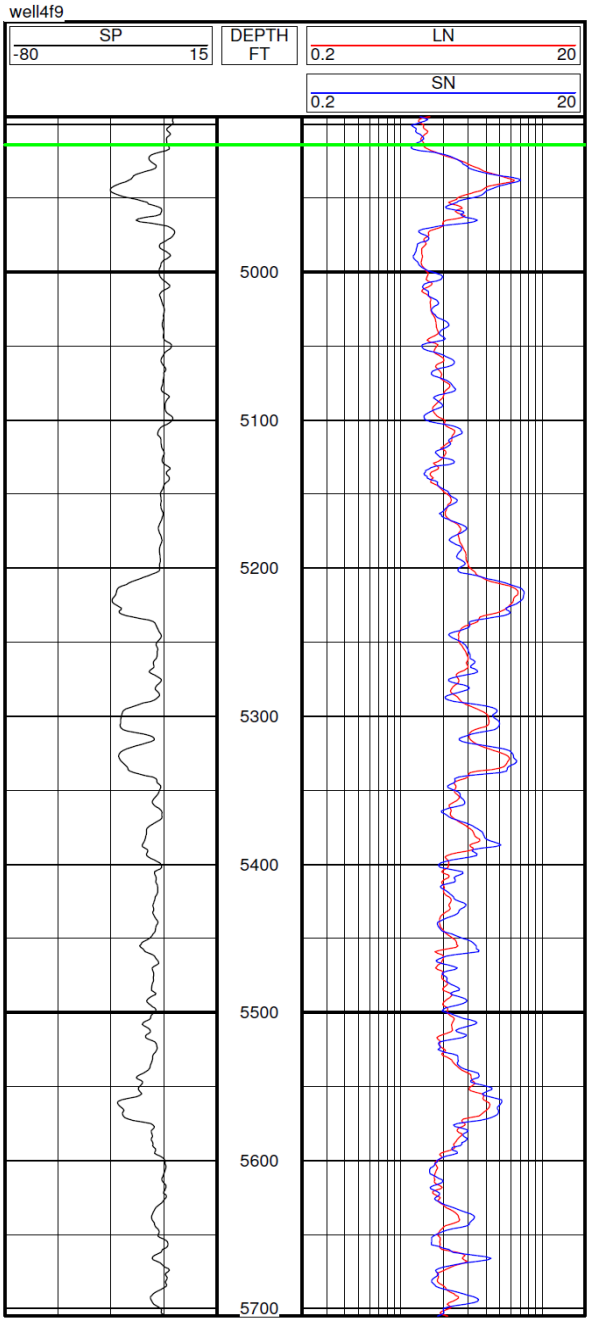

Figure E.16 Testing Well 4 (flattened to well 9), Note: older E-log data set

GC2L Target: Channel Class, early channel topped with splays
GC1U Target: No C38 Basal Reservoir Class at 5080
GC2U Target: D11 Channel Class, D11 channel topped with another channel

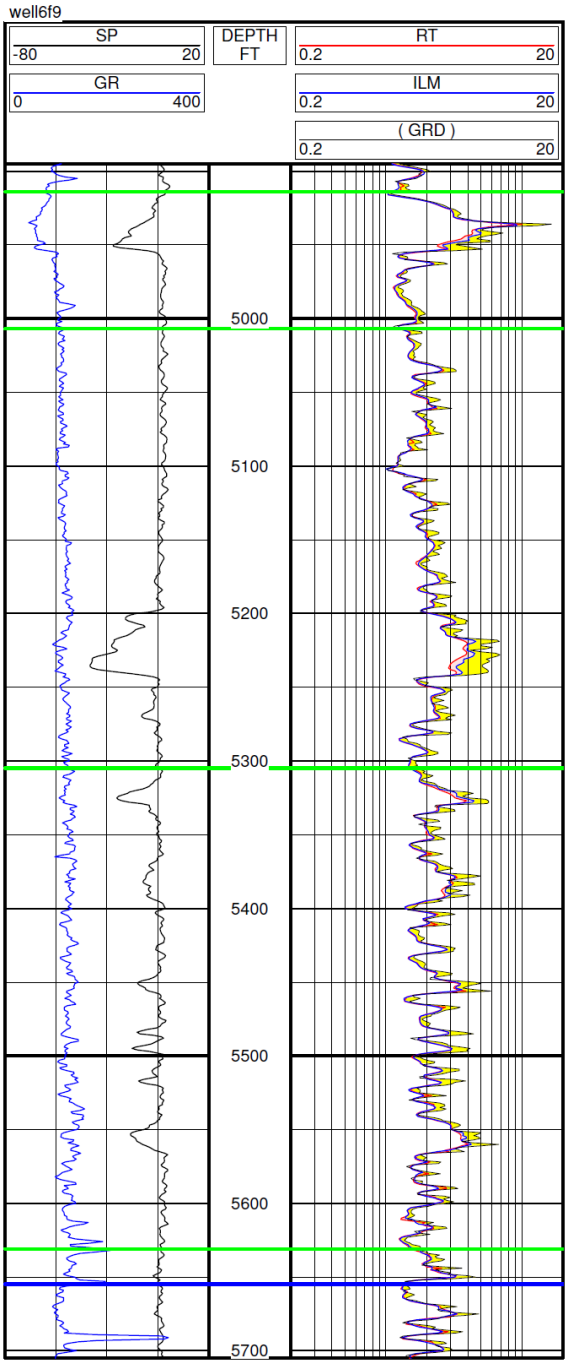

Figure E.17 Testing Well 6 (flattened to well 9), Modern logging suite without RHOB and NPSS

GC2L Target: Channel Class, A single channel from 5545 to 5570
GC1U Target: No C38 Basal Reservoir Class. Flood plain at 5080
GC2U Target: D11 Splay Class, single splay at 5330

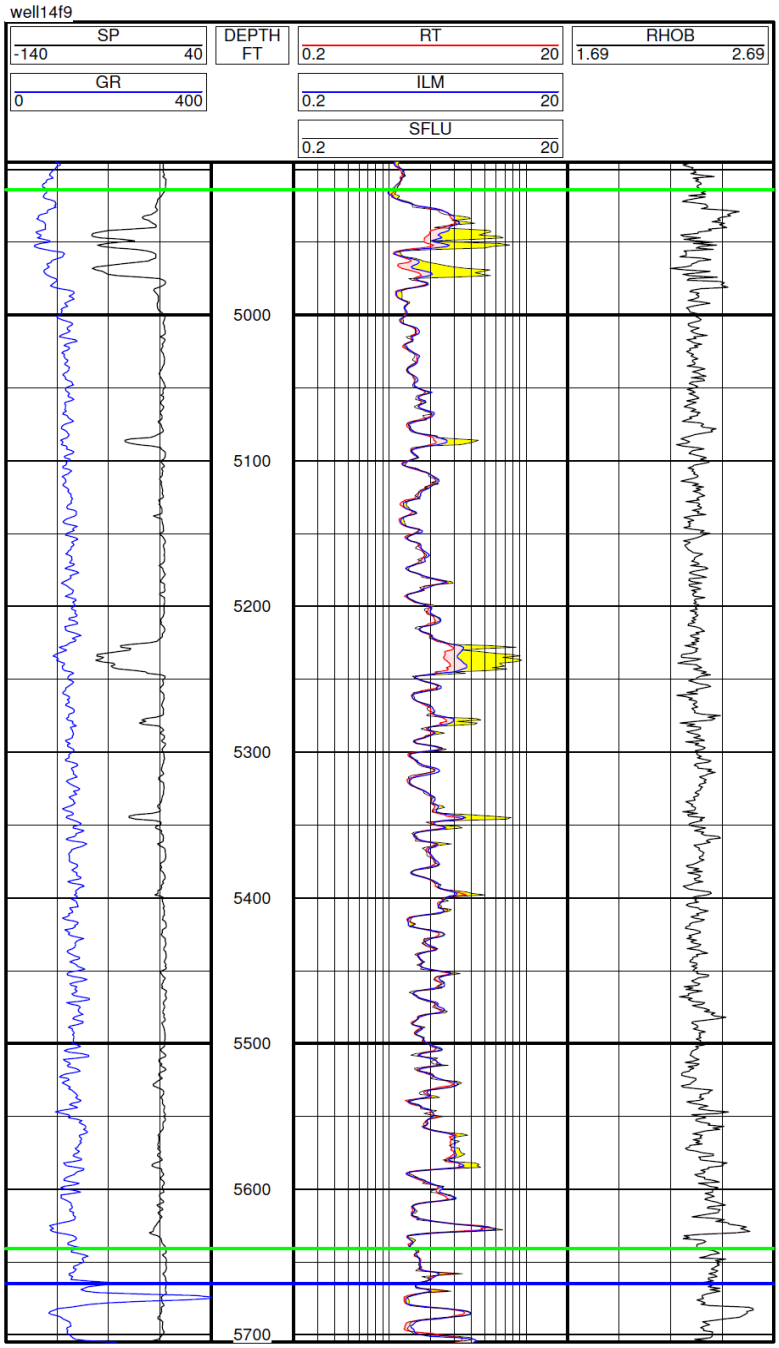

Figure E.18 Testing Well 14 (flattened to well 9), Modern logging suite without NPSS

GC2L Target: Floodplain Class
GC1U Target: Has C38 Basal Reservoir Class. Barely make it with a thin sand
GC2U Target: D11 Splay Class, several tight splays, one permeable sand

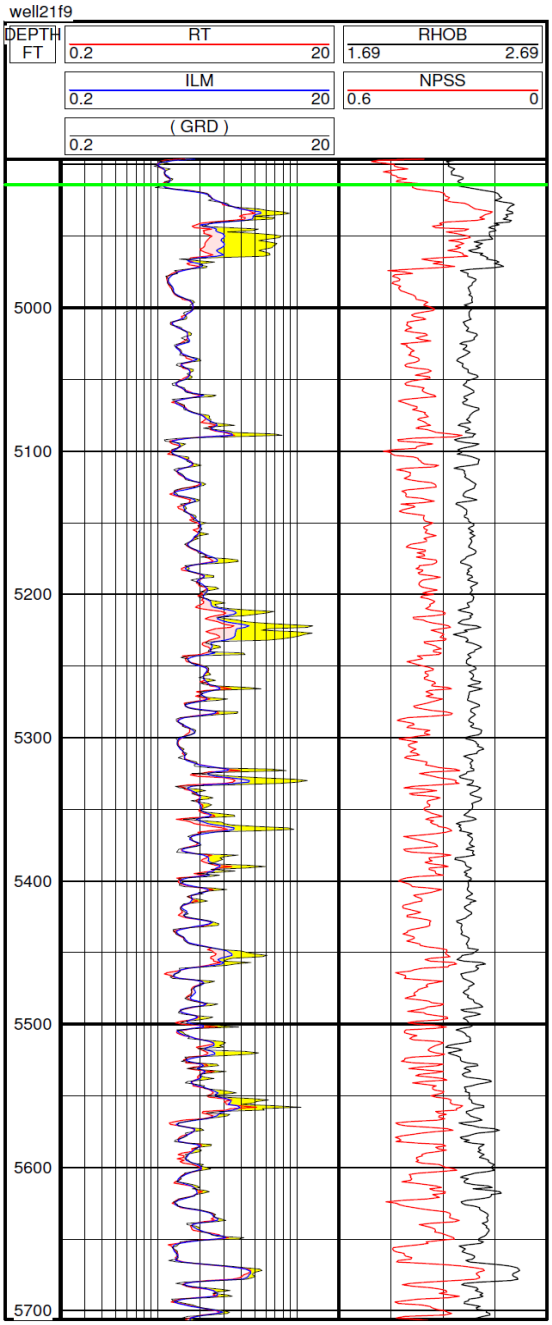

Figure E.19 Testing Well 21 (flattened to well 9), Modern logging suite without SP, GR. RHOB and NPSS

GC2L Target: Splay Class, permeable streaks in splays can be seen in resistivity profile
GC1U Target: Has C38 Basal Reservoir Class. Barely makes it with a thin sand
GC2U Target: D11 Splay Class, tough choice, RHOB and resistivity profile has stacked character, not mixed like channel reworking.

REFERENCES

Ambrose, W.A., Rodgers, Scott D., Andrews, J.R., and Stokes, Jonathan, 2000, AGIWEB Module 3 – Facies mapping of fluvial gas reservoirs in Seeligson field, south Texas: The University of Texas at Austin, Bureau of Economic Geology, and American Geological Institute, www.beg.utexas.edu/agi/mod3/m3-title.htm.

Box, George E.P., and Draper, Norman R., 1987, Empirical model building and response surface methodology: John Wiley & Sons, New York, ISBN 0-471-81003-9.

Chopra, Satinder, Castagna, John, Portiaguine, Oleg, Seismic Resolution and thin-bed reflectivity inversion, CSEG Reporter, January 2006, p. 19 – 25.

Dorrington, K. P., and Link, C.A., 2004, Genetic-algorithm/neural network approach to attribute selection for well-log prediction: Geophysics Vol. 69, No. 1.

Edwards, Marc B., 2002, The case for the regressive systems tract with examples from the Tertiary and Pleistocene of the northern gulf coast basin: Transactions of the Gulf Coast Association of Geological Societies, Volume 52, p243-255.

El-Mowafy, Hamed and Marfurt, Kurt J., 2008, Structural interpretation of the middle Frio formation using 3D seismic and well logs: an example from the Texas Gulf Coast of the United States: The Leading Edge, Vol. xx, p. xx.

Francis, Ashley, 1997, Acoustic impedance inversion pitfalls and some fuzzy analysis: The Leading Edge, Vol. 16, p. 275-280.

Fukunaga, K., Introduction to Statistical Pattern Recognition: 1990, Academic Press, 2nd Edition.

Galloway, W.E., 1982, Depositional architecture of Cenozoic gulf coastal plain fluvial systems: B.E.G. Geological circular 82-5, reprinted from SEPM Special Publication No.31.

Gelinsky, Stephan, Shapiro, Sergei A., 1997, Poroelastic Backus averaging for anisotropic layered fluid- and gas-saturated sediments: Geophysics Vol. 62, No. 6, pages 1867-1878.

Gilreath, J.A., and Stephens, Ray W., 1975, Interpretation of log response in a deltaic environment: AAPG Marine Geology Workshop, Dallas, Texas.

Grigsby, Jeffry D., and Kerr, Dennis R., Diagenetic variability in middle Frio reservoirs (Oligocene), Seeligson and Stratton fields, south Texas: Transactions of the Gulf Coast Association of Geological Societies, Volume XLI, pages 308–319.

Hardage, B. A., Levey, R.A., Pendleton, V., Simmons, J., and Edson, R., 1994, A 3-D seismic case history evaluating fluvially deposited thin-bed reservoirs in a gas-producing property: Geophysics Vol. 59, No. 11.

Holbrook, John, Scott, Robert W., and Oboh-Ikuenobe, Francisca E., 2006, Base-level buffers and buttresses: A model for upstream versus downstream control on fluvial geometry and architecture within sequences: Journal of Sedimentary Research, vol. 76, p. 160-172.

Imhoff, M. G., 2003, Scale dependence of reflection and transmission coefficients: Geophysics Vol. 68, no. 1, p. 322-336

IPNNL, 2004a, NuClass 7.10: Non-linear Networks for Classification: Image Processing and Neural Network Lab, www-ee.uta.edu\eeweb\ip\

IPNNL, 2004b, NuMap 7.10: Non-linear Networks for Regression/Approximation: Image Processing and Neural Network Lab, www-ee.uta.edu\eeweb\ip\

Kerr, Dennis R., and Grigsby, Jeffry D., 1991, Recognition and implications of volcanic glass detritus in the fluvial deposits of the middle Frio formation, south Texas: Transactions of the Gulf Coast Association of Geological Societies, Volume XLI, p. 353–358.

Kerr, Dennis R., and Jirik, Lee A., 1990, Fluvial architecture and reservoir compartmentalization in the Oligocene middle Frio formation, south Texas: Transactions of the Gulf Coast Association of Geological Societies, Volume XL, p. 373–380.

Li, Jiang, Manry, Michael T., Narasimha, Pramod, and Yu, Changhua, 2006a, Feature selection using a piecewise linear network", IEEE Trans. on Neural Networks, Vol. 17, no. 5, p. 1101-1115.

Li, Jiang, Yao, Jianhua, Summers, Ronald M., Petrick, Nicholas, Manry, Michael T. and Hara, Amy K., 2006b, An efficient feature selection algorithm for computer-aided polyp detection: special issue of the International Journal on Artificial Intelligence Tools (IJAIT), vol. 15, no. 6, p. 893-915.

Liu, Yinbin, Schmitt, Douglas R., 2003, Amplitude and AVO responses of a single thin bed: Geophysics Vol. 68, no.4, p. 1161–1168.

Loermans, ir A.M., Kimminau, S., Bolt, H., 1999, On the quest for depth: Transactions of the SPWLA 40th Logging Symposium, May 30, Paper B.

Loucks, R.G., Bebout, D.G., Galloway, W.E., 1977, Relationship of porosity formation and preservation to sandstone consolidation history – Gulf Coast lower tertiary Frio formation: geological circular 77-5, reprinted from transactions of the Gulf Coast Association of Geological Societies, Vol. 27.

Manry, M.T., Dawson, M.S., Fung, A.K., Apollo, S.J., Allen, L.S., Lyle, W.D., and Gong, W., 1994, Fast training of neural networks for remote sensing: Remote Sensing Reviews, Vol. 9.

Mundim, Evaldo C., Schots, Heron A., de Araujo, Joao M., WTdecon, a colored deconvolution implemented by wavelet transform, SEG The Leading Edge, April 2006, p. 398 – 401.

Pennington, W., Acevedo, H., Green, A., Haataja, J., Len, S., Minaeva, A., and Xie, D., 2002, Calibration of seismic attributes for reservoir characterization: Final Technical report for DOE award DE-AC26-98BC15135.

Rio, P., Mukerji, T., Mavko, G., and Marion, D., 1996, Velocity dispersion and upscaling in a laboratory-simulated VSP: Geophysics Vol. 61, no. 2, p. 584–593.

Sinha,Satish, Routh, Partha S., Anno, Phil D., and Castagna, John P., 2005, Spectra decomposition of seismic data with continuous-wavelet transform: : Geophysics Vol. 70, no. 6, p. 19-25.

Skopec, Robert A., and Ross, Christopher P., 1994, Amplitude-versus-offset interpretation, scaling factors,and other challenges associated with acoustic data integration: Society of Core Analysis paper 1994-17.

Widess, M. B., 1973, How thin is a thin bed?, Geophysics Vol. 38, p 1176–1180.

Wiener, Norbert, 1949, Extrapolation, interpolation and smoothing of stationary time series, Wiley, New York ISBN 0-262-73005-7

BIOGRAPHICAL INFORMATION

Richard Odom received a B.S. in Geophysics from New Mexico Tech in 1980. In the decades since, his primary work is the design of well-logging systems and research in nuclear geophysics. He has authored many symposium and journal publications in this discipline and has 11 patents. The M.S. in Geology program was an act of renaissance, to lure the generalist out of the specialist, to get a fresh view of a bigger picture. Mr. Odom plans to use his recently-expanded brain in the search for energy in the subsurface.